5. SITE 672[1]

Shipboard Scientific Party[2]

HOLE 672A

Date occupied: 1110, 15 July 1986

Date departed: 1430, 22 July 1986

Time on hole: 7 days, 3 hr, 20 min

Position: 15°32.40′N, 58°38.46′W

Water depth (sea level, corrected m; echo-sounding): 4975

Water depth (rig floor, corrected m; echo-sounding): 4986

Bottom felt (rig floor, m; drill-pipe measurement): 4983

Distance between rig floor and sea level (m): 10.5

Total depth (rig floor, m): 5477

Penetration (m): 493.8

Number of cores (including cores with no recovery): 53

Total length of cored section (m): 493.8

Total core recovered (m): 381.3

Core recovery (%): 77

Oldest sediment cored:
Depth sub-bottom (m): 493.8
Nature: radiolarian mudstone
Age: early Eocene
Measured velocity (km/s): 1.9

[1] Mascle, A., Moore, J. C., et al., 1988. *Proc., Init. Repts. (Pt. A), ODP*, 110: College Station, TX (Ocean Drilling Program).

[2] J. Casey Moore (Co-Chief Scientist), Dept. of Earth Sciences, University of California at Santa Cruz, Santa Cruz, CA 95064; Alain Mascle (Co-Chief Scientist), Institut Français du Pétrole, 1–4 Ave Bois-Preau, B.P. 311, 92506 Rueil Malmaison Cedex, France; Elliott Taylor (Staff Scientist), Ocean Drilling Program, Texas A&M University, College Station, TX 77840; Francis Alvarez, Borehole Research Group, Lamont-Doherty Geological Observatory, Columbia University, Palisades, NY 10964; Patrick Andreieff, BRGM, BP 6009, 45060 Orleans Cedex-2, France; Ross Barnes, Rosario Geoscience Associates, 104 Harbor Lane, Anacortes, WA 98221; Christian Beck, Département des Sciences de la Terre, Université de Lille, 59655 Villeneuve d'Ascq Cedex, France; Jan Behrmann. Institut für Geowissenschaften und Lithosphärenforschung, Universität Giessen, Senckenbergstr. 3, D6300 Giessen, FRG; Gerard Blanc, Laboratoire de Géochimie et Métallogénie U. A. CNRS 196 U.P.M.C., 4 Place Jussieu, 75252 Paris Cedex 05, France; Kevin Brown, Dept. of Geological Sciences, Durham University, South Road, Durham, DH1 3LE, U.K. (current address: Dept. of Earth Sciences, University of California at Santa Cruz, Santa Cruz, CA 95064); Murlene Clark, Dept. of Geology, LSCB 341, University of South Alabama, Mobile, AL 36688; James Dolan, Earth Sciences Board, University of California at Santa Cruz, Santa Cruz, CA 95064; Andrew Fisher, Division of Marine Geology and Geophysics, University of Miami, 4600 Rickenbacker Causeway, Miami, FL 33149; Joris Gieskes, Ocean Research Division A-015, Scripps Institution of Oceanography, La Jolla, CA 92093; Mark Hounslow, Dept. of Geology, Sheffield University, Brook Hill, Sheffield, England S3 7HF; Patrick McLellan, Petro-Canada Resources, PO Box 2844, Calgary, Alberta Canada (current address: Applied Geotechnology Associates, 1-817 3rd Ave. NW, Calgary, Alberta T2N OJ5 Canada); Kate Moran, Atlantic Geoscience Centre, Bedford Institute of Oceanography, Box 1006, Dartmouth, Nova Scotia B2Y 4A2 Canada; Yujiro Ogawa, Dept. of Geology, Faculty of Science, Kyushu University 33, Hakozaki, Fukuoka 812, Japan; Toyosaburo Sakai, Dept. of Geology, Faculty of General Education, Utsunomiya University, 350 Minemachi, Utsunomiya 321, Japan; Jane Schoonmaker, Hawaii Institute of Geophysics, 2525 Correa Road, Honolulu, HI 96822; Peter J. Vrolijk, Earth Science Board, University of California at Santa Cruz, Santa Cruz, CA 95064; Roy Wilkens, Earth Resources Laboratory, E34-404 Massachusetts Institute of Technology, Cambridge, MA 02139; Colin Williams, Borehole Research Group, Lamont-Doherty Geological Observatory, Columbia University, Palisades, NY 10964.

Principal results: Site 672, located 6 km east of the Barbados Ridge deformation front, penetrated 500 m of Pleistocene to Eocene deposits of the locally 800-m-thick Atlantic sedimentary cover. Lower Pleistocene to the lower Miocene massive hemipelagic clay(stones) and mud(stones) include numerous ash layers. Middle Eocene to upper Oligocene alternating sandstones and siltstones, claystones, calcareous mudstones, marlstones and limestones record lateral clastic and biogenic input, respectively, from the South American continent and the upper slope of the Tiburon Rise, in addition to the background hemipelagic sedimentation. Lower Eocene and lowermost middle Eocene deposits consist of siliceous claystones. The carbonate content of these sediments is high from middle Eocene to lower–upper Oligocene and from upper Miocene to Pleistocene, whereas lower Eocene and upper Oligocene through middle Miocene sediments contain almost no carbonates. Radiolarian-bearing claystones accumulated during early Miocene and early Eocene.

Normal faults and low to very low bedding dips prevail in most of the core section. However, local steep dips, mud-filled en-echelon veins in subhorizontal shear zones, and reverse faults occur in a lower Miocene interval extending from 175 to 195 mbsf. These deformational features are interpreted as an incipient compressional failure that could be related to an anomalous porosity high and to a probable correlative decrease of sediment strength. This high-porosity and structurally anomalous zone correlates with the top of the décollement zone at Sites 671 and 541. Anomalies in chloride and methane pore-water content occur near the potential future décollement surface as well as deeper in the hole. A low chloride content at 365 mbsf (upper Eocene) and a modest increase in methane content at 425 mbsf (middle Eocene) suggest lateral fluid advection in sandy layers. A prominent methane high at about 200 mbsf (lower Miocene or uppermost Oligocene) is succeeded upsection by a slowly decreasing diffusive gradient. This high value of methane content also requires lateral fluid advection at a depth broadly correlative to the future décollement.

BACKGROUND AND OBJECTIVES

The portion of Atlantic abyssal plain facing the Lesser Antilles island arc has decreasing water depths ranging from more than 6000 m north of the arc, to less than 3000 m to the south. This bathymetric gradient is related to the main sedimentary influx to this area from the South American continent, most of which was deposited during the late Miocene to Holocene time (mainly through the Amazon and Orinoco drainage system). Bottom-water currents, moving from the south to the north (Damuth and Fairbridge, 1970; Embley and Langseth, 1977) provide the transportation mechanism for these sediments. As a result of this supply, sediment thickness on the Atlantic ocean floor decreases from over 7 km south of 11°N to about 200 m at 19°N in the Antillean region (Speed, Westbrook, et al., 1984; Mascle et al., 1985). The underlying oceanic crust north of 12°N is of Senonian age, and presumably of Late Jurassic-Early Cretaceous age to the south (Westbrook et al., 1984). The oceanic crust north of 12°N shows WNW- to ESE-trending fracture zones which are probably remnant transform faults. These faults clearly offset magnetic anomalies and have generated troughs and flanking asymmetrical ridges (Peter and Westbrook, 1976; Westbrook et al., 1984). The two most prominent of these ridges are the Barracuda and Tiburon Ridges at 16°33′N and 15°N, respectively.

Site 672 is located on the Atlantic abyssal plain at 15°30′N, i.e., at the northwestern extremity of the Tiburon Rise where it intersects the accretionary complex (Fig. 1). The average seafloor slope at this location is about 1.5°, dipping to the northwest. A similar dip is observed at the top of the oceanic basement. Site 672 is 6 km east of the deformation front, 10 km east of Site 671 and 20 km south of Site 543, the reference site of DSDP Leg 78A. The sedimentary cover at the selected site is about 800 m thick, and has a well-defined seismic sequence, thus making it an attractive site to document the lithostratigraphy of the Atlantic plain sediments (Fig. 2). Site 672 is designed as the reference hole of the ODP Leg 110 site transect that also includes DSDP Holes 541 and 542. Accordingly, Site 672 should provide an important set of data on lithology, biostratigraphy, physical properties, and geochemistry of the oceanic stratigraphic units prior to accretion or subduction. These data will allow critical direct comparisons to be made between sedimentary deposits of the same age cored in the accretionary complex and on the oceanic plate, and thus will provide a better understanding of the acting tectonic processes.

During DSDP Leg 78A, a reference site (Site 543) was drilled 3 km east of the deformation front but 20 km north of the present site transect (Fig. 3). A complete sedimentary section ranging in age from Campanian to early Pleistocene was cored at Site 543, but lower Pliocene, middle Miocene, middle Eocene, and Maestrichtian sections were significantly condensed, and the Paleocene was missing. Furthermore, the seismic sequences on Line A1C at Site 543 look quite different from these on Line CRV 128 (Fig. 2) and no correlation between the two lines has been possible. Obviously, Site 543 could not be considered as an appropriate reference site for ODP Leg 110, and Site 672 is proposed as a new and more convenient one. It is believed, however, that comparisons of sedimentary processes between the two sites will allow a better understanding of sediment paleoenvironment on the slopes of Tiburon Rise.

OPERATIONS

Hole 672A is located about 5 nmi seaward of Site 671. The site was positioned immediately east of the Barbados forearc accretion and subduction zone and was selected as a reference site for the holes drilled on the prism. The stratigraphy and sediment properties of the oceanic abyssal plain sediments prior to accretion/subduction could then be compared to the sediments cored on the forearc. Site 672 is situated at 15°32.40′N, 58°38.46′W in 4973 m of water.

The hole was located from seismic line CRV-128 and dead reckoning as the ship's position was outside of the GPS window and satellite information was not available during transit. The beacon was dropped at 1110 hr on 15 July 1986 and the site spudded at 2030 hours. The BHA consisted of a long-toothed APC-XCB 11-7/6″ diameter core bit with a 6-drill collar bottom hole assembly. The flapper was removed from the float valve in the bit-sub to allow logging without dropping a bit.

The hole was cored using the APC to 123.3 mbsf where the sediment stiffness caused high pullout forces. APC recovery was excellent (100%). Temperature measurements were taken on Cores 110-672A-2H, -4H, and -6H using the APC temperature recorder. The new pore-water-temperature-pressure (WSTP) sampler probe was deployed after Cores 110-672A-5H and -10H.

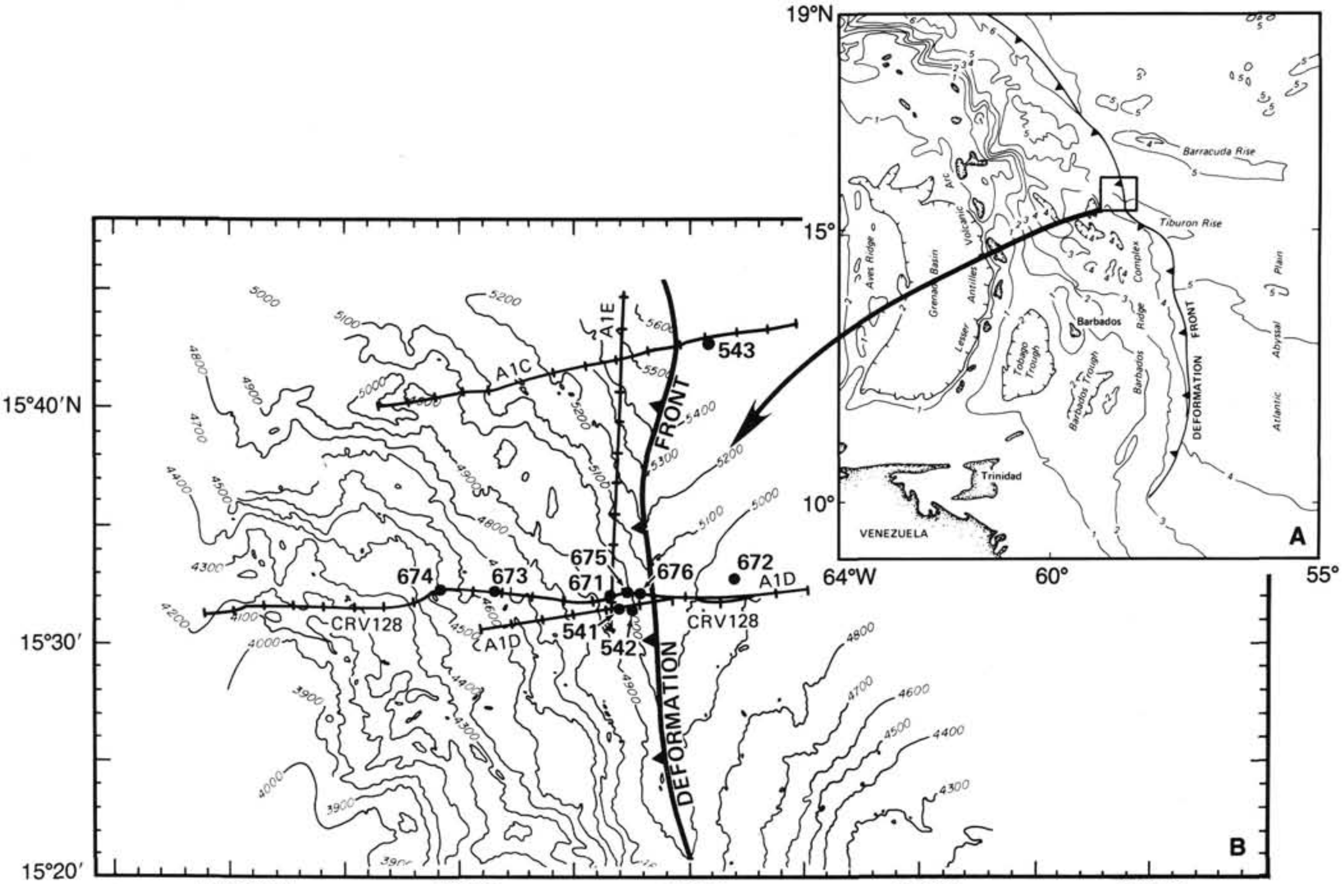

Figure 1. Regional and detailed location maps of Site 672.

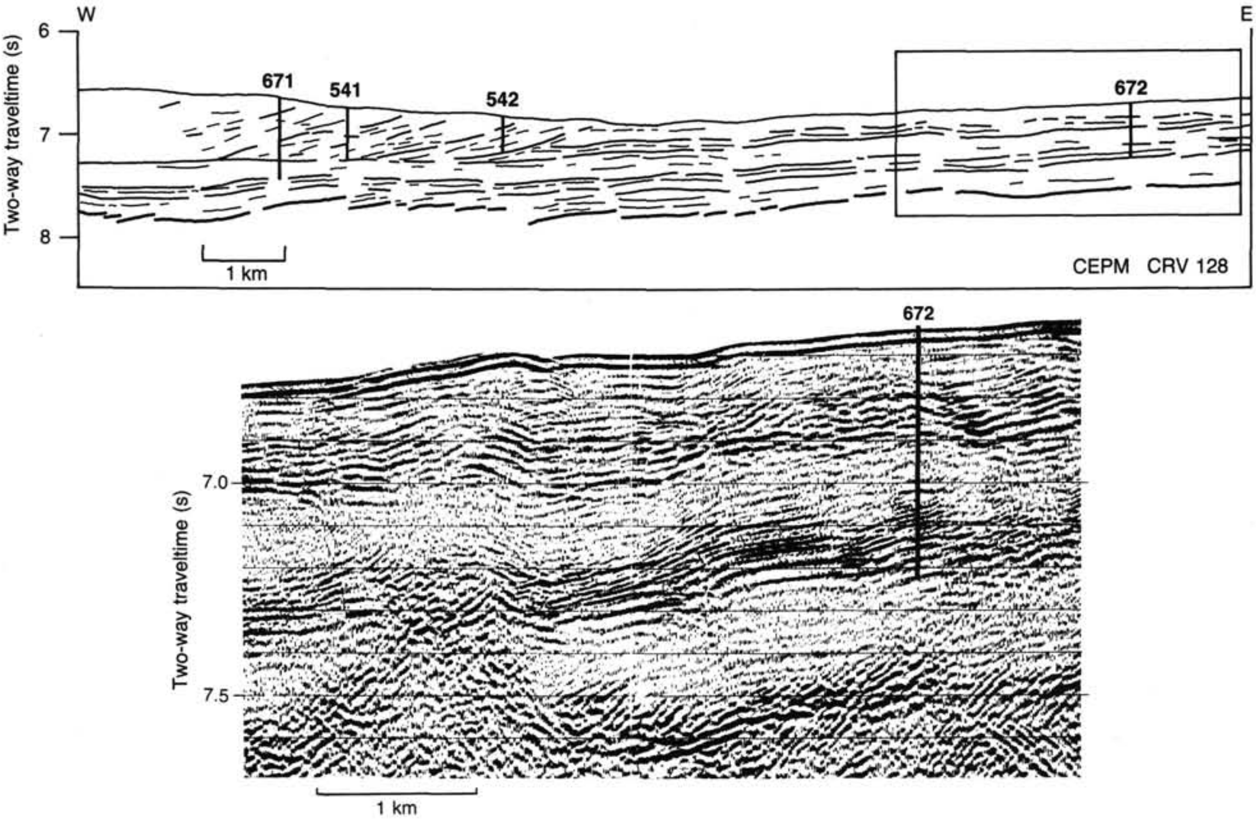

Figure 2. Top: Line drawing of migrated high-resolution multichannel line CRV 128. Bottom: Detailed seismic section and location of Site 672.

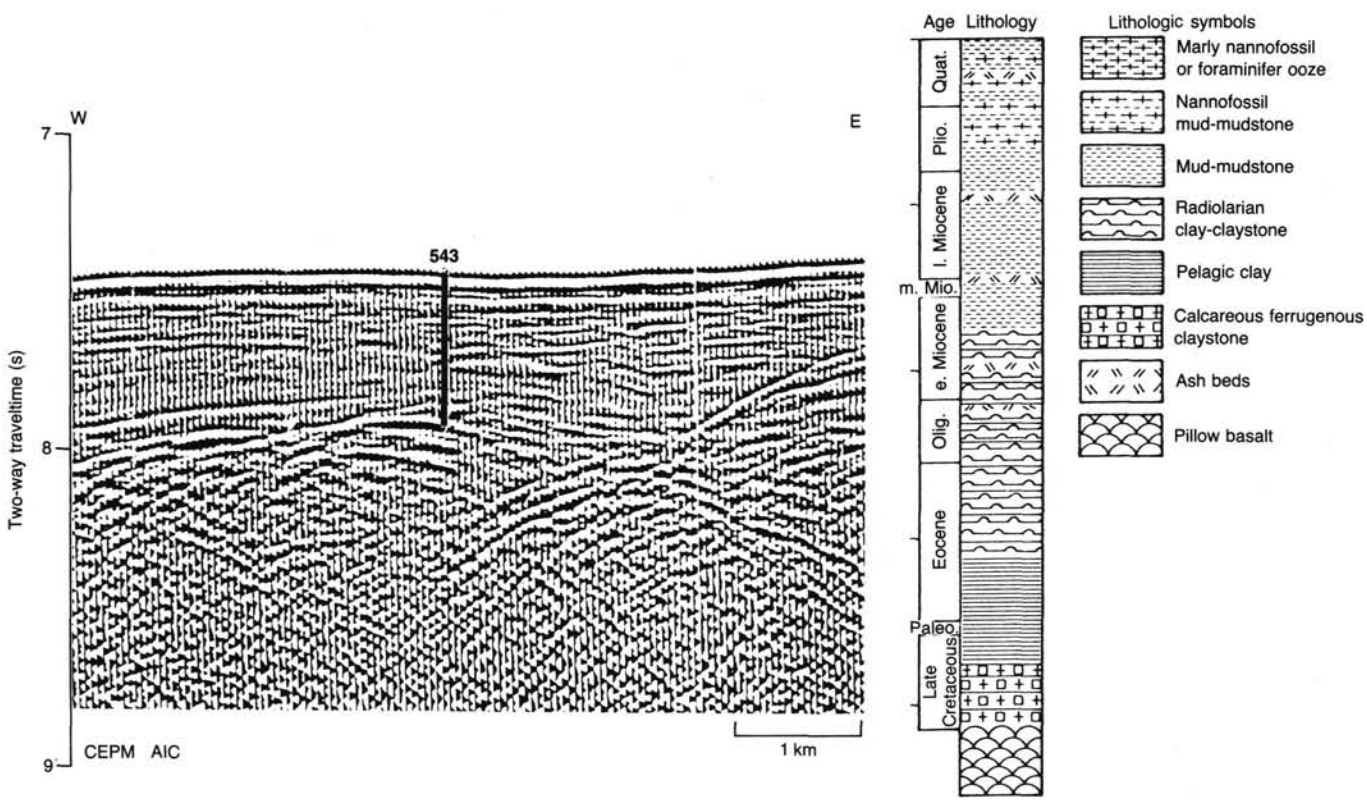

Figure 3. Summary lithology of Site 543 and presumed location of Site 543 on seismic line A1C. The positioning of this line is very poor and correlations with other lines suggest that it is actually located 2 km to the south.

The XCB coring system was deployed after Core 110-672A-14H and used until hole termination at 493.8 mbsf. XCB recovery was 69.3%. The WSTP sampler was deployed after Cores 110-672A-15X and -20X. The second sampler run was aborted when the sampler barrel stuck, 500 m below the rotary table.

Particular attention was given to the drilling parameters of Site 672 to keep cuttings from overwhelming the circulation system. The amount of fill found in the bottom of the hole after each core was reported by the driller. If the fill thickness exceeded 2 m, two annular volumes of seawater were circulated after cutting the next core but before retrieving the core barrel. Pump pressure was increased as the hole deepened and the sediment firmed. The amount of fill increased between cores and the hole became quite sticky as we neared total depth. The operations procedure used for the last few cores was to pull the bit off bottom before retrieving the core and allow the pipe to stand 5 min without circulation. If a significant overpull above the string weight was required to move the pipe after waiting 5 min, the pipe was then moved to a spot higher up the hole, more water was circulated, and the test repeated. The purpose of this test was to approximate the conditions encountered while running into the well to retrieve the core barrel with the sand line. A twenty-barrel mud flush was pumped at 5420 m below rig floor (mbrf) to aid in removing the cuttings. The target depth was obtained at 493.8 mbsf.

The hole was conditioned for logging by pumping a twenty-barrel mud flush and making a short wiper trip back up to 5116 mbrf. The hole was then reamed to bottom to clean out fill from 5460 to 5477 mbrf. The bit was positioned at 5101 mbrf and the Schlumberger DIL-GR-SONIC-CAL tool was run into the hole. The logging tool signal was lost at 5131 mbrf, so the tool was retrieved and inspected. The short bridle between the tool and the torpedo connection was found to be at fault. A second short bridle was installed and the same tool was run back into the hole. The tool signal was once again lost, at 500 mbsf, and was therefore retrieved.

The Lamont multichannel sonic tool was attached to the logging cable and deployed while the Schlumberger cable connections were being repaired. The tool functioned well outside the drill pipe but was stopped by a bridge at 5249 mbrf. The tool was initially stuck but became free after 30 min of repeated pulls at 1800 lb over cable weight. The sonic tool was retrieved and the cable was found to be kinked over the bottom 40 m. Caving conditions in the hole were such that further logging could not be carried on successfully. The pipe was run back to 300 mbsf, and the well was abandoned with heavy mud. Pipe was tripped to surface and the *Resolution* departed Site 672 at 1430 hr, 22 July 1986.

The total operations time at Site 672 was 7.1 days, during which time 493.8 m were cored, 381 m recovered (77.3%) and approximately 30–50 m logged. A core summary for Hole 672A is listed in Table 1.

STRUCTURAL GEOLOGY

Site 672 is especially valuable for assessment of the magnitude of deformation occurring in the incoming oceanic deposits. Thus it provides an important reference for understanding the added structural complexity imprinted onto the sedimentary section during accretion or underthrusting. Unfortunately, cores were not oriented to provide azimuth readings.

There are three discrete zones of bedding disturbance, although in most cores bedding attitudes are horizontal or subhorizontal (Fig. 4). The uppermost zone is limited to Core 110-672A-8H, with bedding dips up to 20°. The second zone shows strongly variable bedding attitudes with dips as steep as 70° in Cores 110-672A-21X and -22X. The third zone of bedding disturbance is found in Core 110-672A-42X. Comparing these positions with the log of faulting intensity, we find that in all three cases bedding disturbance correlates well with sections of intensive faulting of the core, and may therefore be induced by tectonic activity.

In general, Hole 672A displays a low background of fault density with zero to one fault per 10 m throughout most of the section. Dip angles of most fault planes are high, and there is a strong predominance of normal displacement senses. This type of faulting is in line with the structural interpretations of the seismic reflection profiles, which shows normal faulting of the oceanic crust and its sedimentary cover in the vicinity of Site 672. Abundant high-angle faulting is recorded in Core 110-672A-8H, numerous normal faults are observed in Core 110-672A-12H, and high-angle faults are commonly developed in Core 110-672A-42X.

The fault geometries and kinematics of Cores 110-672A-20X and -21X are clearly different from the rest of the section. In addition to normal faults, there are singular fault planes with reverse displacements, and one horizontal fault. In addition there is evidence for low-strain ductile-to-semibrittle shearing in the form of centimeter-scale subhorizontal en echelon arrays of dilation veins filled by clay minerals (Fig. 5). Displacements along the shear zones are either horizontal or reverse, as indicated in one case by the dip and geometry of the vein array. No overprinting relationships between normal and reverse faults could be established, but their geometry makes them mutually exclusive with respect to a particular orientation of the three principal stress axes. We must therefore invoke two independent phases of tectonic activity for their formation. With the exception of one fault in Core 110-672A-10H, all reverse or horizontal faults are concentrated in Cores 110-672A-20X and -21X. In terms of lithostratigraphy and biostratigraphy this is broadly the same horizon that hosts the décollement zone in Hole 671B (see Site 671 chapter, this volume). It is conceivable that the compressive structures encountered in Cores 110-672A-20X and -21X represent the tip strains associated with a slowly propagating horizontal décollement within the Miocene sediment section, well ahead of the megascopically visible deformation front.

Syntectonic subvertical dilation veins with clay mineral fills are developed in Cores 110-672A-12H and -13H. They are spatially associated with a zone of normal faulting, and can be ascribed to the same stress geometry that created the normal faults.

Irregular clay-filled vein networks occur in Cores 110-672A-20X to -22X together with subvertical veins and the en echelon vein arrays described above.

In summary, the rocks penetrated in Hole 672 were found to contain a much stronger tectonic imprint than expected in a pile of sediments riding passively on oceanic crust. Many of the observed structures can be related to the normal faulting also visible on the seismic reflection profiles in the area. The cause of the compressive structures encountered in Hole 672 remains unclear, although they may represent precursors of future thrusting associated with the seaward (eastward) progradation of the Lesser Antilles accretionary prism.

LITHOSTRATIGRAPHY

Sediment Lithology: Description

The 494-m-thick succession cored at Site 672 has been divided into five lithologic units (Table 2). Major sediment types as well as some minor lithologies were used as criteria for subdivision. Units 1, 2, and 5 are characterized by relatively homogeneous hemipelagic sedimentation whereas Units 3 and 4 are composed of cyclic alternations of three or four different lithologies reflecting a significant influx of terrigenous material and possible redeposition by a variety of mechanisms. Unit 2 has been

Table 1. Coring summary for Site 672.

Core no. 110-672A-	Date July 1986	Time	Sub-bottom top (m)	Sub-bottom bottom (m)	Meters cored (m)	Meters recovered (m)	Percentage recovery
1H	15	2110	0.0	3.3	3.3	3.35	101.0
2H	15	2250	3.3	12.8	9.5	10.04	105.7
3H	15	2355	12.8	22.3	9.5	9.69	102.0
4H	16	0155	22.3	31.8	9.5	9.80	103.0
5H	16	0250	31.8	41.3	9.5	9.60	101.0
6H	16	0645	41.3	50.8	9.5	9.81	103.0
7H	16	0825	50.8	60.3	9.5	9.68	102.0
8H	16	1030	60.3	69.8	9.5	9.81	103.0
9H	16	1145	69.8	79.3	9.5	9.65	101.0
10H	16	1300	79.3	88.8	9.5	9.85	103.0
11H	16	1746	88.8	98.3	9.5	9.73	102.0
12H	16	1905	98.3	107.8	9.5	9.81	103.0
13H	16	1958	107.8	117.3	9.5	6.77	71.2
14H	16	2157	117.3	123.3	6.0	5.19	86.5
15X	17	0010	123.3	132.8	9.5	6.71	70.6
16X	17	0410	132.8	142.3	9.5	1.81	19.0
17X	17	0605	142.3	151.8	9.5	8.22	86.5
18X	17	0805	151.8	161.3	9.5	5.55	58.4
19X	17	1003	161.3	170.8	9.5	8.00	84.2
20X	17	1203	170.8	180.3	9.5	4.87	51.2
21X	17	1422	180.3	189.8	9.5	6.28	66.1
22X	17	1613	189.8	199.3	9.5	8.51	89.6
23X	17	1955	199.3	208.8	9.5	9.57	101.0
24X	17	2155	208.8	218.3	9.5	9.40	98.9
25X	17	2358	218.3	227.8	9.5	5.30	55.8
26X	18	0210	227.8	237.3	9.5	5.72	60.2
27X	18	0405	237.3	246.8	9.5	8.98	94.5
28X	18	0605	246.8	256.3	9.5	9.12	96.0
29X	18	0812	256.3	265.8	9.5	9.59	101.0
30X	18	1025	265.8	275.3	9.5	9.47	99.7
31X	18	1215	275.3	284.8	9.5	5.39	56.7
32X	18	1525	284.8	294.3	9.5	7.34	77.2
33X	18	1800	294.3	303.8	9.5	8.66	91.1
34X	18	2010	303.8	313.3	9.5	8.16	85.9
35X	18	2220	313.3	322.8	9.5	9.33	98.2
36X	19	0015	322.8	332.3	9.5	9.51	100.0
37X	19	0231	332.3	341.8	9.5	8.83	92.9
38X	19	0525	341.8	351.3	9.5	9.38	98.7
39X	19	0816	351.3	360.8	9.5	5.01	52.7
40X	19	1100	360.8	370.3	9.5	9.58	101.0
41X	19	1310	370.3	379.8	9.5	3.21	33.8
42X	19	1505	379.8	389.3	9.5	6.72	70.7
43X	19	1715	389.3	398.8	9.5	8.84	93.0
44X	19	1950	398.9	408.3	9.5	5.58	58.7
45X	19	2210	408.3	417.8	9.5	1.38	14.5
46X	20	0145	417.8	427.3	9.5	2.34	24.6
47X	20	0410	427.3	436.8	9.5	0.54	5.7
48X	20	0640	436.8	446.3	9.5	6.04	63.6
49X	20	0900	446.3	455.8	9.5	6.70	70.5
50X	20	1200	455.8	465.3	9.5	5.39	56.7
51X	20	1410	465.3	474.8	9.5	4.32	45.5
52X	20	1750	474.8	484.3	9.5	0.72	7.6
53X	21	0500	484.3	493.8	9.5	8.27	87.0

subdivided into Subunits 2-A, 2-B, and 2-C on the basis of subtle lithologic differences, biostratigraphy, physical properties, and structural data. Subunit 2-B includes the interval that is equivalent to the décollement zone at Site 671.

Lithologic Unit 1 (0–123.3 mbsf)

This unit consists of lower Pleistocene to upper Miocene pale yellowish-brown to greenish-gray calcareous clay, calcareous mud and marl. Transitions between these sediment types are gradational. Carbonate content varies between 5.6% and 48.6% with most sediments containing 20-45% carbonate (Fig. 6). Most smear slides of sediments from Unit 1 show traces (up to 2%) of radiolarians and sponge spicules. Ash layers (vitric, vitric crystalline, and crystalline) are present throughout Unit 1 (2 to 5 discrete ash layers per core on the average; Fig. 7) and are commonly highly bioturbated (Fig. 8).

Lithologic Unit 2 (123.3–227.8 mbsf)

The transition to this unit is marked by a sharp decline in carbonate content of the sediments to near-zero values (Fig. 6).

Subunit 2-A (123.3–170.8 mbsf)

The unit is composed of green and olive gray mud/mudstone and clay/claystone of late Miocene and indeterminate age. Ash content is significantly reduced relative to Unit 1 sediments, especially at depths greater than 128 m (Fig. 7). Ash beds are commonly bioturbated, although the overall intensity of bioturbation in Unit 2 is less than that in Unit 1.

Subunit 2-B (170.8–208.8 mbsf)

The unit consists of claystones and siliceous claystones of early Miocene and indeterminate ages. Radiolarians and sponge

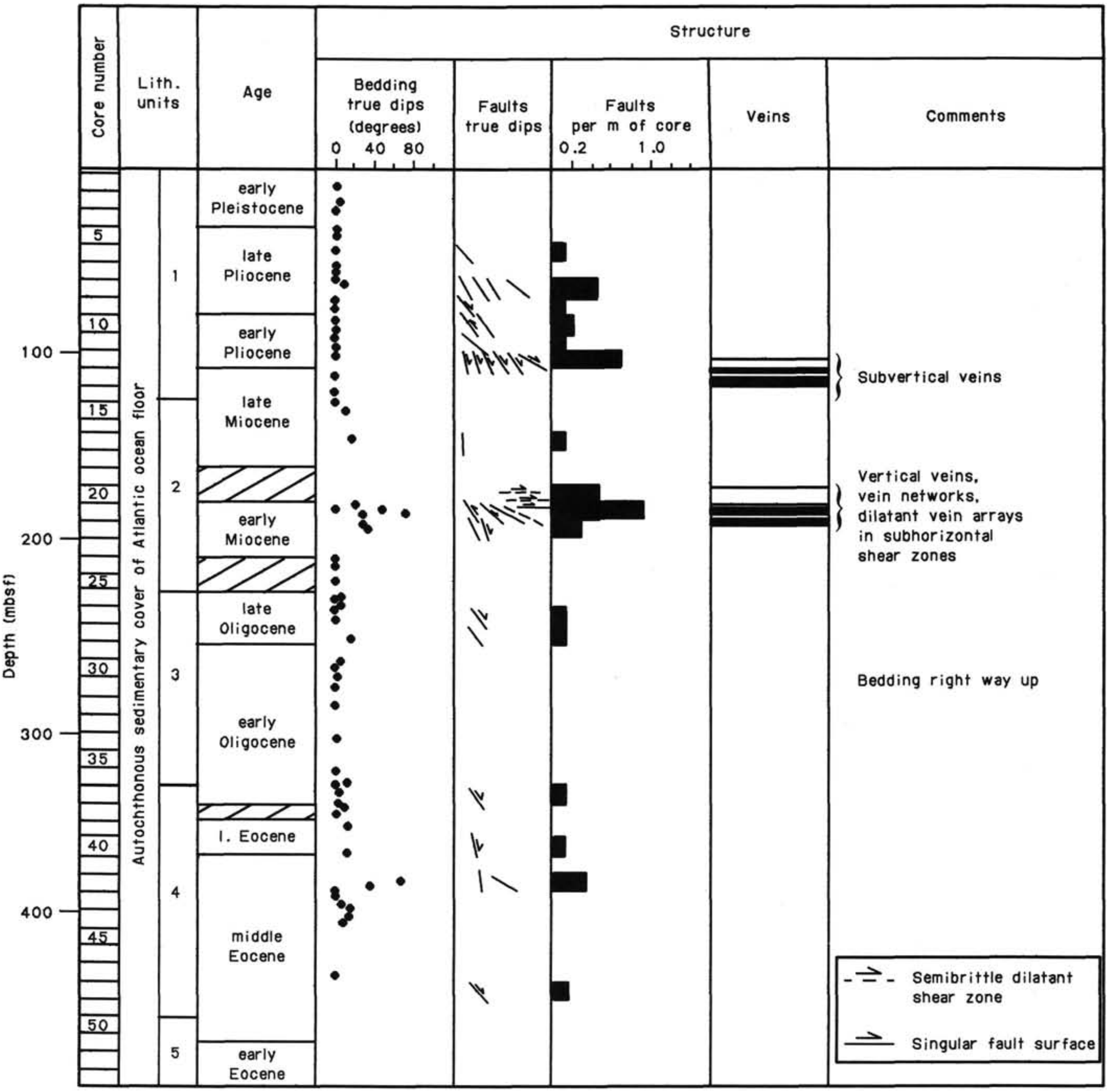

Figure 4. Log of structural data measured on cores of Hole 672A. Singular brittle fault surfaces are depicted as solid lines, the angle with the horizontal indicating the dip angle. The dip of shear zone boundaries of semibrittle dilatant shear zones is indicated by broken lines. Where faulting kinematics could be identified, the sense of movement is indicated by small arrows.

spicules comprise an average of 5–15% of these sediments. The frequency of ash beds and overall ash content of Subunit 2-B are greater than those of Subunit 2-A (Fig. 7). The intensity of bioturbation decreases with depth. Examples of *Zoophycos* and *Chondrites* are shown in Figures 9 and 10, respectively. Subunit 2-B is predominantly brown and orange-brown in color, distinctly different from the green and olive characteristic of Subunit 2-A. Zeolites (probably clinoptilolite) are dispersed throughout much of Core 110-672A-23X in the lower 10 m of Subunit 2-B. In addition to these lithologic differences, Subunit 2-B is characterized by relatively high porosities and the presence of structural features such as veins and faults. Subunit 2-B's lithologic characteristics and precise age (as determined from radiolarians) suggest that these sediments are equivalent to the décollement zone of Site 671.

Subunit 2-C (208.8–227.8 mbsf)

This unit consists of varicolored (brownish green, bluish green, and olive gray) claystones and mudstones of indeterminate age with horizontally laminated quartz silt-rich intervals increasing in number and thickness with depth (Fig. 11). Ash content is low (Fig. 7) and sediments are only mildly bioturbated.

Lithologic Unit 3 (227.8–332.3 mbsf)

The unit is characterized by interbedded marlstones and claystones, mudstones, and siltstones of variable carbonate content.

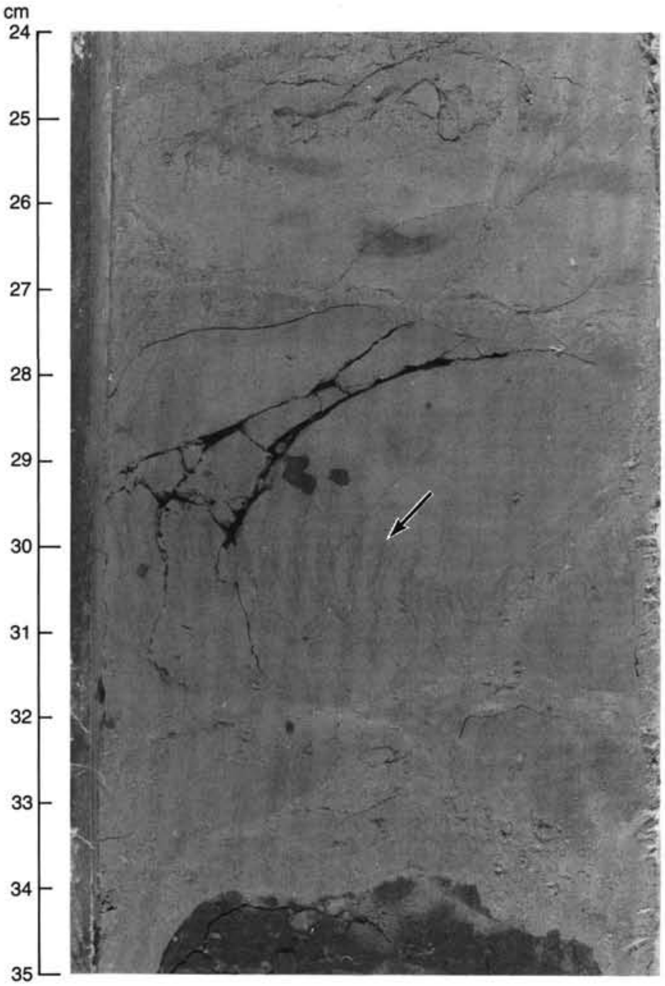

Figure 5. Core photograph shows an en-echelon array of sigmoidal dilatant veins (arrow) in Sample 110-672A-20X, CC (28–30 cm). The vein array is subhorizontal, and vein geometry may be interpreted in terms of top-to-left shearing.

The sediments of Unit 3 have been dated as early to late Oligocene. Unit 3 is distinguished by the presence of common calcareous intervals; Unit 2 is generally noncalcareous (Fig. 6). The claystones are noncalcareous to slightly calcareous, generally green or olive gray, and are commonly mildly bioturbated. The mudstones are brown to dark gray and their carbonate content varies from near-zero to 30% (transition to marlstone). The mudstones are locally parallel laminated and are generally free of bioturbation. The siltstones are dark gray to black and commonly are parallel or cross laminated. They are noncalcareous to slightly calcareous and are commonly transitional to silty mudstones. Silt also occurs as very thin laminae within mudstone intervals, and locally exhibits micro-cross laminations and small-scale convolute features (Fig. 12). The silt-sized grains are dominantly quartz, with traces of glauconite and very rare mafic minerals (glaucophane and mica) and microcline. The marlstones of Unit 3 are pale greenish gray and contain up to 80% carbonate. Some of these carbonate-rich intervals show *Planolites, Teichichnus*, and *Chondrites* burrows. These burrows are commonly more abundant near the top of each carbonate-rich layer, and are generally filled with overlying noncalcareous green claystone.

Both sharp and gradational contacts occur between the different lithologies of Unit 3. Cores 110-672A-26X through -29X (227.8–265.8 mbsf) have few intervals of marlstone and the transitions between claystone, mudstone and siltstone are commonly gradational. In contrast, the lower portion of Unit 3 (Cores 110-672A-30X through -36X, 265.8–332.3 mbsf) is characterized by common marlstones composed of nannofossils and clay. These beds typically exhibit sharp lower contacts, laminated basal intervals, and bioturbated tops (Fig. 13). These carbonate-rich layers either grade upward into, or are overlain with sharp contacts by, less calcareous lithologies.

Lithologic Unit 4 (332.3–455.8 mbsf)

This unit is also characterized by cyclic sedimentation. Ages range from middle to late Eocene/early Oligocene; Cores 110-672A-37X and -38X are barren of microfossils. The sediments of Unit 4 are lithologically very similar to those of Unit 3 and are differentiated primarily by the presence of intercalated, pale green to gray, quartz sandstones in the lower unit. The sandstone horizons are calcareous and slightly glauconitic (Fig. 14) and range in thickness from 1 cm to 60 cm. The quartz grains average 0.5 mm in diameter and are subangular to subrounded. These beds commonly contain a mixture of very fine-grained silt and sand-sized quartz (Fig. 15). The calcareous mudstones locally contain foraminifer fragments, glauconite, and rare detrital grains of microcline (Fig. 16); fragments of benthic foraminifers also occur locally.

The sandstones of Unit 4 are interlayered with dark green, noncalcareous claystones and olive, brown, and dark gray mudstones and siltstones with variable carbonate contents. Claystone layers vary in thickness from 15 cm to 6 m. Mudstones, muddy siltstones and siltstones generally range from 5 to 60 cm in thickness. These beds are generally similar in composition to the calcareous quartz sandstones except for higher clay contents. Pale green marlstones similar to those of Unit 3 (Fig. 13) range from 10 cm to 1.5 m in thickness. These beds are commonly silty or sandy. Many of the marlstone layers are highly indurated and can therefore be classified as limestones.

Cross-lamination and convolute bedding are common in the calcareous sandstones, siltstones, and mudstones (Figs. 17, 18, and 19). Slumps commonly occur at the base of marlstone layers (Fig. 20). The calcareous quartz sandstones and the marlstones both typically exhibit sharp basal contacts and laminated silty lower portions. The beds commonly grade upward to less silty, bioturbated intervals that are in turn overlain by dark green, noncalcareous claystone (Figs. 21 and 22).

Analysis of five thin sections made of limestones from Unit 4 (Cores 110-672A-41X, -43X, and -49X) revealed two different lithologies. The more common of the two lithologies consists of wackestones to packstones that contain well-preserved foraminifers, sand-sized quartz, and rare echinoid fragments dispersed in a micritic and clayey matrix (Fig. 23). Foraminifer tests are generally filled with the matrix material (Fig. 24) although rarely they are filled with glauconite. The second variety of limestone is relatively rare and consists of silty to sandy, laminated, fine-grained limestone that is locally ferruginous (Fig. 25). Foraminifers and radiolarians are fragmented and recrystallized (Fig. 26) and traces of glauconite, microcline, and glaucophane were observed in these limestones.

Lithologic Unit 5 (455.8–493.8 mbsf)

This unit consists of slightly siliceous to siliceous claystones/mudstones of early to middle Eocene age. Carbonate content is essentially zero. Unit 5 exhibits common color changes from dark green to brown to reddish brown. Radiolarian contents vary from 5 to 30% and traces of quartz silt are dispersed throughout the unit. Unit 5 sediments are free of bioturbation.

Sediment thickness versus age is shown in Figure 27. Unit 1 sediments exhibit moderate sedimentation rates whereas Unit 2 exhibits low to very low rates. Unit 3 is characterized by moder-

Table 2. Lithologic subdivisions at Site 672.

Unit	Lithology	Core range (Hole 672A)	Depth (mbsf)	Age
1	Calcareous clay and mud; common ash layers; traces of biogenic silica; $CaCO_3$: 5 to 65%	1H to 14X	0–123.3	Early Pleistocene to late Miocene (upper part)
2-A	Mudstone and claystone; few ash layers; $CaCO_3$: 0–15%	15X to 19X	123.3–170.8	Late Miocene (lower part) and indeterminant
2-B	Claystone and siliceous claystone; common ash layers; $CaCO_3$: 0%	20X to 23X	170.8–208.8	Indeterminant and early Miocene
2-C	Claystone and mudstone with laminated silt intervals; $CaCO_3$: 0%	24X to 25X	208.8–227.8	Indeterminant
3	Interbedded claystone, calcareous mudstone, and marl; frequent thin quartz silt laminae; $CaCO_3$: 0 to 65%	26X to 36X	227.8–332.3	Late Oligocene (lower part) to early Oligocene
4	Interbedded claystone, laminated calcareous mudstone, micritic limestone and calcarenite; glauconitic sand layers; $CaCO_3$: 0 to 90%	37X to 49X	332.3–455.8	Early Oligocene/late Eocene to middle Eocene
5	Siliceous (radiolarian) claystone; shaly in lower part; $CaCO_3$: <10%	50X to 53X	455.8–493.8	Middle Eocene (lowermost) to early Eocene

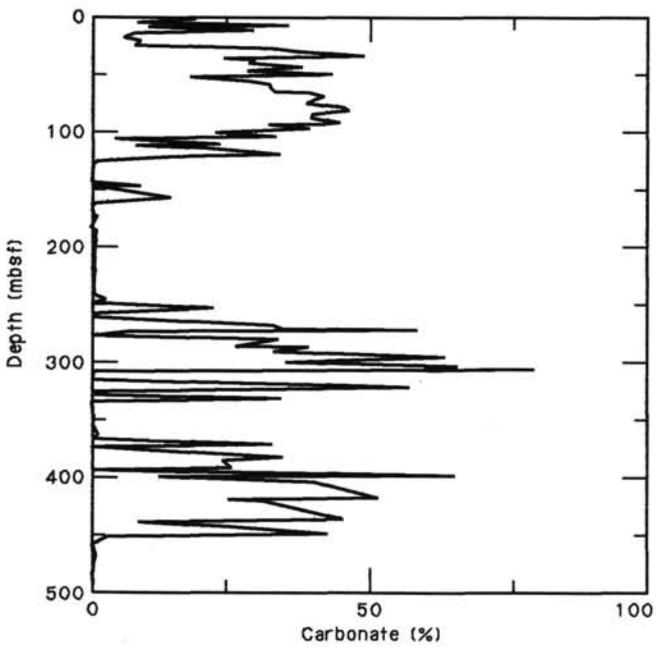

Figure 6. Profile of percentage carbonate in Site 672 sediments.

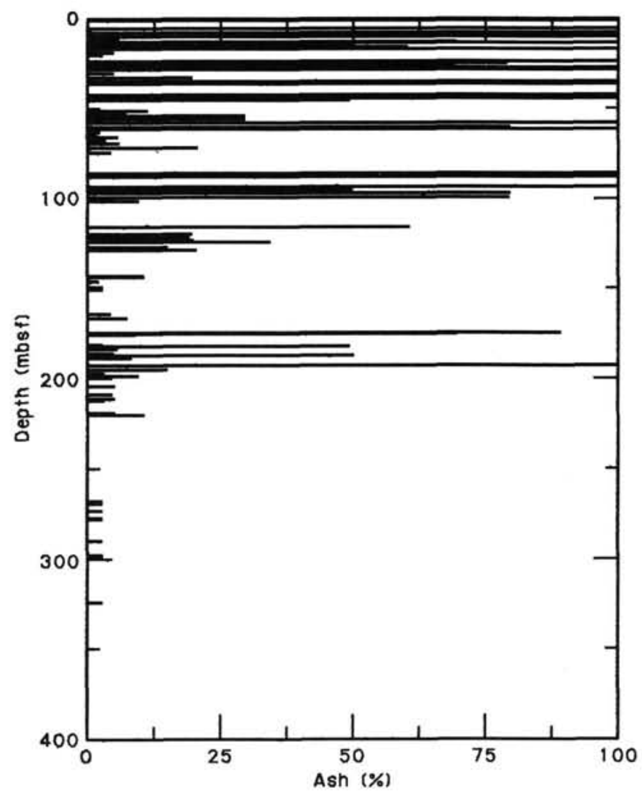

Figure 7. Concentration of ash versus depth for Hole 672A.

ate sedimentation rates whereas Unit 4 is marked by high values. Unit 5 rates are low.

Volcanic Ash Occurrence

As at Site 671, a semiquantitative estimate of the volume of ash deposited in the sedimentary sequence recovered at Site 672 was determined by plotting the intervals over which ash horizons occur and by estimating the concentration in those intervals. The graphic ash log (Fig. 7) results from analysis of core descriptions, core photos, and smear-slide descriptions. In contrast to Site 671, the estimate of ash concentration is probably more accurate here because it was determined in each ash interval by careful core examination and by calibration with smear-slide analysis. The rationale for this painstaking analysis is to identify ash beds that have been diluted and dispersed because

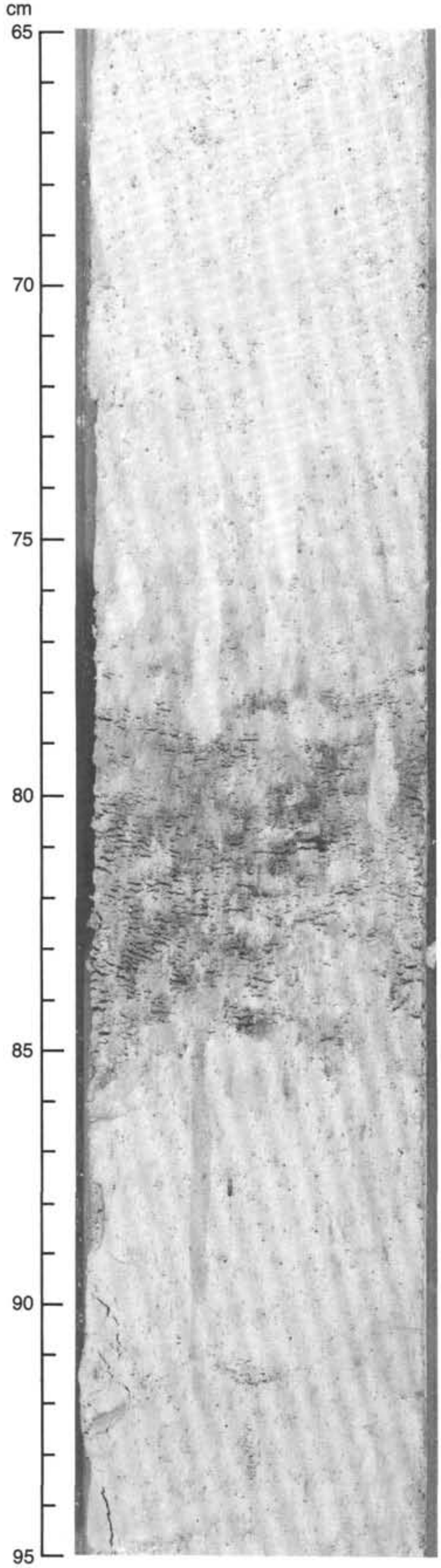

Figure 8. Bioturbated ash bed in Unit 1; photograph of Sample 110-672A-10H-1, 65–95 cm.

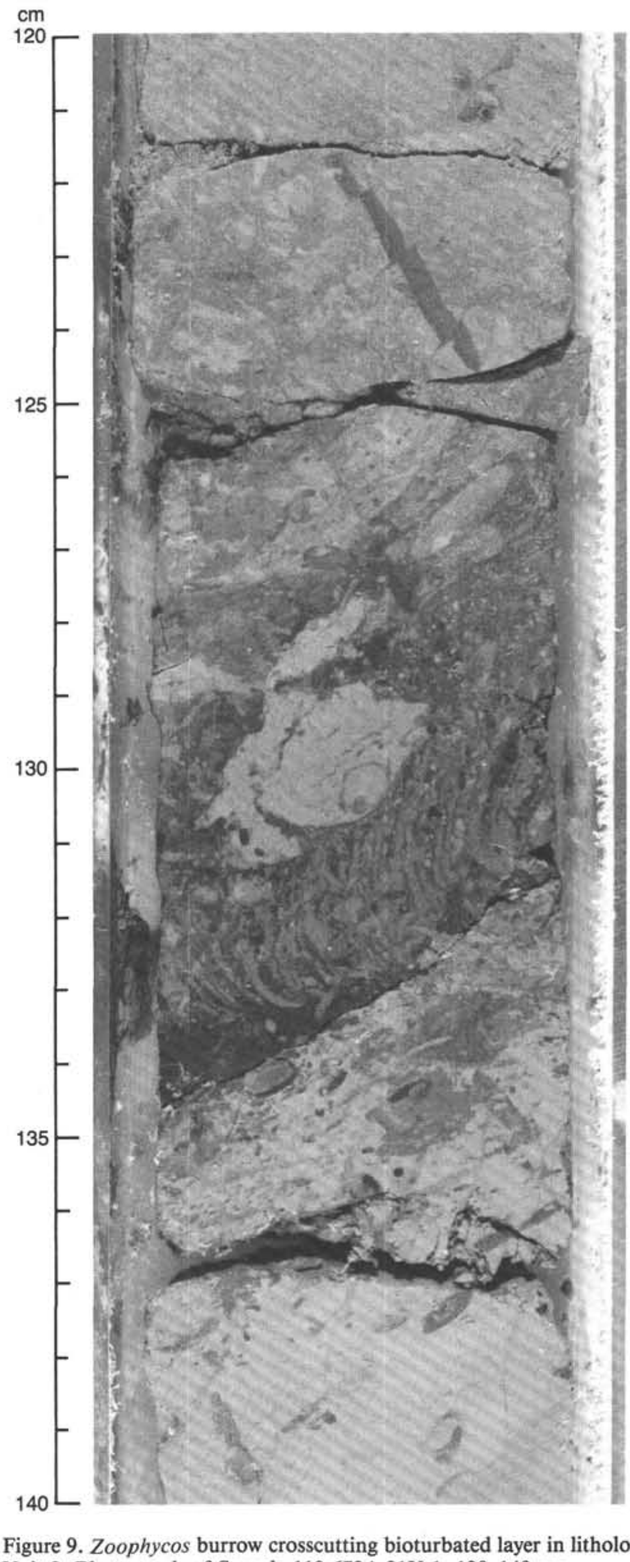

Figure 9. *Zoophycos* burrow crosscutting bioturbated layer in lithologic Unit 2. Photograph of Sample 110-672A-21X-1, 120–140 cm.

of strong bioturbation. At deeper levels, ash concentration information is lost as diagenesis and alteration of unstable constituents (e.g., glass) proceeds.

Ash material consists primarily of plagioclase laths and glass shards (both fresh and devitrified). In thick beds crystals are concentrated near the base and glass near the top, suggesting they accumulated by air-fall. Lack of internal structure of the

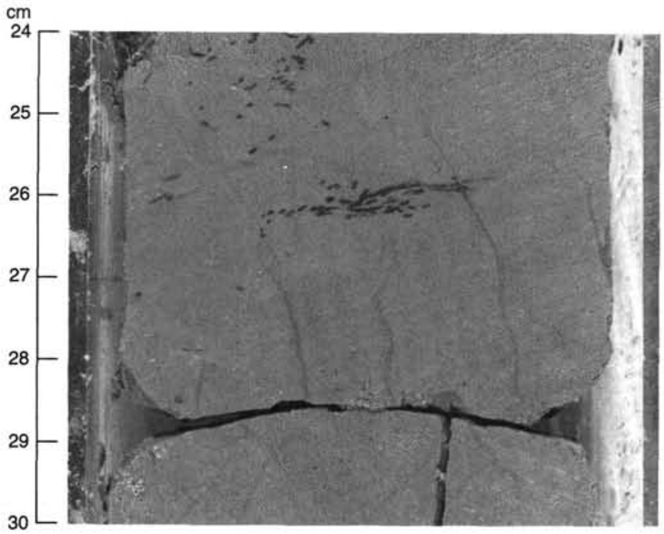

Figure 10. *Chondrites* burrows in claystone of lithologic Unit 2. Photograph of Sample 110-672A-21X-2, 24–30 cm.

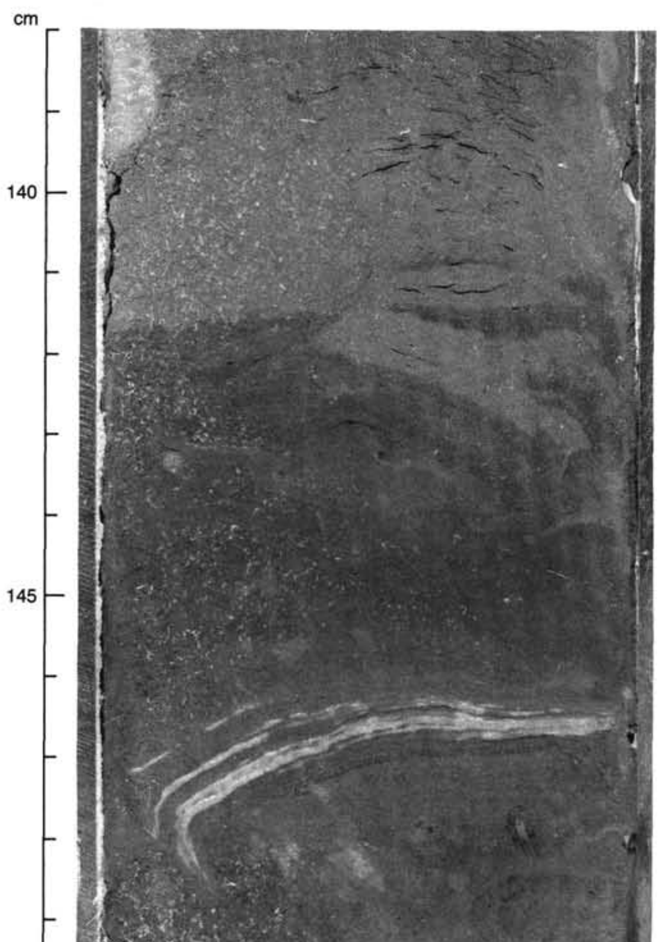

Figure 11. Laminated silt layer from base of lithologic Unit 2. Photograph of Sample 110-672A-25X-1, 138–150 cm.

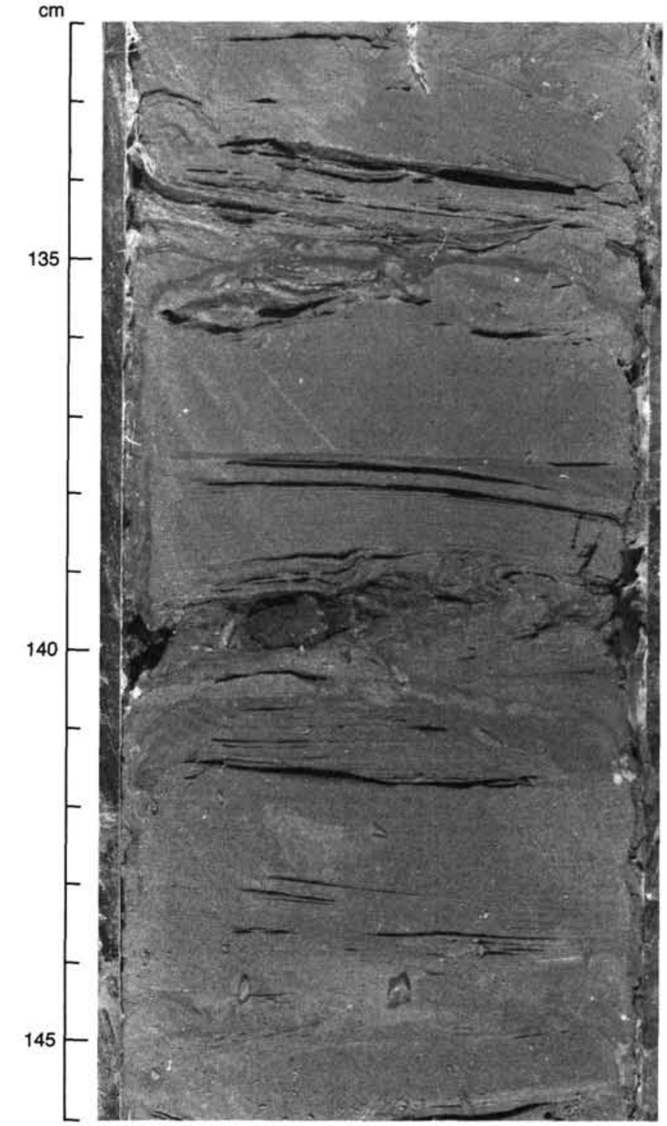

Figure 12. Horizontal and convolute laminations in calcareous mudstone typical of lithologic Unit 4. Photograph of Sample 110-672A-30X-3, 132–146 cm.

ash layers, and homogeneity of particle size, favor the hypothesis of segregation by air-fall rather than by turbidity currents. Although some pure crystalline and vitric ashes do occur, most beds are a mixture of both components.

Comparison of these results with those from Site 671 shows that the ash distribution is generally similar in both holes. Abundant ash was deposited in the Pliocene and Pleistocene, the amount decreases in the Miocene, and ash is nearly absent below the Miocene/Oligocene boundary. The details of this comparison match imperfectly, but this variation can be explained by variable diagenesis and by the current lack of resolution of biostratigraphic boundaries.

Analysis of Sediment Coarse Fractions

Analysis of the coarse fraction (>63 μm) of sediments from Site 672 provides valuable information for sediment provenance interpretation. Grains obtained by sieving sediment through a 63-μm sieve, as well as coarse grains in smear slides, were examined.

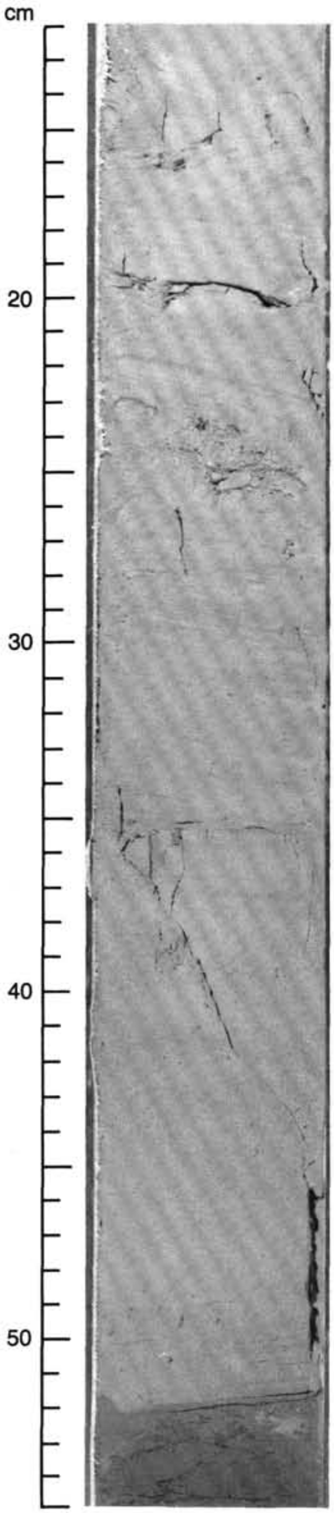

Figure 13. Lower laminated portion of 70-cm-thick, pale green marlstone bed in lithologic Unit 3. Photograph of Sample 110-672A-34X-5, 12–55 cm.

There are three distinct groups of coarse-fraction grains in the Site 672 sediments. The first group is composed of ash components and is characteristic of Cores 110-672A-1H through -22X (lower Pleistocene through lower Miocene). Common minerals are feldspar (mostly plagioclase), hornblende (brown-green or rarely brown-red), orthopyroxene, clinopyroxene, quartz, opaque minerals, and glass (including volcanic rock fragments). The feldspar and quartz grains are usually angular, but some rounded quartz, probably of continental origin, is present. The rounded quartz grains have wavy extinction indicating derivation from metamorphic or granitic rocks.

The second coarse-fraction association, found in Cores 110-672A-22X through -49X, is dominated by continentally-derived quartz. Trace amounts of glaucophane are found in the coarse fractions of sediments from Cores 110-672A-26X through -38X, and minor amounts of microcline are commonly associated with the quartz throughout this interval. Rarely, trace amounts of clinopyroxene also occur in this coarse fraction association. Radiolarians are common in Core 110-672A-21X and rare fish teeth were found in Core 110-672A-24X.

The third coarse-fraction association, found in Cores 110-672A-50X to -53X, consists of radiolarians and fish teeth.

The following conclusions can be drawn from analysis of these coarse -fraction associations:

1. Volcanic ash was supplied to the Site 672 region from at least the early Miocene to the present, probably from the Lesser Antilles Arc. In comparison with Site 671, ash is less abundant and generally more fine-grained at Site 672. Most ash material appears to be associated with calc-alkaline volcanism. The presence of rounded, metamorphic/granitic quartz grains in the lower Miocene-Pleistocene sediments probably reflects periodic terrigenous influx from South America.
2. The quartz-glaucophane-microcline coarse-fraction assemblage reflects a continental sediment source during the lower Miocene to lower to middle Eocene. The lack of ash components indicates either significant distance from the volcanic arc during this time period, or lack of arc activity, or both.
3. The coarse fractions from lower Eocene sediments reflect pelagic sedimentation with no arc-derived or continent-derived coarse grains.

Depositional Environments and Processes

The combination of clay and biogenic siliceous materials in Unit 5 sediments indicates that sedimentation during the early Eocene and early middle Eocene was hemipelagic and below the carbonate compensation depth (CCD). During the middle Eocene, and continuing through the late Eocene/early Oligocene (Unit 4 sediments), there was a significant influx of coarser (silt- and sand-sized) terrigenous detritus. These sediments presumably were originally delivered to the region as turbidites originating from the South American continent. Their presence on the slope top of the Tiburon rise is problematic. They may represent either: (a) very distal turbidites that flowed upslope to their present depositional site, or (b) redeposition by bottom currents. Biogenic siliceous sediment occurs only sporadically, and sponge spicules observed in mudstones and sandstones of Unit 4 are blackened and appear to be reworked. The pale green marlstones of Unit 4 commonly have sharp basal contacts, prominent laminations, cross-bedding, and slump structures. The common restriction of bioturbation to the upper portions of these beds suggests rapid deposition, probably by turbidity currents. The presence of slumps composed of pale green nannofossil marlstone within the marlstone beds coupled with the occurrence of these beds on the slope of the Tiburon Rise suggests a source area higher on the Rise. The presence of minor silt-sized quartz (as well as rare glaucophane and microcline) in the calcareous deposits of Unit 4 is somewhat problematic in that it requires deposition of terrigenous silt on the Tiburon Rise before redeposition in the marlstone beds.

From the late Eocene/early Oligocene through the late Oligocene (Unit 3 sediments) delivery of silt and clay-sized terrigenous debris to the Site 672 region continued, but sand deposi-

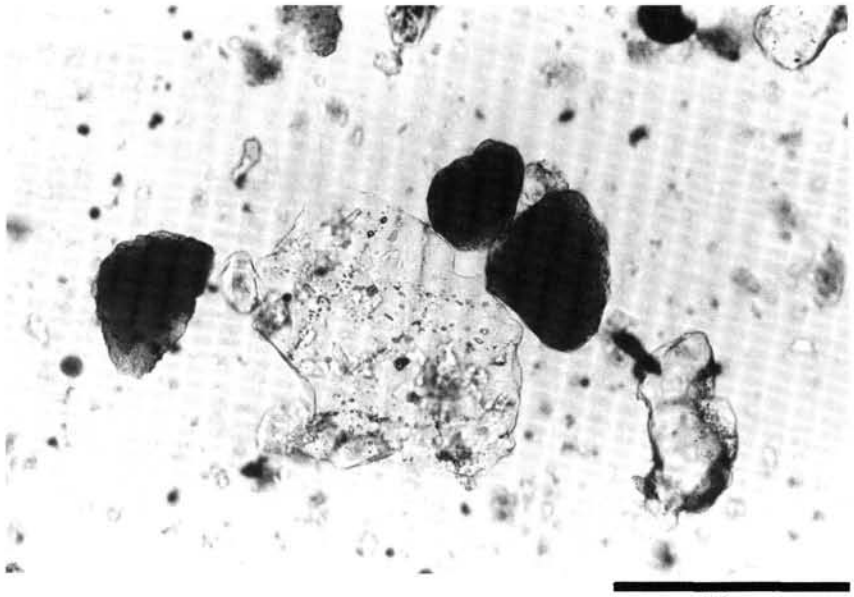

Figure 14. Glauconitic quartz sand (smear slide), Sample 110-672A-40X-1, 29–31 cm; lithologic Unit 4.

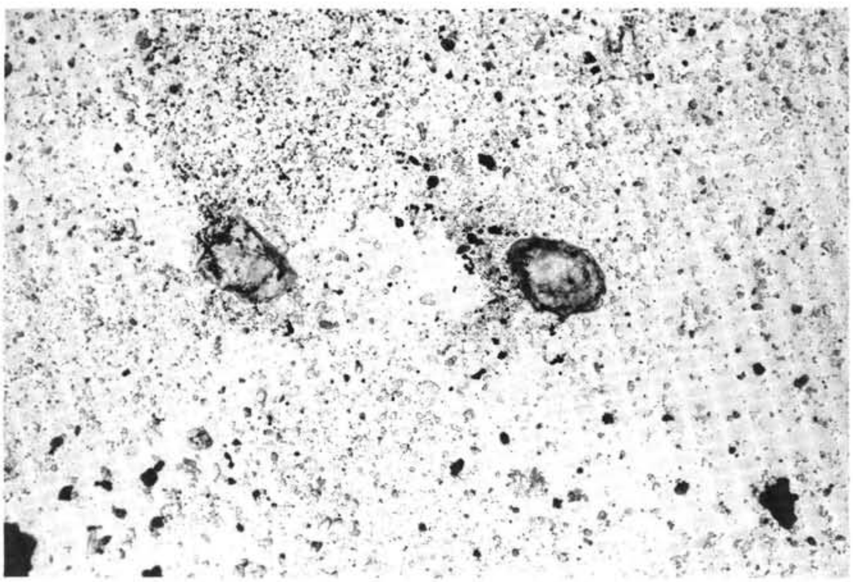

Figure 15. Silty sand from lithologic Unit 4; note contrast in grain size between sand and silt fractions (smear slide). Sample 110-672-37X-5, 71–73 cm.

tion ceased. Deposition of biogenic silica continued sporadically. The marlstones of Unit 3 may represent a combination of true pelagic accumulation and turbidity current deposition; differentiation between the two origins is difficult and requires further investigation. Interpretation of the position of Site 672 with respect to the CCD during deposition of Unit 3 sediments depends on the origin of the calcareous intervals. If some marlstone layers contain carbonate accumulations of pelagic origin, the site can be assumed to have been above the CCD, or perhaps between the compensation depths for foraminifers and nannofossils. If, however, all carbonate is considered to have been delivered to the site from a topographically higher lateral source (Tiburon Rise), it can be concluded that the site remained below the CCD during deposition of Unit 3 sediments. The presence of noncalcareous clay and mudstone interlayered with the carbonate-rich horizons provides support for the second hypothesis.

The upper Oligocene to upper Miocene sediments of Unit 2 record a return to hemipelagic deposition. Terrigenous input is limited principally to clay-sized material. The biogenic silica content of Unit 2 sediments is generally low, but is somewhat variable. Sediments of Subunit 2-B are notably siliceous. Carbonate is either absent or present in very low concentrations in Unit 2, indicating that Site 672 was below, or very near, the CCD during deposition of Unit 2 sediments. Bioturbation increased during the Miocene. The appearance of ash layers in

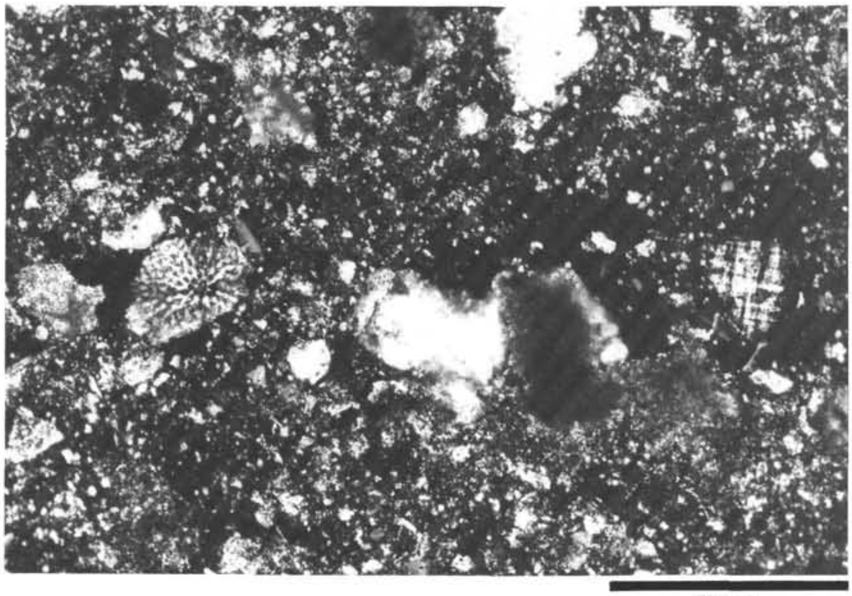

Figure 16. Foraminifer fragment and quartz, glauconite, and microcline grains in calcareous mudstone of lithologic Unit 4 (smear slide), Sample 110-672A-42X-1, 20–22 cm.

Miocene sediments indicates increasing proximity of the site to the Lesser Antilles Arc, or an upsurge in Neogene arc activity, or both.

Deposition of the upper Miocene to lower Pleistocene sediments of Unit 1 was dominated by accumulation of terrigenous clay, pelagic carbonate, and ash layers. The predominance of both foraminifers and nannofossils indicate sedimentation above the CCD. The biogenic silica content of Unit 1 sediments is relatively low. Bioturbation is very well developed.

Bulk Mineralogy

The bulk mineralogy of sediments from Site 672 is presented in terms of cumulative percentage of the four phases: total clay minerals, quartz, plagioclase, and calcite (Fig. 28). Methods of sample preparation, X-ray diffraction analysis, and semiquantitative analysis are given in the Explanatory Notes chapter. Several major trends in the percentages of the four primary components are evident. In general, these trends can be related to the changing influence of hemipelagic sedimentation vs. lateral influxes of terrigenous and calcareous sediment, overprinted by deposition of volcanic ash from the Lesser Antilles Arc.

The percentage of total clay minerals in the upper 100 m of section varies widely between about 20%–60% with an average of about 40%. From 100 to 190 mbsf, the percentage of total clay increases, with wide fluctuations, to values between 80% and 90%. This high clay content is characteristic of the sediments from about 190 to 250 mbsf. The sediments in the upper 250 m of section reflect hemipelagic sedimentation and correspond to lithologic Units 1, 2, and the uppermost part of Unit 3. The wide fluctuations of percentage total clay in Unit 1, and the overall increase from Unit 1 to Unit 2, are related to changes in carbonate content (discussed below). Below 250 mbsf, the cyclic sediment sequences of the lower Oligocene and middle to upper Eocene (Units 3 and 4) have variable clay contents reflecting the alternations of lithologies (noncalcareous clay/mudstones, marlstones and calcareous siltstones, and sandstones). The lower part of the middle Eocene section marks a return to dominantly hemipelagic sedimentation (Unit 5, 456 to 494 mbsf). The siliceous clay/mudstones of this unit have total clay contents ranging from 82% to 94%.

There are sharp fluctuations in percentage calcite throughout Unit 1 sediments with average values increasing slightly with depth from roughly 25 to 30%, to about 40% at a depth of 80 mbsf. Below 80 mbsf, calcite content decreases until the section becomes calcite-free at the base of Unit 1 (123 mbsf). With the exception of two samples containing 11% to 16% calcite at about 157 mbsf, Unit 2 sediments are calcite-free. Calcite first reappears at a depth of 252 mbsf in Unit 3. The trend in percentage calcite in Unit 1 and 2 sediments may reflect a shallowing of the CCD through the late Oligocene. The calcite content of Unit 3 and 4 sediments is highly variable and largely reflects periodic lateral influxes of carbonate sediment, probably derived from the Tiburon Rise, during the early Oligocene and middle to late Eocene. The carbonate-rich horizons of Units 3 and 4 are interbedded with noncalcareous claystone and mudstone layers, which probably represent background sedimentation. The upper portion of Unit 4 (335–370 mbsf) is calcite-free. The sediments of Unit 5 are calcite-free and record deposits below the CCD.

The plagioclase content of Site 672 sediments reflects the occurrence of ash layers and dispersed ash. In Units 1 and 2 sediments, plagioclase varies from 0% to 64%, reflecting the abundant ash layers in these units (Fig. 7). The sediments of Units 3, 4, and 5 have no discrete ash layers and their plagioclase contents are between 0% and 9%.

In Units 1 and 2 sediments, quartz varies between 2% and 23% with one sample containing 48% (128 mbsf). Most samples contain about 10% quartz, a value similar to that of the hemipelagic sediments in the upper 500 m at Site 671. Units 3 and 4 sediments show widely varying quartz contents reflecting the influence of terrigenous silts and sands derived from South America. The quartz content of Unit 5 sediments is about 10%, similar to that of Units 1 and 2 sediments.

Sediments of Subunit 2B were noted in the lithologic descriptions as having characteristics like those of the décollement zone at Site 671. In terms of bulk mineralogy, Cores 110-672A-22X and -23X within this subunit are most similar to those of the décollement observed in other Leg 110 sites. These sediments are clay-rich, containing 80% to 95% total clay minerals. They are calcite-free, and contain 2% to 10% quartz and 0% to 5% plagioclase.

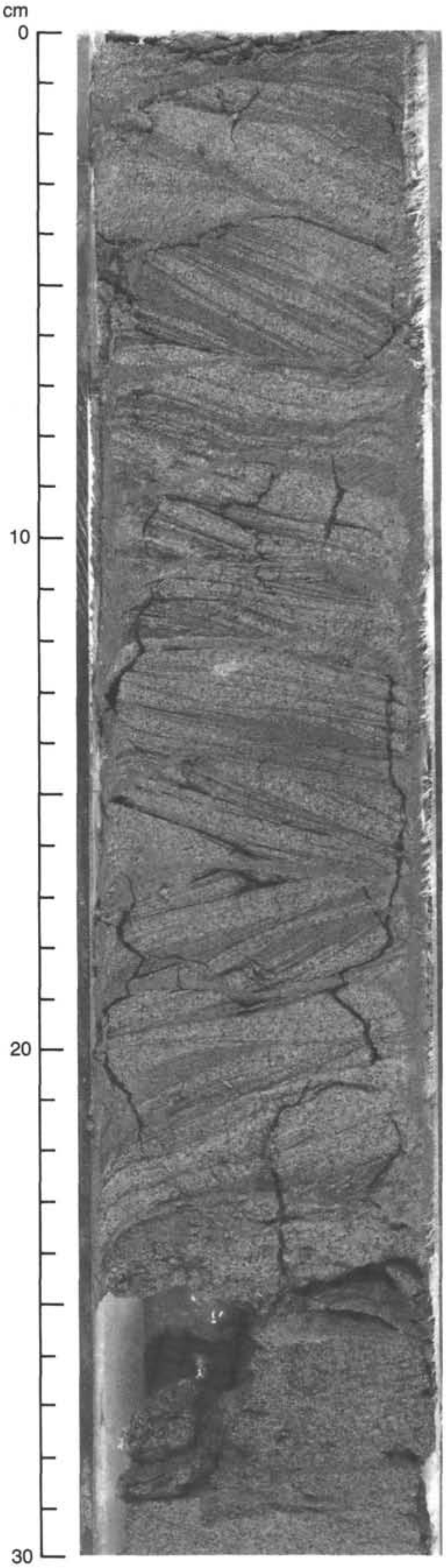

Figure 17. Cross-lamination in calcareous sandy siltstone. Photograph of Sample 110-672A-48X-2, 0–30 cm.

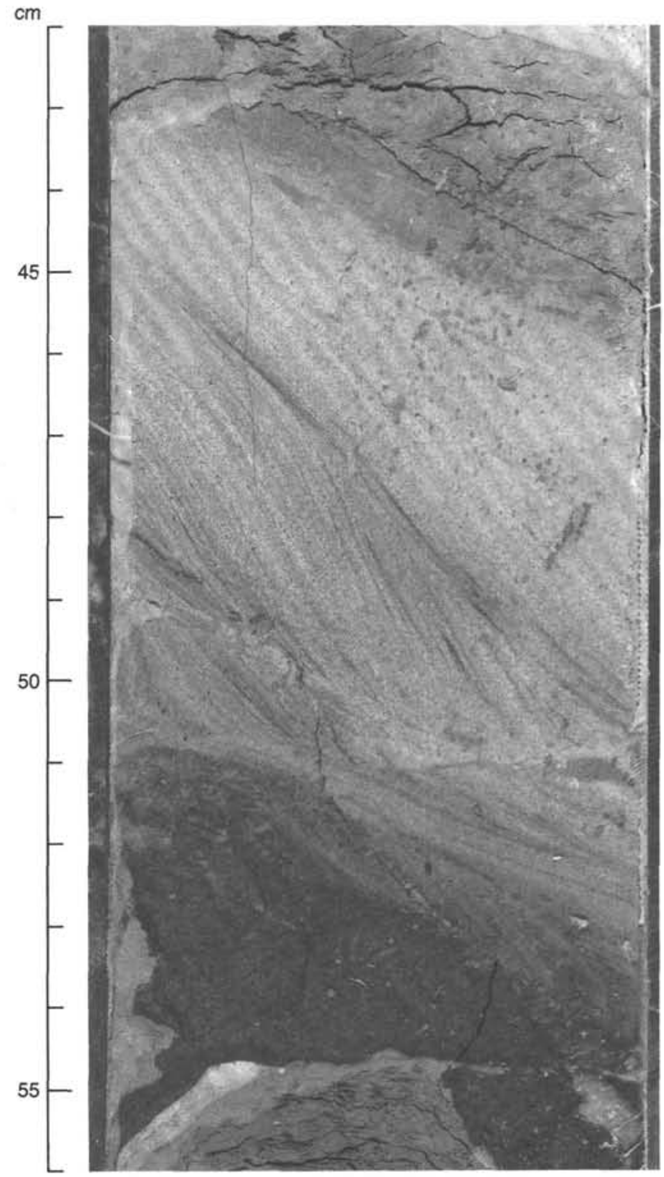

Figure 18. Relatively large-scale, nonplanar cross-stratification in calcareous mudstone of lithologic Unit 4. Photograph of Sample 110-672A-40X-5, 42–56 cm.

The bulk mineralogy of most of the sediments sampled at Site 672 is adequately described in terms of the four phases: total clay, calcite, quartz, and plagioclase. Many of the samples of early to middle Eocene age, however, contain significant concentrations of opal-CT that are not accounted for in the semiquantitative analysis. Opal-CT is a form of silica ($SiO_2 \cdot 2H_2O$) that is an intimate admixture of cristobalite and tridymite. It is a common product of the diagenesis of the opaline silica (opal-A) in radiolarian and diatom tests. Opal-CT first appears with depth in some of the carbonate-rich horizons of the middle Eocene between 409 and 441 mbsf. It is present in all samples analyzed below 448 mbsf and is a major component of the lower and middle Eocene sediments of Unit 5.

BIOSTRATIGRAPHY

Summary

Site 672 was drilled in the previously presumed undeformed sediments of the Atlantic abyssal plain as a biostratigraphic ref-

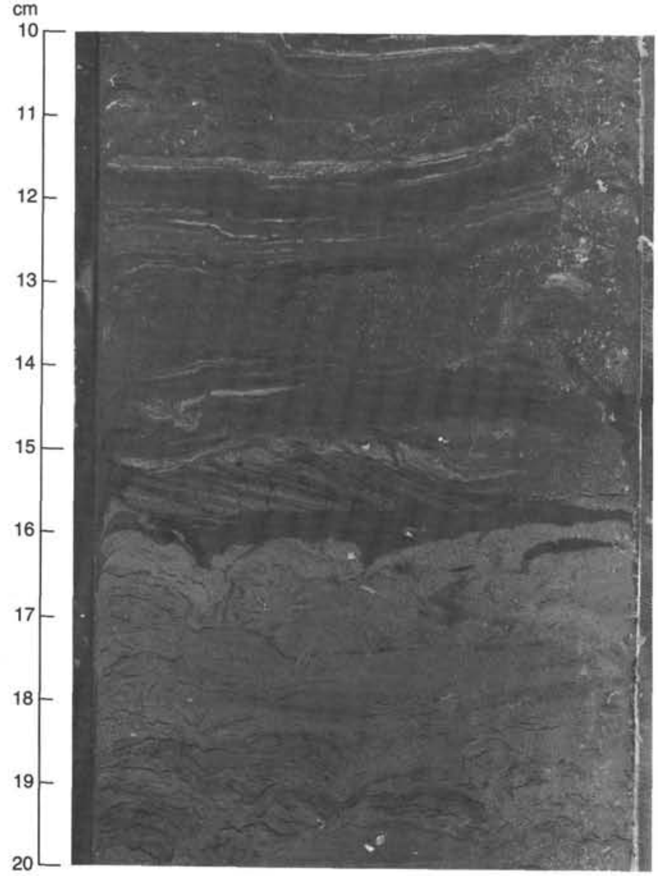

Figure 19. Oblique stratification (ripple drift ?) in intercalated sand and silt layers, lithologic Unit 4. Photograph of Sample 110-672A-38X-7, 10–20 cm.

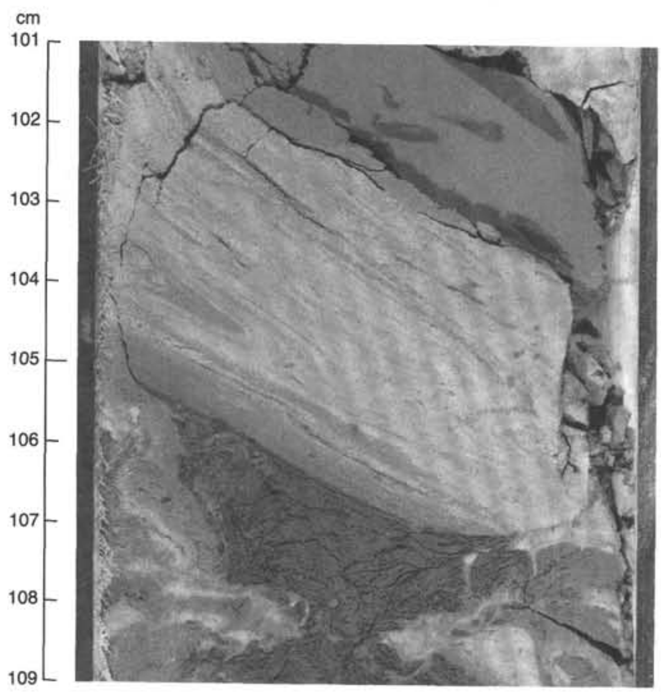

Figure 20. Slump folding in pale green silty marlstone. Photograph of Sample 110-672A-40X-2, 101–109 cm.

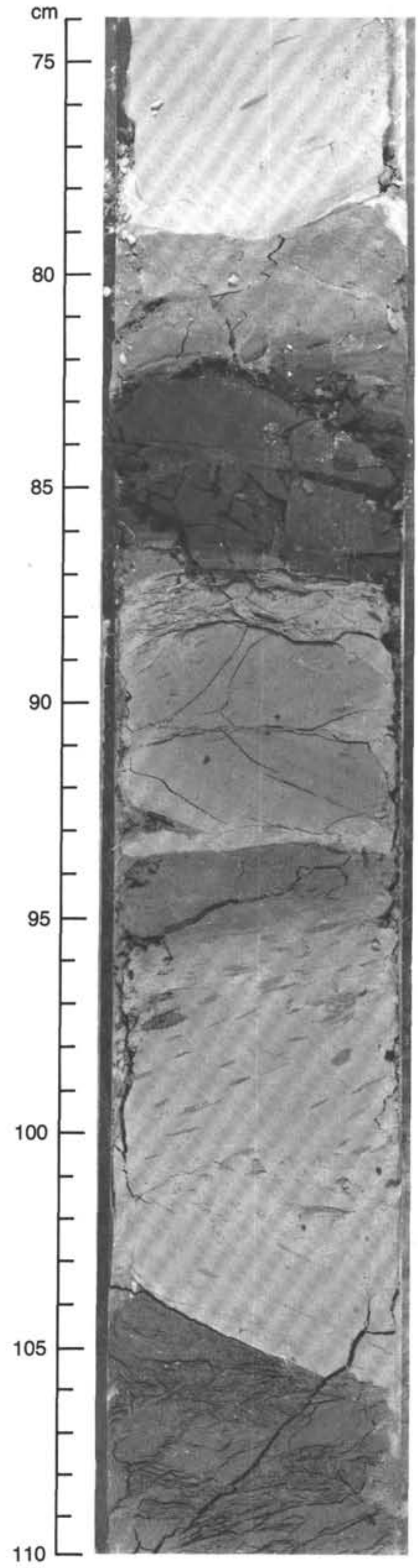

Figure 21. Cyclic sequences in lithologic Unit 4; noncalcareous claystones (dark) and marlstones (light). Note sharp base of marlstone layer at 104 cm and gradational, bioturbated upper contact of same bed into dark green claystone at 96 cm. Photograph of Sample 110-672A-48X-4, 74–110 cm.

Figure 22. Idealized stratigraphic section showing major sediment types in cyclically bedded lithologic Unit 4.

erence for structurally deformed sections in the Barbados accretionary wedge. The biostratigraphy at Site 672 (Fig. 29) is based on a combination of data from calcareous nannofossils, foraminifers, and radiolarians. These fossil groups define an early Pleistocene through early Eocene age for the reference section. The biostratigraphic record is not complete at Site 672, largely owing to the effect of Miocene dissolution.

A significant biostratigraphic gap is indicated between Sections 110-672A-4H-CC and -5H-CC by missing zones in both calcareous fossil groups. This gap in the sedimentary record contains the Pleistocene/Pliocene boundary and may span 1.4 to 2.4 Ma.

The Miocene section in Hole 672A is highly dissolved, and remains for the most part, biostratigraphically unresolved by calcareous microfossil groups. Upward migrations of the CCD during Miocene time are probably responsible for the carbonate-poor intervals observed in sediments of this portion of the Atlantic abyssal plain. Radiolarian species are abundant and well preserved in the lower Miocene section and provide excellent biostratigraphic control between Samples 110-672A-21X-1, 27–29 cm and -23X-4, 97–99 cm. Based on radiolarian ages, the décollement zone in Hole 671C is correlative with the lower Miocene silica-rich sediments in Hole 672A.

Oligocene sediments between Samples 110-672A-26X-1, 48–49 cm and -36X-CC include clastic and bioclastic sequences which originated from either the upper slope of the Tiburon Rise or the South American continent. Eocene taxa of all three fossil groups are reworked into the Oligocene section. Reworking is particularly apparent in Sections 110-672A-31X-CC through -35X-CC. Preservation of carbonate assemblages in pelagic Oligocene deposits is moderate to good.

Recovery of Eocene sediments in Hole 672A was poor, owing to variations in lithification and consequent difficulty in coring. Calcareous fossils are locally recrystallized in the middle and upper Eocene but retain a moderate level of preservation down through Section 110-672A-48X-CC. Below this point, silica-rich clays underlie the calcareous sediments. The basal portion of the sequence contains radiolarian assemblages which range from middle to early Eocene in age.

Calcareous Nannofossils

Nannofossiliferous sediments in Hole 672A range from early Pleistocene to middle Eocene in age. The biostratigraphic succession in Hole 672A is frequently interrupted by intervals of strong dissolution which are particularly apparent in the Miocene. Preservation is generally good in the Pliocene and Pleistocene but deteriorates in older sediments. The Paleogene section is affected by dissolution and recrystallization and is of moderate preservation.

Samples 110-672A-1H-1, 71–73 cm to -4H-CC are early Pleistocene in age. These samples are placed within the *Pseudoemiliania lacunosa* small gephyrocapsa Zone of Gartner (1977) because of the presence of *Pseudoemiliania lacunosa* without *Helicosphaera sellii*. Upper Pleistocene sediments were not observed at this site.

Between Samples 110-672A-4H-CC and -5H-1, 80–81 cm a significant amount of missing sediment section is indicated. The base of Core 110-672A-4H is above the *H. sellii* datum of early Pleistocene age and Sample 110-672A-5H-1, 80–82 cm is within the *Calcidiscus macintyrei* Zone (Gartner, 1977) of late Pliocene age. The *Helicosphaera sellii* Zone of Gartner (1977) was not observed in the section. Samples 110-672A-5H-1, 80–82 cm through -5H-3, 80–82 cm are assigned to the *Calcidiscus macintyrei* Zone (Gartner, 1977) based on the presence of *C. macintyrei* without *D. brouweri*. Samples 110-672A-5H-4, 80–82 cm through 6H-3, 98–100 cm are zoned into the late Pliocene CN12d Zone of Okada and Bukry (1980) owing to the presence of *D. brouweri* without *D. pentaradiatus*. Subzone CN12c of Okada and Bukry (1980) is found between Samples 110-672A-6H-4, 98–100 cm and -6H-6, 98–100 cm. The presence of *D. surculus* in Samples 110-672A-6H-CC through -7H-3, 80–82 cm indicates the Subzone CN12b of Okada and Bukry (1980). The *D. tamalis* Subzone CN12a occurs between Samples 110-672A-7H-4, 80–82 cm through -10H-3, 80–82 cm and is designated by the presence of *D. tamalis* without *Reticulofenestra pseudoumbilica*. The early/late Pliocene boundary is defined in Sample 110-672A-10H-4, 80–82 cm by the LAD of *R. pseudoumbilica*. Zone CN11 of early Pliocene age is restricted to the interval between Samples 110-672A-10H-4, 80–82 cm and -12H-1, 82–84 cm and was not refined to subzone level. Rare specimens of *Amaurolithus primus* are observed in Sample 110-672A-12H-1, 82–84 cm. The top of species *A. primus* is not consistent in this geographic area (Bergen, 1984) and is not used as a marker in Hole 672A. *A. tricorniculatus* occurs in Sample 110-672A-12H-2, 82–84 cm and indicates the top of the early Pliocene Zone CN10c. The range of *Ceratolithus acutus* designates the CN10b Subzone of Okada and Bukry (1980) in Samples 110-672A-12H-6, 82–84 cm through -13H-2, 87–89 cm. Sample 110-672A-13H-

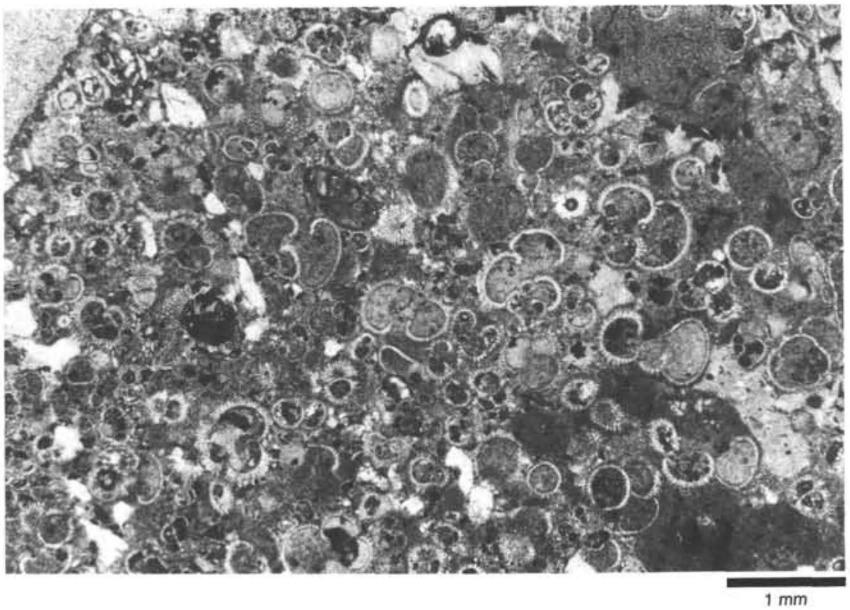

Figure 23. Limestone (packstone to wackestone) from lithologic Unit 4, composed predominantly of planktonic foraminifers (thin section); Sample 110-672A-41X-CC, 18–19 cm.

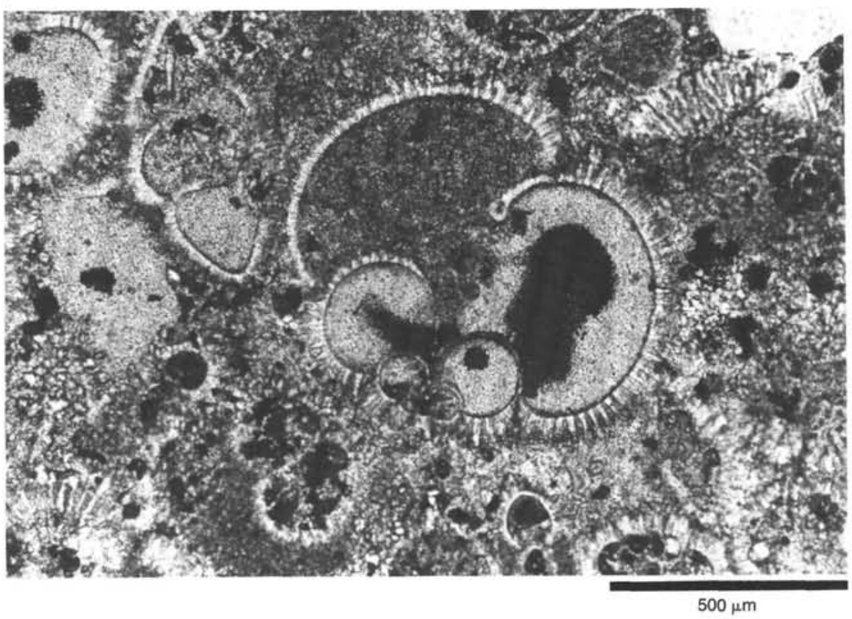

Figure 24. Thin-section detail of packstone shown in Figure 23. Planktonic foraminifer showing both clay infilling (light) and micrite infilling (dark); Sample 110-672A- 41X-CC, 18–19 cm.

3, 97–99 cm does not contain *C. acutus* or *D. quinqueramus* and is placed within Subzone CN10a (Okada and Bukry, 1980), which is latest Miocene in age.

Upper Miocene sediment occurs in Sample 110-672A-13H-4, 97–99 cm, below the LAD of *Discoaster quinqueramus*. The co-occurrence of *D. quinqueramus* and *Amaurolithus primus* in Samples 110-672A-13H-4, 97–98 cm through -15X-2, 70–72 cm defines the CN9b Subzone of Okada and Bukry (1980). A barren interval extends from Sample 110-672A-15X-3, 70–72 cm to -17X-2, 110–112 cm and is probably the result of a late Miocene dissolution episode. The CN9a Zone of Okada and Bukry (1980) occurs in Samples 110-672A-17X-3, 110–112 cm through -18X-4, 39–41 cm based on the presence of *Discoaster berggrenii* without *Amaurolithus primus*.

Sample 110-672A-18X-CC is assigned to Zone CN7 of Okada and Bukry (1980) owing to the tentative identification of *D. hamatus*. Specimens of *D. hamatus* are six-rayed forms which often appear near the top of the range of this taxon. Poor preservation makes positive recognition of this species difficult. Section 110-672A-18X-CC is the last nannofossiliferous interval in the Miocene section. Below this a long barren zone persists between Samples 110-672A-19X-1, 78–80 cm and -25X-CC, a circumstance attributed to a rather extensive upward excursion of the Miocene CCD.

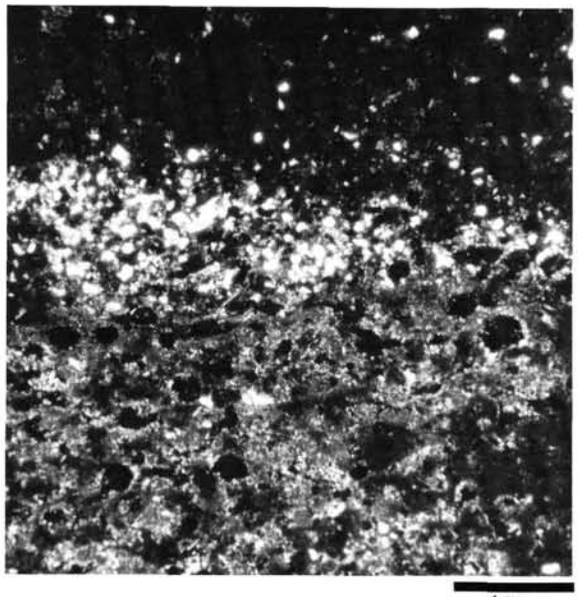

Figure 25. Laminated ferruginous limestone (thin section), Sample 672A-49X-3, 116–118 cm, lithologic Unit 4.

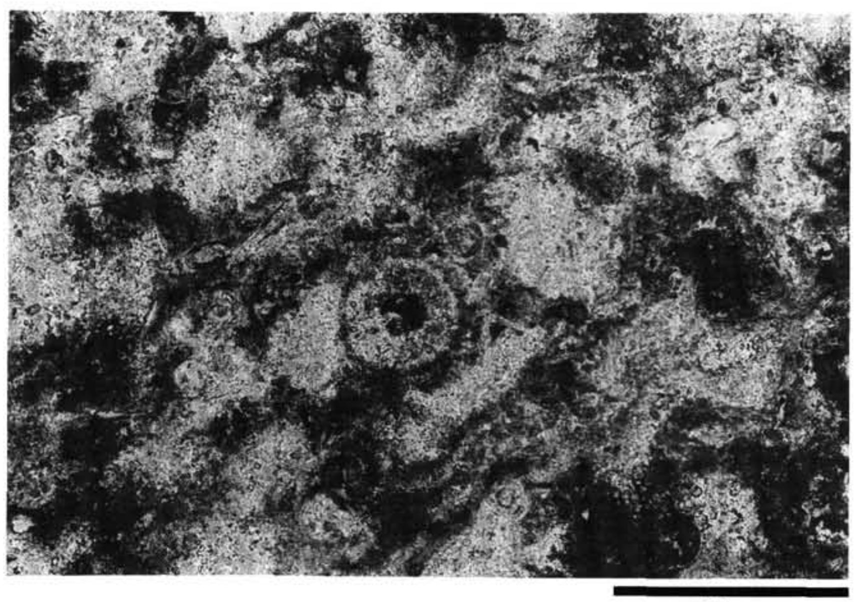

Figure 26. Radiolarian "ghost" in recrystallized limestone shown in Figure 25 (thin section), Sample 110-672A-49X-3, 116–118 cm.

The top of the Paleogene is marked in Core 110-672A-26X by *Sphenolithus ciperoensis* which is the range marker for the late Oligocene CP19 Zone of Okada and Bukry (1980). Sediments belonging to the latest Oligocene CN1 Zone are not found in the section and may have been removed by dissolution. The *S. ciperoensis* Zone (CP19) of Okada and Bukry (1980) is identified from Samples 110-672A-26X-1, 86–88 cm through -28-CC by the presence of *S. ciperoensis*. Zone CP18, defined by the occurrence of *S. distentus* in the absence of *S. ciperoensis*, is observed in Samples 110-672A-29X-1, 85–87 cm through -37-X-1, 67–69 cm. Many barren intervals were noted in the CP18 section. Zone CP18 is reassigned to the early Oligocene by Berggren, Kent, and Flynn (1985) from its earlier designation as late Oligocene by Okada and Bukry (1980). Reworking of Eocene nannofossils into the CP18 section is common especially in Section 110-672A-31X-CC.

Lower Oligocene sediment is also observed in Sample 110-672A-37X-6, 67–69 cm. The Oligocene section is slightly recrystallized and of moderate preservation overall. Early Oligocene zone CP16b of Okada and Bukry (1980) is recognized in Core 110-672-37X samples above because of the occurrence of *Reticulofenestra umbilica* and *Cyclicargolithus formosus*.

Upper Eocene sediments are confined to Samples 110-672A-39X-2, 26–28 cm through -40X-5, 13–15 cm. This section is often very recrystallized and is of moderate to poor preservation. The co-occurrence of *Discoaster sipanensis* and *D. barbadiensis*

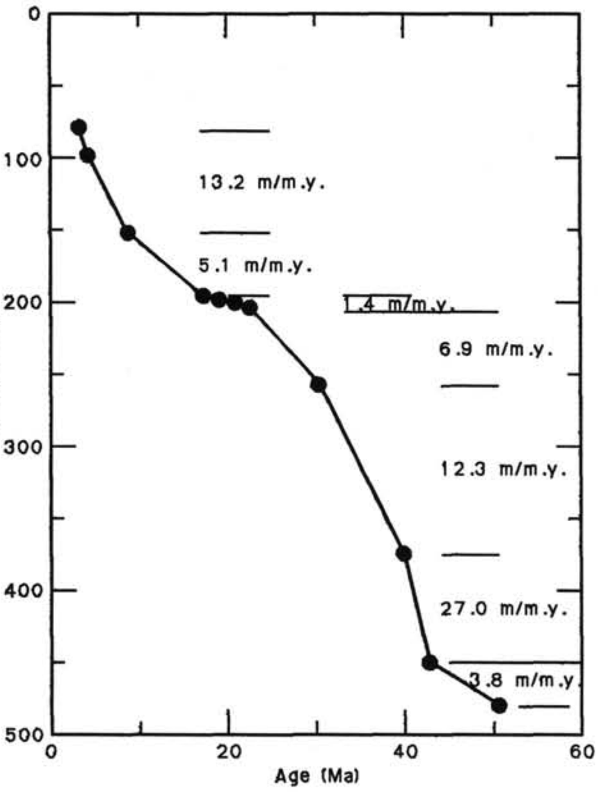

Figure 27. Sediment thickness vs. age for Site 672. Sedimentation rates for each interval are also shown.

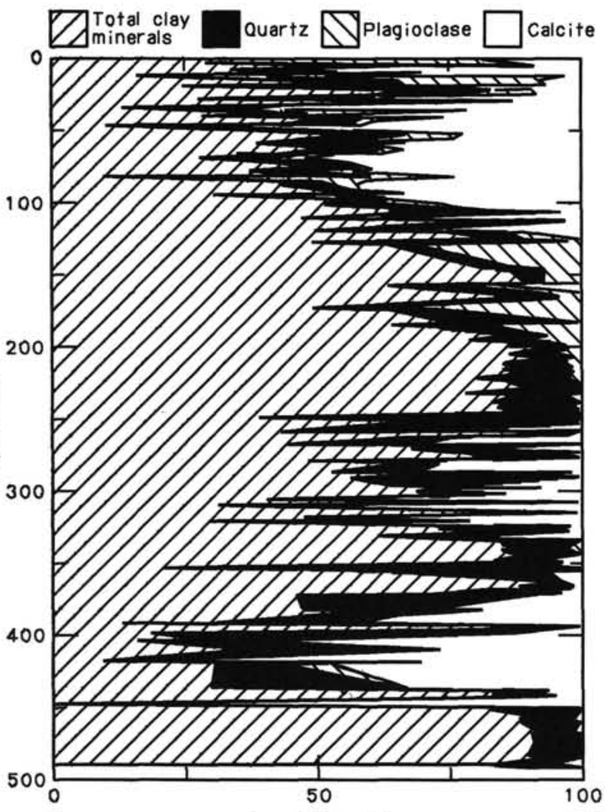

Figure 28. Bulk mineralogy of Site 672 samples expressed as cumulative percentages of total clay minerals, quartz, plagioclase, and calcite.

without *Chiasmolithus grandis* suggests Zone CP15 of Okada and Bukry (1980).

An expanded middle Eocene section is recognized in Samples 110-672A-40X-6, 44-46 cm through -49X-2, 70-72 cm. This interval is confined to the CP14 Zone of Okada and Bukry (1980) by the presence of *C. grandis* and *Reticulofenestra umbilica*. Samples 110-672A-49X-3, 79-81 cm through -53X-CC are barren of nannofossils.

Planktonic Foraminifers

Planktonic foraminifer-bearing sediments at Site 672 range from early Pleistocene to Eocene in age. Foraminifers are generally abundant and well preserved throughout the Pleistocene and the Pliocene. As at Site 671, the Pliocene-Miocene passage is marked by an increase in dissolution which reduced drastically the number of species and, finally, gave way to a long interval barren of foraminifers. Below this barren interval, which corresponds to almost the whole Miocene, sediments yield some well-preserved and generally poor assemblages belonging to the Oligocene and the Eocene.

The Pleistocene assemblage, recovered between Sections 110-672A-1H-CC and -4H-CC, is dominated by *Globorotalia truncatulinoides, G. hessi, Neogloboquadrina dutertrei, Sphaeroidinella dehiscens, Pulleniatina obliqueloculata, Globigerinoides conglobatus, G. trilobus* and *G. ruber*. The *Globorotalia menardii-G. tumida* complex is well represented only in Cores 110-672A-1H and -2H. This interval is placed within the lower Pleistocene *Globorotalia hessi* subzone of the *G. truncatulinoides* Zone, owing to the presence of the subzonal marker in the absence of younger or older species, such as *Globigerina calida* or *Globorotalia viola*.

The lowermost Pleistocene *G. viola* Subzone of the *G. truncatulinoides* Zone has not been identified here; sediments corresponding to this relatively long time (ca. 1 Ma, according to Berggren, Kent and Van Couvering, 1985) are probably missing from the section.

The last downhole occurrence of *G. truncatulinoides* is noted in Section 110-672A-4H-CC, while the first downhole occurrence of *G. miocenica* is in Section 110-672A-6H-CC. Consequently, Core 110-672A-5H falls in the uppermost Pliocene *G. tosaensis* Zone, which is bracketed by these two events. Nannofossils from the same core are assigned to Zone CN12a, which corresponds to a lower level in our planktonic foraminifer zonal scheme, i.e., to the *Globorotalia miocenica* Zone. This discrepancy is perhaps due to the somewhat erratic distribution of the thin-shelled *G. miocenica* and *G. exilis*, appearance of which may have been by dissolution. Following this hypothesis, Core 110-672A-5H should be placed within the *G. miocenica* Zone instead of within the *G. tosaensis* Zone. In this case, the abovementioned hiatus between lower Pleistocene and uppermost Pliocene would represent on the order of 1.8 m.y. of sedimentation.

Sections 110-672A-6H-CC and -7H-CC are assigned to the *G. miocenica* Zone (upper part: *G. exilis* Subzone or Berggren's PL5) because of the (apparent?) first occurrence of the zonal and subzonal markers, frequent and very well preserved in Core 110-672A-7H.

The short Zone PL4, defined by the coexistence of last *Sphaeroidinella dehiscens* s.s. (large flange) and first *Globoquadrina altispira*, has not been recognized. These two events were successively noted, however, in Sections 110-672A-7H-CC and -8H-CC; the zone could nevertheless be represented in Core 110-672A-8H.

The lower part of the *G. miocenica* Zone (PL3) was observed in Sections 110-672A-8H-CC and -9H-CC. The assemblage is dominated by *Globorotalia limbata, G. multicamerata, Globoquadrina altispira, Globigerinoides extremus, Globigerina vene-*

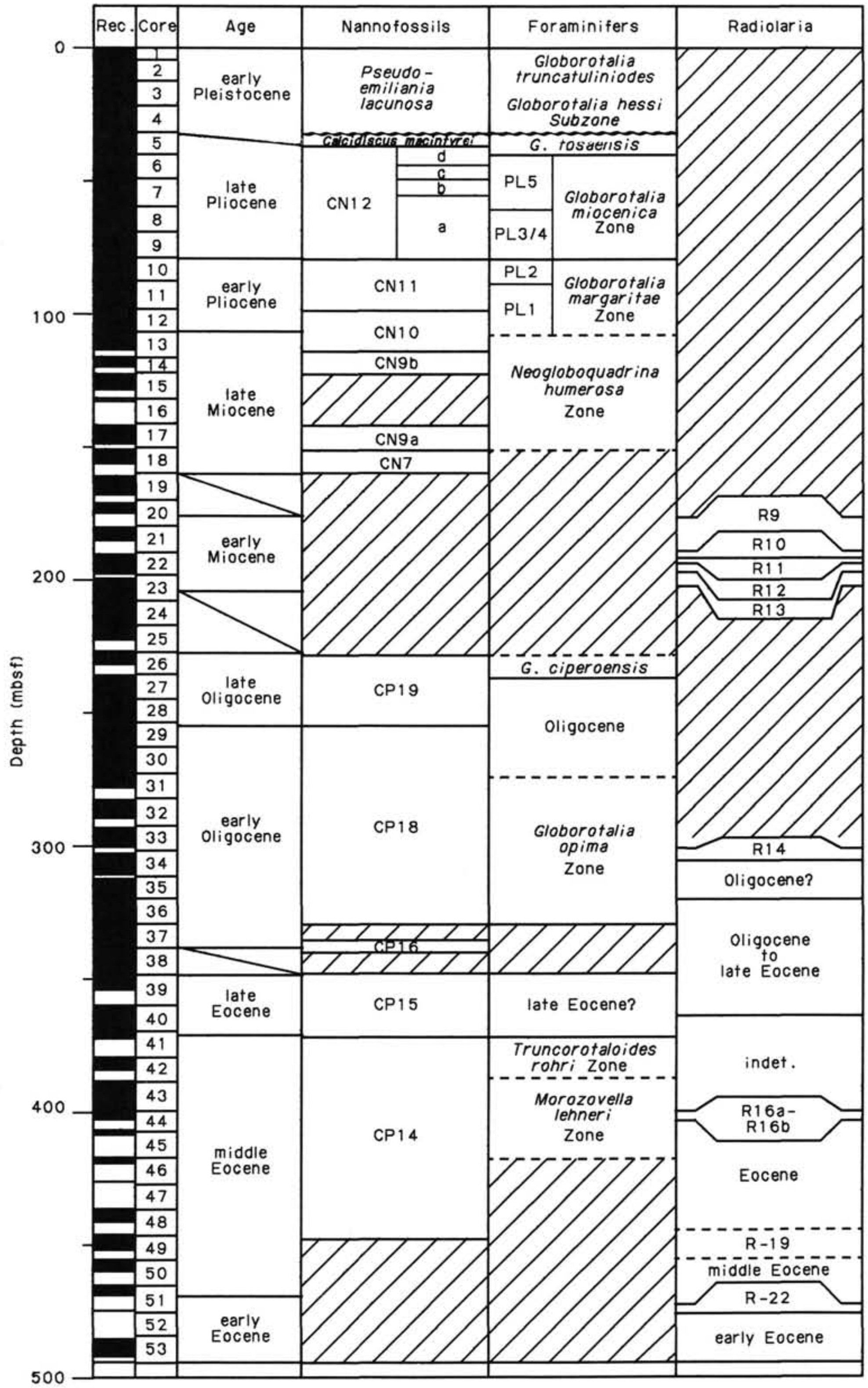

Figure 29. Biostratigraphic summary, Site 672. R9: *Calocycletta costata* Zone; R10: *Stichocorys wolffii* Zone; R11: *Stichocorys delmontensis* Zone; R12: *Cyrtocapsella tetrapera* Zone; R13: *Lychnocanoma elongata* Zone; R14: *Dorcadospyris ateuchus* Zone; R16: *Thyrsocyrtis bromia* Zone; R16a: *Carpocanistrum azyx* Zone; R16b: *Calocyclas bandyca* Zone; R19: *Podocyrtis mitra* Zone; R22: *Dictyoprora mongolfieri* Zone.

zuelana, Sphaeroidinellopsis seminulina and *S. sphaeroides*. The zonal marker is lacking, probably removed by dissolution.

Sections 110-672A-10H-CC through -12H-CC belong to the lower Pliocene, *Globorotalia margaritae* Zone, although the nominate taxon has not been identified in the core-catcher samples. As at Site 671, this zone can nevertheless be recognized in using the alternative markers *Pulleniatina primalis, Globorotalia plesiotumida* and *Globigerinoides obliquus*. The first downhole occurrence of *Globigerina nepenthes* and *Globorotalia cibaoensis* in Section 110-672A-11H-CC marks the lower part of the zone (PL1a to early PL1b).

The Pliocene/Miocene boundary is placed between Cores 110-672A-12H and -13H on the basis of the nannofossil data. Section 672A-13H-CC, however, contains rare specimens of *Globigerinoides conglobatus*. Estimated age of the FAD of this taxon (5.3 Ma; cf. Berggren, Kent, and Van Couvering, 1985) seems to need further investigations in the Caribbean because it occurs here together with *Discoaster quinqueramus*, of which the LAD is calibrated at 5.6 Ma (Berggren, Kent, and Van Couvering, 1985).

Cores 110-672A-14H through -16X and -18X through -25X are barren of planktonic foraminifers. Core 110-672A-17X yields a poor assemblage composed of the dissolution-resistant species *Globigerina nepenthes* and *Sphaeroidinellopsis seminulina*; the core is tentatively dated from the upper Miocene, *Neogloboquadrina humerosa* Zone.

Sections 110-672A-26X-CC through -36X-CC are placed within the Oligocene. Characteristic taxa include *Cassigerinella chipolensis, Globigerina* gr. *ciperoensis, G.* gr. *praebulloides, G. angulio fficinalis, G.* gr. *tripartita, G. gortanii, G. officinalis* and *Globorotalia nana*.

Core 110-672A-26X is tentatively assigned to the late Oligocene, *Globigerina ciperoensis* Zone owing to the presence of the zonal marker and on the basis of nannofossil data.

Globorotalia opima was noted from Samples 110-672A-30X-3, 77–79 cm to -35X-CC, which thus belong to the lower Oligocene, *G. opima* Zone (Bolli, 1957a).

The last definite Oligocene microfauna is found in Core 110-672A-36X, which yields rare *Cassigerinella chipolensis* and *Globigerina* sp. Cores 110-672A-37X and -38X are barren of foraminifers.

Reworked Eocene assemblages are common within this Oligocene interval, especially in its lower part where relatively frequent *Globorotalia pseudoscitula, Acarinina broedermanni, A. bullbrooki* and *Pseudohastigerina micra* have been identified.

An upper Eocene interval is suspected between Cores 110-672A-39X and -40X, according to the absence of either definite Oligocene or middle Eocene species.

Sections 110-672A-41X-CC through -45X-CC belong to the middle Eocene. A very rich assemblage, including *Globorotalia cerroazulensis, G. pomeroli, Morozovella lehneri, M. spinulosa, Truncorotaloides rohri, T. topilensis, Globigerinatheka index, G.* gr. *mexicana* and *Hantkenina mexicana*, occurs in Core 110-672A-41X, which is dated from the uppermost middle Eocene, *Truncorotaloides rohri* Zone of Bolli (1957b).

Cores 110-672A-43X and -44X are assigned to the *Morozovella lehneri* Zone, because of the occurrence of the nominate taxon together with *Acarinina broedermanni, A. bullbrooki, Globorotalia pomeroli, G. bolivariana, G. subscitula*, and *Globigerinatheka* gr. *subconglobata*.

Cores 110-672A-46X through -53X are barren of foraminifers.

Benthic Foraminifers

Benthic foraminifer evidence suggests that Hole 672A material was deposited at abyssal depths throughout its Pliocene-Pleistocene history. Sections 110-672A-1H-CC through -11H-CC contain well-preserved benthic assemblages which are dominated by the following species: *Nuttallides umboniferus, Planulina wuellerstorfi, Pyrgo murrhina*, and *Oridorsalis umbonatus. Epistominella exigua, Globocassidulina subglobosa, Pullenia bulloides, Eggerella bradyi*, and *Gyroidinoides* sp. are consistantly found within the section but are not dominant faunal components. All of the above species are collectively indicative of the Atlantic abyssal environment. Upper Neogene population changes are inferred as abundance patterns shift among the four dominant taxa. Abyssal population dynamics in this portion of the Atlantic are controlled by changes in Antarctic bottom-water volume which responds, in turn, to episodic glaciation.

Pliocene sediments between Sections 110-672A-5H-CC and -11H-CC show marked variation in the percentages of *Nuttallides umboniferus. N. umboniferus* is indicative of Antarctic bottom water and is assumed to peak in abundance during times of increased Antarctic bottom-water flow. Miliolid taxa are associated with warmer bottom-water temperatures and vary inversely with percentage *N. umboniferus*. Two periods of bottom-water cooling are inferred from the distribution of these species: the first occurred during the late Pliocene and the second during the early Pleistocene. The late Pliocene cooling event is signaled by a pronounced peak in *N. umboniferus* in Sample 110-672A-8H-CC. The age of this sample is based on planktonic foraminifer zone PL5 which is dated paleomagnetically as 2.2 to 3 Ma. Weissert et al. (1983) presented evidence of increased bottom-water flow in the South Atlantic at 2.5 Ma that they attributed to an episode of Pliocene glaciation. The increased amount of *N. umboniferus* in Core 110-672A-8H may be synchronous with the cooling event observed in the South Atlantic sediment record.

A second increase in *N. umboniferus* occurs between Sections 110-672A-3H-CC and -4H-CC. This early Pleistocene shift in population dominance may be coincident with the Illinoian Glacial event. The relative percentage of *N. umboniferus* remains elevated in Section 110-672A-1H-3.

Radiolaria

No radiolarians are preserved in the sediments in the Sections 110-672A-1H-CC to -19X-CC, although some sponge spicules are found in the upper part of the interval. A few radiolarians are found in Core 110-672A-20X, although they are conspicuously dissolved and no speciation is possible.

Samples 110-672A-21X-1, 27–29 cm through -23X-2, 65–66 cm contain well-preserved, lower Miocene, extremely diverse, radiolarian assemblages. Samples 110-672A-21X-1, 27–29 cm through -22X-3, 105–106 cm (180.6–193.6 mbsf) are assigned to the *Calocycletta costata* Zone (Riedel and Sanfilippo, 1978) because of the presence of *C. costata* and *Dorcadospyris dentata*, and the absence of *Dorcadospyris alata*. The last occurrence of *Carpocanistrum cingulata* is in Section 110-672A-21X-CC. Samples 110-672A-22X-4, 115–116 cm through -22-5, 46–48 cm (195.5–196.3 mbsf) are assigned to the *Stichocorys wolffii* Zone (Riedel and Sanfilippo, 1978). *Cyrtocapsella tetrapera, C. cornuta, Calocycletta virginis, Stichocorys delmontensis*, and *S. wolffii* are present in these samples whereas *C. costata, D. dentata* and *Liriospyris stauropora* are absent. Samples 110-672A-22X-6, 35–36 cm and -22X-CC (197.7–199.3 mbsf) are assigned to the *Stichocorys delmontensis* Zone (Riedel and Sanfilippo, 1978). *C. tetrapera, C. cornuta, C. virginis, Carpocanopsis bramlettei*, and *S. delmontensis* are present and *S. wolffii, D. dentata*, and *C. costata* are absent in these samples. Samples 110-672A-23X-1, 65–66 cm and -23X-2, 65–66 cm (200.0–201.5 mbsf) are assigned to the *Cyrtocapsella tetrapera* Zone (Riedel and Sanfilippo, 1978) because of the presence of *C. tetrapera, C. cornuta, C. virginis*, and *Lychnocanoma elongata*, and the absence of *S. delmontensis, S. wolffii*, and *C. costata. Calocycletta serrata* is common in the lower sample and absent in the upper sample. Sample 110-672A-23X-3, 65-66 cm and -23X-4, 97-98 cm (203.0-204.8 mbsf) are assigned to the *Lychnocanoma elongata* Zone (Riedel and Sanfilippo, 1978) because of the presence of *L. elongata, C. cingulata* and *Dorcadospyris ateuchus*, and the absence of *C. tetrapera, C. cornuta*, and *C. serrata*.

In Samples 110-672A-23X-5, 97-98 cm and -23X-CC (206.3-208.8 mbsf), radiolarians are still abundant, but the quality of preservation decreases rapidly with increased dissolution. Orosphaerid fragments are common in this interval. No zonal assignments were attempted with these samples.

Samples from Cores 110-672A-24X to -39X are barren or contain scarce, badly dissolved, and/or opaque (probably replaced with pyrite) radiolarian specimens. No age indicator is present except in Samples 110-672A-32X-CC; -34X-3, 87-88 cm; -34X-5, 87-88 cm; -35X-5, 87-85 cm through -36X-1, 78-79 cm; and -39X-2, 36-37 cm.

Tristyrospyris triceros, ranging from upper Eocene to Oligocene (from *Thyrsocystis bromia* Zone of Riedel and Sanfilippo (1978) or *Carpocanestrum azyx* Zone of Riedel and Sanfilippo, 1978) to *Dorcado spyris ateuchus* Zone of Reidel and Sanfilipo (1978), is always found in these samples. In addition to this species, the following indicators, all of which are replaced by opaque minerals, are found in Section 110-672A-32X-CC:

Calocyclas turris	*Lithochytris vespertilio*
Calocyclas hispida	*Podocyrtis mitra*
Dictyoprora mongolfieri	

in Sample 110-672A-34X-5, 87-88 cm:

Artophormis gracialis	*Theocyrtis annosa*
Dorcadospyris ateuchus	

Section 110-672A-32X-CC is assigned to the lower Oligocene from the calcareous nannofossils and foraminifers. *T. triceros* is consistent with this age, but the ranges of five Eocene species identified in this interval represent notable inconsistency with the early Oligocene age. These opaque Eocene radiolarians may be regarded as reworked specimens. Sample 110-672A-34X-5, 87-88 cm is assigned to *D. ateuchus* Zone owing to the presence of *T. annosa*. In this interval, opaque sponge spicules also occur rather frequently.

In Cores 110-672A-40X through -53X, radiolarians are few to abundant, but their state of preservation is poor owing to high silica cementation. Cores 110-672A-40X to -42X contain few to common radiolarians, but age assignments could not be made. Cores 110-672A-43X through -53X are placed in the Eocene, based on the nearly continuous occurrence of *Lithocyclia ocellus* and *Calocyclas hispida*. In addition to these two species, the radiolarian assemblages of Samples 110-672A-43X-1, 94-95 cm and -43X-2, 94-95 cm include *T. triceros* and *T. bromia* and are assigned to *C. azyx* Zone—*Calocyelas bandyca* Zone of Saunders, et al. (1984) (late Eocene). Sections 110-672A-45X-CC, -47X-CC, -48X-CC, and Sample 49X-4, 73-75 cm include *Sethochytris triconiscus*. Samples 110-672A-49X-1, 73-75 cm through -49X-3, 73-75 cm include the late form of *Podocyrtis mitra* with large pores of elongate abdomen. These latter samples are assigned to *P. mitra* Zone of Riedel and Sanfilippo (1978) (middle Eocene). Samples 110-672A-49X-CC and -50X-1, 80-82 cm include *Podocyrtis trachodes, P. mitra*, and *Lithapium mitra*, and Section 110-672A-50X-CC contains *Podocyrtis sinuosa* and *P. mitra*, thus being assigned to *Podocyrtis ampla* Zone—*Podocyrtis mitra* Zone of Riedel and Sanfilippo (1978) (middle Eocene). Sample 110-672A-51X-2, 68-70 cm contains *Eusyringium lagena*, and Section 110-672A-51X-CC assigned to *Dictyoprora* (= *Theocampe*) *mongolfieri* Zone—*P. mitra* Zone of Riedel and Sanfilippo (1978) (middle Eocene), contains *P. sinuosa* and *Thyrosocyrtis triacantha*. Sample 110-672A-52X-1, 23-24 cm contains frequent occurrences of *P. mitra* and *T. sinuosa* and is barren of *P. mitra* and *T. triacantha* as well as *Dictyoprora mongolfieri, Eusyringium fistuligerum*, and *Rhopalocanium ornatum*. This sample is assigned to *D. mongolfieri* Zone of Riedel and Sanfilippo (1978) (middle Eocene). In the lowest samples, Sections 110-672A-52X-CC through -53X-CC, *D. mongolfieri* is absent, and *L. ocellus* and *C. hispida* are present as mentioned above. Cores 110-672A-51X and -52X are therefore assigned to *Buryella clinata* Zone—*Theocotyle cryptocephala* Zone of Riedel and Sanfilippo (1978) (early Eocene).

Ichthyoliths were frequently found in Cores 110-672A-24X through -38X.

PALEOMAGNETICS

Paleomagnetic samples where not collected at this site because of the time constraints of measuring the samples. However, the site provided an opportunity to measure a reference section for magnetic susceptibility to compare to the susceptibility log at Site 671.

The methodology used in measuring the susceptibility was the same as at Site 671, as were the constraints on the reliability of the measurements (see Chapter 1, this volume). The susceptibility log for this site (Fig. 30) shows the Pleistocene to upper Miocene section to have an average value of about 60 G Oe^{-1} compared to the slightly higher average at Site 671 of about 70 to 80 G Oe^{-1}. The susceptibility shows the same broad low in the upper Pliocene which was present at Site 671. The reduction in the susceptibility at about 200 mbsf in the lower Miocene sequence corresponds to the reduction in the ash content of the sediments and the change in provenance of the coarse fraction. The low values (average of 16 G Oe^{-1}) in the Oligocene section (220 to 350 mbsf) correspond to lithologic Unit 3 (Lithostratigraphy Section, this chapter). From visual observations it was noted that the small-scale fluctuations in this section correspond to variations in the carbonate content such that chalk horizons have low susceptibility values compared to the marls and claystones. This is likely to be a result of the diluting influence of calcite, which has a small negative susceptibility. A decline in the susceptibility at about 360 mbsf corresponds to lithologic Unit 4, which is comparatively richer in silt and sand than the Oligocene section. The sand/silt rich layers in this part of the sequence tend to have lower susceptibilities than the surrounding marls, suggesting that the source for the magnetic minerals in this part of the sequence is associated with clay-sized particles.

The correlation between the lower Pliocene-upper Miocene sections from Sites 671 and 672 is exceptionally good (Fig. 31) and indicates the degree to which the ash beds, which give rise to these fluctuations, are uniformly deposited on the abyssal plain. The correlation of Core 110-671B-1H with Cores 110-672A-1H and -2H is also good (Fig. 32), although this breaks down in the lower part of the Pleistocene. A small repeated section is present from the base of Core 110-672A-2H to near the base of Core 110-672A-3H, which is seen again in Core 110-672A-4H. The correlation between these two repeated sections is exceptionally good (Fig. 33). Such a correlation is consistent with the nannofossil stratigraphy, which over these cores have the same zone. This repeated section is probably caused by a small fault or rotational slip plane at the base of Core 110-672A-3H (21 mbsf). In comparison to the sequence at Hole 672A, the susceptibility stratigraphy over the core interval 110-671B-2H to -4H is considerably expanded. This is corroborated by the expanded biostratigraphic interval at Hole 671B.

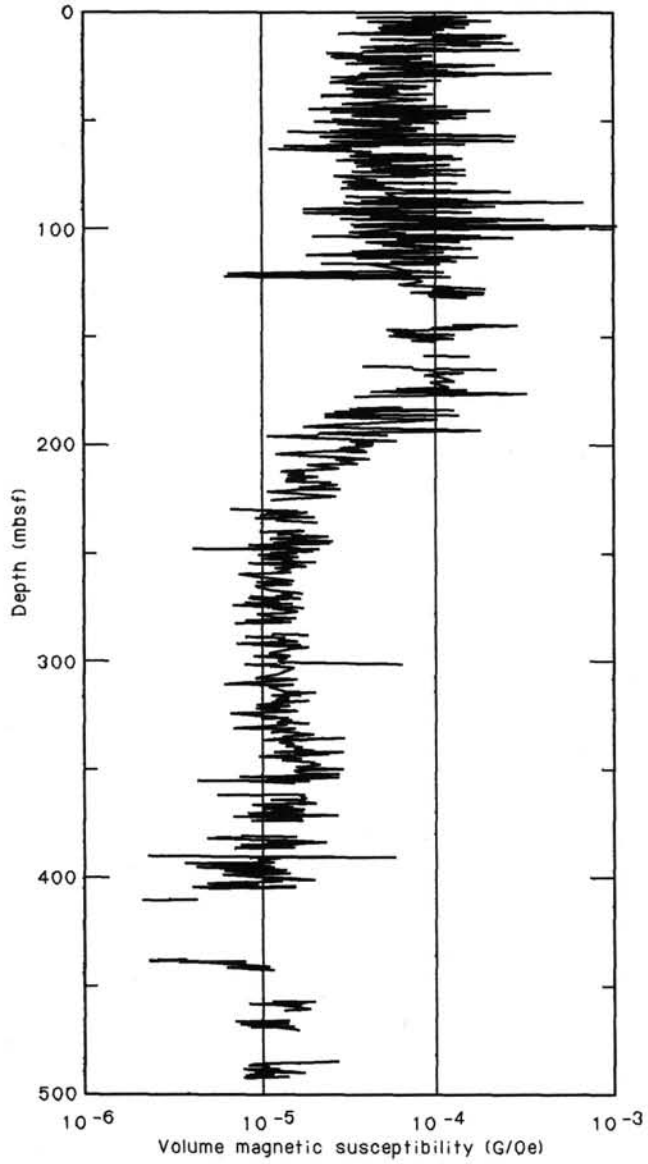

Figure 30. Susceptibility log for Site 672.

GEOCHEMISTRY

Introduction

Site 672 was drilled as an oceanic reference site for the transect of holes drilled during Legs 78A and 110 across the accretionary prism of the Barbados subduction zone complex at about 15°32′N. In this report we discuss the geochemical data collected at Site 672, and compare it with Site 671.

Inorganic Geochemistry

Results

The data collected on interstitial waters are presented in Tables 3 and 4, and also in Figure 34.

Discussion

Chloride

The concentration-depth profile of dissolved chloride shows remarkable complexity, with chloride extremes occurring at various depths in the sediment column (Fig. 34). In the upper 100 mbsf a classic profile is observed with a slight maximum in dissolved chloride. Below 100 mbsf chloride generally decreases toward a concentration of 505 mmol/L at 367 mbsf in a zone of sand-layer lenses. However, there are some notable excursions in this general trend. High chloride concentrations are present in the radiolaria-rich zone at 190 mbsf and in three other horizons, especially at 310 and 352 mbsf. In addition, a slight minimum occurs at 216 mbsf, i.e., at the base of the zone characterized as the "future décollement."

The chloride minimum in the sandy horizons at Site 672 parallels the apparent low chloride concentration in the sand underlying the lowest point cored in Site 671, suggesting horizontal advection of low-chloride waters east of the deformation front. Slightly higher methane concentrations within the sand layers (Fig. 35) support this concept. A pronounced methane peak is also associated with the chloride minimum at the bottom of "future décollement." It is quite possible that water is already moving along this "zone of future décollement"; if so, some of the hydrological characteristics of the accretionary prism extend seaward of the deformation front.

We see no *a priori* reason to reject the chloride values that are distinctly above the general trend of the profile. On closer analysis, each chloride maximum is accompanied by a distinct positive excursion in the ammonia and (Na + K) concentrations (Fig. 34). On the other hand, there is no distinct effect on the concentrations of Ca, Mg, or SO_4 (Fig. 34), in part because of the relatively minor chloride concentration changes (maximum difference in Cl at 350 mbsf is about 12%).

Are the observed chloride maxima real or are they due to artifacts? First we examine the apparent correlation between changes in NH_4, Cl, and Na in the high-chloride samples. The following table presents the relevant information.

Sample 110-672A-	Lithology	ΔCl	ΔNa	ΔNH_4 (mmol/L)
21X-2, 140-150 cm	Radiolarian mudstone	10	15	160
34X-4, 140-150 cm	Marl	30	38	110
39X-2, 145-150 cm	Quartzose muddy siltstone	70	60	300
53X-4, 145-150 cm	Mudstone	10	10	70

Δ Values calculated from "expected" values on trend lines.

ΔCl and ΔNa are roughly correlated with ΔNH_4. This suggests the possibility that the maxima in NH_4 are caused by ion-exchange processes, in which enhanced Na concentrations may displace some NH_4 ions from exchange positions in clay minerals. The ion-exchange process will be quite different in various lithologies, clayey sediments having higher exchange capacities than sands or silts. The radiolaria-containing sample has the highest relative increase in NH_4. Thus, some of the increases in ammonia may also be due to enhanced bacterial activity.

Artifact?

It is difficult to support the artifact hypotheses for the very high observed chloride concentrations. Contamination by seawater appears most unlikely, especially because this is not supported by the data on Ca, Mg, and SO_4 (Fig.34). Furthermore, the chloride values are higher than that of seawater. Because the high chloride concentrations occur in different lithologies, there does not appear to be any common compositional cause. A squeezing artifact is not likely, especially because two sections (110-672A-21X-2 and -53X-4) yielded water quite easily without using high pressures. Water was extracted from the other samples with more difficulty, but surrounding samples with similar lithologies required similar treatment and did not show anomalies. Further chemical analysis is planned for the squeezed cakes,

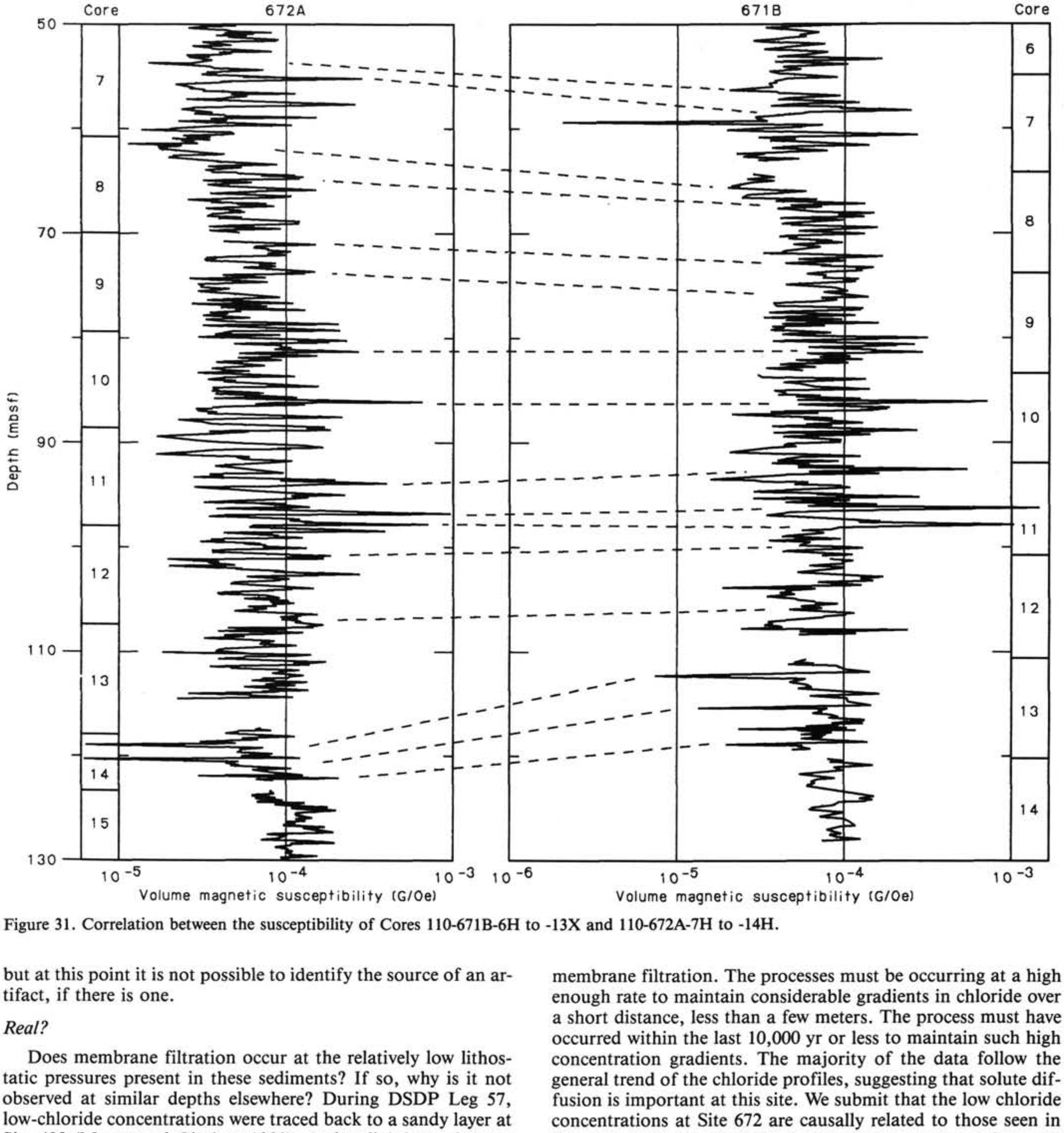

Figure 31. Correlation between the susceptibility of Cores 110-671B-6H to -13X and 110-672A-7H to -14H.

but at this point it is not possible to identify the source of an artifact, if there is one.

Real?

Does membrane filtration occur at the relatively low lithostatic pressures present in these sediments? If so, why is it not observed at similar depths elsewhere? During DSDP Leg 57, low-chloride concentrations were traced back to a sandy layer at Site 438 (Moore and Gieskes, 1980). A site slightly to the east (Site 440) did not show any chloride decreases despite a thick sedimentary section and similar lithologies. The low chloride concentrations found in Leg 57 sites were probably related to a freshwater aquifer, not to dewatering. Similarly, low chloride concentrations at Site 241 of DSDP Leg 25 (Gieskes, 1974) can best be understood in terms of an aquifer, and not in terms of dewatering. We could be misinterpreting both cases, but the question remains why dewatering, accompanied by membrane filtration, does not occur more frequently in deep-sea sediments.

Now let us assume that membrane filtration does account for observed depletions and increases in Cl concentrations. The assumption is that salt is retained in the dewatered zone during membrane filtration. The processes must be occurring at a high enough rate to maintain considerable gradients in chloride over a short distance, less than a few meters. The process must have occurred within the last 10,000 yr or less to maintain such high concentration gradients. The majority of the data follow the general trend of the chloride profiles, suggesting that solute diffusion is important at this site. We submit that the low chloride concentrations at Site 672 are causally related to those seen in Site 671, and that significant advection may occur along the sandy aquifers. Perhaps *in situ* dewatering is superimposed on this phenomenon. It may be possible that high pore-water pressures or local deformation creates a localized environment for processes resembling membrane desalination.

Alkalinity

A good alkalinity profile was obtained to a depth of 300 mbsf (Fig. 34). Just below the sediment-seawater interface there is a small alkalinity maximum largely attributed to the production of HCO_3 during sulfate reduction processes associated with the bacterial oxidation of organic matter. Below approximately 25 mbsf, the alteration of volcanic ash, which also causes sharp

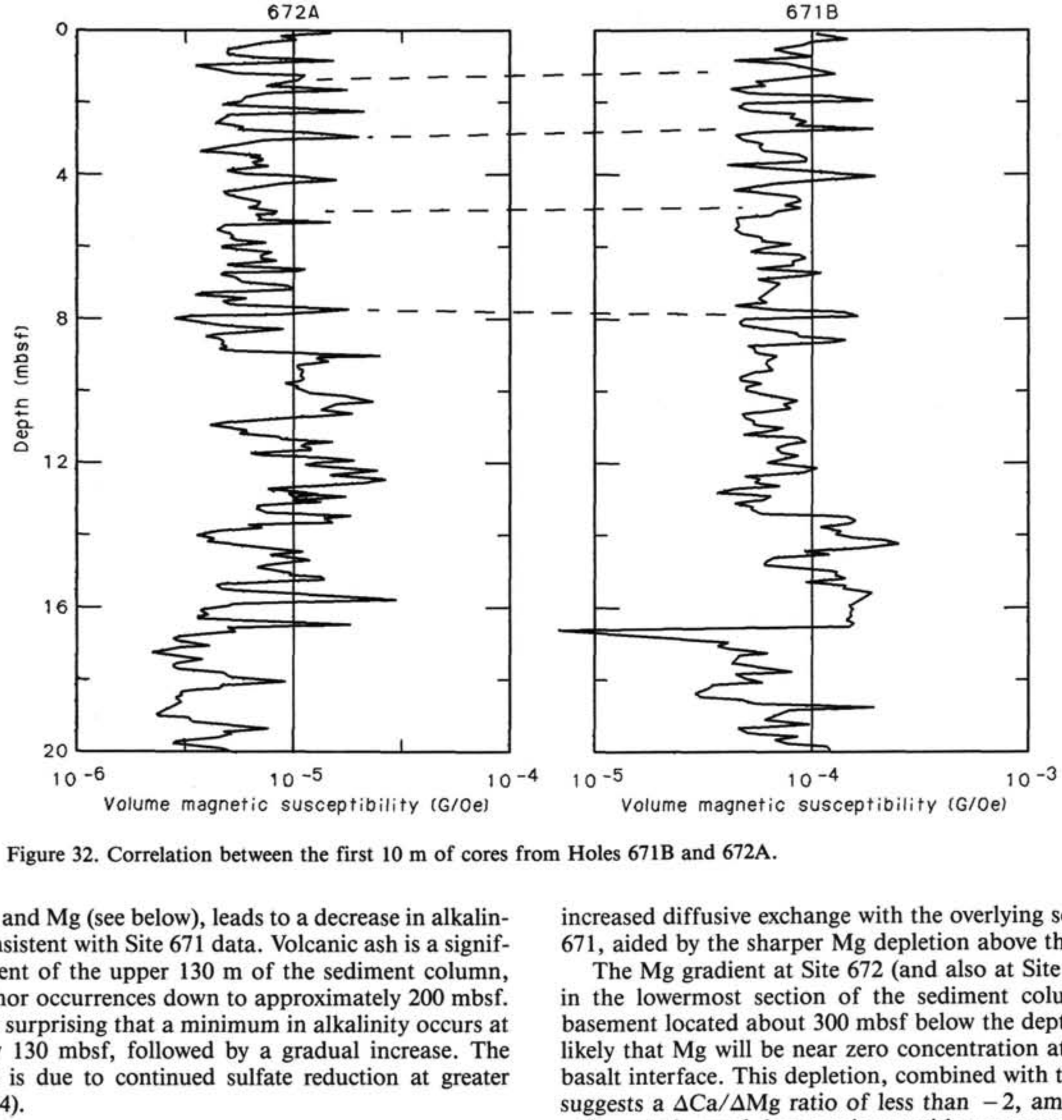

Figure 32. Correlation between the first 10 m of cores from Holes 671B and 672A.

changes in Ca and Mg (see below), leads to a decrease in alkalinity. This is consistent with Site 671 data. Volcanic ash is a significant component of the upper 130 m of the sediment column, with some minor occurrences down to approximately 200 mbsf. Thus, it is not surprising that a minimum in alkalinity occurs at approximately 130 mbsf, followed by a gradual increase. The latter increase is due to continued sulfate reduction at greater depths (Fig. 34).

Calcium and Magnesium

The concentration-depth profiles for Ca and Mg at Sites 671 and 672 are compared in Figure 34B. As discussed in the Site 671 report, the Ca profile above the décollement chiefly reflects the alteration of volcanic materials in the sediment column. Below the décollement, however, the almost linear and sharply increasing Ca gradients suggest diffusive supply from greater depth (Fig. 35). Below 200 mbsf a change in slope of the Ca profile is apparent, with a minor change in slope in the upper part of the sand/silt/limestone section at 325 to 375 mbsf. We surmise that the changes result from enhanced diffusivities and boundary conditions created by advection of "low-chloride" fluids. The Site 672 Ca profile, as well as the Mg profiles discussed below, confirm our hypothesis that the concentration gradients below the décollement at Site 671 are largely "fossil gradients."

Mg profiles are presented in Figure 34B. Alteration of volcanic ash creates a minimum in Mg at approximately 125 mbsf, below which concentrations increase to a maximum of 43 mmol/L at approximately 275 mbsf. The similarity with the Mg profile below the décollement at Site 671 is striking, and supports the idea that the radiolarian zone around 200 mbsf is the zone of the future décollement. The Mg concentration maximum at Site 671 is less than at Site 672, presumably because of increased diffusive exchange with the overlying sediment in Site 671, aided by the sharper Mg depletion above the décollement.

The Mg gradient at Site 672 (and also at Site 671) decreases in the lowermost section of the sediment column, and with basement located about 300 mbsf below the depths drilled, it is likely that Mg will be near zero concentration at the sediment-basalt interface. This depletion, combined with the Ca gradient suggests a $\Delta Ca/\Delta Mg$ ratio of less than -2, among the lowest ratios yet observed, but consistent with our speculation that formation waters in this old basement are essentially depleted in Mg (McDuff, 1981).

Sodium and Potassium

As mentioned in the Site 671 chapter, we can only estimate the sum of (Na + K) from charge balance calculations. The (Na + K) concentration-depth profile and the ratio (Na + K)/Cl is presented in Figure 34.

Below 100 mbsf there is a gradual decrease in (Na + K) with increasing depth, with a minimum in the low-chloride sandstone layers. As we suggested for Site 671, the (Na + K) gradient appears to be caused by a sink in the deeper undrilled section, presumably in the underlying basalts.

Typically, the high Cl samples also show high (Na + K) concentrations when compared with the general trend line. Similarly, the ratio of (Na + K)/Cl is anomalous for at least the three upper anomalous Cl levels. A slight minimum in (Na + K)/Cl occurs in the sand layers, related to the probable presence of an advective component in the low-chloride layer.

Sulfate and Ammonia

The sulfate concentration-depth profile at Site 672 (Fig. 34) shows an almost linear decrease with depth to about 375 mbsf, i.e., to below the section characterized by sand and silts. In

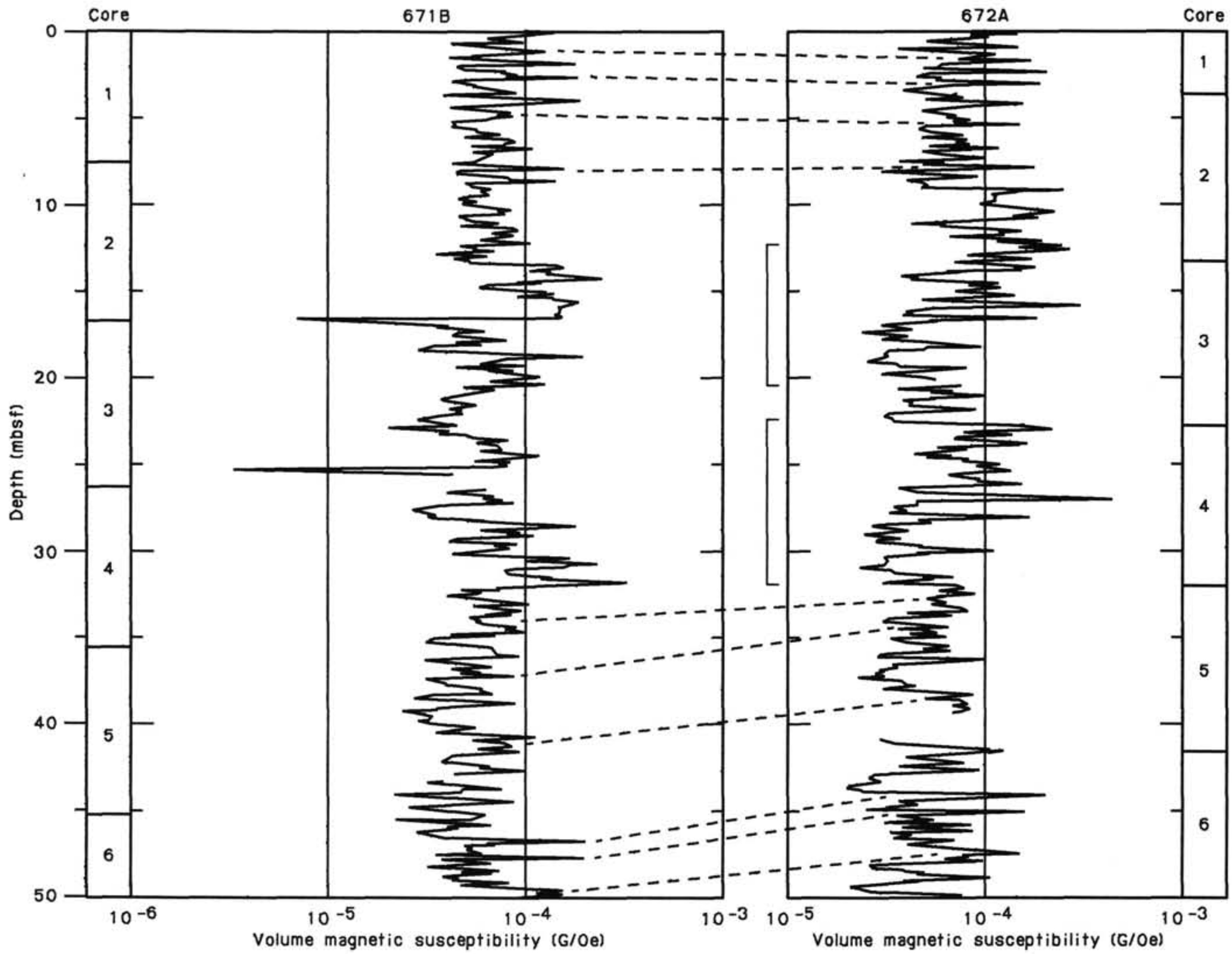

Figure 33. Correlation between the first six cores of Holes 671B and 672A, with the repeated interval in Hole 672A indicated by brackets.

comparison with Site 671, SO_4 depletions are less pronounced at Site 672, but sulfate reduction is still important in the presubduction sediments below the zone of "future décollement."

Notwithstanding the larger depletions in SO_4 at Site 671, ammonia concentrations in Site 672 (Fig. 34) are about the same as at Site 671. This is perhaps owing to the gradual absorption of NH_4 into clay minerals.

The anomalously high NH_4 concentrations in the high-Cl sediments have already been alluded to.

Silica

As at Site 671, the concentrations of dissolved silica typically reflect the local lithology (Fig. 34).

Conclusions

1. The inorganic geochemistry of interstitial waters obtained at Site 672 suggests that this site is not a true reference site, representative of a "normal" oceanic environment. This is particularly clear from the chloride profiles, which indicate a continuation of low-chloride water flow through permeable sand beds perhaps associated with *in situ* dewatering.

2. Based on the occurrence of a chloride minimum and a CH_4 maximum in Hole 672A, we suggest that indeed the "zone of future décollement" is already a horizon of active fluid transport.

Dissolved Gases and Organic Carbon

Methane

The methane data from Site 672 are given in Table 5. The dissolved methane profile (Fig. 35) shows a maximum concentration of about 208 μmol/L at 216 mbsf, comparable to the concentrations found at the thrust above the décollement in Hole 671B.

How can we explain the high concentration at this level? The thermal gradient found at Site 672A is 79°C/Km (see Heat Flow section). This thermal gradient does not support a thermogenic origin for methane production at the depths cored. The large sulfate concentrations are inconsistent with a biogenic origin of methane from microbial anaerobic respiration (Claypool and Kaplan, 1974). We therefore propose that the methane measured at Site 672 is not produced *in situ*, but is instead advected with low-chloride waters, probably originating from the west.

The sharp methane concentration gradient in the upper 160 m suggests methane diffusion. Below 245 mbsf, the observed variations in dissolved methane concentrations are complex, probably related to similar variations in dissolved chloride. The increasing methane concentration with increasing depth probably results from thermogenic production of methane at greater depth and a diffusive supply from this source. It is not immediately apparent why methane concentrations away from zones of

Table 3. Interstitial water compositions: pH, alkalinity, salinity, chlorinity, Hole 672A.

Core	Sec.	Interval (cm)	Depth (mbsf)	pH	Alkalinity (mmol/L)	Salinity (‰)	Chlorinity (mmol/L)
1H	4	145–150	6	n.d.	n.d.	n.d.	560
2H	6	145–150	12	7.43	2.99	35.5	563
3H	4	145–150	18	7.65	3.19	36	563
4H	5	145–150	29	7.68	3.20	35.3	562
5H	5	145–150	38.5	7.70	2.05	35.3	563
*I.S.1			40	7.43	2.23	35	561
7H	5	145–150	57.5	7.81	1.74	35	563
9H	5	145–150	76	7.70	1.26	n.d.	562
*I.S.2			89	7.95	1.63	35	564
12H	5	145–150	105	7.79	1.17	n.d.	562
15X	3	140–150	130	7.96	1.13	34.5	559
*I.S.3			132	8.51	1.85	35	550
18X	3	140–150	158	7.90	1.32	34.3	552
21X	2	140–150	185	7.60	2.06	35	565
24X	5	140–150	216	7.70	3.33	35	540
27X	5	140–150	245	7.69	3.46	34.2	554
30X	5	140–150	274	7.80	4.47	34.0	549
32X	4	140–150	290	7.70	5.49	35	549
34X	4	140–150	309	7.40	5.17	35	573
36X	4	140–150	327	n.d.	n.d.	34.2	532
38X	5	145–150	346	n.d.	n.d.	33.8	518
39X	2	145–150	352	7.69	n.d.	36.2	576
40X	5	145–150	367	n.d.	n.d.	32.2	505
41X	1	145–150	376	n.d.	n.d.	n.d.	n.d.
42X	2	145–150	382	n.d.	n.d.	33	522
43X	4	145–150	395	n.d.	n.d.	n.d.	529
46X	1	140–150	425	n.d.	n.d.	34.3	535
48X	3	140–150	447	n.d.	n.d.	34	527
51X	2	140–150	470	n.d.	n.d.	n.d.	545
53X	4	145–150	489	6.52	7.64	33.8	572

* Denote *in-situ* pore-water samples.

possible fluid transport are significantly higher at Site 672 than at Site 671.

Organic Carbon

Rock-Eval data are given in Table 6. The total organic carbon (TOC) contents in Hole 672A are very low (<0.6%). We provide an interpretation of the Rock-Eval parameters for only three samples (at 290, 327, and 352 mbsf) ranging in age from early Oligocene to late Eocene. The plot of total organic carbon (TOC) vs. depth (Fig. 35) suggest a division of the Hole 672A sediment column into five parts:

1. From the seafloor to 105 mbsf, in lower Pleistocene and lower Pliocene sediments, the TOC values are very low (average = 0.04%).

2. Below 105 mbsf, the TOC increases from 0.01% to 0.29%. This increase in TOC could result from a change in organic matter deposition rates during late Miocene. From 160 to 275 mbsf, the observed increase with decreasing burial depth could be caused by a slight increase in the rate of deposition of organic matter from the lower Oligocene to the upper Miocene.

3. From 270 to 375 mbsf, the TOC are variable with three peaks that decrease with burial depth (from lower Oligocene to upper Eocene). For these three peaks, the S2/S3 ratios and the plot of HI versus OI (Fig. 36) both indicate that terrestrial organic carbon is the major component of organic matter in these samples. We propose that terrestrial organic matter input increased from the upper Eocene to the lower Oligocene. The average temperature of maximum S_2, T_{max}, for these three samples of about 404°C indicates an immature zone.

4. From 375 to 450 mbsf, in middle Eocene to lower Eocene sediments, the TOC is very low (average = 0.05%). Thus, the Oligocene sediments could be the most important series relative to the amount of organic matter.

Table 4. Interstitial water compositions: Ca, Mg, NH_4, Si, SO_4, Na+K,(Na+K)/Cl, Site 672.

Core	Depth (mbsf)	Ca (mmol/L)	Mg (mmol/L)	NH_4 (µmol/L)	Si (mmol/L)	SO_4 (mmol/L)	Na+K (mmol/L)	(Na+K)/Cl
1	6	11.6	51.5	0	369	26.3	489	0.87
2	12	12.7	49.9	27	420	27.1	495	0.88
3	18	14.1	48.0	60	218	25.4	493	0.87
4	29	13.7	48.2	30	337	26.6	494	0.88
5	38.5	16.6	44.7	125	195	25.2	493	0.87
*I.S.1	40	16.6	49.8	80	124	26.3	483	0.86
7	57.5	19.3	41.9	206	169	24.2	491	0.87
9	76	21.8	39.1	225	137	23.3	489	0.87
*I.S.2	89	22.6	42.8	122	58	26.3	487	0.86
12	105	26.2	36.7	232	168	22.5	483	0.86
15	130	29.0	35.9	215	151	21.5	473	0.85
*I.S.3	132	23.9	43.8	200	65	23.3	463	0.84
18	158	32.2	38.4	230	150	21.1	454	0.82
21	185	32.8	35.0	400	1030	20.4	471	0.83
24	216	34.7	41.6	223	428	17.9	426	0.79
27	245	37.4	42.2	210	255	16.8	432	0.78
30	274	40.4	42.8	245	253	15.3	418	0.76
32	290	42.2	41.8	255	323	14.1	415	0.75
34	309	44.5	38.9	345	572	12.8	437	0.76
36	327	50.2	42.1	235	463	13.9	381	0.72
38	346	51.1	40.9	265	612	12.1	364	0.70
39	352	53.2	38.2	560	740	13.0	425	0.74
40	367	52.6	39.0	305	606	11.8	351	0.70
41	376	52.7	35.9	280	509	10.8	—	—
42	382	51.3	37.5	335	777	10.3	371	0.71
43	395	56.5	37.5	320	682	12.4	372	0.70
46	425	62.7	37.7	300	622	12.0	364	0.68
48	447	61.6	38.8	315	472	15.8	364	0.69
51	470	71.9	36.4	325	773	13.9	363	0.65
53	489	79.2	35.4	405	676	11.8	374	0.65

* Denote *in-situ* pore-water samples.

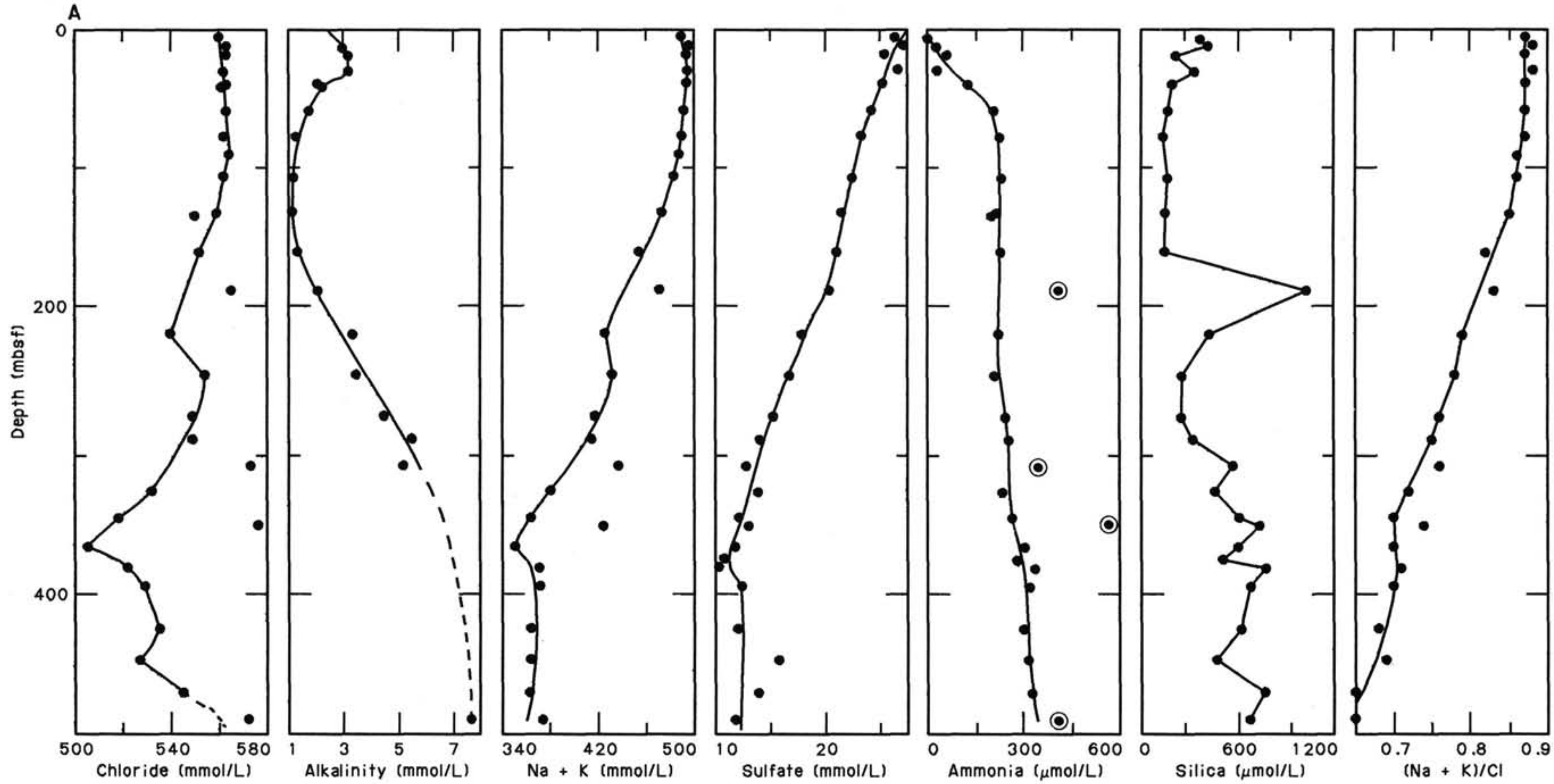
A
Depth (mbsf)
0
200
400
500 540 580
Chloride (mmol/L)
1 3 5 7
Alkalinity (mmol/L)
340 420 500
Na + K (mmol/L)
10 20
Sulfate (mmol/L)
0 300 600
Ammonia (μmol/L)
0 600 1200
Silica (μmol/L)
0.7 0.8 0.9
(Na + K)/Cl

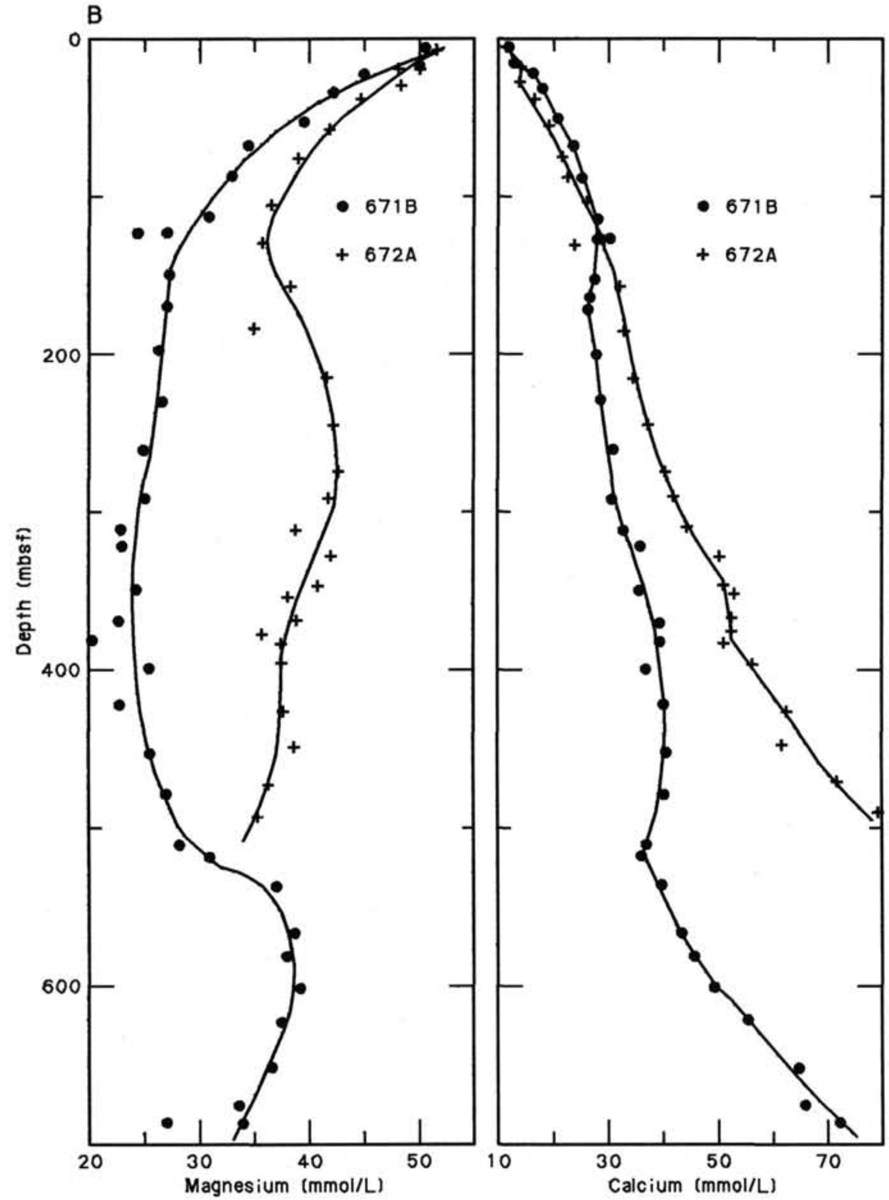

Figure 34. A. Pore-water chloride, alkalinity, (Na + K), (Na + K)/Cl, sulfate, ammonia, and silica profiles, Site 672. Open symbols indicate *in situ* water samples. Ammonia concentrations at chloride maxima are circled. B. Calcium and magnesium profiles, Sites 671 and 672.

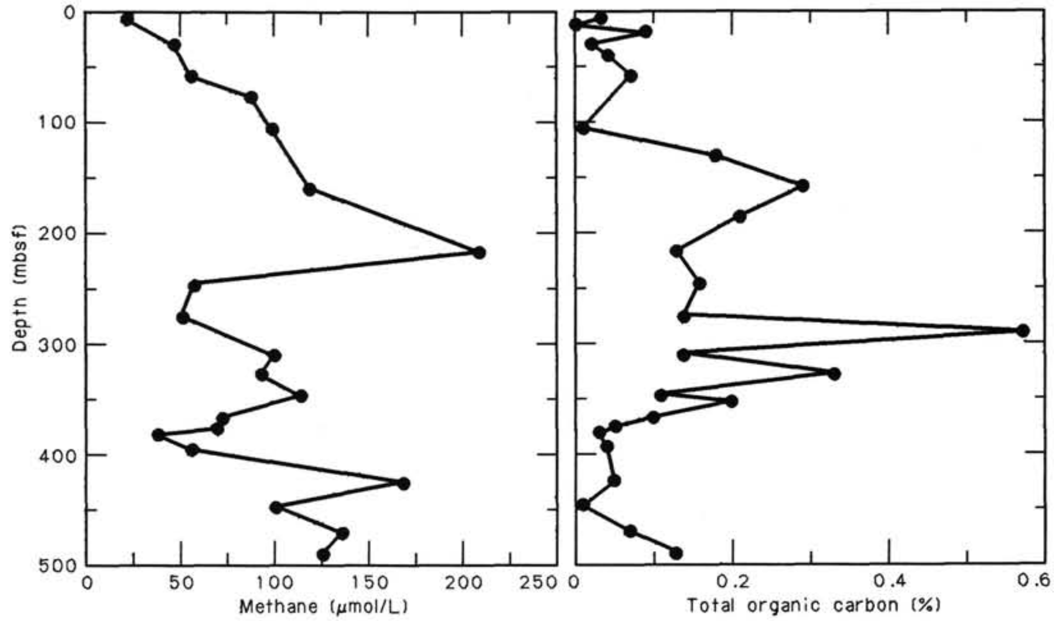

Figure 35. Plot of methane and total organic carbon vs. depth, Hole 672A.

Table 5. Geochemistry data: organic carbon, inorganic carbon, and methane, Hole 672A.

Core	Sec.	Interval (cm)	Depth (mbsf)	Organic carbon (%)	Inorganic carbon (%)	CH_4 (µmol/L)
1	4	145-150	6	0.03	4.43	22
2	6	145-150	12	0.00	0.14	n.d.
3	4	145-150	18	0.09	3.77	n.d.
4	5	145-150	29	0.02	1.97	46
5	5	145-150	38.5	0.04	4.32	n.d.
7	5	145-150	57.5	0.07	4.43	55
9	5	145-150	76	n.d.	n.d.	88
12	5	145-150	105	0.01	2.78	99
15	3	140-150	130	0.18	0.01	n.d.
18	3	140-150	158	0.29	0.06	119
21	2	140-150	185	0.21	0.02	n.d.
24	5	140-150	216	0.13	0.02	208
27	5	140-150	245	0.16	0.02	57
30	5	140-150	274	0.14	0.04	50
32	4	140-150	290	0.57	0.90	n.d.
34	4	140-150	309	0.14	0.07	100
36	4	140-150	327	0.33	7.68	93
38	5	145-150	346	0.11	0.05	114
39	2	145-150	352	0.20	0.48	n.d.
40	5	145-150	367	0.10	0.05	72
41	1	145-150	376	0.05	0.11	69
42	2	145-150	382	0.03	3.09	37
43	4	145-150	395	0.04	0.71	55
46	1	140-150	425	0.05	0.03	168
48	3	140-150	447	0.01	0.67	101
51	2	140-150	470	0.07	0.70	136
53	4	145-150	489	0.13	0.03	126

Conclusion

The dissolved chloride data, like the dissolved pore-water methane data, indicates that Site 672 is not a true reference site representative of a "normal" oceanic environment. Methane and chloride anomalies were found at the base of the stratigraphic equivalent to the décollement zone described at Site 671. These anomalies indicate active fluid flow at least 6 km seaward of the encroaching accretionary wedge. In contrast to Site 671, some dissolved methane diffusion with seawater occurs.

The most important organic matter-bearing levels are contained in the lower Oligocene to upper Eocene sediments. At Site 671, the most important organic matter-bearing levels are in the upper Oligocene sediments. These results suggest that the most important terrestrial organic matter inputs are Oligocene in age and that lateral variations of organic matter-bearing levels can be expected in the underthrust and accreted sediments. The maturation of the Oligocene terrestrial organic matter could be the main source of gas once the sediment below the décollement zone reaches proper thermal conditions.

PHYSICAL PROPERTIES

Introduction

Site 672 was chosen as the reference site for the Leg 110 transect. With respect to the physical property measurements for the study area, Site 672 serves as a reference by defining the physical character of sediments that are considered to have been uninfluenced by the stresses induced in the region of the active margin front. Although *in situ* measurements of stresses were not made at the site, it is assumed that the location (6 km east of the deformation front as defined by the geophysical reflection data) is not influenced by stresses propagating laterally from the accretionary prism. Physical property data from this site raise questions about this assumption.

Data presented in this section include index properties (water content, bulk and grain densities, and porosity), compressional wave velocity, formation factor, undrained shear strength (peak and residual), and thermal conductivity. All of the data are from recovered core samples. Data above 123 mbsf were measured on good quality advanced piston core (APC) samples and the remainder of the data were collected from samples cored with the extended core barrel (XCB). Within the APC zone, all physical property measurements were made on one sample from every other section of core (nominally). Within the XCB zone, strength and formation factor were not measured owing to sample disturbance. Index property and compressional velocity measurements were made on selected coherent sediment blocks or 'biscuits' within the XCB zone and thermal conductivity mea-

Table 6. Rock Eval geochemistry data, Hole 672A.

Core	Sec.	Interval (cm)	Depth (mbsf)	Temp. (°C)	S_1	S_2	S_3	PI	S_2/S_3	PC	TOC	HI	OI
1	4	145-150	6	427	0.03	0.01	3.19	0.75	0.00	0.00	0.03	33	10633
2	6	145-150	12	304	0.05	0.00	1.71	1.00	0.00	0.00	0.00	0	0
3	4	145-150	18	253	0.02	0.00	3.13	1.00	0.00	0.00	0.09	0	3477
4	5	145-150	29	214	0.04	0.01	3.12	1.00	0.00	0.00	0.02	50	15600
5	5	145-150	38.5	332	0.04	0.03	3.30	0.67	0.00	0.00	0.04	75	8250
7	5	145-150	57.5	190	0.03	0.00	2.67	1.00	0.00	0.00	0.07	0	3814
12	5	145-150	105	246	0.02	0.00	2.82	1.00	0.00	0.00	0.01	0	28200
15	3	140-150	130	469	0.02	2.25	0.14	0.01	16.07	0.18	0.18	1250	77
18	3	140-150	158	469	0.03	3.56	0.46	0.01	7.73	0.29	0.29	1227	158
21	2	140-150	185	568	0.10	2.48	0.07	0.04	35.42	0.21	0.21	1180	33
24	5	140-150	216	465	0.03	1.62	0.14	0.02	11.57	0.13	0.13	1246	107
27	5	140-150	245	471	0.03	1.81	0.23	0.02	7.86	0.15	0.16	1131	143
30	5	140-150	274	542	0.05	1.25	0.35	0.04	3.57	0.10	0.14	892	250
32	4	140-150	290	407	0.05	0.16	1.39	0.25	0.11	0.01	0.57	28	243
34	4	140-150	309	484	0.06	1.27	0.55	0.05	2.30	0.11	0.14	907	392
36	4	140-150	327	393	0.05	0.10	2.17	0.36	0.04	0.01	0.33	30	657
38	5	145-150	346	482	0.03	1.33	0.42	0.02	3.16	0.11	0.11	1209	381
39	2	145-150	352	412	0.01	0.05	0.63	0.17	0.07	0.00	0.20	25	315
40	5	145-150	367	576	0.06	1.11	0.58	0.05	1.91	0.09	0.10	1110	580
41	1	145-150	376	542	0.02	0.60	0.54	0.03	1.11	0.05	0.05	1200	1080
42	2	145-150	382	381	0.04	0.04	1.19	0.50	0.03	0.00	0.03	133	3966
43	4	145-150	395	355	0.05	0.06	1.24	0.50	0.04	0.00	0.04	150	3100
46	1	140-150	425	548	0.05	0.62	0.62	0.08	1.00	0.05	0.05	1240	1240
48	3	140-150	447	386	0.03	0.04	1.25	0.50	0.03	0.00	0.01	400	12500
51	2	140-150	470	530	0.04	0.83	0.10	0.05	8.30	0.07	0.07	1185	142
53	4	145-150	489	545	0.05	1.37	0.12	0.04	11.41	0.11	0.13	1053	92

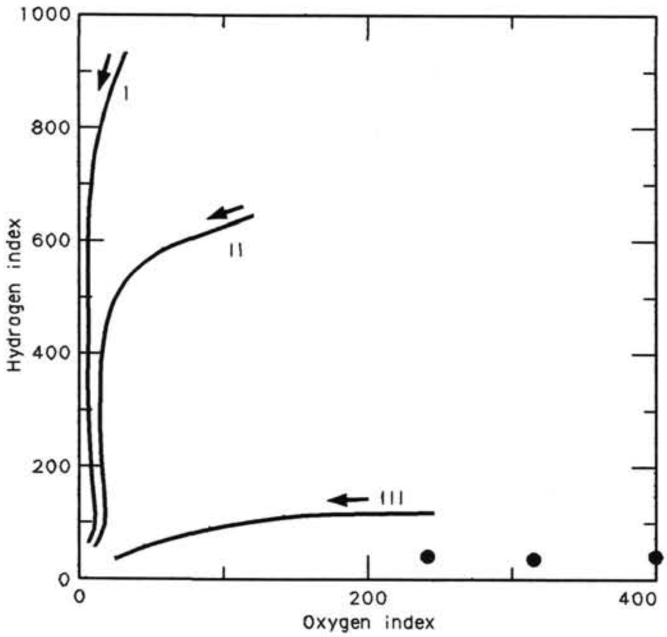

Figure 36. Plot of hydrogen index (HI) vs. oxygen index (OI), Site 672.

surements were made selectively, based on recovered sample quality.

Index Properties

Methods

The methods used to measure the index properties at Site 672 are detailed in Chapter 1, this volume. Samples collected within the upper 190 m of core were first oven-dried for 24 hr at 60°C and then freeze-dried. Index measurements were nominally made at an interval of one every two sections (3 m). In addition to index measurements on selected samples, densities were measured using the GRAPE on all core sections.

Results

The index properties measured at Site 672 include bulk density, porosity, water content (reported as a percentage of total sample weight and a percentage of dry sample weight), and grain density. Water content is presented as a percentage of dry sample weight except as noted. Both calculations of water content (total and dry) are listed with the other index properties (Table 7).

All of the index properties follow similar downhole trends at Site 672 (Fig. 37). The index data can be separated into four distinct zones. The zones are closely associated with the lithologic subdivisions at the site with the exception of the Unit 3/Unit 4 lithologic boundary; however, lithologic breaks in Hole 672A do not correlate exactly with changes in the index properties. This inconsistency is expected because the changes in porosity, density, and water content are influenced not only by the lithology and sedimentological facies, but also by the stress history at the site. Consequently, the correlation between the lithologic boundaries and the index properties should include transition zones where the index data show variability between the major lithologic units. This summary describes the index properties in the context of four zones of similar index data character. The zones are associated with the lithology as follows:

Index zone 1 = lithologic Unit 1
Index zone 2 = lithologic Unit 2
Index zone 3 = lithologic Units 3 and 4
Index zone 4 = lithologic Unit 5

Index property subdivisions (Fig. 37) show an upper zone between the seafloor and 101 mbsf (lithologic Unit 1 equivalent). Below Zone 1, the index properties change significantly in a transitional region above Zone 2 between 101 and 126 mbsf. Zone 2, the equivalent to lithologic Unit 2, extends to a depth of 186 mbsf. Below Zone 2, the index properties are again transitional to a depth of 204 mbsf. The index properties are consistent within Zone 3 to a depth of 442 mbsf (lithologic Units 3 and 4 equivalents). Significant changes in index properties define Zone 4, which extends to the bottom of Hole 672A.

Table 7. Index properties summary, Hole 672A.

Core	Sec.	Int. (cm)	Depth (mbsf)	% Water (wet)	% Water (dry)	Porosity[a] (%)	Bulk density[a] (g/cm^3)	Grain density (g/cm^3)	Bulk density[b] (g/cm^3)	Porosity[b] (%)
1	2	73	2.23	44.7821	81.1008	68.9890	1.5783	2.6337	1.5414	67.8773
2	2	73	5.53	53.9261	117.0430	76.6479	1.4562	2.6926	1.4289	75.7598
2	3	134	7.64	50.9187	103.7440	74.5897	1.5008	2.6971	1.4679	73.4896
2	4	73	8.53	53.5764	115.4070	76.4687	1.4622	2.6442	1.4268	75.1645
2	6	73	11.53	48.1716	92.9445	73.2379	1.5576	2.7443	1.5124	71.6285
3	4	75	18.05	54.7303	120.8980	78.1329	1.4626	2.5909	1.4058	75.6602
3	6	75	21.05	42.6927	74.4980	69.4674	1.6670	2.6657	1.5783	66.2555
4	2	75	24.55	55.7991	126.2400	79.0699	1.4518	2.7344	1.4109	77.4017
4	4	75	27.55	45.7920	84.4746	71.0889	1.5905	2.7990	1.5560	70.0462
4	6	75	30.55	42.1416	72.8358	67.1882	1.6334	2.7169	1.5970	66.1702
5	2	69	33.99	42.7487	74.6685	68.5615	1.6431	2.6470	1.5737	66.1509
5	3	133	36.13	49.9121	99.6488	73.5585	1.5099	2.5775	1.4626	71.7911
5	4	75	37.05	48.8986	95.6893	74.0350	1.5511	2.6195	1.4825	71.2851
5	6	74	40.04	45.7774	84.4250	71.8270	1.6075	2.7202	1.5428	69.4362
6	2	71	43.51	42.0515	72.5671	67.7768	1.6512	2.6650	1.5879	65.6568
6	4	75	46.55	41.6701	71.4387	67.2693	1.6539	2.7072	1.6025	65.6530
6	6	75	49.55	43.2946	76.3500	70.1162	1.6592	2.6058	1.5574	66.3036
7	2	20	52.50	39.4489	65.1498	64.9680	1.6872	2.7161	1.6401	63.6110
7	4	10	55.40	38.7422	63.2445	63.6887	1.6842	2.6845	1.6446	62.6461
7	6	20	58.50	38.8158	63.4409	63.7046	1.6814	2.7127	1.6498	62.9612
8	2	50	62.30	40.7701	68.8336	67.0514	1.6849	2.7766	1.6311	65.3774
8	4	50	65.30	38.9763	63.8707	64.7005	1.7007	2.8043	1.6673	63.8834
8	4	80	65.60	41.6041	71.2449	66.6731	1.6418	2.6958	1.6012	65.4969
8	6	50	68.30	41.5474	71.0788	66.0702	1.6292	2.7020	1.6033	65.4951
9	2	70	72.00	42.7126	74.5584	67.9711	1.6303	2.7104	1.5869	66.6413
9	4	70	75.00	39.0189	63.9852	63.7368	1.6735	2.7046	1.6446	63.0921
9	6	70	78.00	40.0418	66.7828	64.9228	1.6611	2.6776	1.6220	63.8583
10	2	70	81.50	44.2327	79.3166	69.1727	1.6021	2.6998	1.5618	67.9248
10	4	70	84.50	41.8718	72.0336	67.0165	1.6397	2.6743	1.5926	65.5671
10	6	70	87.50	36.9000	58.4786	61.9637	1.7204	2.7159	1.6831	61.0616
11	2	70	91.00	39.5474	65.4189	64.8212	1.6792	2.7061	1.6362	63.6221
11	3	137	93.17	38.4969	62.5935	63.9046	1.7007	2.7013	1.6525	62.5483
11	4	70	94.00	42.9517	75.2900	68.2872	1.6288	2.7099	1.5831	66.8550
11	6	70	97.00	39.5388	65.3954	64.5285	1.6720	2.6591	1.6259	63.2101
12	2	75	100.55	41.9272	72.1977	67.3051	1.6446	2.7065	1.5983	65.8859
12	4	75	103.55	34.2333	52.0526	58.9227	1.7634	2.6930	1.7245	58.0455
12	6	75	106.55	34.7139	53.1720	60.1492	1.7752	2.6886	1.7147	58.5249
13	2	75	110.05	34.1765	51.9215	59.0690	1.7707	2.7399	1.7381	58.4012
13	3	130	112.10	34.5986	52.9018	60.0159	1.7771	2.7004	1.7199	58.5066
13	4	75	113.05	33.3770	50.0983	57.9630	1.7792	2.6778	1.7359	56.9688
14	2	82	119.31	36.6117	57.7577	62.2121	1.7409	2.6752	1.6781	60.4073
14	3	60	120.59	36.1062	56.5098	61.7073	1.7509	2.7595	1.7077	60.6196
15	2	78	125.58	46.6283	87.3653	71.8045	1.5777	2.7485	1.5352	70.3766
15	4	53	128.33	49.6270	98.5192	74.4055	1.5360	2.6248	1.4738	71.9227
17	2	83	144.63	43.8364	78.0514	69.5685	1.6259	2.4284	1.5127	65.2304
17	3	133	146.63	40.8579	69.0843	63.8436	1.6009	2.3067	1.5221	61.1958
17	4	86	147.66	40.7060	68.6511	65.1446	1.6396	2.3676	1.5395	61.6562
18	4	58	156.88	38.8088	63.4223	62.6386	1.6536	2.5490	1.6114	61.5026
19	2	7	162.87	50.0113	100.0450	74.2060	1.5201	2.6665	1.4753	72.5462
19	4	90	166.70	47.4867	90.4281	72.1095	1.5557	2.7202	1.5182	70.8831
20	1	35	171.15	45.0552	82.0008	69.3283	1.5764	2.5892	1.5291	67.7507
20	2	88	173.18	47.2392	89.5348	72.0047	1.5616	2.6111	1.5032	69.8284
21	2	137	183.17	59.6316	147.7190	80.4787	1.3827	2.4497	1.3342	78.2655
21	4	99	185.79	58.7182	142.2370	79.4904	1.3869	2.4727	1.3465	77.7680
22	2	115	192.45	50.9014	103.6720	74.0822	1.4911	2.5392	1.4441	72.2955
22	4	74	195.04	46.2381	86.0054	69.8585	1.5479	2.5878	1.5126	68.7785
22	6	27	197.57	41.5382	71.0519	65.8160	1.6233	2.5529	1.5716	64.2032
23	1	25	199.55	40.6492	68.4898	64.1538	1.6169	2.5699	1.5885	63.5025
23	1	49	199.79	40.0294	66.7485	64.3770	1.6476	2.6014	1.6051	63.1825
23	2	67	201.47	40.7939	68.9016	66.2351	1.6634	2.6078	1.5948	63.9777
23	4	61	204.41	42.8379	74.9411	66.8665	1.5992	2.5860	1.5599	65.7132
23	6	70	207.50	34.6153	52.9411	59.4978	1.7609	2.6268	1.6998	57.8574
24	2	64	210.94	35.5970	55.2724	60.9100	1.7530	2.5079	1.6506	57.7910
24	4	75	214.05	33.7215	50.8785	58.1539	1.7668	2.2586	1.6023	53.1785
24	6	94	217.24	33.4548	50.2739	57.6941	1.7668	2.9753	1.8126	59.5995
25	2	98	220.78	32.4516	48.0420	58.4051	1.8439	2.6012	1.7305	55.2241
25	3	83	222.13	29.3074	41.4575	54.9181	1.9198	2.7721	1.8437	53.1221
25	4	40	223.20	31.0761	45.0876	58.3016	1.9220	2.7550	1.8022	55.0602
26	2	40	229.70	32.1098	47.2966	57.7333	1.8420	2.4859	1.7008	53.7184
26	4	75	233.05	29.7927	42.4354	54.1478	1.8620	2.9305	1.8808	55.0743
27	2	74	239.54	31.2023	45.3538	55.2173	1.8130	2.3956	1.6860	51.7546
27	4	74	242.54	33.9326	51.3606	61.0821	1.8442	2.0549	1.5285	51.0835
27	6	74	245.54	38.4451	62.4565	67.6848	1.8037	2.4542	1.5929	60.2406
28	2	71	249.01	31.1887	45.3249	55.4135	1.8203	2.2957	1.6514	50.6845
28	4	90	252.20	27.9955	38.8802	50.8770	1.8619	3.0035	1.9446	53.5044
29	2	75	258.55	32.0618	47.1926	55.7502	1.7814	2.4279	1.6830	53.0809
29	4	72	261.52	34.0221	51.5659	59.0769	1.7790	2.5434	1.6863	56.4259

Table 7 (continued).

Core	Sec.	Int. (cm)	Depth (mbsf)	% Water (wet)	% Water (dry)	Porosity[a] (%)	Bulk density[a] (g/cm³)	Grain density (g/cm³)	Bulk density[b] (g/cm³)	Porosity[b] (%)
30	2	62	267.92	26.4328	35.9301	49.6360	1.9238	2.6731	1.8713	48.6351
30	4	32	270.62	28.5868	40.0300	51.3379	1.8399	2.6708	1.8259	51.3221
30	6	66	273.96	32.0063	47.0724	56.2726	1.8012	2.6636	1.7572	55.2998
31	1	74	276.04	34.4701	52.6020	60.3356	1.7933	2.5675	1.6858	57.1458
31	4	30	280.10	29.2478	41.3384	53.4347	1.8717	2.6425	1.8033	51.8636
32	2	40	286.70	27.4067	37.7538	50.3168	1.8809	2.7004	1.8603	50.1288
32	4	65	289.95	28.9234	40.6932	52.6093	1.8635	2.6789	1.8218	51.8088
33	2	22	296.02	23.2892	30.3598	44.7572	1.9689	2.7441	1.9689	45.0808
33	4	90	299.70	30.2767	43.4242	54.7621	1.8530	2.7018	1.8020	53.6431
33	6	54	302.34	30.7308	44.3642	55.4064	1.8471	2.7153	1.7972	54.3002
34	2	49	305.79	25.0787	33.4733	47.8010	1.9527	2.6267	1.8828	46.4310
34	4	48	308.78	26.9057	36.8096	50.7075	1.9308	2.6549	1.8549	49.0720
35	2	49	315.29	30.8584	44.6308	55.9480	1.8575	2.5568	1.7452	52.9644
35	4	118	318.98	26.6505	36.3337	49.7356	1.9119	2.6657	1.8640	48.8465
36	2	64	324.94	31.4141	45.8027	56.2808	1.7800	2.5900	1.7400	53.8900
36	4	92	328.22	32.6800	48.5500	56.8700	1.7800	2.5900	1.7200	55.3700
36	6	25	330.55	27.4982	37.9276	51.0434	1.9017	2.6223	1.8312	49.5146
36	6	70	331.00	27.3800	37.7100	50.5900	1.8900	2.6600	1.8500	49.7400
37	2	60	334.40	27.5100	37.9500	51.5100	1.9180	2.5800	1.8200	49.1100
37	4	48	337.28	27.2800	37.5100	50.5100	1.8970	2.6430	1.8430	49.4300
37	6	80	340.60	28.5990	40.0500	52.6870	1.8870	2.6730	1.7550	51.2320
38	2	91	344.21	28.4940	39.8480	52.6370	1.8930	2.6730	1.8290	51.2330
38	5	58	348.38	31.1942	45.3366	56.0807	1.8418	2.5759	1.7453	53.5407
39	2	90	353.70	26.5730	36.1896	49.6148	1.9129	2.6515	1.8606	48.6145
39	2	104	353.84	27.6940	38.3011	51.5038	1.9053	2.6127	1.8239	49.6691
39	3	88	355.18	30.6946	44.2888	56.1582	1.8744	2.6276	1.7708	53.4471
39	3	104	355.34	25.5095	34.2453	48.8829	1.9632	2.6000	1.8635	46.7468
40	2	84	363.14	33.7879	51.0298	58.3409	1.7690	2.6527	1.7215	57.1930
40	4	126	366.56	32.8714	48.9677	57.7498	1.7999	2.6274	1.7307	55.9428
40	6	46	368.76	26.2189	35.5360	49.1139	1.9191	2.6425	1.8647	48.0732
41	1	125	371.55	20.4837	25.7603	40.6666	2.0340	2.6834	2.0114	40.5094
41	2	61	372.41	28.7013	40.2551	52.1244	1.8606	2.6633	1.8211	51.3930
42	2	100	382.30	25.4902	34.2106	47.9126	1.9257	2.6401	1.8792	47.1007
42	4	79	385.09	27.0219	37.0274	50.1359	1.9008	2.5971	1.8317	48.6728
43	2	44	391.24	26.7322	36.4856	48.7785	1.8694	2.5981	1.8378	48.3132
43	4	12	393.92	30.2910	43.4534	53.4874	1.8090	2.5272	1.7457	52.0070
43	6	85	397.65	19.5407	24.2864	39.8606	2.0899	2.6816	2.0340	39.0796
44	1	8	398.88	25.4911	34.2122	47.3572	1.9033	2.5100	1.8289	45.8529
44	4	15	403.45	28.1456	39.1703	50.5974	1.8418	2.6259	1.8195	50.3567
46	1	0	417.80	21.5729	27.5069	42.1977	2.0040	2.4918	1.9002	40.3196
46	1	112	418.92	24.9589	33.2603	46.8391	1.9226	2.5819	1.8679	45.8472
48	1	1	436.81	24.6975	32.7977	46.9326	1.9468	2.5851	1.8746	45.5295
48	1	124	438.04	24.2176	31.9568	46.5704	1.9701	2.4790	1.8411	43.8571
48	4	73	442.03	18.4058	22.5577	35.7861	1.9919	2.7755	2.1077	38.1379
49	2	75	448.55	23.6969	31.0563	43.9626	1.9007	2.4970	1.8590	43.3287
49	4	119	451.99	26.4093	35.8868	48.0395	1.8636	2.4848	1.8014	46.7948
50	2	58	457.88	27.4828	37.8983	48.8244	1.8201	2.4256	1.7592	47.5616
50	3	143	460.23	25.2024	33.6941	46.3277	1.8833	2.4238	1.7995	44.6146
51	2	78	467.58	27.7511	38.4104	50.6232	1.8689	2.5539	1.8018	49.1755
51	3	11	468.41	30.9109	44.7406	54.4968	1.8062	2.5752	1.7502	53.2027
52	1	0	474.80	27.2619	37.4795	49.4785	1.8594	2.4907	1.7878	47.9393
53	1	1	484.31	35.8109	55.7896	62.4161	1.7856	4.3522	2.0055	70.5184
53	6	40	492.20	33.4710	50.3103	58.8346	1.8009	1.3396	1.2124	40.3723

[a] Calculated on basis of wet and dry measurements.
[b] Calculated on basis of dry volumetric measurements.

Within the uppermost zone (lithologic Unit 1 equivalent), the bulk density increases slightly from 1.46 g/cm^3 near the seafloor to 1.64 g/cm^3 at 100.6 mbsf (Fig. 37). The maximum and minimum densities within this zone are 1.72 g/cm^3 and 1.45 g/cm^3, respectively. The porosity and water content follow this same trend by decreasing within this zone, with maxima at 24.5 mbsf of 126% (water content) and 79.1% (porosity) and minima at 87.5 mbsf of 58% (water content) and 62% (porosity). The grain density is consistent within this zone, with a range of 2.58 to 2.80 g/cm^3 and a mean value of 2.61 g/cm^3 (Fig. 37), although the data for the upper 50 mbsf is quite scattered. With the exception of the data scatter near the seafloor within Zone 1, the sediment behaves as a normally consolidating sequence with similar ranges of water content, porosity, and density as Unit 1 at Site 671.

The transition between Zones 1 and 2 shows little variation in index properties (Fig. 37). The bulk density is consistently higher than the overlying zone with little variability (1.74 to 1.78 g/cm^3). Similarly, the water content varies between 50% and 58% and the porosity between 58% and 62%, both of which are lower than in Zone 1. The grain density (Fig. 37) is comparable to the overlying unit, with little change (2.68 to 2.75 g/cm^3).

Below the transition within Zone 2 (lithologic Unit 2 equivalent), the index properties change sharply (Fig. 38). The bulk density decreases from 1.63 g/cm^3 at 145 mbsf to 1.39 g/cm^3 at 186 mbsf. The porosity and water content data both increase within this zone to maxima at 183 mbsf of 81% and 148%, respectively. The grain density is quite scattered throughout, but generally increases with depth below seafloor. The mean grain density within the Unit 2 equivalent is 2.56 g/cm^3.

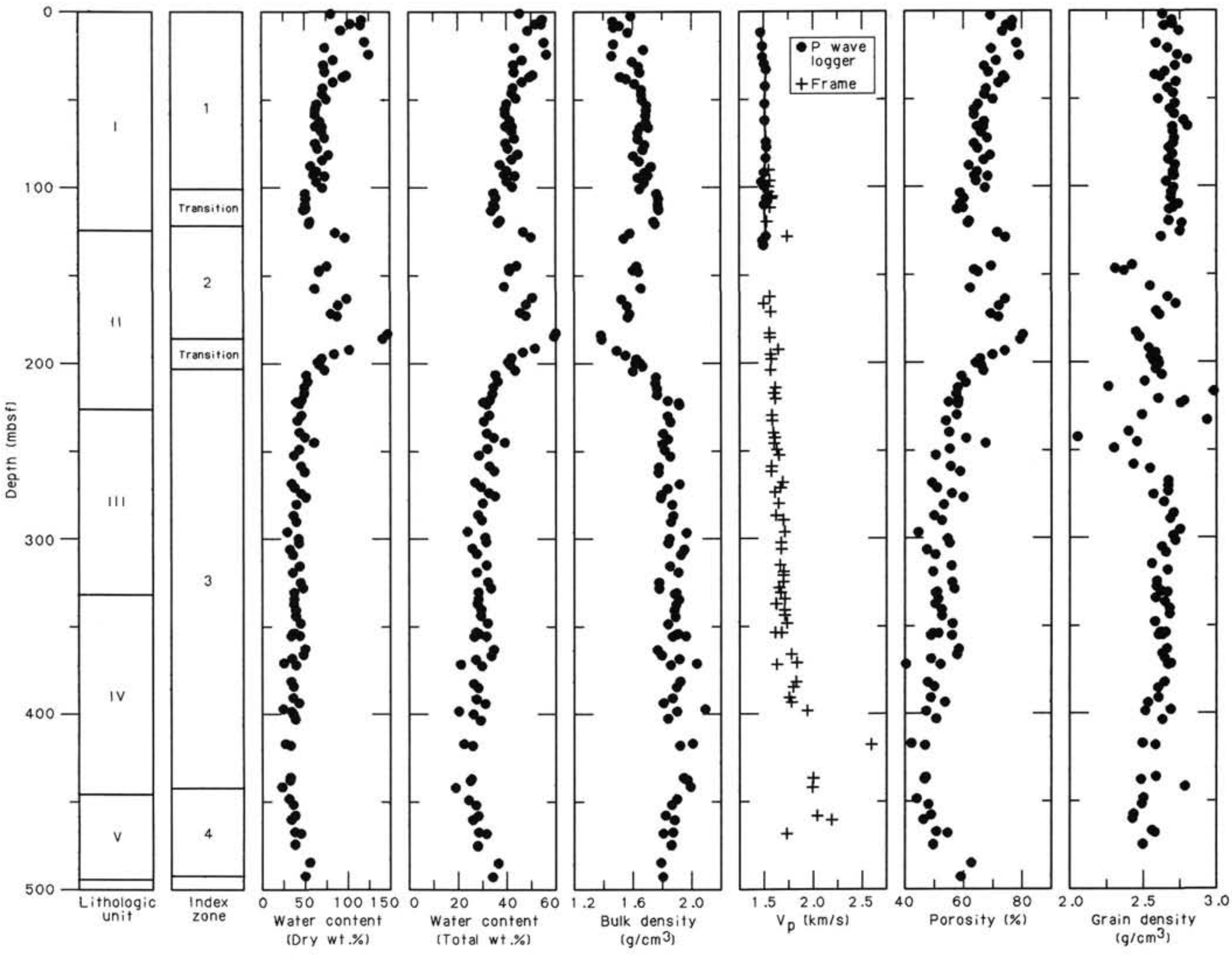

Figure 37. Index property zones, lithologic units, grain density, water content (calculated as the percentage of the total sample weight), water content (calculated as a percentage of the dry sample weight), porosity, bulk density and compressional wave velocity plotted vs. depth below seafloor.

Below Zone 2, the index properties reverse trends within a transition zone (Fig. 37). Between 186 mbsf and 204 mbsf, the water content decreases from 104% to 75%. The porosity decreases over the same interval from 74% to 67% and the bulk density increases from 1.44 to 1.56 g/cm^3. The grain density within this transition zone shows a distinct increase with depth that contrasts with the scatter in Zone 2. The grain density increases from a low value of 2.48 g/cm^3 at 192 mbsf to a high of 2.61 g/cm^3 at 201 mbsf. This transition zone lies above the lithologic boundary between Units 2 and 3 at 228 mbsf and may extend to that depth.

In Zone 3, below 204 mbsf, the index properties become more consistent with depth. The properties show increasing bulk density, decreasing water content and porosity, and generally decreasing grain density with depth below seafloor. The water content ranges from 55% at 211 mbsf to 25% at 398 mbsf. The porosity varies between 61% and 40% at 243 and 398 mbsf, respectively. The bulk density low within this zone (1.75 g/cm^3) occurs at 211 mbsf and the highest density (2.09 g/cm^3) occurs at 398 mbsf. The grain density data are scattered at the top of this zone, but vary between 2.30 and 2.98 g/cm^3 with a mean of 2.61 g/cm^3. The variation of water content, density, and porosity within this zone suggests a normally consolidating sequence, similar to that of Zone 1.

Within Zone 4, the equivalent to lithologic Unit 5, the properties again reverse trend, although not as dramatically as in the transition above Zone 3. The water content and porosity increase from 22% and 36% at 442 mbsf to 50% and 59% respectively at the bottom of the hole (492 mbsf). The bulk density decreases from 1.99 g/cm^3 to 1.80 g/cm^3 within this zone and the grain densities, with a mean value of 2.53 g/cm^3, are slightly lower than those within Zone 3.

Discussion

The index properties at Site 672 are divided into four zones. Of these divisions, Zones 1 and 3 can be described as sediment sequences which appear to be normally consolidated and therefore useful as reference sediment units. The reverse trend in porosity in Zone 2 may have been caused by anisotropic loading conditions (e.g., overpressure lateral stresses higher than the vertical overburden stress) or by compositional changes within the zone (e.g., changes in radiolarian distribution). Zone 4 may have also been affected by lateral loading, although the change in lithology coincident with the boundary between Zones 3 and

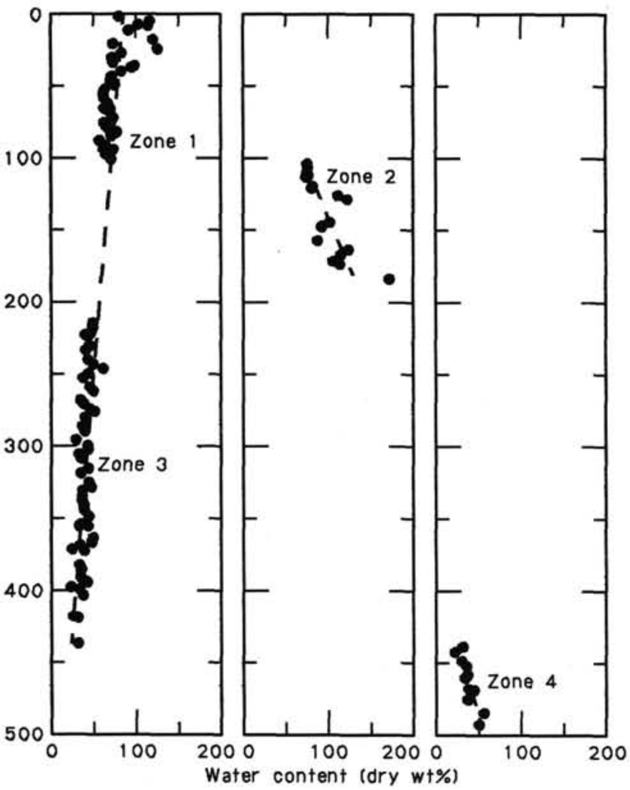

Figure 38. A. Linear least-squares approximation of water content vs. depth below seafloor in index Zones 1 and 3 and Zones 2 and 4.

4 could result in the changed water content profile. These trends are shown in Figure 38, where linear approximations to the water content vs. depth profile are shown for Zones 1 and 3 and Zones 2 and 4. A normally (one-dimensional, axial) consolidating sedimentary sequence is suggested in Zones 1 and 3, while Zones 2 and 4 show a reverse behavior.

Compressional Wave Velocity

Methods

The methods employed at Site 672 for measurement of sediment compressional wave velocity are detailed in Chapter 1 of this volume. Compressional wave velocities were measured using the *P*-wave logger and, for samples deeper than Core 110-672A-10H, also with the Hamilton frame velocimeter. Velocities were measured in the whole-round core with the logger and in two directions with the Hamilton frame.

Results

Compressional wave velocities measured on samples from the core are listed in Table 8. In general, the velocities measured with the propagation direction parallel to the axis of the core (vertical) are slightly slower than those measured with propagation normal to the axis of the core (horizontal). This slight anisotropy has been observed many times before in ocean sediment samples and may be the result of stress release opening fine cracks parallel to bedding as a result of overburden loss during core recovery. These fine cracks tend to reduce V_p in the vertical direction. There is also the possibility of a preferred fabric anisotropy induced by stress anisotropy (and potential shear failure) or depositional processes.

In the uppermost section of Hole 672A, between 90 and 120 mbsf, velocities were selected from the *P*-Wave Logger and in-

Table 8. Compressional wave velocity, Hole 672A.

Core	Sec.	Int. (cm)	Depth (mbsf)	Vel (A)[a] (km/s)	Vel (B)[b] (km/s)
11	2	68	90.98	1.5900	1.5800
11	4	68	93.98	1.5400	1.5500
11	6	68	96.98	1.5700	1.5800
12	2	72	100.52		1.5600
12	4	72	103.52	1.5800	1.5700
12	6	72	106.52	1.5800	1.6000
13	2	70	110.00	1.5600	1.5800
13	4	70	113.00	1.5600	1.5900
14	3	60	120.59	1.5500	1.5500
15	4	53	128.33	1.7700	1.7600
19	2	7	162.87	1.6300	1.5800
19	4	90	166.70	1.4900	1.5200
20	1	35	171.15		1.5900
21	2	137	183.17	1.5800	1.5800
21	4	99	185.79		1.5800
22	2	115	192.45	1.6000	1.6700
22	4	74	195.04	1.5900	1.5900
22	6	27	197.57	1.5800	1.6000
23	4	61	204.41	1.5800	1.5900
24	4	76	214.06	1.6000	1.6400
24	6	94	217.24	1.6000	1.6200
25	2	98	220.78	1.6000	1.6400
26	2	46	229.76	1.5900	1.6000
26	4	75	233.05	1.6000	1.6100
27	2	74	239.54	1.6000	1.6200
27	4	74	242.54	1.6300	1.6400
27	6	74	245.54	1.5400	1.6300
28	2	71	249.01	1.6200	1.6600
28	4	90	252.20	1.6400	1.6900
29	2	75	258.55	1.6100	1.6100
29	4	72	261.52		1.6000
30	2	62	267.92	1.6900	1.7200
30	4	32	270.62	1.6600	1.6900
30	6	66	273.96	1.6200	1.6400
31	2	74	277.54	1.6000	
31	4	30	280.10	1.6300	1.6800
32	2	40	286.70	1.6500	1.6500
32	4	65	289.95	1.6700	
32	4	65	289.95	1.6700	1.7300
33	2	22	296.02	1.7000	1.7400
33	6	54	302.34	1.6600	1.7000
34	2	49	305.79	1.6800	1.7000
34	4	48	308.78	1.6900	
35	2	49	315.29	1.6400	1.6900
35	4	118	318.98	1.6700	1.7300
35	6	25	321.05	1.6600	1.7200
36	2	64	324.94		1.7200
36	4	92	328.22		1.6800
36	6	70	331.00	1.6600	1.7000
37	2	59	334.39	1.6600	1.7400
37	4	48	337.28	1.6900	1.6500
37	6	80	340.60	1.5800	1.7400
38	2	91	344.21		1.7400
38	5	58	348.38	1.6800	1.7600
39	2	90	353.70	1.8300	1.7000
39	2	104	353.84		1.6400
40	2	84	363.14	1.6500	
40	4	126	366.56	1.6800	1.8000
41	1	125	371.55	1.8500	1.8600
41	2	61	372.41		1.6500
42	2	100	382.30	1.8200	1.8500
42	4	79	385.09	1.8700	1.8200
43	2	44	391.24	1.7300	1.7700
43	4	12	393.92		1.8000
44	1	8	398.88		1.9600
46	1	45	418.25		2.6100
46	1	112	418.92	1.7900	
46	2	35	419.65		3.1800
48	1	1	436.81		2.0100
48	4	73	442.03	2.0000	2.0000
49	2	75	448.55	2.6600	
49	4	75	451.55	2.2300	
50	2	58	457.88	1.9500	2.0500
50	3	143	460.23	2.0600	2.1900
51	2	78	467.58	1.9300	
51	3	11	468.41	1.7300	1.7400
52	1	1	474.81	1.9400	
53	1	1	484.31		2.0300
53	6	40	492.20		2.0000

[a] Velocity measured parallel to cored direction.
[b] Velocity measured perpendicular to cored direction.

cluded on the plot of Hamilton frame velocities vs. depth presented in Figure 37. The general agreement between the two measurements is quite good, although the logger appears to have an offset of approximately -0.03 km/s when compared to the Hamilton Frame. It was observed that an interval of recovered core consisting of 100% water was indicating a V_p of 1.48 km/s, also suggesting an offset on the order of 0.02–0.03 km/s for the logger data.

Both the logger and the Hamilton Frame describe a very gradual increase in velocity with depth to almost 375 mbsf, at which point the sediments become more indurated. Velocities in claystones recovered from below 375 mbsf increase to near 1.90 km/s, while velocities in carbonate and sand-rich layers are often greater. The single "slow" data point recorded at approximately 475 mbsf may be the result of sample disturbance and is suspect.

Discussion

Perhaps the major observation to be made about the velocity profile at Site 672 is its lack of expression. Much like the upper 500 m of Site 671, there are very few excursions in velocity at this site which might be chosen as the possible sources for reflectors in the seismic data. It is particularly interesting that the local maximum in porosity seen between 180 and 200 mbsf appears to have no expression at all in the velocity data. This can be explained by the fact that soft sediments have very little variation in their acoustic properties unless there are major changes in water content. In Figure 39 the velocity-water content data from both Sites 671 and 672 are shown. There is little change in velocity from changes in water content when the water contents are large (>30% of total sample weight). It is only at the lower water content values that velocity variation is seen, and these are the result of lithification. Figure 39 illustrates that, for unlithified sediments, there is little variation of velocity with water content, and for partially lithified sediments there is very little variation of water content with velocity. This suggests that in the upper sediments seismic reflections will be related to density changes, while lower in the sediment sequence reflections will be related to changes in compressional velocity.

Thermal Conductivity

Methods

Measurements of thermal conductivity were made using the needle probe technique of Von Herzen and Maxwell (1959), which is described in detail in Chapter 1, this volume. Thermal conductivity measurements were attempted on every other section of a core, but disturbed areas were avoided when they were seen through the core liner. Several measurements were eliminated after viewing the split core on the sampling table, and several others remain questionable based on core observations after measurement.

Results

Determinations of the thermal conductivity of cored sediments from Site 672 are plotted vs. depth below seafloor in Figure 40 and listed in Table 9. Thermal conductivity values quickly increase from a near-surface low of 0.88 W/m °C to a local maximum in excess of 1.5 W/m °C at around 30 mbsf. Below this level the thermal conductivity fluctuates between 1.1 and 1.3 W/m °C until near the Unit 1/Unit 2 boundary. The exact nature of the change from this regime into lower values between 140 and 210 mbsf is unclear because of the disturbed state of the core recovered in this interval.

Although the low values of thermal conductivity seem to coincide with lithologic Unit 2, it is worth noting that the measured values increase above the Unit 2/Unit 3 boundary. The thermal conductivities measured in the bottom 20 m of Unit 2

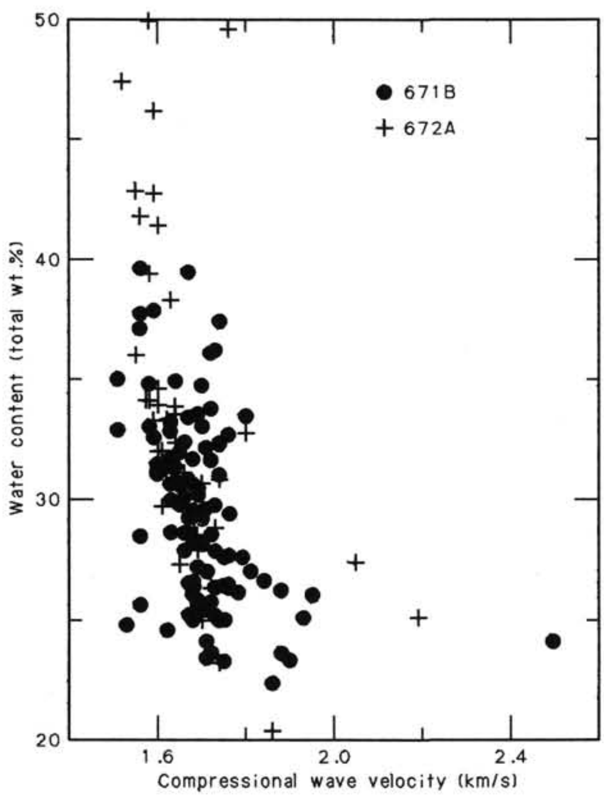

Figure 39. Compressional wave velocity vs. water content calculated as weight percentage of the total sample. Hole 672A is compared to Hole 671B.

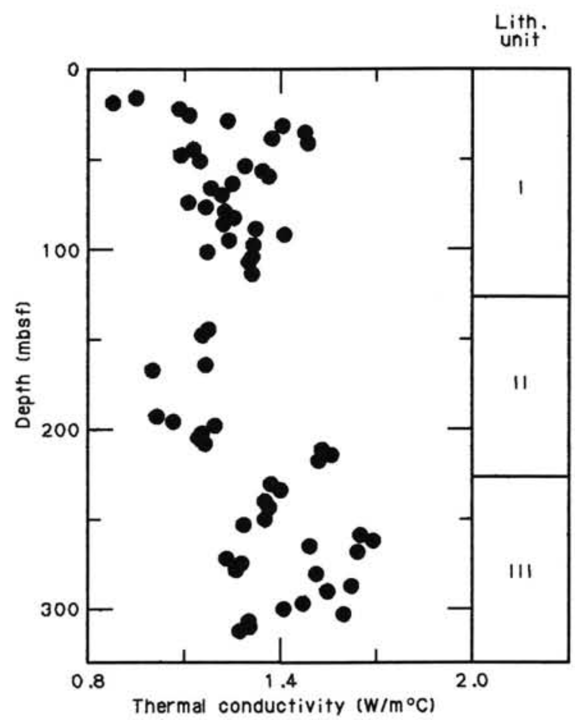

Figure 40. Thermal conductivity variation with depth below seafloor, Hole 672A.

Table 9. Thermal conductivity, Hole 672A.

Core	Sec.	Int. (cm)	Depth (mbsf)	Cal/cm·°C·s ($\times10^{-4}$)	W/m°C
3	2	75	15.05	22.8000	0.9530
3	4	75	18.05	20.9000	0.8800
3	6	75	21.05	25.7000	1.0800
4	2	75	24.55	26.6000	1.1100
4	4	75	27.55	29.4000	1.2300
4	6	75	30.55	33.4000	1.4000
5	2	75	34.05	35.2000	1.4700
5	4	75	37.05	32.6000	1.3700
5	6	75	40.05	35.4300	1.4800
6	2	75	43.55	26.9000	1.1200
6	4	75	46.55	26.0000	1.0900
6	6	75	49.55	27.3000	1.1400
7	2	20	52.50	30.8000	1.2900
7	4	10	55.40	31.9000	1.3400
7	6	20	58.50	32.4000	1.3600
8	2	50	62.30	29.9000	1.2500
8	4	50	65.30	28.3000	1.1800
8	6	50	68.30	29.0000	1.2100
9	2	70	72.00	26.5000	1.1100
9	4	70	75.00	27.8000	1.1600
9	6	70	78.00	29.1000	1.2200
10	2	70	81.50	29.7800	1.2500
10	2	70	81.50	29.8000	1.2500
10	4	70	84.50	29.1000	1.2200
10	4	70	84.50	29.1300	1.2200
10	6	70	87.50	31.5000	1.3200
10	6	70	87.50	31.4500	1.3200
11	2	70	91.00	33.6200	1.4100
11	4	70	94.00	29.7000	1.2400
11	6	70	97.00	31.3400	1.3100
12	2	75	100.55	27.9000	1.1700
12	4	75	103.55	31.2300	1.3100
12	6	75	106.55	31.1200	1.3000
13	4	75	113.05	31.3500	1.3100
17	2	75	144.55	27.9900	1.1700
17	4	75	147.55	27.5000	1.1500
19	2	100	163.80	27.7000	1.1600
19	4	100	166.80	23.8600	0.9990
22	2	80	192.10	24.2000	1.0100
22	4	80	195.10	25.2800	1.0600
22	6	30	197.60	28.4900	1.1900
23	2	70	201.50	27.5700	1.1500
23	4	70	204.50	27.2500	1.1400
23	6	70	207.50	27.7900	1.1600
24	2	70	211.00	36.5900	1.5300
24	4	70	214.00	37.3700	1.5600
24	6	70	217.00	36.1900	1.5200
26	2	75	230.05	32.6200	1.3700
26	4	75	233.05	33.5200	1.4000
27	2	75	239.55	32.3500	1.3500
27	4	75	242.55	32.5500	1.3600
28	2	75	249.05	32.2100	1.3500
28	2	75	249.05	32.2100	1.3500
28	4	75	252.05	30.7200	1.2900
28	4	75	252.05	30.7200	1.2900
29	2	75	258.55	39.4600	1.6500
29	4	75	261.55	40.2800	1.6900
29	6	83	264.63	35.6100	1.4900
30	2	64	267.94	39.1300	1.6400
30	4	83	271.13	29.2900	1.2300
30	6	71	274.01	30.6400	1.2800
31	2	75	277.55	30.0300	1.2600
31	4	48	280.28	36.1700	1.5100
32	2	40	286.70	38.8000	1.6200
32	4	60	289.90	37.0400	1.5500
33	2	60	296.40	35.1000	1.4700
33	4	60	299.40	33.6800	1.4100
33	6	60	302.40	38.2900	1.6000
34	2	100	306.30	30.5100	1.3000
34	4	70	309.00	31.1000	1.3000
34	6	15	311.45	30.2200	1.2700
35	2	75	315.55	21.9400	0.9180
35	4	75	318.55	19.5600	0.8190

are similar to those of Unit 3, alternating between values of 1.2 and 1.3 W/m °C. Measurements were terminated near 300 mbsf when the sediments became too indurated for probe placement.

Discussion

Thermal conductivity values are plotted vs. water content in Figure 41. The Site 672 data present a picture similar to that of Site 671, but with more data scatter in the upper unit. The four determinations from the lower section of lithologic Unit 2, plus all of the data from Unit 3, are in better agreement with the Unit 2 data from Site 671. This trend may reflect a system that is becoming dominated by the framework mineralogy, while the Unit 1–Unit 2 trend, which is in general agreement with previous soft sediment determinations, represents a water-dominated system.

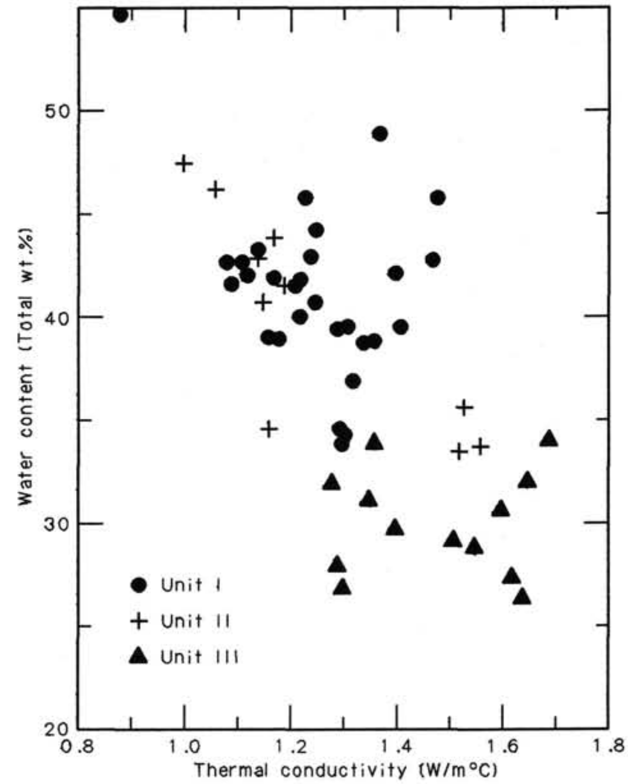

Figure 41. Thermal conductivity vs. water content calculated as weight percentage of the total sample at Hole 672A.

Formation Factor

Methods

Formation-factor measurements were made on even-numbered sections of split cores from the upper 10 cores of Hole 672A. Electrical problems developed with the sensor while we measured Core 110-672A-11X, so the program was terminated pending repair of the tool. Procedures were essentially those outlined in Chapter 1, this volume.

Results

Formation-factor values are plotted vs. depth below seafloor in Figure 42 and listed in Table 10. These values generally increase with depth and show some regular variation that is probably related to small fluctuations in the water content of the core. The increase in the formation factor (F) over the first 90 mbsf at Site 671 is a little greater than at Site 672. This may be attributed to a greater concentration of pelagic carbonate in the upper sediments of Site 672 and, consequently, a more open, less electrically resistive, fabric.

Discussion

Data from both Holes 672A and 671B are plotted in Figure 43 as a function of water content calculated as a percent of total sample weight. The formation-factor data from Hole 672A sed-

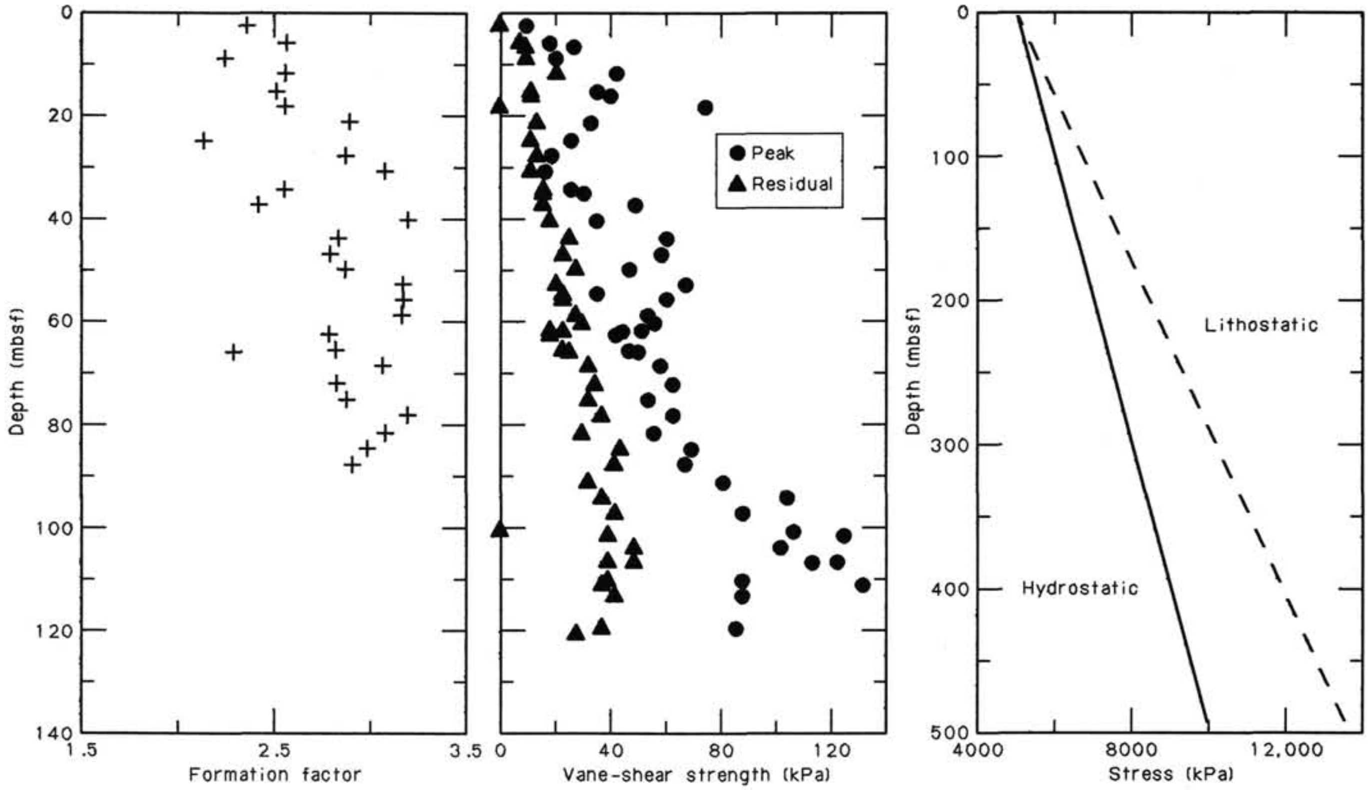

Figure 42. Formation factor, peak and residual vane shear strengths measured in the APC-recovered sediments from Hole 672A, and hydrostatic and total overburden stress curves calculated for the sedimentary section cored at Site 672.

Table 10. Sediment formation factor, Hole 672A.

Core	Sec.	Int. (cm)	Depth (mbsf)	F-horiz.	F-vert.
1	2	72	2.22	2.1000	2.3000
2	2	72	5.52	2.2000	2.5000
2	4	72	8.52	2.1000	2.2000
2	6	72	11.52	2.2000	2.5000
3	2	70	15.00	2.2600	2.4500
3	4	70	18.00	2.2000	2.5000
3	6	67	20.97	2.7000	2.8200
4	2	72	24.52	2.0000	2.1000
4	4	72	27.52	2.6000	2.8000
4	6	72	30.52	2.9000	3.0000
5	2	71	34.01	2.4600	2.5000
5	4	69	36.99	2.2300	2.3800
5	6	68	39.98	2.5600	3.1200
6	2	72	43.52	2.4600	2.7700
6	4	69	46.49	2.4800	2.7200
6	6	69	49.49	2.6400	2.8000
7	2	12	52.42	3.0900	3.1000
7	4	15	55.45	2.9800	3.0900
7	6	12	58.42	2.8400	3.1000
8	2	44	62.24	2.7000	2.7400
8	4	42	65.22	2.7200	2.7600
8	4	86	65.66	2.5000	2.2600
8	6	42	68.22	2.7100	3.0000
9	2	60	71.90	2.5200	2.7700
9	4	65	74.95	2.6800	2.8100
9	6	64	77.94	2.9100	3.1300
10	2	64	81.44	2.9200	3.0100
10	4	58	84.38	2.7000	2.9200
10	6	74	87.54	2.8000	2.8600

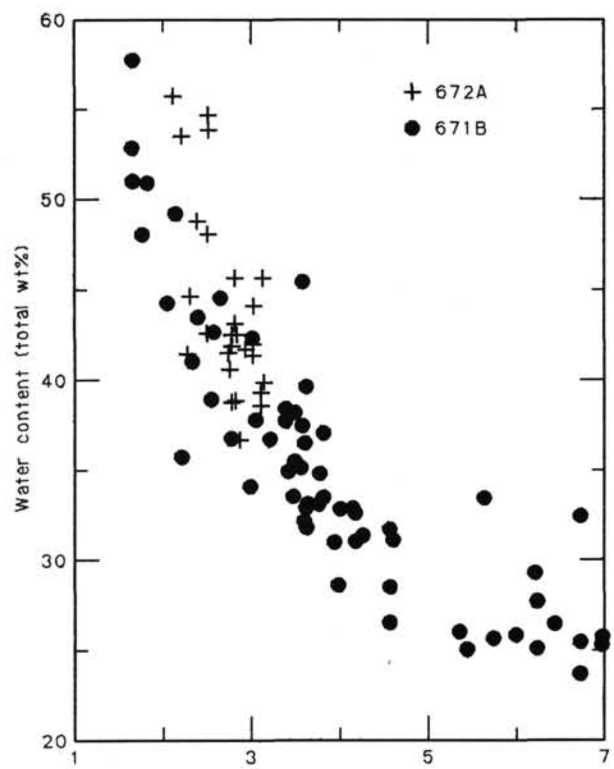

Figure 43. Formation factor vs. water content calculated as weight percentage of the total sample from Hole 672A. Results from Hole 671B are shown for comparison.

iments are in agreement with the trend observed at Site 671, although there seems to be a broader range of water content values for a given formation factor than was seen previously.

Undrained Shear Strength

Results

The methods used to measure the undrained shear strength of the sediment at Site 672 are described in Chapter 1. A total of 48 strength measurements were made from 2.25 to 120.6 mbsf in the APC section of Hole 672A (Table 11). The peak shear strength vs. depth profile shows three major trends within the tested portion of the hole, and a secondary trend in the lower 20 m (Figure 42). Peak strength increases monotonically within the upper trend from 9.2 kPa at 2.25 mbsf to nearly 74 kPa at 18 mbsf. This rapid strength increase in the upper 20 m ends with a downcore drop in peak strength to values between 16 and 33 kPa. The second strength trend extends from 20 to 55 mbsf. Peak strengths in this depth range are approximately 60 kPa, although the data are scattered.

Table 11. Vane shear strength, Hole 672A.

Core	Sec.	Int. (cm)	Depth (mbsf)	Peak (kPa)	Residual (kPa)
1	2	75	2.25	9.2000	
2	2	75	5.55	17.5000	7.4000
2	3	1	6.31	26.3000	9.5000
2	4	75	8.55	19.8000	9.9000
2	6	65	11.45	41.5047	20.7410
3	2	75	15.05	34.5835	11.5278
3	3	1	15.81	39.1901	11.5278
3	4	75	18.05	73.7736	
3	6	75	21.05	32.2689	13.8198
4	2	75	24.55	25.3703	11.5278
4	4	75	27.55	18.4264	13.7744
4	6	75	30.55	16.1344	11.5278
5	2	70	34.00	25.3703	16.1344
5	3	1	34.81	29.9542	16.1344
5	4	75	37.05	48.4260	16.1344
5	6	74	40.04	34.5835	18.4491
6	2	70	43.50	59.9538	25.3703
6	4	75	46.55	57.6846	23.0527
6	6	75	49.55	46.1113	27.6623
7	2	19	52.49	66.8524	20.7410
7	3	50	54.30	34.5835	23.0557
7	4	10	55.40	59.9538	23.0557
7	6	20	58.50	53.0326	27.6623
7	7	20	60.00	55.3245	29.9542
8	1	118	61.48	50.7179	18.4491
8	1	130	61.60	43.7967	23.0557
8	2	50	62.30	41.5047	18.4491
8	4	50	65.30	46.1113	23.0557
8	4	80	65.60	49.5606	25.3703
8	6	50	68.30	57.6392	32.2689
9	2	70	72.00	62.2458	34.5835
9	4	70	75.00	53.0326	32.2689
9	6	70	78.00	62.2458	36.8981
10	2	70	81.50	55.3245	29.9769
10	4	70	84.50	69.1670	43.7967
10	6	70	87.50	66.8524	41.5047
11	2	70	91.00	80.6948	32.2689
11	4	70	94.00	103.7510	36.8981
11	6	70	97.00	87.6161	41.5047
12	2	75	100.55	106.0650	
12	3	1	101.31	124.4920	39.1901
12	4	75	103.55	101.4360	48.4260
12	6	60	106.40	122.1770	39.1901
12	6	75	106.55		48.4260
13	2	75	110.05	112.9640	39.1901
13	3	1	110.81	87.6161	36.8981
13	4	75	113.05	131.4130	41.5047
14	2	88	119.37	87.6161	36.8981
14	3	60	120.59	85.3014	27.6623
33	2	18	259.98	179.8340	

The third principal trend in the vane shear strength data is from 55 to 120 mbsf. The overall depth trend within this lower segment exhibits a well-constrained depth dependency, increasing from 40 to 131 kPa over the interval. This lower section can, however, be subdivided into two secondary trends. The upper subgroup extends from 55 to 87 mbsf, and the other subgroup is below this latter depth. The lower subgroup has a high-strength gradient and the upper boundary correlates with the transition from upper to lower Pliocene sediments.

Residual vane strengths at Site 672 range from a low of 7.4 kPa at 5.6 mbsf to a maximum of 48.4 kPa at 103 and 106 mbsf. The residual strengths slowly and steadily increase with depth (Figure 42). The sensitivity of the tested sediments is calculated assuming the residual strength approximates the remolded value (Pyle, 1984). Using this criteria, sensitivities range from 1.5 to about 3.3.

The effective overburden stress and total overburden (or lithostatic) stress were calculated for the Site 672 sedimentary section using bulk density measurements and assuming hydrostatic pore-pressure conditions. The two stress curves show a slight deviation from a linear increase with depth (Fig. 42). This deviation is more pronounced in the effective overburden curve. The source of this feature at approximately 180–200 mbsf is the siliceous composition (higher porosity and lower density) of lithologic Unit 2. Numerous faults and en echelon veins also occur at this sub-bottom depth, and the interval corresponds to the equivalent stratigraphic position of the top of the décollement zone found at Site 671.

Discussion

The physical properties of the hemipelagic sediment blanket at Site 672 serve as a reference against which the measurements from the accreted and subducted sequences can be compared. Undrained vane shear strengths within the upper 110 mbsf of Site 672 sediments have a lower rate of strength increase with depth compared to those in the upper 270 mbsf for Site 671. Linear regressions computed only for the APC-recovered sediments at each site yield the following relationships:

Site 671- Strength = 8.6 + 1.51 * Depth $r = 0.92$
Site 672- Strength = 16.5 + 0.70 * Depth $r = 0.89$

where strength units are in kPa and depth in meters. The slightly greater strength of the sediments from Site 671 may be a reflection of tectonic strengthening of this accreted material and/or the result of diagenesis.

Summary

The physical property data define four major zones in Hole 672A. These zones are primarily defined by the index property data, but are consistent with the thermal conductivity, shear strength, and formation-factor measurements. The zones show two different characteristics. First, a character that can probably be attributed to a normally consolidated sequence (Zones 1 and 3); and second, a character that shows increasing water content with depth (Zones 2 and 4) which may either be attributed to stress conditions not expected at a "reference" site, to compositional changes within the zone, or both.

The compressional velocity data do not resolve the zones, primarily because of the dependence of the measurement on the water within the sediment-water matrix. The shear strength data, although limited to the upper index zone, shows lower strength than at Site 671. As defined by the index data, Zone 1 shows no evidence of influence from stresses at the deformation front, suggesting that the higher strengths at Site 671 are owing to stresses induced within the sediment column during accretion.

When compared to the biostratigraphy, the transition between index Zone 1 and Zone 2 is coincident with the lower Pliocene/lower Miocene boundary. Below Zone 2, the transition falls within the lower Miocene/lower Oligocene lower bound. The distinct physical property break between Zones 3 and 4 does not correlate with any break in age.

The structural geologic profile at Site 672 shows very good correlation with the physical properties. At the upper physical property transition zone where low water content and porosity occur, the structural picture is a zone of normal faults and subvertical veins. At the base of Zone 2, where there is a peak in the water content and porosity profiles, the sediments show shear zones, fault surfaces and vein networks. Although the index data trends are opposed for the upper normal fault zone (110 mbsf) and the lower reverse fault zone (180 mbsf), the physical character of the sediments may be indicative of the maturity of the "future" décollement zone.

LOGGING RESULTS

Bad hole conditions similar to those encountered at Site 671 hindered attempts to log Hole 672A, and logging at two different levels in the hole yielded only 45 m of measurements. The first logging run utilized a Schlumberger DIL-LSS-GR-CAL string (see Logging Results section, Site 671, for a description) with the pipe set at 146.5 mbsf. We hoped that this would be far enough into the formation to avoid the sloughing problems which commonly plague logging operations in soft sediments. However, the tool string hit an obstruction 13 m out of the bit; after we raised the pipe the tool recorded over an open hole interval from 141.5 to 116 mbsf (Cores 110-672A-16X to -13H).

After pulling the tools out of the pipe, the bit was lowered to 188 mbsf. Some extra pipe was retained above the rig floor to push past any obstructions developed during the 3 hr required for logging tool rig-up and transit through pipe to open hole. Hitting the bridge on the first logging run damaged the Schlumberger cable head, and the backup cable head failed in the water column 200 m below the rig floor, necessitating a run with the Lamont Multichannel Sonic (MCS) tool. The MCS tool encountered a bridge only 33 m into the open hole. After obtaining a log in this section and pulling the MCS out of the hole, logging was discontinued because of the poor hole conditions.

Schlumberger Run

Figure 44 displays the open-hole section of the log from the DIL-LSS-GR-CAL tool string. The Caliper and gamma-ray traces are in track 1, the three resistivity traces (ILD, ILM, SFLU) are in track 2, and the two slowness traces from the LSS tool (DT and DTL) are in track 3. Two important observations are immediately available from these logs.

First, the borehole diameter stays in the range of 7 to 8 in. over most of the open-hole section, despite the bit size of 11.4 in. This is a clear indication of the difficult hole conditions, with the constrictions forming as a result of some combination of slumping of the borehole wall and hole deformation. An observed increase in the cable tension across this interval also serves as an indicator of the confining hole size.

Second, the logs over this section are remarkably uniform in character, with almost all of the major changes in value (especially for the gamma-ray and resistivity curves) corresponding to changes in hole diameter and not to formation properties. All of the measured properties are consistent in magnitude with the same properties measured in Hole 671C. The ILD and ILM, which still seem to be the most accurate resistivity measurements, vary in a range from 1.5 to 3.0 ohm-m, with the minimum values occurring at depths of increased hole diameter. Except for hole size-affected sections, the gamma-ray curve maintains a nearly constant value of approximately 55 API units, while both the DT and DTL slowness curves remain between 190 μs/ft (1.60 km/s) and 195 μs/ft (1.56 km/s). The sonic velocities derived from these curves are compared with physical properties measurements in Table 12. Considering the uncertainties inherent in both types of measurement, the close correspondence is surprising, especially in light of the fact that the core velocities have not been corrected for decompaction resulting from removal of the weight of the sediment column. This correction usually raises the measured velocities by a few percent; in this case, an increase of a few percent in the core velocities would give even better agreement between the core and log values.

The logged section in Hole 672A extends from 116 to 141.5 mbsf, an interval almost identical in depth to the 110- to 132-mbsf logged section in Hole 671C. While these two sections contain different stratigraphic intervals (a lower Pliocene to upper Miocene section in Hole 671C as opposed to an upper Miocene section in Hole 672A) and are in what are thought to be two different tectonic environments (the toe of an accretionary prism and the undisturbed Atlantic abyssal plain), the almost identical values of resistivity and sonic velocity suggest that depth of burial is the dominant factor in determining the bulk, *in situ* physical properties. Sonic and resistivity logs, being sensitive to changes in porosity, are valuable tools for estimating the onset of overpressuring in a formation. By comparing a log from an overpressured zone with one from a hydrostatically pressured zone of the same lithology, it is possible to arrive at an estimate of the amount and extent of overpressuring (Ransom, 1986 and Fertl, 1976). Overpressuring shows up both in the value of a log measurement and in the gradient with depth. For the resistivity logs from Holes 672A and 671C, the gradients (approximately 0.01 ohm-m/m) and the values of resistivity have basically the same value, which implies that, over the sub-bottom depths covered by the logs, near-lithostatic pore pressures are either absent in the prism or present in both the toe of the prism and in the abyssal plain in front of the prism. Of course, overpressuring is often limited to intervals below a discrete low-permeability boundary, so the possible absence of large overpressures in the upper section of Hole 671C does not necessarily invalidate the numerous models of accretionary prisms which invoke the presence of near-lithostatic fluid pressures (e.g., Davis et al., 1983).

Lamont Multichannel Sonic Log

The MCS is a variable spacing, single-source 12- receiver sonic logging tool that records the full sonic waveforms produced by the interaction of the source signal with the formation. A MASSCOMP 561 computer at the surface controls the tool during logging, digitizes the data uphole, and records the digitized data on magnetic tape. The large number of receivers and their close (15 cm) spacings enable the operator to arrive at accurate estimates of the acoustical properties of the formation surrounding the borehole; these estimates are generally superior to those obtainable from a standard sonic log. The accuracy of the MCS tool, even under bad hole conditions, has been established in a number of holes on land and at sea (Salisbury, Scott, Auroux, et al., 1986). A typical analysis of the waveforms yields an estimate of compressional velocity and, in moderately fast formations, an estimate of shear velocity, allowing calculation of the formation's dynamic elastic constants.

Usually, for moderatly fast formations, four dominant modes of wave motion are found in an acoustic log waveform. The first two are the compressional and shear (or composite shear-pseudo Rayleigh after Tsang and Rader, 1979) head waves, which travel along the interface between the formation and the borehole fluid. The other two are the tube (or Stoneley) wave, a form of surface wave that propagates along the wall of the borehole at a speed slightly below the borehole fluid speed, and the normal modes,

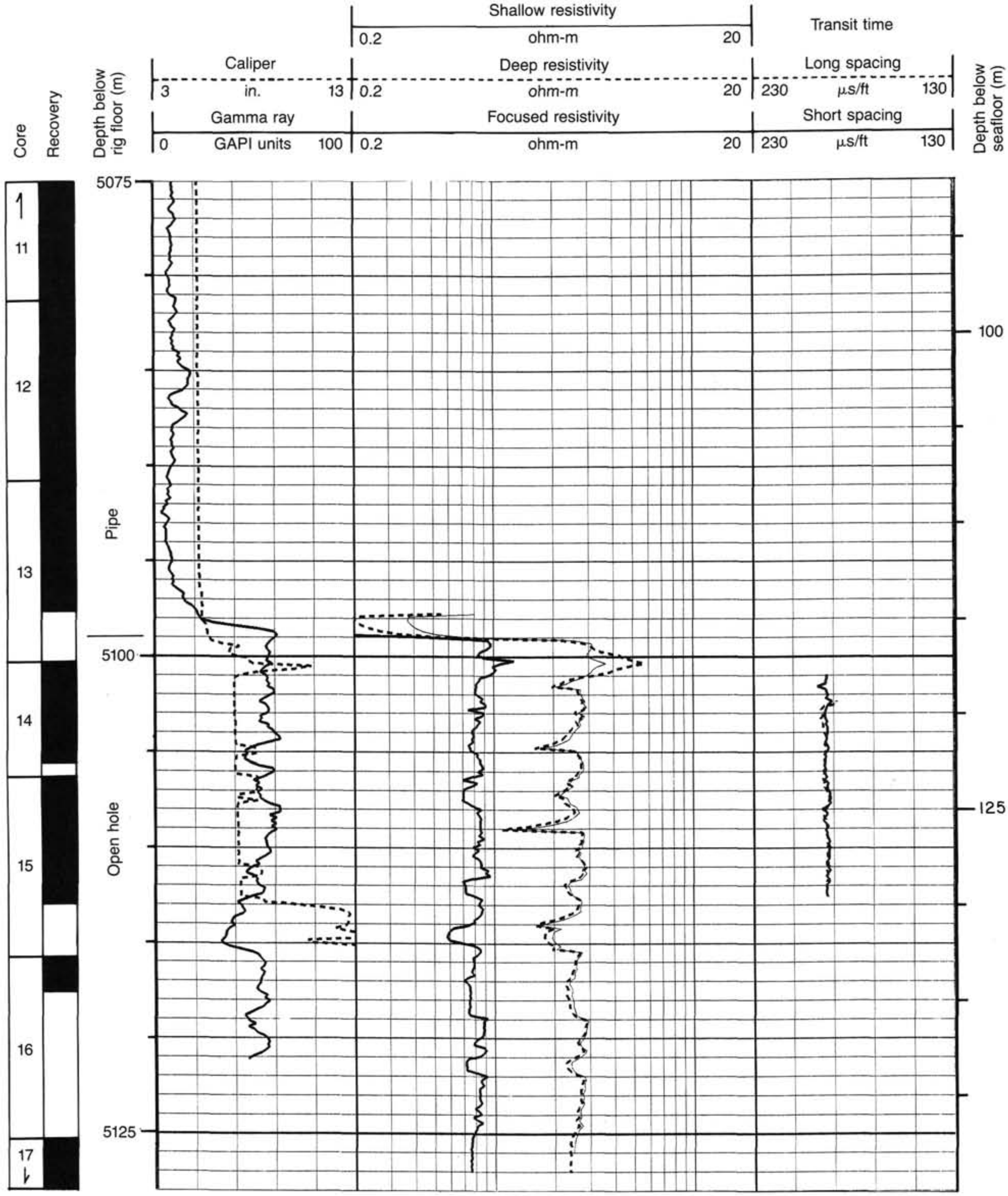

Figure 44. Schlumberger logs run in Hole 672A. Note the small caliper readings and the correspondence of low resistivity and gamma-ray values with increases in hole diameter.

which are trapped or guided waves propagating in the borehole. In a fast formation, the compressional and shear waves arrive at the receivers ahead of the other waves, allowing for the calculation of both compressional and shear velocity (see Fig. 45). In a slow formation, however, such as the soft claystone/mudstone penetrated at all of the Leg 110 sites, the weak shear wave is refracted away from the borehole, making calculation of the shear velocity impossible without the use of an inversion technique (e.g., Cheng et al., 1986). Figure 46 shows typical waveforms recorded in Hole 672A; note that while the compressional wave is visible, the fluid wave dominates the entire waveform behind the compressional arrival.

Velocity for the compressional part of the full waveform is determined by a semblance technique similar to that used in

Table 12. Comparison of LSS-derived velocities with core data.

Depth (m) rig floor	Depth (m) sub-bottom	V_{DT} (km/s)	V_{DTL} (km/s)	V_{core} (km/s)
5102.81	119.11	1.57	1.57	
5102.96	119.26	1.57	1.57	
5103.11	119.41	1.57	1.57	
5103.26	119.56	1.54	1.54	
5103.42	119.72	1.57	1.57	
5103.57	119.87	1.58	1.58	
5103.72	120.02	1.58	1.58	
5103.87	120.17	1.57	1.57	1.55
5104.03	120.33	1.60	1.60	1.55
5104.18	120.48	1.58	1.58	1.55
5104.33	120.63	1.58	1.58	1.55
5104.48	120.78	1.57	1.57	
5104.64	120.94	1.57	1.57	
5104.79	121.09	1.57	1.57	
5104.94	121.24	1.57	1.57	
5105.09	121.39	1.58	1.58	
5105.25	121.55	1.57	1.57	
5105.40	121.70	1.58	1.58	
5105.55	121.85	1.58	1.58	
5105.70	122.00	1.58	1.58	
5105.86	122.16	1.58	1.58	
5106.01	122.31	1.58	1.58	
5106.16	122.46	1.57	1.57	
5106.31	122.61	1.58	1.58	
5106.46	122.76	1.58	1.58	
5106.62	122.92	1.58	1.58	
5106.77	123.07	1.57	1.57	
5106.92	123.22	1.57	1.57	
5107.07	123.37	1.57	1.57	
5107.23	123.53	1.57	1.57	
5107.38	123.68	1.57	1.57	
5107.53	123.83	1.57	1.57	
5107.68	123.98	1.56	1.56	
5107.84	124.14	1.57	1.57	
5107.99	124.29	1.58	1.58	
5108.14	124.44	1.57	1.57	
5108.29	124.59	1.58	1.58	
5108.45	124.75	1.58	1.58	
5108.60	124.90	1.58	1.58	
5108.75	125.05	1.59	1.59	
5108.90	125.20	1.59	1.59	
5109.06	125.36	1.59	1.59	
5109.21	125.51	1.59	1.59	
5109.36	125.66	1.59	1.59	
5109.51	125.81	1.58	1.58	
5109.67	125.97	1.56	1.56	
5109.82	126.12	1.58	1.58	
5109.97	126.27	1.58	1.58	
5110.12	126.42	1.57	1.57	
5110.28	126.58	1.56	1.56	
5110.43	126.73	1.58	1.58	
5110.58	126.88	1.58	1.58	
5110.73	127.03	1.57	1.57	
5110.89	127.19	1.58	1.58	
5111.04	127.34	1.58	1.58	
5111.19	127.49	1.58	1.58	
5111.34	127.64	1.59	1.59	
5111.50	127.80	1.58	1.58	
5111.65	127.95	1.59	1.59	1.76 (anomalous
5111.80	128.10	1.59	1.59	1.76 readings from
5111.95	128.25	1.59	1.59	1.76 ash layer)
5112.11	128.41	1.59	1.59	
5112.26	128.56	1.59	1.59	
5112.41	128.71	1.58	1.58	
5112.56	128.86	1.58	1.58	
5112.72	129.02	1.58	1.58	
5112.87	129.17	1.59	1.59	
5113.02	129.32	1.58	1.58	
5113.17	129.47	1.57	1.57	
5113.33	129.63	1.58	1.58	
5113.48	129.78	1.59	1.59	
5113.63	129.93	1.58	1.58	
5113.78	130.08	1.58	1.58	
5113.94	130.24	1.58	1.58	
5114.09	130.39	1.58	1.58	
5114.24	130.54	1.58	1.58	

multichannel seismic surveys (Neidell and Taner, 1971). The semblance analysis is a statistical method used to detect arrival and associated slowness. This method assumes only that the formation is homogenous over the span of the receiver array; if discontinuities, such as fractures, are present on a smaller scale, then those discontinuities show up as isolated low values of semblance. The method is applied by passing a set of time windows of assumed arrival times and values of slowness through the waveforms. After this, the scalar semblance is computed for each windowed waveform, resulting in a measure of the presence or absence of an arrival with the specified slowness and arrival time. A high value of semblance (close to 1.0) indicates that the segments delimited by the window are identical in both shape and magnitude; thus, the window has identified a coherent arrival. A low value of semblance (less than 0.5) indicates that there is no coherent arrival for the specified value of slowness.

The result of a preliminary semblance calculation over 13 m of MCS data is shown in Figure 47. The high value of semblance (approximately 0.7) indicates that the estimated velocities are reasonably accurate. There appear to be four separate zones of slowness. From 201 to 202.5 mbsf the slowness is 192 μs/ft (1.59 km/s). This changes to approximately 187 μs/ft (1.63 km/s) from 202.5 to 204.5 mbsf and then to 190 μs/ft (1.60 km/s) from 204.5 to 210 mbsf. From 210 to 214 mbsf, the slowness drops to 185 μs/ft (1.65 km/s). As with the Schlumberger sonic data, the MCS velocity values correlate well with the physical properties values as is shown in Table 13.

The lithology of the section covered by the MCS data is a fairly homogenous mudstone/claystone (see Lithostratigraphy section, this chapter), so it is not certain what accounts for the small-scale velocity variations seen in the log. It should be noted, however, that Core 110-672A-23X, which is thought to contain part of the future décollement, spans most of this section of the log (199.3 to 208.8 mbsf). Given the steady steplike increase in velocity with depth shown in the log, it is possible that the formation of the décollement at this depth is partially determined by a transition from material of higher porosity and lower strength to material of lower porosity and greater strength.

SEISMIC STRATIGRAPHY

Seismic line CRV 128 clearly depicts five seismic sequences in the area of Site 672 (Fig. 48). Because of some inaccuracy in the location of the seismic line with respect to the hole, the correlation of the limits of the seismic sequences with the lithologies and physical properties observed at Site 672 are not perfectly constrained, and uncertainties of about 20 m (2 cores) are likely.

Seismic Unit A

The top of Unit A is the seafloor and its base is reflector A (depths: 0–110 mbsf). The unit shows little variation in thickness (0.130 s) except between SP90 to 130 where the thickness increases to 0.180 s, apparently owing to young down-faulting of a small block. This seismic unit comprises weak to very weak, discontinuous, parallel reflectors. Age control from Site 672 indicates a latest Miocene to early Pleistocene age, and its dominant facies are calcareous clays, calcareous muds, and marls.

Seismic Unit B

Unit B is bound by the weak reflector A at the top and the strong reflector B at the bottom (depths: 110–205 mbsf). It is parallel to unit A, and composed of discontinuous, parallel, weak to strong reflectors of relatively uniform thickness. Unit B is Miocene in age, bearing in mind the indeterminate two-core age at the lower boundary, reflector B. The dominant facies in Unit 3 are mudstones and claystones. Reflector A may be re-

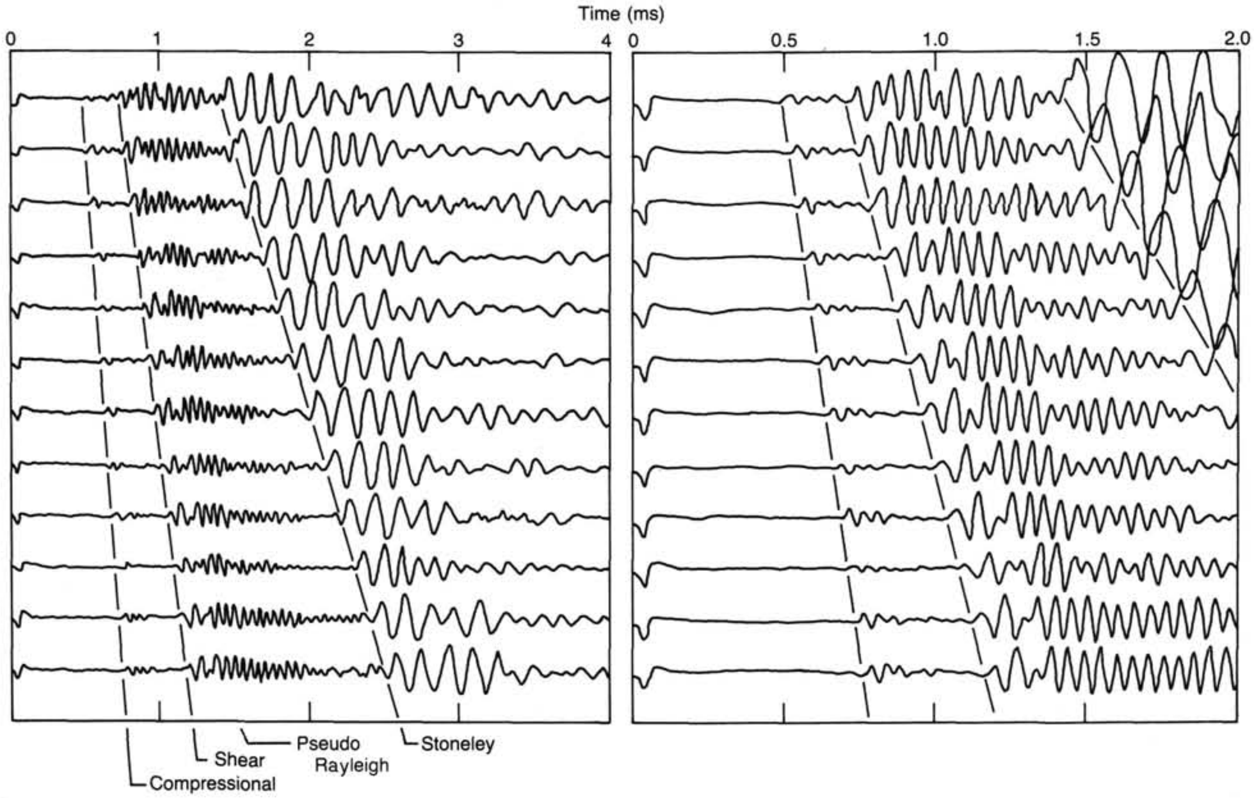

Figure 45. Typical multichannel sonic data recorded in granitic rock. In such fast formations the various wave arrivals are well separated.

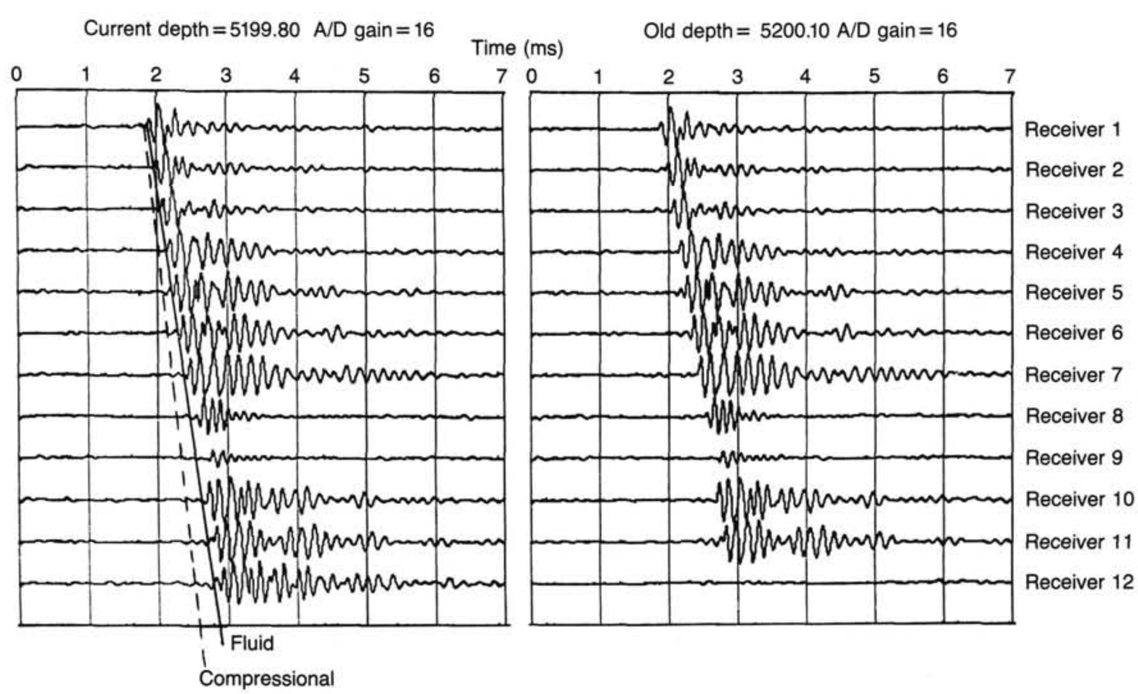

Figure 46. Waveforms recorded by the MCS tool in Hole 672A. Here the fluid arrival is slightly later than the compressional arrival, obscuring the later head and surface wave modes.

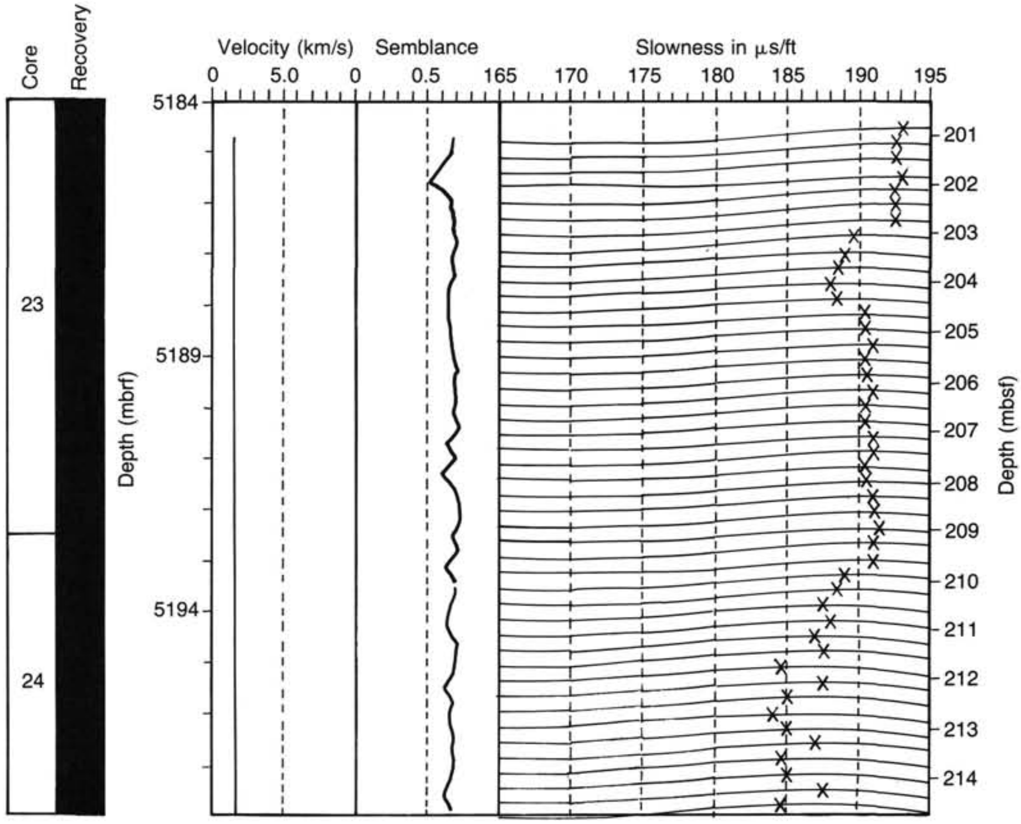

Figure 47. Velocity, semblance, and slowness for the interval 5184 m (200 mbsf) to 5198 m (214 mbsf). Note the steplike increase in velocity (decrease in slowness) across the section; this could be linked to the future location of the décollement. Points on slowness curve mark positions of maximum semblance.

lated to a slight decrease in bulk density (about 10%) just below the Pliocene/Miocene boundary (depth: 120 mbsf).

Seismic Unit C

The top of Unit C is the strong low-frequency reflector B and its base is at reflector C, a prominent reflector with a slightly higher frequency than reflector B (depth: 205–370 mbsf). This unit is almost transparent, is parallel to the overlying seismic units and thickens from east to west (0.190 s at Site 672 to 0.240 s at SP 200). Unit C is late Oligocene to late Eocene in age; however, the exact age of reflector C is poorly constrained in the late Eocene. The lithology is made of alternating claystones, calcareous claystones and mudstones, mudstones, and thin beds of silt. Reflector B is probably generated by a nearly 20% increase in density at a 200 mbsf; however, velocities do not show any significant change at this depth.

Seismic Unit D

Unit D consist of prominent, moderately strong and continuous reflectors. The upper boundary of Unit D is reflector C, whereas its lower boundary is reflector D (depth: 370–470 mbsf). This seismic unit is 0.100 to 0.130 s thick along most of CRV 128 and is parallel to the overlying units. Unit D is of middle Eocene age and consists of alternating claystones, calcareous mudstones, marls and sands. Slight density and velocity variations explain the unit's acoustically layered appearance (see Physical Properties section).

Seismic Unit E

Unit E is the sedimentary seismic sequence immediately overlying oceanic crust (reflector E) and underlying Unit D from which it is separated by the strong, low-frequency reflector D (depth: 470–800 mbsf). Unit E shows weak to very weak parallel reflectors especially in its lower half. Large thickness variations occur in this unit owing to basement faulting; the highest measured thickness is 0.300 s at SP 70. Reflector D might be related to the slight decrease of density between 450 and 470 msbf. The age and lithology of this unit are not known, as only its uppermost part was drilled at Site 672. The three cores that penetrated into the top of this unit consist of lower Eocene siliceous claystones. Correlation with DSDP Site 543 suggests that the remainder of Unit E is made of clays and calcareous clays, ranging from early Eocene to Campanian age. Reflector E is the top of the faulted oceanic crust, found to be of Late Cretaceous age at DSDP Site 543.

Several normal faults have been described in Hole 672A (see Structural Geology section). These faults might be related to the subtle but clearly depicted ones observed on the seismic record (Fig. 49). Subtle variations of the seafloor topography are clearly related to recent normal displacements along these faults.

HEAT FLOW

Introduction

To determine the magnitude of any heat-flow anomalies within the Lesser Antilles accretionary complex, it is first necessary to establish a background reference. Site 672 is located on the northwestern edge of the Tiburon Rise, 6 km east of the deformation front and 20 km south of Site 543, the reference for Deep Sea Drilling Project Leg 78A (Biju-Duval, Moore, et al., 1984). Langseth et al. (1986) conducted the Leg 110 site survey, which included transects at 14°20′N and 14°35′N. The authors noted

Table 13. Comparison of MCS velocities with core velocities.

Depth (m) rig floor	Depth (m) sub-bottom	V_{MCS} (km/s)	V_{core} (km/s)
5184.7	201.0	1.58	
5185.0	201.3	1.58	
5185.3	201.6	1.58	
5185.6	201.9	1.58	
5185.9	202.2	1.58	
5186.2	202.5	1.58	
5186.5	202.8	1.58	
5186.8	203.1	1.61	
5187.1	203.4	1.61	
5187.4	203.7	1.61	1.59
5187.7	204.0	1.62	1.59
5188.0	204.3	1.62	1.59
5188.3	204.6	1.60	
5188.6	204.9	1.60	
5188.9	205.2	1.60	
5189.2	205.5	1.60	
5189.5	205.8	1.60	
5189.8	206.1	1.60	
5190.1	206.4	1.60	
5190.4	206.7	1.60	
5190.7	207.0	1.60	
5191.0	207.3	1.60	
5191.3	207.6	1.60	
5191.6	207.9	1.60	
5191.9	208.2	1.60	
5192.2	208.5	1.60	
5192.5	208.8	1.59	
5192.8	209.1	1.60	
5193.1	209.4	1.60	
5193.4	209.7	1.61	
5193.7	210.0	1.62	
5194.0	210.3	1.63	
5194.3	210.6	1.62	
5194.6	210.9	1.63	
5194.9	211.2	1.63	
5195.2	211.5	1.65	
5195.5	211.8	1.63	
5195.8	212.1	1.65	
5196.1	212.4	1.66	
5196.4	212.7	1.65	
5196.7	213.0	1.63	
5197.0	213.3	1.65	
5197.3	213.6	1.65	1.64
5197.6	213.9	1.63	1.64
5197.9	214.2	1.65	1.64

progressively lower heat-flow values from the abyssal plain westward, as is theoretically predicted. They also found no evidence of pore-water movement through the prism at these latitudes. However, at 15°30′N nearly the same latitude as ODP Site 672, they reported progressively higher heat flow values while moving up the accretionary complex. Langseth et al. (1986) suggested that local heat-flow highs at 15°30′N indicate significant upward flow of interstitial water through the sediment of the complex. One such high (125 mW/m^2) is located just 3 km west of Site 672. Moore and Biju-Duval (1984) noted the presence of a penetrating thrust on a seismic line east of the deformation front (their Figure 5A). Langseth (pers. comm., 1986) suggested that this thrust may act as a conduit for migration of warm fluid, resulting in the large measured heat flow.

Methods and Results

See Chapter 1 for a discussion of experimental methods, intertool calibration, and data reduction. Tool properties are summarized in Table 14 and measured temperatures are summarized in Table 15.

Hole 672A

The APC tool was deployed during collection of Cores 110-672A-2H, -4H, -6H, -8H, and -10H with a sampling interval of 15 s. Prior to taking Core 110- 672A-2H, the shoe was lowered past the bit, 3 m below mudline, to measure bottom-water temperature. The shoe was held in this position for 10 min and equilibrated to 2.20°C, which was corroborated (± 0.05°C) by later deployments of the same tool as well as the T-probe. After measuring bit temperature, the APC was fired into the sediment. Accurate sediment temperatures were determined with the APC tool at depths of 13.3 mbsf (Core 110-672A-2H, Fig. 50); 32.3 mbsf (Core 110-672A-4H, Fig. 51); and 52.3 mbsf (Core 110-672A-6H, Fig. 52). Records from deployments 110-672A-2H and -6H display frictional heating during penetration, followed by cooling of the coring shoe and tool. Temperatures for these deployments were extrapolated to 3.66°C (±0.05) and 6.65°C (±0.05), respectively. The temperature record from deployment for Core 110-672A-4H suggests that the APC tool moved slightly while in the sediment, so an equilibrium temperature of 4.30°C (±0.05) was calculated from only the first portion of the record. Probe malfunctions resulted in no data being recorded during lowerings for Cores 110-672A-8H and -10H.

The T-probe, mounted in the WSTP tool, was run successfully after Cores 110-672A-5H and -15X to depths of 42.3 and 133.8 mbsf, respectively (Figs. 53, 54). The APC tool and WSTP tool were run in tandem after Core 110-672A-15X. During this run the APC thermistor sat 60 cm behind the tip of the T-probe. The T-probe record for this lowering indicates sediment penetration and subsequent cooling while the APC tool record (Fig. 55) indicates that the shoe did not penetrate the sediment surface. The temperatures that were recorded with the T-probe after Core 110-672A-15X were extrapolated to an equilibrium temperature of 5.25°C (±0.05°C).

The temperature record for run after Core 110-672A-15X (Fig. 55) indicates that the WSTP-probe penetrated sediment after latch-in to the bit, but before lowering to the bottom of the hole. The probe was probably in contact with sediment fill that had fallen from the borehole wall. This fill was probably approaching the ambient sediment temperature at this depth when the probe was pressed in further to sample pore water. The temperature drops continuously during the 20 min that the probe remained in this position. Analysis of the pore-water sample collected at the time indicates seawater contamination. This evidence suggests that the fill was penetrated and cracked, allowing inflow of seawater. The 12.7°C temperature determined for this lowering was calculated from the cooling of the T-probe prior to penetration and cracking of the hole bottom, and is thus a lower bound. This value has an estimated error of 0.1°C.

Interpretations

A linear-least-squares best fit of the temperature values from Hole 672A yields a thermal gradient of 79°C/km (Fig. 56). This gradient is 160% higher than the sediment gradient estimated at Site 543 (Davis and Hussong, 1984). There is apparent concave-down curvature of the gradient from 0 to 35 mbsf, followed by a lesser degree of concave-up curvature from 35 to 50 mbsf. Thermal conductivity varies over this same interval (Fig. 56), with a steady increase to 40 mbsf (as the thermal gradient decreases) and a sharp decrease after 40 mbsf coinciding with a thermal gradient increase.

To calculate the heat flow at Site 672, changes in sediment thermal properties were taken into account by calculating the integrated thermal resistance of the sediment column at the depth of each temperature measurement (as in Bullard, 1939). Thermal conductivities were converted to thermal resistances with variations between adjacent thermal conductivity measurements assumed to be linear, and the thermal resistance was numerically integrated at each temperature-measurement depth using Simpson's rule (Burington, 1973). This method should be more precise than assuming thermal conductivity is a linear function of depth (as in Becker et al., 1983). The gradient of the linear-

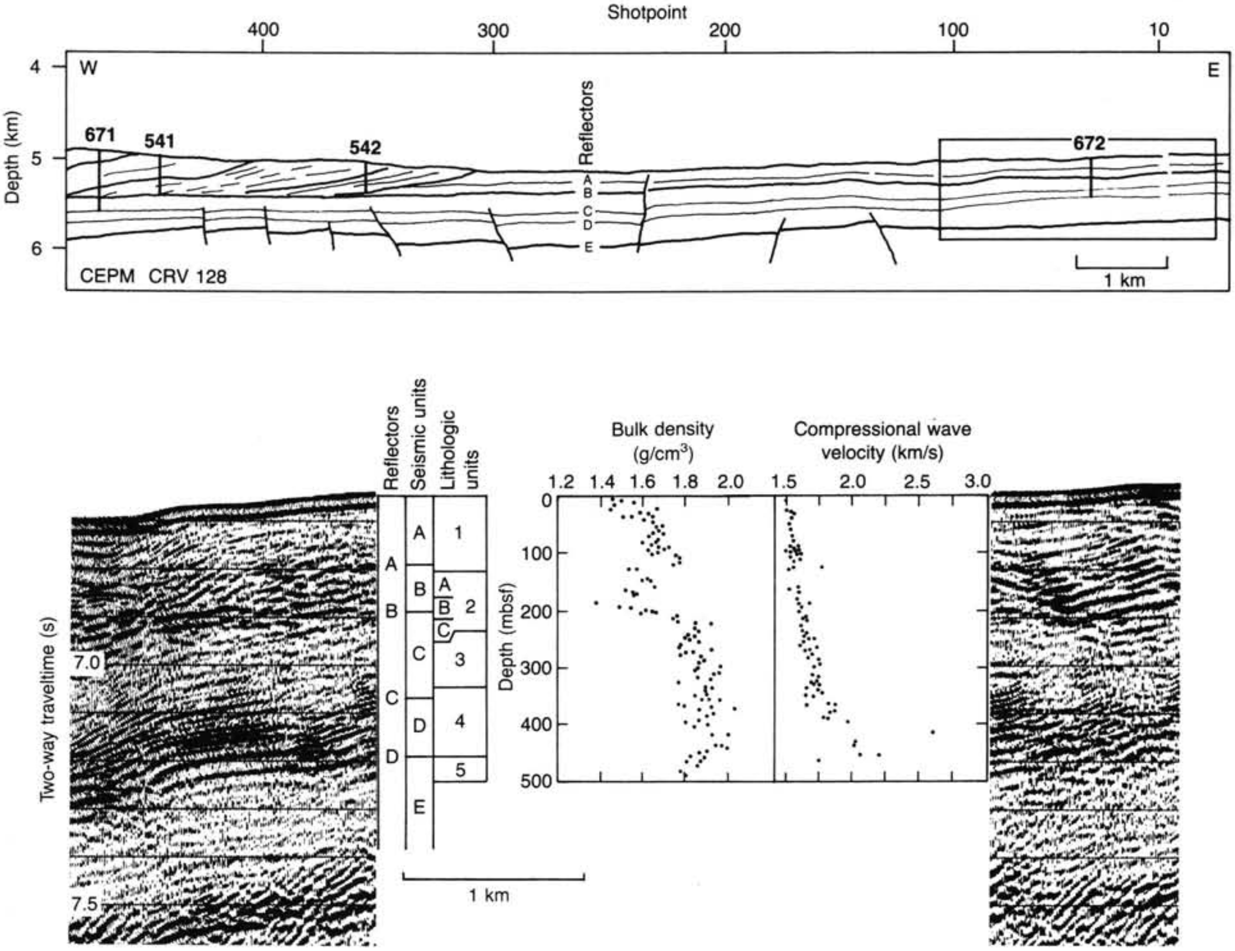

Figure 48. Top: Depth section of Line CRV 128 from Site 672 to Site 671. No vertical exaggeration. Bottom: Correlation of lithologic units and physical properties with seismic sequences of Line CRV 128.

least-squares best-fitting line through these temperature-thermal resistance values is the conductive heat flow (Fig. 57). Since there was no thermal conductivity data for the upper 15 m of sediment, it was necessary to assume a surface value. Langseth et al. (1986) reported surface conductivity values of 0.82 W/m °C from piston cores taken just east of the deformation front at 14°20′N. Davis and Hussong (1984) assumed a thermal conductivity of 1.04 W/m °C for the upper portion of the sediment column at Site 543. A series of values ranging from 0.75 to 1.00 W/m °C were used in the current analysis with resulting variations in the calculated heat flow ranging from 91 to 92 mW/m^2.

The heat flow found at Site 672 is approximately 80% greater than that theoretically predicted for 90-Ma crust. Earlier surveys of the Barracuda Ridge (Birch, 1970; Schubert and Peter, 1974), which is tectonically similar to the Tiburon Rise (Moretti and Ngokwey, 1985), revealed anomolously small heat-flow values. These were attributed to hydrothermal circulation in the basement and a lateral thermal conductivity contrast. By analogy, one might expect to find similar low values at reference Site 672, near the Tiburon Rise.

Two possible explanations for the large heat flow observed at Site 672 are:

1. Anomolously warm oceanic crust is maintaining a linear gradient of 70°C/km through the entire sediment column. This gradient requires a temperature of about 65°C at the base of the sedimentary sequence.

To maintain a strong geothermal gradient through the entire sediment column without fluid migration, the oceanic crust would have to be unusually thin. The Moho is anomolously shallow beneath the thick sedimentary sequence on the northern flank of the Barracuda Ridge (Moretti and Ngokwey, 1985). By analogy, the Tiburon Rise may be flanked to the north by thin oceanic crust. However, if the Moho is in fact shallower than normal beneath the northern flanks of both aseismic ridges, it would seem likely that the two would yield similar heat-flow values. The two yield dissimilar values, suggesting that different processes dominate the thermal regimes over the two features.

2. There is a steady supply of heat within the sedimentary sequence below 140 m. This heat source may be warm fluid moving through the sand layer(s) encountered at around 400 mbsf, through normal faults that penetrate the sedimentary sequence and basement, or through the "future décollement zone" at 175 to 195 mbsf (see sections on Structural Geology and Lithostratigraphy, this chapter). If at a depth of 400 mbsf, the heat source would have to maintain a sediment temperature of 32°C.

Geochemical evidence (Geochemistry section, this chapter), and the linear thermal gradient encountered at Site 672, do not suggest significant pore-water movement up through the sediment column, although lateral flow is still conceptually feasible

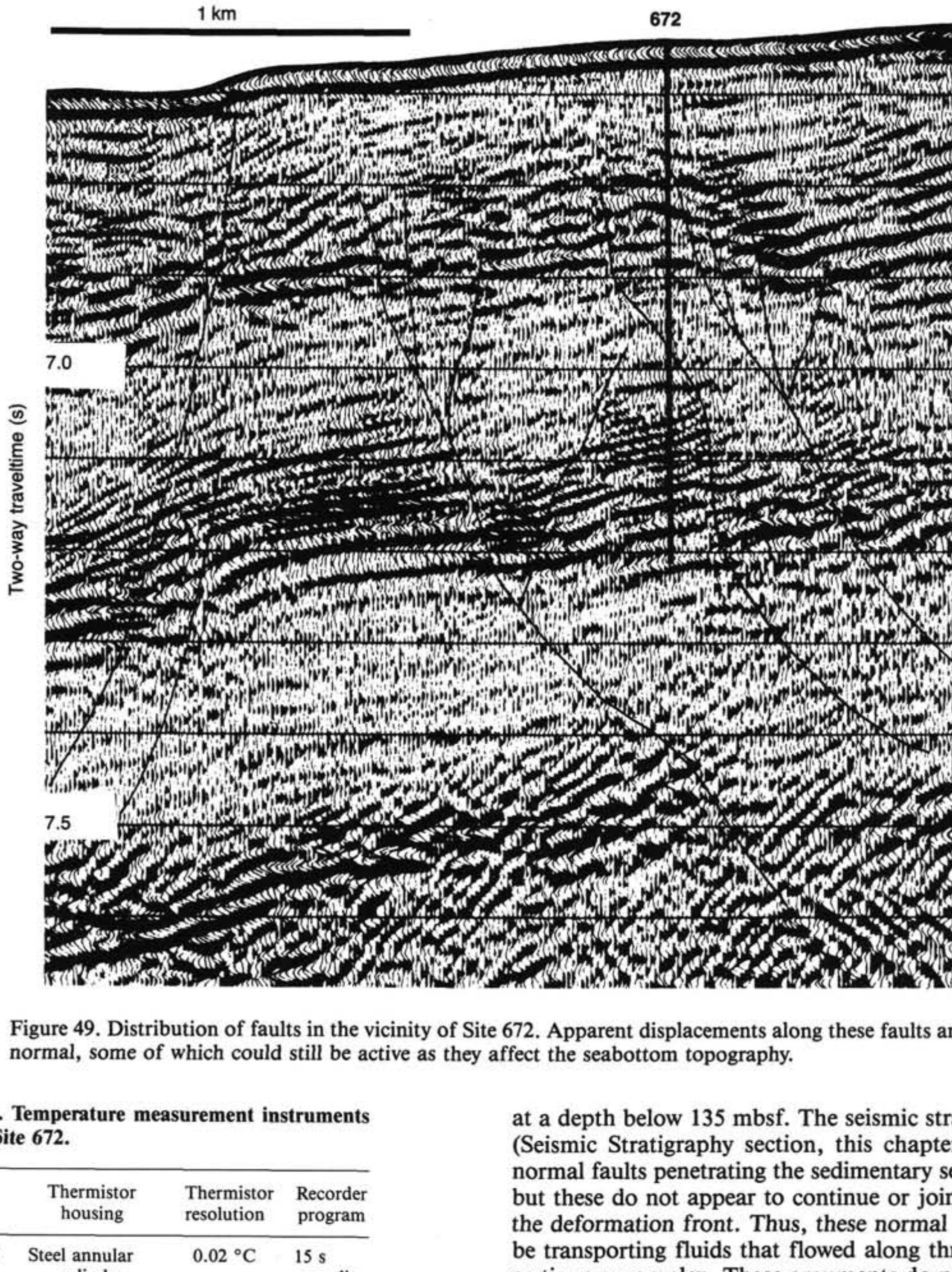

Figure 49. Distribution of faults in the vicinity of Site 672. Apparent displacements along these faults are normal, some of which could still be active as they affect the seabottom topography.

Table 14. Temperature measurement instruments used at Site 672.

Tool	Thermistor housing	Thermistor resolution	Recorder program
APC Tool	Steel annular cylinder ID: 0.0617 m OD: 0.0786 m	0.02 °C	15 s recording interval
T-probe	Steel cylindrical 0.0125-m dia	0.05 °C	5.12 s recording interval

Table 15. Temperature measurement summary, Hole 672A.

Depth (mbsf)	Tool	Equilibrium temp. (est. error) (°C)	Sediment/water temperature
0	APC-tool #6	2.20 (0.05)	Water
13.3	APC-tool #6	3.66 (0.05)	Sediment
32.3	APC-tool #6	4.30 (0.05)	Sediment
42.3	T-probe #14	5.25 (0.05)	Sediment
51.3	APC-tool #6	6.65 (0.05)	Sediment
133.8	T-probe #14	12.7 (0.10)	Sediment

at a depth below 135 mbsf. The seismic stratigraphy of Site 672 (Seismic Stratigraphy section, this chapter) reveals high-angle normal faults penetrating the sedimentary sequence to basement, but these do not appear to continue or join other faults west of the deformation front. Thus, these normal faults are unlikely to be transporting fluids that flowed along thrusts through the accretionary complex. These arguments do not, however, rule out lateral migration of fluid at a depth below the bottom of the hole.

The question remaining is whether the large heat flow measured at Site 672 is truly anomalous or indicative of the region. If it is the former, then it will be difficult to establish a regional "reference" to which heat flow over the accretionary complex may be compared.

SUMMARY AND CONCLUSIONS

Site 672 is located 6 km east of the deformation front of the northern Barbados Ridge on the transect including DSDP Sites 541-542 and ODP Site 671. The principal aim of Site 672 was to core a reference section on the seaward side of the accretionary complex and to provide complete data on the biostratigraphy, lithologies, physical properties, and geochemistry of the incoming oceanic sedimentary cover (Fig. 58).

Four lithologic units have been recognized at Site 672, which range in age from early Pleistocene to early Eocene.

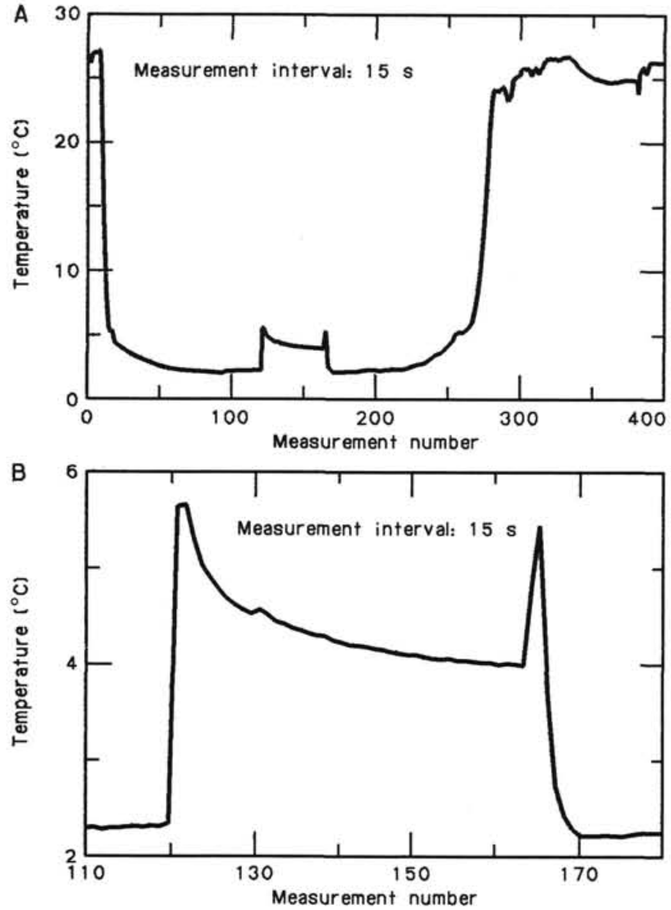

Figure 50. A. Temperature vs. time record for first deployment of APC tool, Core 110-672A-2H, 13.3 mbsf. B. Detail of record, showing sediment temperature.

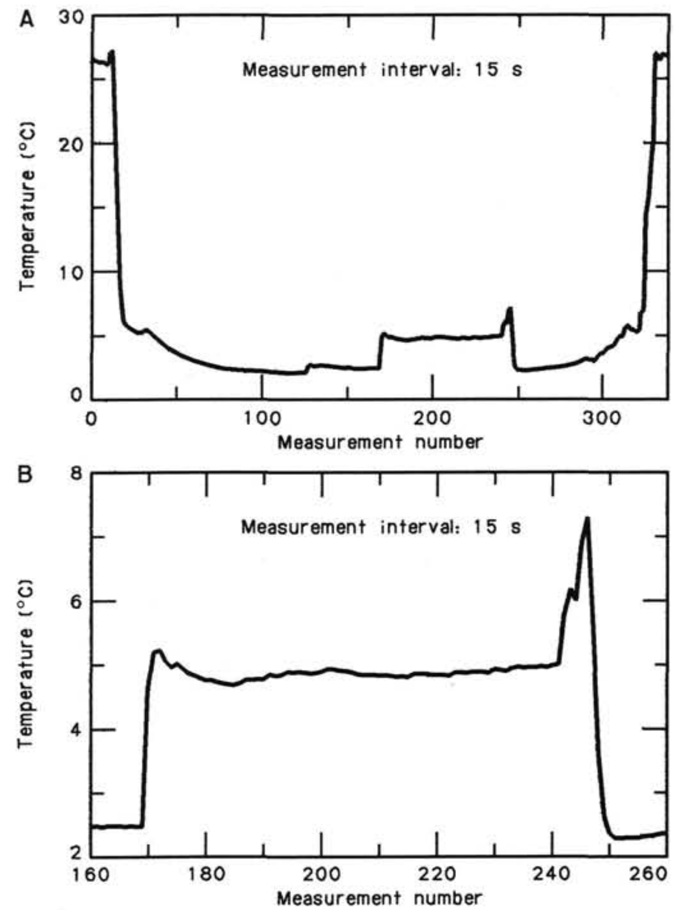

Figure 51. A. Temperature vs. time record for second deployment of APC tool, Core 110-672A-4H, 32.3 mbsf. B. Detail of record, showing sediment temperature.

Unit 1 (0–123 mbsf) consists of calcareous clays and mud, marls, and frequent ash layers. This unit is of early Pleistocene to upper late Miocene age.

Unit 2 (123–228 mbsf) includes mudstones, claystones, and ash layers, with a locally conspicuous biogenic siliceous component. This unit is of late Miocene to early Miocene age (but the two deepest cores are of undeterminate age). Units 1 and 2 show quite homogenous hemipelagic facies and contrast with the two following units where alternating lithologies suggest lateral clastic and biogenic input and reworking in addition to the background hemipelagic sedimentation.

Unit 3 (228–332 mbsf) consists of Oligocene interbedded claystones, calcareous claystones/mudstones, marls, and thin silt layers.

Unit 4 (332–446 mbsf) records significant lateral clastic and biogenic inputs in the form of cyclic alternation of claystones, laminated calcareous mudstones and marls, micritic limestones, and calcarenites (in the lower part only) and sandstones. Unit 4 is of latest to middle Eocene age.

Unit 5 (446–494 mbsf), the deepest cores of Site 672, consist of pelagic siliceous claystone of early middle to early Eocene age. This is the upper part of transparent seismic sequence which extends down to the oceanic basement about 300 m below the bottom of the hole. The oceanic crust is presumed to be of Senonian age according to results from DSDP Site 543, located 20 km to the north.

Obvious seismic evidence of normal faulting is supported by small-scale normal faults observed in cores. Most of these faults appear between 60 and 110, and 170 and 200 msbf. Dilatant subvertical veins filled with clays also occur within these depth intervals. In the interval 180–200 mbsf some of these faults show a conspicuous subhorizontal en-echelon pattern. Displacements along these shear zones are predominantly horizontal, but in one case a reverse movement has been documented. A few reverse faults were also observed at the same depth. This 180–200 mbsf interval, with dilatent veins plus low-angle faults, is of early Miocene age and shows evidence of compressive stresses whereas most of the cored section is affected by normal faulting only.

Bulk densities increase regularly with depth except in two anomalous intervals. The first interval is between 120 msbf (upper late Miocene) and 215 msbf (Oligocene-Miocene boundary). Over this interval average density decreases about 10% with a local pronounced low at a depth of 190 mbsf (lower Miocene). This 95-m-thick interval corresponds quite well with lithologic Unit 2, characterized by a low to very low carbonate content and a relatively high siliceous content. The central portion of this interval, Subunit 2b, also corresponds to the cores that include en-echelon dilatant veins in subhorizontal shear zones.

The second low-density interval is between 450 msbf and the bottom of the hole. It is of early Eocene to early middle Eocene age and exactly correlates with lithologic Unit 5. Here, too, the lithology is characterized by a lack of carbonates and a high siliceous content.

An unexpected result at Site 672 is the large heat flow values (79°C/km) calculated from the temperature measurements in

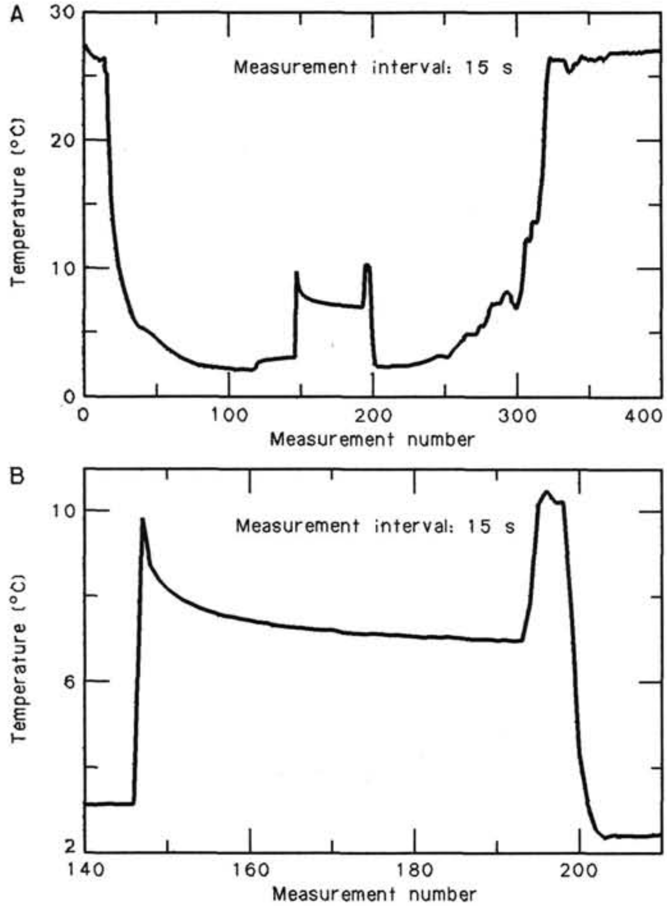

Figure 52. A. Temperature vs. time record for third deployment of APC tool, Core 110-672A-6H, 51.3 mbsf. B. Detail of record, showing sediment temperature.

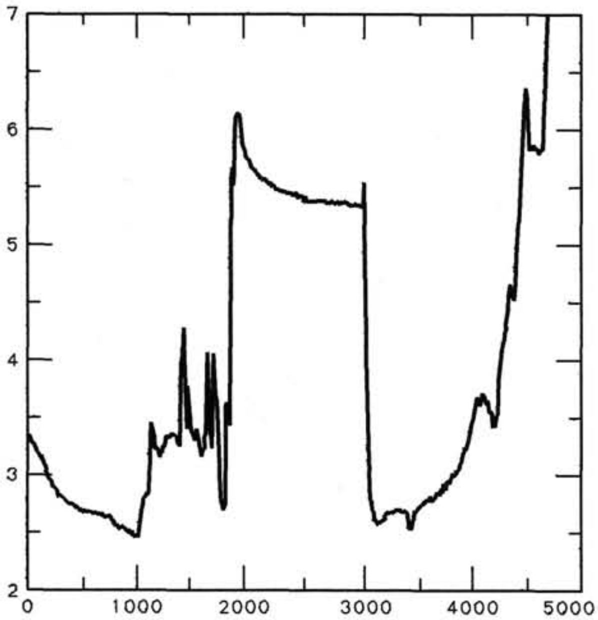

Figure 53. Temperature vs. time record for first deployment of T-probe, after Core 110-672A-5H, 42.3 mbsf.

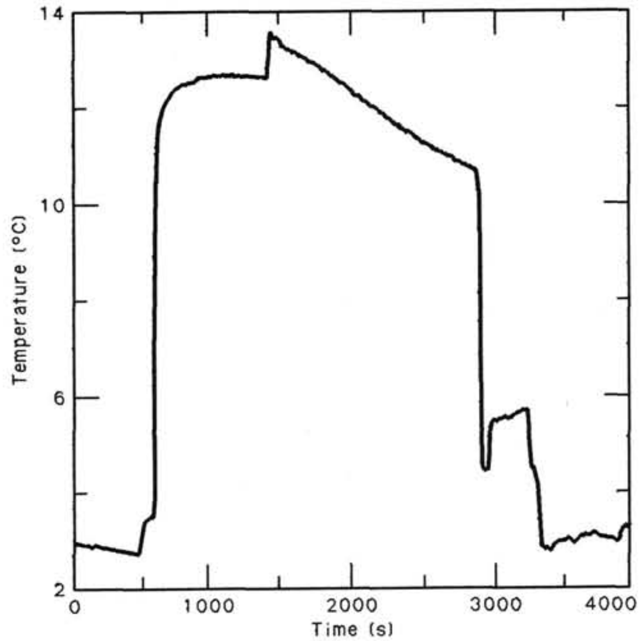

Figure 54. Temperature vs. time record for second deployment of T-probe, after Core 110-672A-15X, 133.8 mbsf.

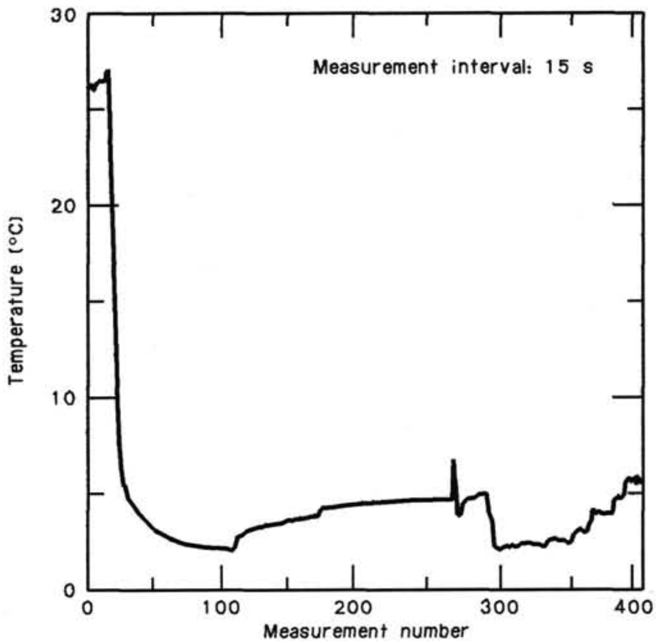

Figure 55. Temperature vs. measurement number for deployment of APC tool, run in tandem with T-probe after Core 110-672A-15X, 133.3 mbsf.

the hole. Interpretation of this result is still debatable but these heat flows could have originated from a superficial source in the sediments rather than far below in the crust or upper mantle. Another spectacular result came from the magnetic susceptibility measurements that have shown quite distinct average values above and below 180–200 mbsf (lower Miocene). These two magnetic susceptibility zones are correlated to a rapid source change for the magnetic minerals. The Neogene magnetic minerals are related to ash beds from the volcanic arc, whereas Pa-

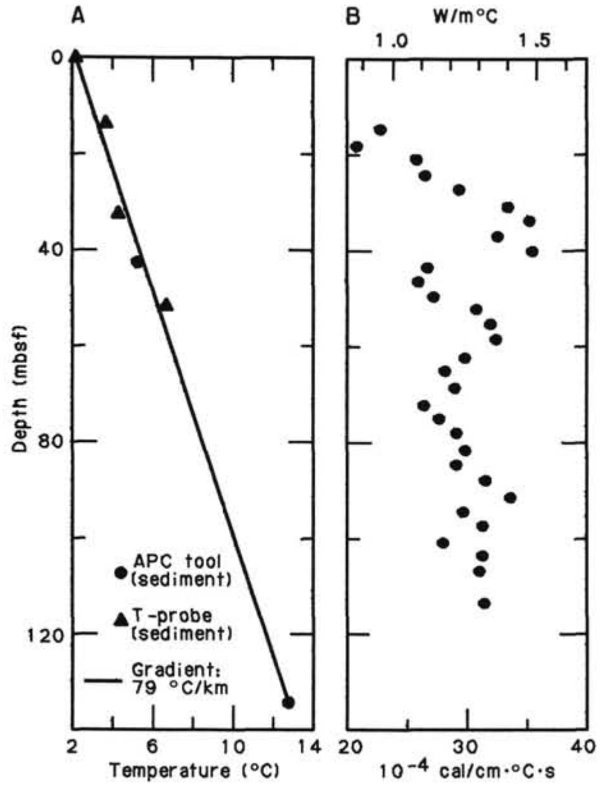

Figure 56. Plots of A. temperature and B. thermal conductivity vs. depth for Hole 672A.

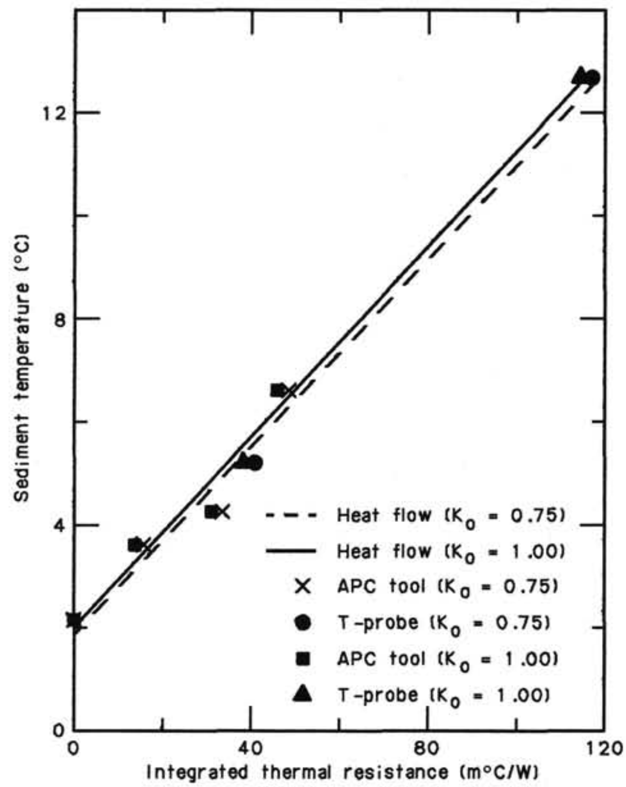

Figure 57. Plot of downhole temperature vs. integrated thermal resistance in Hole 672A. Linear least-squares best-fitted curves generated with different assumed surface sediment thermal conductivities.

leogene magnetic minerals are more probably derived from clays originating on the South American continent. A similar distribution of magnetic minerals had already been proposed at Site 671.

Site 672, as an oceanic abyssal plain reference hole, was intended to reveal standard trends in pore-water chemistry. The decrease of magnesium and the increase of calcium with depth both reflect the alteration of volcanic ashes in the upper level (0–120 mbsf), and respective diffusion of these elements to or from the oceanic crust in the lower half of the hole (300–500 mbsf). A slight increase in curve slopes between 325 and 375 mbsf is related to greater diffusivity of the sand layers at the top of the lithologic Unit 4. The concentration-depth profile of dissolved chloride is more complex as several anomalies are superimposed. A normal slight decrease in chloride occurs from 0 to 300 msbf. The major anomaly is a sharp decrease in chloride content below 300 msbf with a prominent low value at 367 mbsf. This depth corresponds to the principal sand layer of lithologic Unit 4. Apparently, advection of freshwater is the origin of the low chloride content. A single low value at 216 msbf would probably have been neglected if it had not been 25 m below the previously described lower Miocene shear zone. Furthermore, it correlates with a high value of methane content. These observations suggest advection of freshwater just below the lower Miocene shear zone. A few anomalously high values of chloride content remain difficult to explain. The only presently known process leading to very local variation in chloride concentration and perhaps other ions is recent membrane filtration.

From this brief summary of Site 672, three major points are especially noteworthy:

1. DSDP Site 543 and ODP Site 672 are both located on the moderate slopes (average: 1.5%) of the Tiburon Rise, a broad NW-SE trending and 40-km-wide oceanic ridge that culminates at about 1500 m above the surrounding abyssal plains (Fig. 59). Site 672 is on an westward-facing slope at a water depth of 4983 m, whereas Site 543 is on a northward-facing slope at a water depth of 5633 m. The sediment thickness is about twice as great at Site 672 as at Site 543. Most of this thickening occurs in pre-Neogene strata, and is particularly well documented in middle Eocene and Oligocene time (Fig. 60). At Site 672, these two intervals are each 100 m thick and they correspond to relatively high rates of sedimentation with clastic and biogenic influxes from the South American continent as well as from the upper slope of the Tiburon Rise (see Lithostratigraphy section). At the same time, a cumulative thickness of 40 m consisting only of pelagic clays was deposited at the location of Site 543. These differences can be explained by two processes. First, the lack of biogenic components is probably related to the greater depth of Site 543: if located well below the CCD, both primary (pelagic) and reworked foraminifers or nannofossils have been dissolved. Second, the absence of any silt or sand layers at Site 543 could be a result of some obstructing effect of the Tiburon Rise, particularly if the main source of these clastic influxes is South America. This however, does not explain why we found these silts and sands at Site 672 which, in its present setting, is some 650 m higher than Site 543. On line CRV-128, the related seismic sequences do not show any evidences of thinning or pinch outs from west to east as would be expected if they onlapped the Tiburon Rise at the edge of a deeper basin to the south or to the west. These sands and silts could be distal turbiditic deposits although they lack true Bouma sequences. Alternatively, they could be explained as sediments transported and reworked by bottom currents coming from the south. These currents could have decreased in velocity and energy upon topping the Tiburon Rise leading to the deposition of the entrained clastic particles.

The lower third of the sedimentary cover at Site 672 was not drilled. From the seismic section, it appears to be significantly thicker than the equivalent interval at Site 543. As the oceanic crust is apparently not of different age, the sedimentation rates were probably higher from Campanian to early Eocene at Site 672 than at Site 543. Notably, the Paleocene (8.6 m.y.) is missing and the Maestrichtian (7 m.y.) is very reduced at Site 543.

2. Structural features related to compressive stresses (reverse faults, en-echelon veins) are restricted to the lower Miocene interval whereas normal faults occur within Pliocene to middle Eocene sediments. This lower Miocene section correlates exactly with the top of the décollement zone defined at Site 671. Why are these veins and faults concentrated in this peculiar interval from 175 to 200 mbsf? Data show a sharp increase in porosity in this interval, perhaps indicating significant underconsolidation and elevated pore pressure plus consequent lower strength than sediments above and below. This anomalously weak interval permits the development of the compressive structural features. Apparently, some of the stresses related to the developing accretionary complex are propagating a few kilometers forward of the deformation front (here defined as the first appearance of large-scale folds and faults).

3. A first comparison of Ca, Mg, Cl, and CH_4 content between Sites 671 and 672 shows strong similarities in absolute values and trends when stratigraphic intervals are plotted at the same depth (Fig. 61). In the upper 100 m the fits are almost perfect except for methane, where diffusion from 225 mbsf can be inferred. A similar trend agreement is also observed within the repeated upper Miocene-Pleistocene section below thrust T4. The Miocene interval is too disturbed by faulting and folding at Site 671 to allow direct comparison with Site 672. However, if we correlate the décollement as defined at Site 671 with the shear zone we encountered at Site 672, the three elements and the methane below the décollement zone show remarkable similarities in both values and trends. This is quite consistent with a scenario of recent underthrusting of the Paleogene series, which has an overall low diffusive permeability (with the noticeable exception of some sand layers). The high methane content below the shear zone at Site 672 mimics that measured in the décollement zone of Site 671. This supports the hypothesis that water is laterally advecting from the accretionary complex to Site 672 along an incipient shear zone that will become the future décollement.

REFERENCES

Becker, K., Von Herzen, R., and Karoto, S., 1983. Geothermal measurements from drilling of sediments near the Galapagos Spreading Center, 86° W, Deep Sea Drilling Project Leg 70. *In*, Honnorez, J., Von Herzen, R. P., et al., *Init. Repts. DSDP,* 70: Washington (U.S. Govt. Printing Office), 445–458.

Bergen, J., 1984. Calcareous nannoplankton from Deep Sea Drilling Project Leg 78A: evidence for imbricate underthrusting at the Lesser Antillian active margin. *In* Biju-Duval, B., Moore, C., et al., *Init. Repts. DSDP*, 78A: Washington (U. S. Govt. Printing Office), 411–445.

Berggren, W. A., Kent, D. V., and Flynn, J. J., 1985. Paleogene geochronology and chronostratigraphy, *In*: Snelling, N. J., The geochronology and the geologic record. *Geol. Soc. London, Mem.* 10:141–195.

Berggren, W. A., Kent, D. V., and Van Couvering, J. A., 1985. Neogene geochronology and chronostratigraphy. *In*: Snelling, N. J., The geochronology and the geologic record. *Geol. Soc. London, Mem.* 10: 211–260.

Biju-Duval, B., Moore, J. C., et al., 1984. *Init. Repts. DSDP*, 78A: Washington (U.S. Govt. Printing Office).

Birch, F. S., 1970. The Barracuda Fault zone in the western North Atlantic: geological and geophysical studies., *Deep Sea Res.*, 17:847–859.

Bolli, H. M., 1957a. Planktonic foraminifera from the Oligocene-Miocene Cipero-Lengua Formations of Trinidad, B.W.I. *Bull. U.S. Nat. Museum*, 215:92–123.

Bolli, H. M., 1957b. Planktonic foraminifera from the Eocene Navet and San Fernando Formations of Trinidad, B.W.I. *Bull. U.S. Nat. Museum*, 215:155–172.

Bullard, E. C., 1939. Heat flow in South Africa, *Proc. Roy. Soc. London,* A173:474–502.

Burington, R. S., 1973. *Handbook of Mathematical Tables and Formulas,* New York (McGraw-Hill).

Cheng, C. H., Wilkens, R. H., and Meredith, J. A., 1986. Modeling of the fluid waveform acoustic log in soft marine sediments. *SPWLA 27th Annual Logging Symposium.*

Claypool, G. E., and Kaplan, I. R., 1974. The origin and distribution of methane in marine sediments. *In* Kaplan, I. R., (Ed.), *Natural Gases in Marine Sediments*. Plenum Press: 99–140.

Damuth, J. E., and Fairbridge, R. W., 1970. Equatorial Atlantic deep-Sea arkosic sands and ice-age aridity in tropical South America. *Geol. Soc. Am. Bull.*, 81:189–206.

Davis, D., and Hussong, D., 1984. Geothermal observations during Deep Sea Drilling Project Leg 78A. *In* Biju-Duval, B., Moore, J. C., et al., *Init. Repts. DSDP,* 78A: Washington (U.S. Govt. Printing Office), 593–598.

Davis, D., Suppe, J., and Dalhen, F. A., 1983. Mechanism of fold-and-thrust belts and accretionary wedge. *J. Geophys. Res.*, 88:1153–1172.

Embley, R. W., and Langseth, M. G., 1977. Sedimentation processes on the continental rise of northeastern South America. *Mar. Geol.*, 25: 297.

Fertl, W. H., 1976. *Abnormal Formation Pressure*: Amsterdam (Elsevier Scientific Publishing Company).

Gartner, S., 1977. Calcareous nannofossil biostratigraphy and revised zonation of the Pleistocene. *Mar. Micropaleontology*, 2:1–25.

Gieskes, J. M., 1974. Interstitial water studies, Leg 25. *In* Simpson, E. S., Schlich, R., et al., *Init. Repts. DSDP*, 25: Washington (U.S. Govt. Printing Office), 361–394.

Langseth, M., Westbrook, G., and Hobart, M., 1986. Geothermal transects of the lower trench slope of the Barbados accretionary prism, [paper presented at the 11th Annual Caribbean Geological Conference, Bridgetown, Barbados].

McDuff, E., 1981. Major cation gradients in DSDP interstitial waters: the role of diffusive exchange between sea water upper ocean crust. *Geochim. Cosmochim. Acta*, 45:1705.

Mascle, A., Cazes, M., and Le Quellec P., 1985. Structure des marges et bassins Caraibes: une revue. *In* Mascle, A. (Ed.), *Symposium sur la Geodynamique des Caraibes*: Paris (Edition Technip.)

Moore, G. W., and Gieskes, J. M., 1980. Interaction between sediment and interstitial water near the Japan Trench, Leg 57, Deep Sea Drilling Project. *In* Scientific Party, *Init. Repts. DSDP*, 57: Washington (U.S. Govt. Printing Office), 1269–1275.

Moore, J. C., and Biju-Duval, B., 1984. Tectonic synthesis, Deep Sea Drilling Project Leg 78A: structual evolution of offscraped and underthrust sediment, Northern Barbados Ridge Complex. *In* Biju-Duval, B., Moore, J. C., et al., *Init. Repts. DSDP*, 78A: Washington (U.S. Govt. Printing Office), 601–621.

Moretti, I., and Ngokwey, K., 1985. Aseismic ridge subduction and vertical motion of an overiding plate. *In*, Mascle, A. (Ed.), *Geodynamique des Caraibes*: Paris (Editions Technip.), 245–253.

Neidell, N., and Taner, H., 1971. Semblance and other coherency measure for multichannel data. *Geophysics*, 36:482–497.

Okada, H., and Bukry, D., 1980. Supplementary modification and introduction of code numbers to the low latitude coccolith biostratigraphic zonation (Bukry 1973, 1975). *Mar. Micropaleontology*, 5: 321–325.

Peter, G., and Westbrook, G. K., 1976. Tectonics of southwestern north Atlantic. *Bull. Soc. Assoc. Pet. Geol.*, 60:1078–1106.

Pyle, M. R., 1984. Vane shear data on undrained residual strength. *J. Geotech. Div.*, Am. Soc. Civ. Eng., 110:543–547.

Ransom, R. C., 1986. A method for calculating pore pressure from well logs. *Log Analyst SPWLA*, Mar.–Apr.:72–76.

Riedel, W. R., and Sanfilippo, A., 1978. Stratigraphy and evolution of tropical Cenozoic radiolarians. *Micropaleontology*, 24:61–96.

Salisbury, M. H., Scott, J. H., Auroux, C., et al., 1986. *Proc., Init. Repts. (Pt. A), ODP.* 102.

Sanfilippo, A., and Riedel, W. R., 1982. Revision of the radiolarian genera *Theocotyle, Theocotylissa* and *Thyrsocyrtis*. *Micropaleontology*, 28:170–188.

Saunders, J. B., Bernoulli, D., Müller-Merz, E., Oberhaensli, H., Perch-Nielsen, K., Riedel, W. R., Sanfilippo, A., and Torrini, R. Jr., 1984. Stratigraphy of late Middle Eocene to Early Oligocene in Bath Cliff section Barbados, West Indies. *Micropaleontology*, 30:390–425.

Schubert, C. E., and Peter, G., 1974. Heat flow northeast of Guadeloupe Island, Lesser Antilles, *J. Geophys. Res.*, 79:2139–2140.

Speed, R. C., Westbrook, G. K., et al., 1984. Lesser Antilles Arc and adjacent terranes; Ocean Margin Drilling Program. *Atlas 10, Regional Atlas Series*, Woods Hole (Marine Science International).

Tsang, L., and Rader, D., 1979. Numerical evaluation of the transient acoustic waveform due to a point source in a fluid filled borehole. *Geophysics*, 44:1706–1720.

Von Herzen, R. P., and Maxwell, A. E., 1959. The measurement of thermal conductivity of deep-sea sediments by a needle probe method. *J. Geophys. Res.*, 65:1535–1541.

Weissert, H. J., McKenzie, J. A., Wright, R. C., Clark, M., Oberhansli, H., and Casey, M., 1983. Paleoclimatic record of the Pliocene at Deep Sea Drilling Sites 519, 521, 522, and 523 (central South Atlantic). *In* Hsu, K. J., LaBreque, J. L., et al., *Init. Repts. DSDP*, 73: Washington (U.S. Govt. Printing Office), 701–715.

Westbrook, G. K., Mascle, A., and Biju-Duval, B., 1984. Geophysics and the structure of the Lesser Antilles Forearc. *In* Biju-Duval, B., Moore, J. C., et al., *Init. Repts. DSDP* 78A: Washington (U.S. Govt. Printing Office), 23–38.

Ms 110A-106

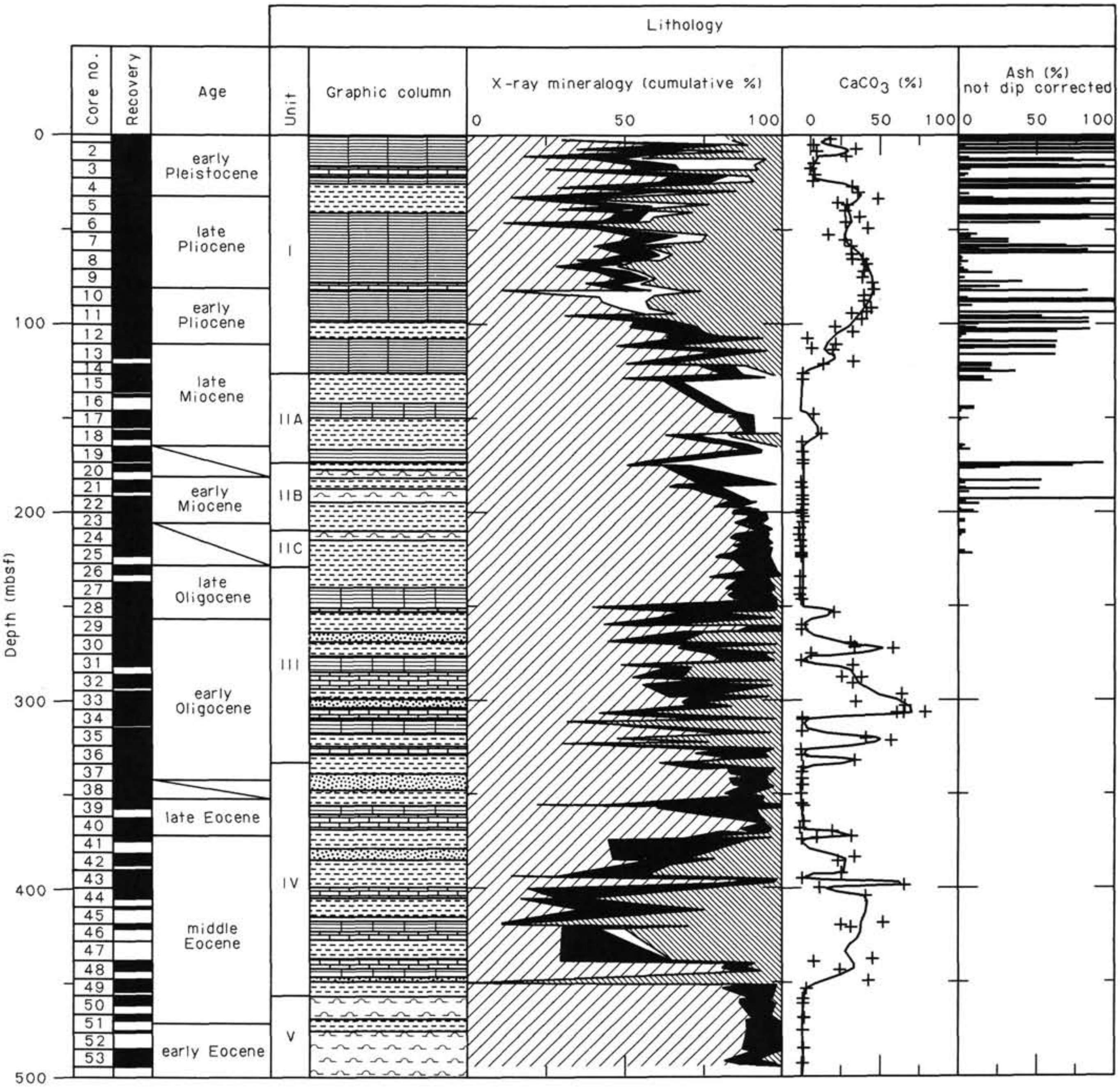

Figure 58. Summary of Site 672.

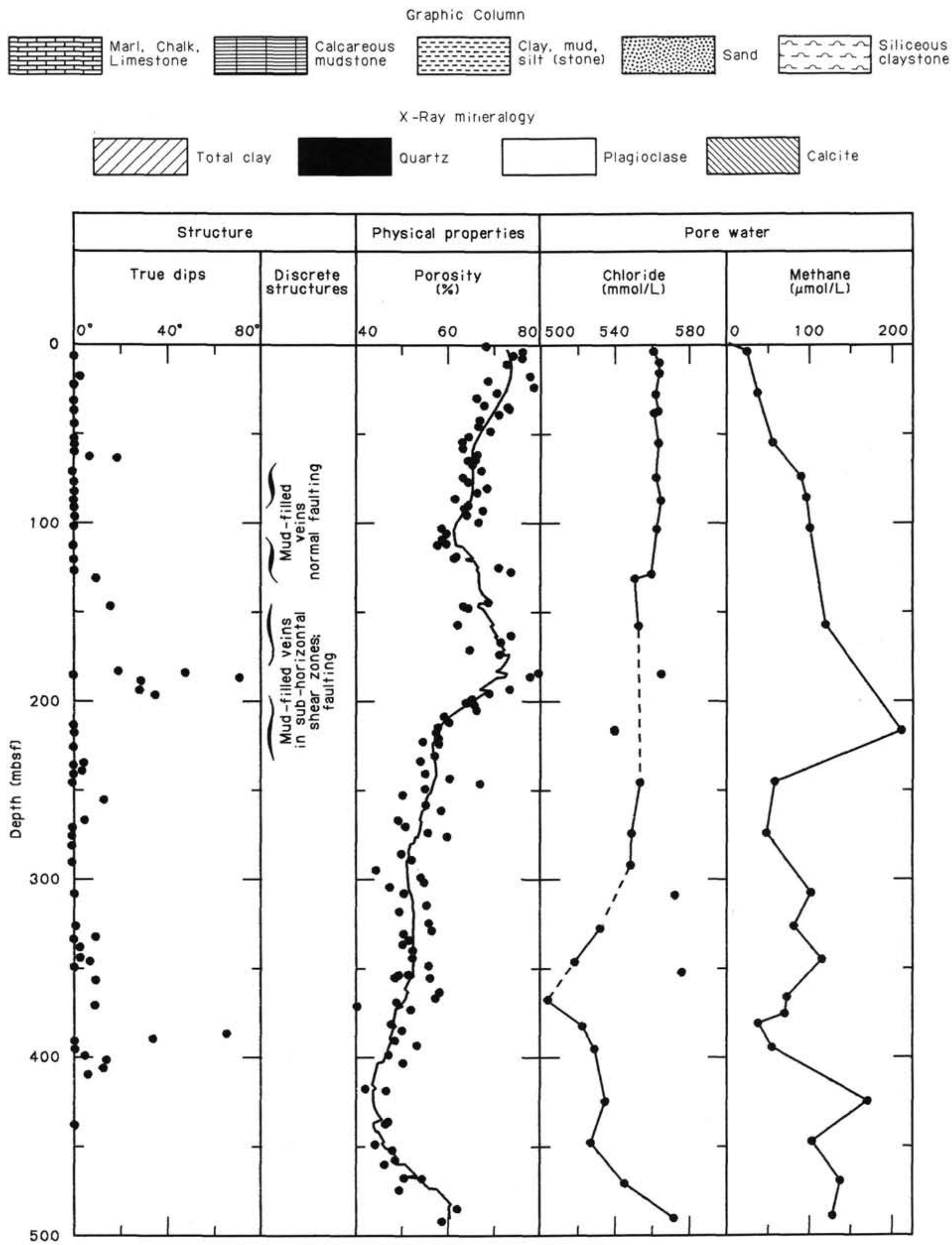

Figure 58 (continued).

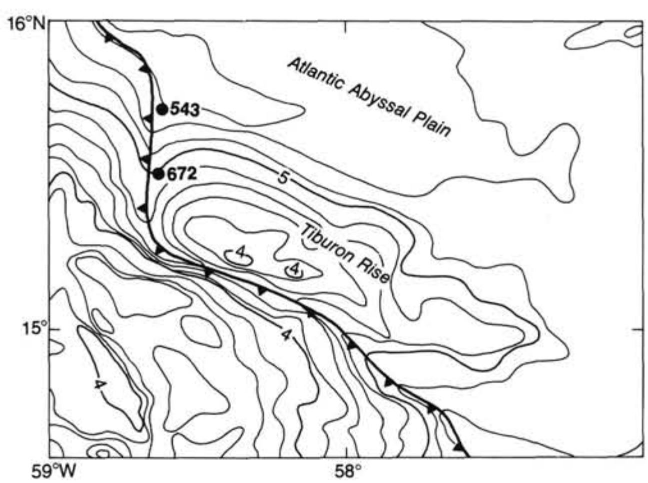

Figure 59. Location of DSDP Site 543 and ODP Site 672 with respect to the Tiburon Rise and the deformation front. Contours are water depths in kilometers.

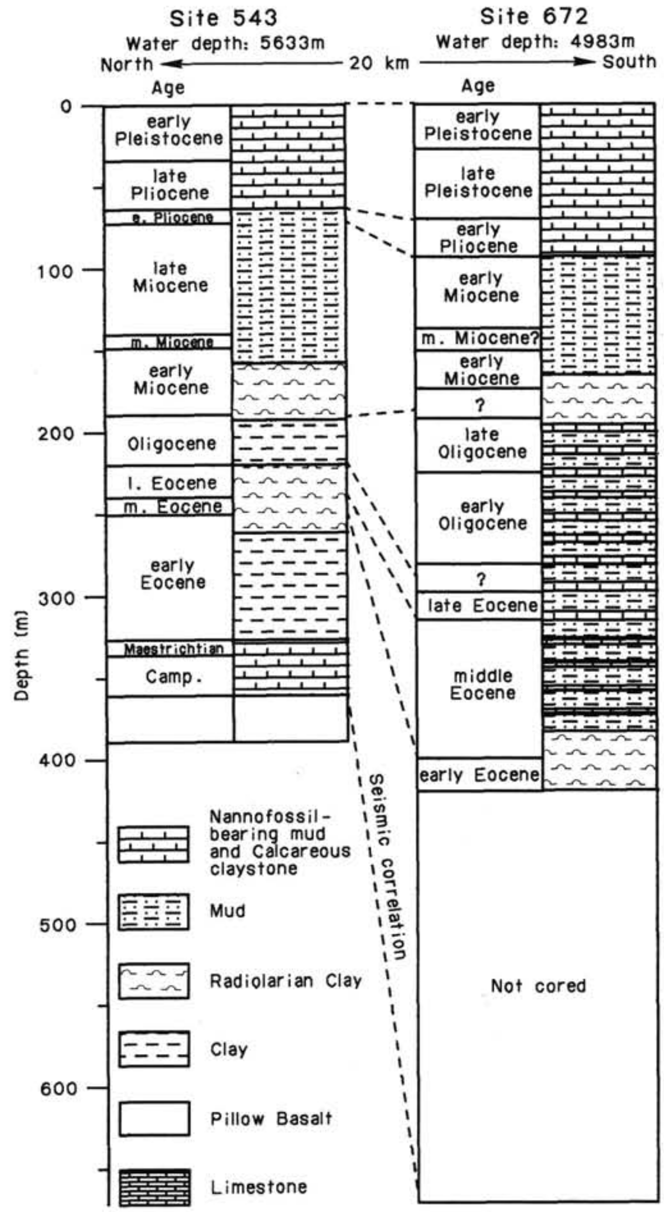

Figure 60. Comparison of DSDP Site 543 lithologies with those cored at ODP Site 672.

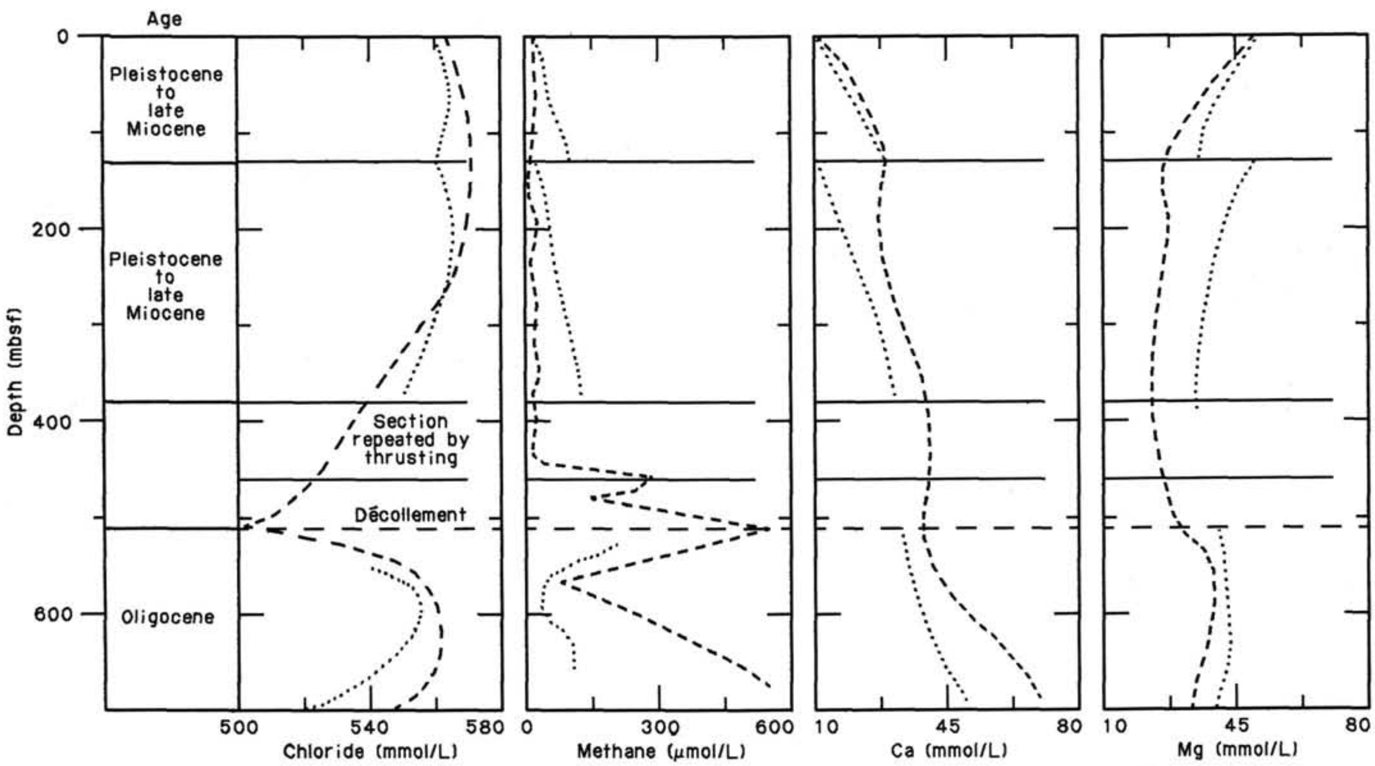

Figure 61. Comparison of Sites 671 (dashed) and 672 (dotted) diagrams in calcium, magnesium, chloride and methane in pore water. The values for Site 672 have been projected onto the Site 671 diagram, taking into account the stratigraphic intervals and the tectonic repetitions.

SITE 672 HOLE A CORE 1 H CORED INTERVAL 4973.0-4976.3 mbsl; 0.0-3.3 mbsf

TIME-ROCK UNIT	FORAMINIFERS	NANNOFOSSILS	RADIOLARIANS	DIATOMS	PALEOMAGNETICS	PHYS. PROPERTIES	CHEMISTRY	SECTION	METERS
LOWER PLEISTOCENE	*Globorotalia truncatulinoides* Zone *G. hessi* subzone C/P	*Pseudomiliania lacunosa* Zone C/P	Barren B			●1.58	●18.35%	1, 2, 3, CC	0.5, 1.0

LITHOLOGIC DESCRIPTION

CALCAREOUS CLAY and MUD plus MARL

CALCAREOUS CLAY and MUD plus MARL, yellowish brown (10YR5/8, 10YR5/4, 10YR4/4), nannofossil-rich.

Minor lithology: interbeds of vitric and minor crystalline ash in Section 1, 90–92 cm and 133–139 cm, and in Section 2, 139–143 cm; light to medium gray (10YR6/2–10YR5/1).

SMEAR SLIDE SUMMARY (%):

	1, 92 M	1, 107 D	1, 135 M	2, 84 D	2, 142 M
TEXTURE:					
Sand	10	—	90	2	85
Silt	90	5	10	12	15
Clay	—	95	—	86	—
COMPOSITION:					
Quartz	—	Tr	Tr	—	—
Feldspar	20	Tr	60	—	60
Clay	—	65	—	71	—
Volcanic glass	76	—	15	—	33
Calcite/dolomite	—	—	—	Tr	
Accessory minerals					
Orthopyroxene	1	—	—	—	1
Clinopyroxene	1	—	2	—	1
Opaques	2	—	2	5	2
Hornblende	—	—	20	—	3
Foraminifers	—	4	—	3	—
Nannofossils	—	25	—	20	—
Sponge spicules	—	2	—	1	—
Bioclasts	—	2	—	—	—

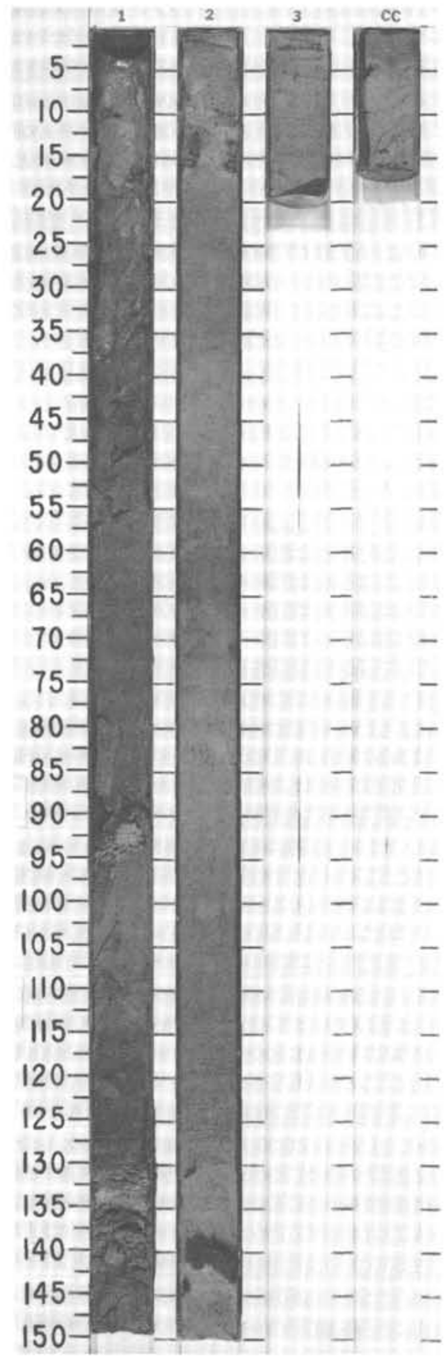

SITE 672 HOLE A CORE 2 H CORED INTERVAL 4976.3-4985.8 mbsl; 3.3-12.8 mbsf

TIME-ROCK UNIT	FORAMINIFERS	NANNOFOSSILS	RADIOLARIANS	DIATOMS	PALEOMAGNETICS	PHYS. PROPERTIES	CHEMISTRY	SECTION	METERS	GRAPHIC LITHOLOGY	DRILLING DISTURB.	SED. STRUCTURES	SAMPLES
LOWER PLEISTOCENE	*Globorotalia truncatulinoides* Zone *G. hessi* subzone; A/G	*Pseudomiliania lacunosa* Zone; A/G	Barren; B			$\gamma=1.46$ $\phi=77$; $\gamma=1.50$ $\phi=75$; $\gamma=1.46$ $\phi=76$; $\gamma=1.56$ $\phi=73$	8.0 %; 35.0 %; 9.8 %; 23.8 %	1, 2, 3, 4, 5, 6, 7, CC	0.5, 1.0				*; *; *; PP; *; *; IW; *

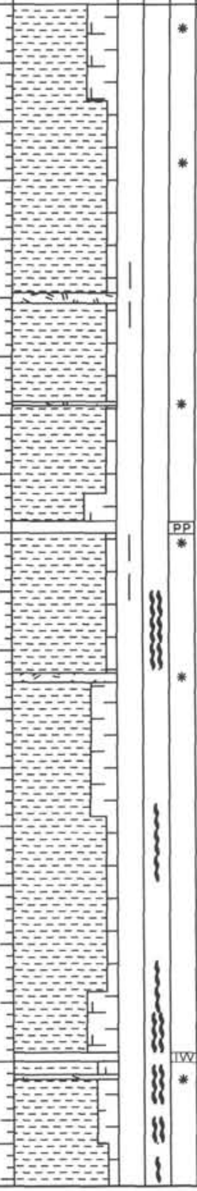

BIOSTRAT. ZONE/FOSSIL CHARACTER

LITHOLOGIC DESCRIPTION

MUD plus CALCAREOUS CLAY and MUD plus MARL

MUD plus CALCAREOUS CLAY and MUD plus MARL; very pale brown, yellowish brown, and brown (10YR4/4, 10YR5/4, 10YR6/4, 10YR7/4, 10YR7/3, 2.5Y5/4, 2.5Y4/2, 2.5Y5/2); nannofossil-rich.

Minor lithology: interbeds of vitric and minor crystalline ash, light brown to dark grayish brown (7.5YR6/4–10YR3/2); pyrite locally developed.

SMEAR SLIDE SUMMARY (%):

	1, 19 D	1, 129 D	3, 40 M	4, 6 M	4, 124 M	7, 15 M
TEXTURE:						
Sand	Tr	2	15	80	80	—
Silt	40	8	80	20	20	70
Clay	60	90	5	—	—	30
COMPOSITION:						
Quartz	Tr	—	1	—	—	—
Feldspar	2	1	20	40	50	20
Rock fragments	—	—	—	43	40	Tr
Clay	65	80	5	—	—	30
Volcanic glass	—	—	70	5	—	40
Accessory minerals	—	Tr	2	2	—	8
Orthopyroxene	—	—	—	10	10	—
Clinopyroxene	Tr	1	2	—	—	—
Hornblende	2	—	1	—	Tr	—
Foraminifers	4	2	—	—	—	—
Nannofossils	25	10	—	—	—	—
Radiolarians	Tr	—	Tr	—	—	—
Sponge spicules	Tr	1	—	—	—	—
Bioclasts	4	—	—	—	—	—

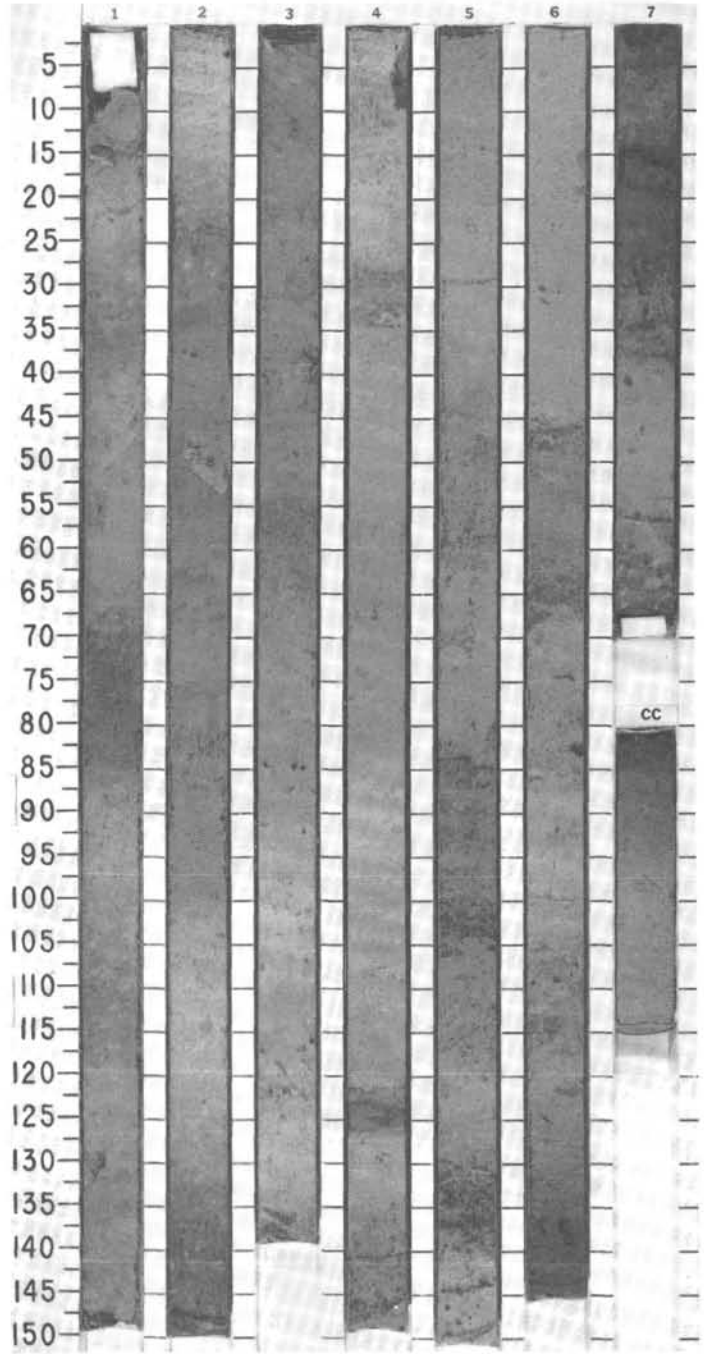

SITE 672 HOLE A CORE 3 H CORED INTERVAL 4985.8-4995.3 mbsl; 12.8-22.3 mbsf

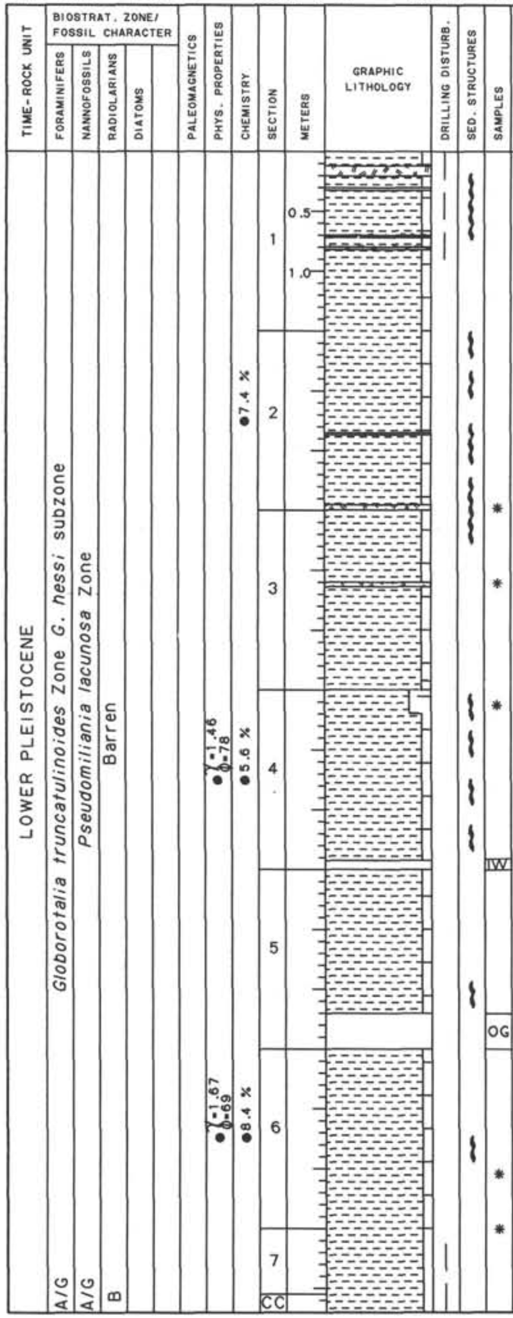

LITHOLOGIC DESCRIPTION

CALCAREOUS CLAY and minor CALCAREOUS MUD plus MARL

CALCAREOUS CLAY and minor CALCAREOUS MUD plus MARL; light yellowish brown to light olive-gray (10YR4/1–10YR6/6, 5Y6/2–5Y6/3); nannofossil-rich, and locally foraminifer-rich.

Minor lithology: interbeds of vitric and minor crystalline ash, dark to light gray (10YR5/1–5Y4/1); horizontal bedding dips.

SMEAR SLIDE SUMMARY (%):

	2, 149 M	3, 64 M	4, 12 D	6, 103 D	6, 150 D
TEXTURE:					
Sand	90	95	—	3	—
Silt	10	5	5	17	6
Clay	—	—	95	80	94
COMPOSITION:					
Quartz	—	—	Tr	—	—
Feldspar	20	10	Tr	—	1
Rock fragments	35	50	—	—	—
Clay	—	—	78	77	79
Volcanic glass	35	37	—	—	—
Calcite/dolomite	—	—	—	—	3
Accessory minerals					
Zeolites	—	—	Tr	—	—
Orthopyroxene	6	2	—	—	—
Clinopyroxene	3	—	—	—	—
Opaques	2	1	—	—	1
Olivine	Tr	Tr	—	—	—
Foraminifers	—	—	Tr	5	1
Nannofossils	—	—	20	15	15
Sponge spicules	—	—	—	—	Tr
Chitinozoa	—	—	—	Tr	—
Bioclasts	—	—	3	—	—

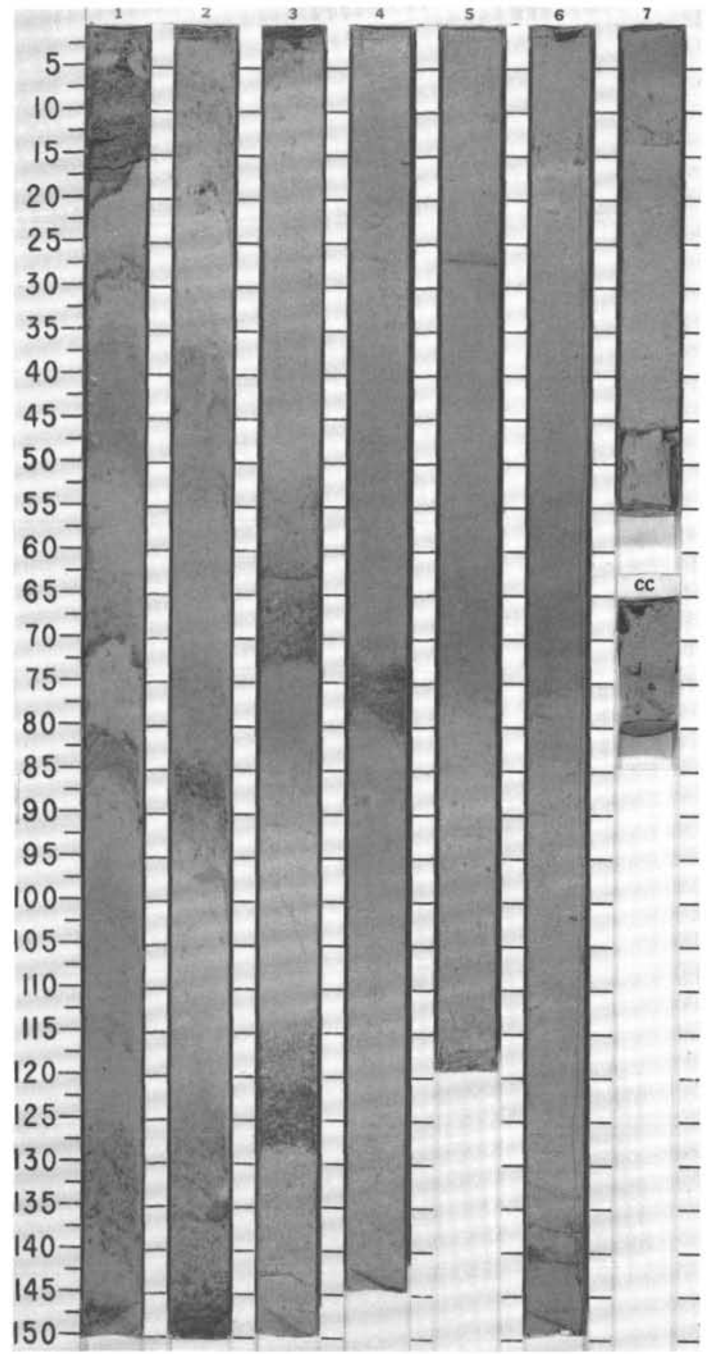

SITE 672 HOLE A CORE 4 H CORED INTERVAL 4995.3-5004.8 mbsl; 22.3-31.8 mbsf

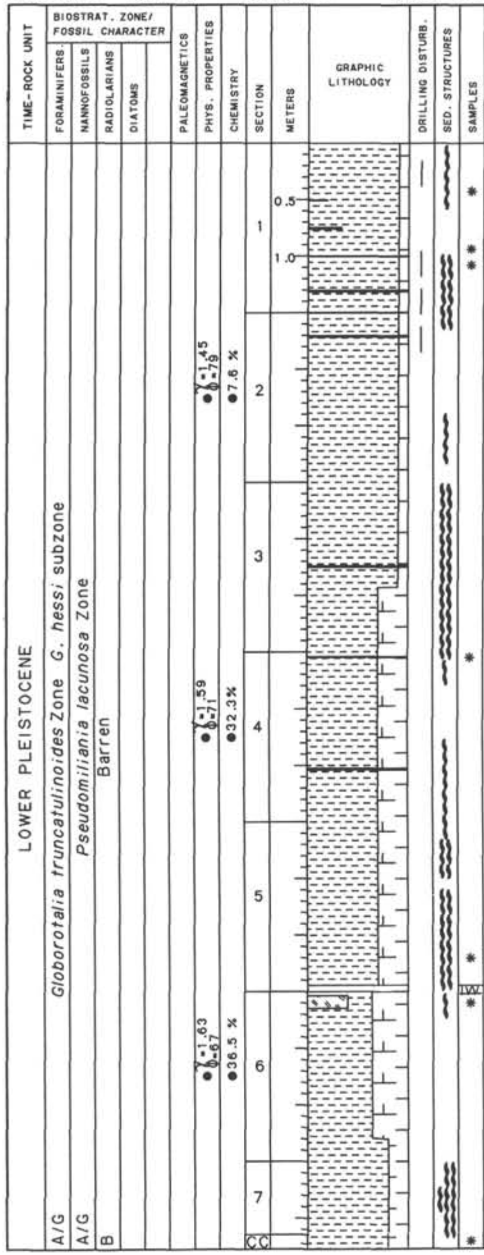

LITHOLOGIC DESCRIPTION

CALCAREOUS CLAY and MUD plus MARL

CALCAREOUS CLAY and MUD plus MARL; light yellowish brown, brownish gray, and light olive-gray (2.5Y6/3, 2.5Y7/2, 5Y6/2); nannofossil-rich.

Minor lithology: lithic and vitric ash occurs dispersed throughout the sediment and as ash beds, gray (2.5Y5/1, 7.5YR6/0).

SMEAR SLIDE SUMMARY (%):

	1, 51 M	1, 87 M	1, 106 D	4, 6 M	5, 120 D	6, 10 M	CC, 5 D
TEXTURE:							
Sand	10	—	—	90	—	2	—
Silt	90	50	10	10	10	20	5
Clay	—	50	90	—	90	78	95
COMPOSITION:							
Quartz	—	—	—	Tr	—	Tr	Tr
Feldspar	3	35	1	40	Tr	10	Tr
Rock fragments	90	—	—	54	—	—	—
Clay	—	40	85	—	74	65	75
Volcanic glass	5	5	Tr	2	—	20	—
Accessory minerals							
Zeolites	—	—	—	—	Tr	—	Tr
Pyroxene	—	3	Tr	3	—	2	—
Opaques	2	3	—	1	—	Tr	—
Hornblende	—	8	—	Tr	—	—	—
Foraminifers	—	Tr	Tr	—	4	—	1
Nannofossils	—	2	10	—	20	10	20
Sponge spicules	—	Tr	Tr	—	—	—	—
Bioclasts	—	—	2	—	2	—	3

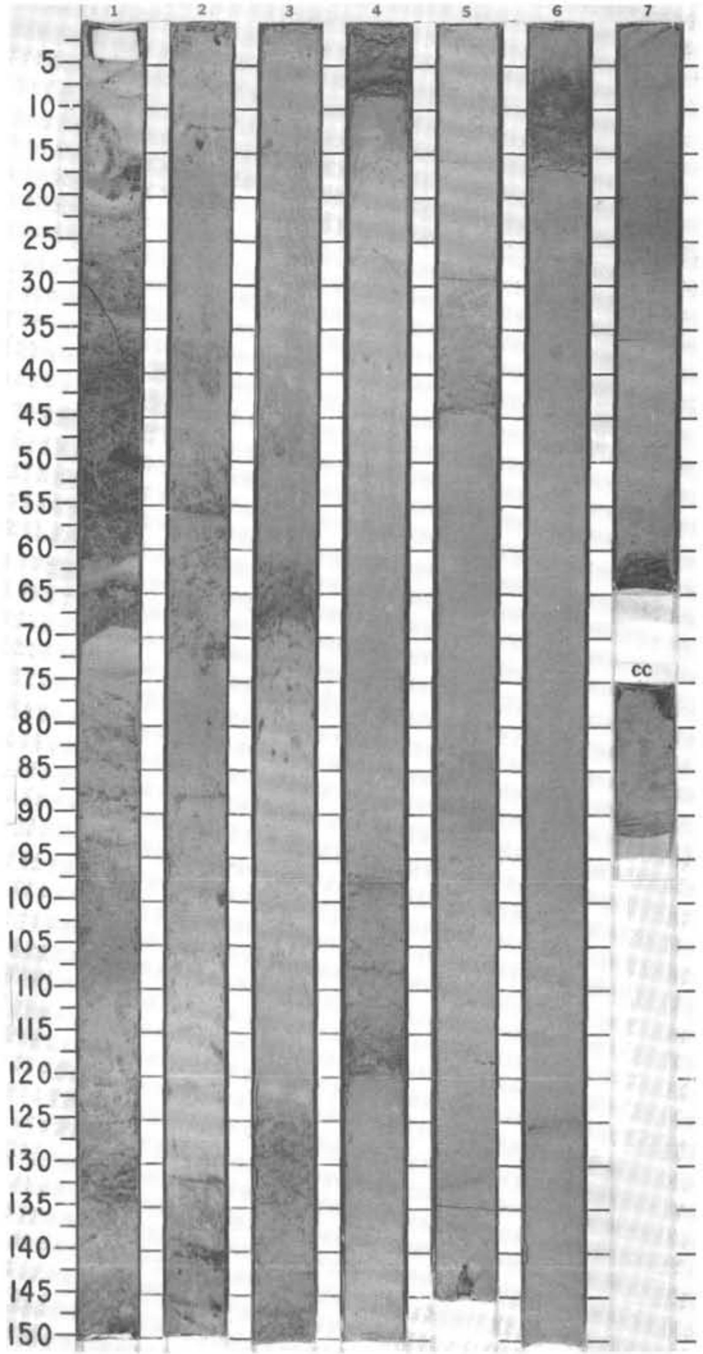

SITE 672 HOLE A CORE 5 H CORED INTERVAL 5004.8-5014.3 mbsl; 31.8-41.3 mbsf

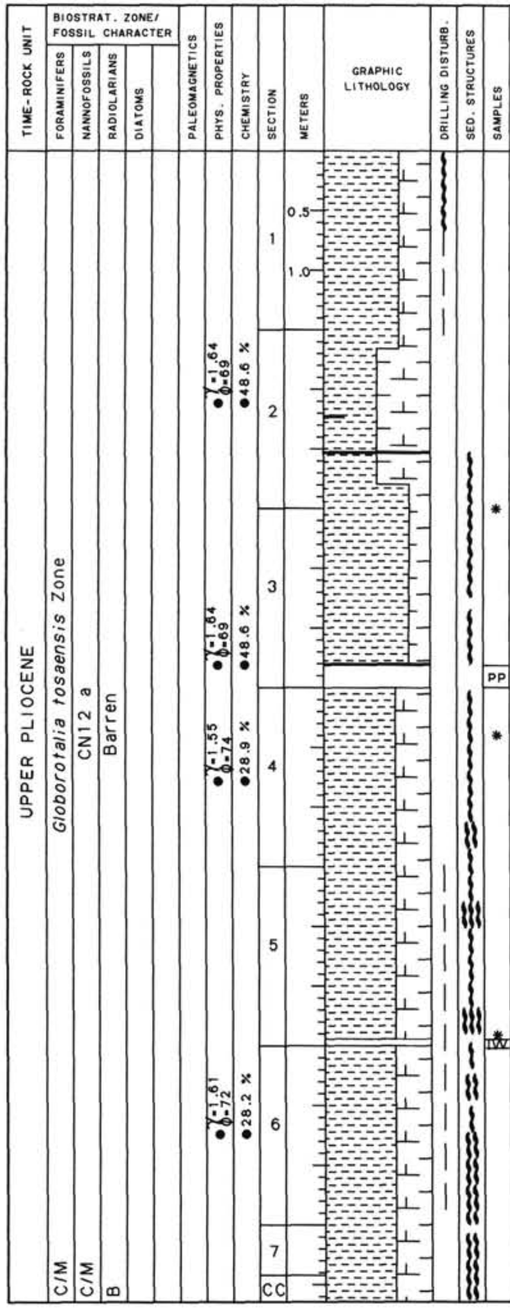

LITHOLOGIC DESCRIPTION

CALCAREOUS CLAY plus MARL

CALCAREOUS CLAY plus MARL; light gray to light olive-gray (2.5Y5/2, 2.5Y7/2, 5Y6/2); nannofossil-rich.

Minor lithology: minor thin ash beds, dark gray (2.5Y3/0); manganese-oxide(?) particles dispersed through sediment; horizontal bedding dips.

SMEAR SLIDE SUMMARY (%):

	3, 6 D	4, 43 D	5, 140 D
TEXTURE:			
Sand	2	—	—
Silt	18	10	4
Clay	80	90	96
COMPOSITION:			
Quartz	1	—	—
Feldspar	1	—	1
Clay	65	60	76
Accessory minerals			
Glauconite?	—	Tr	—
Opaque (Mn oxide)	15	—	Tr
Foraminifers	2	4	3
Nannofossils	15	30	20
Bioclasts	3	3	—

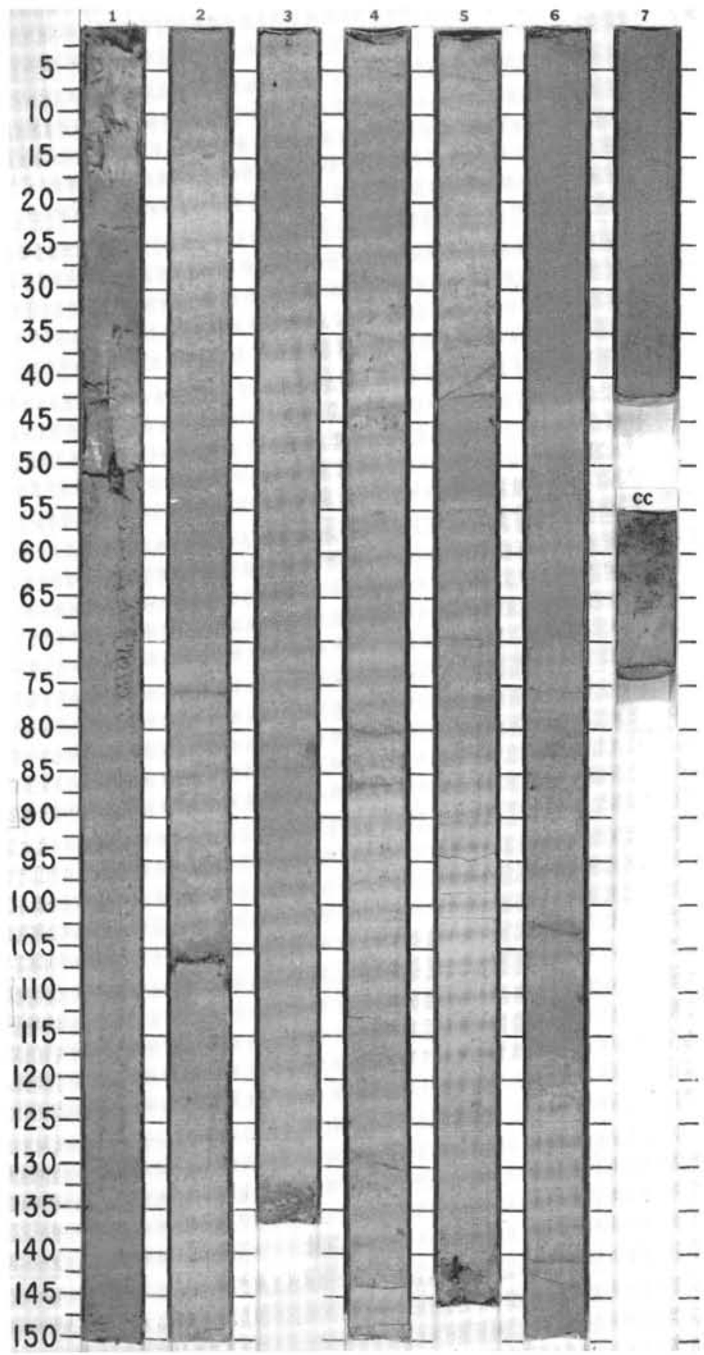

SITE 672 HOLE A CORE 6 H CORED INTERVAL 5014.3-5023.8 mbsl; 41.3-50.8 mbsf

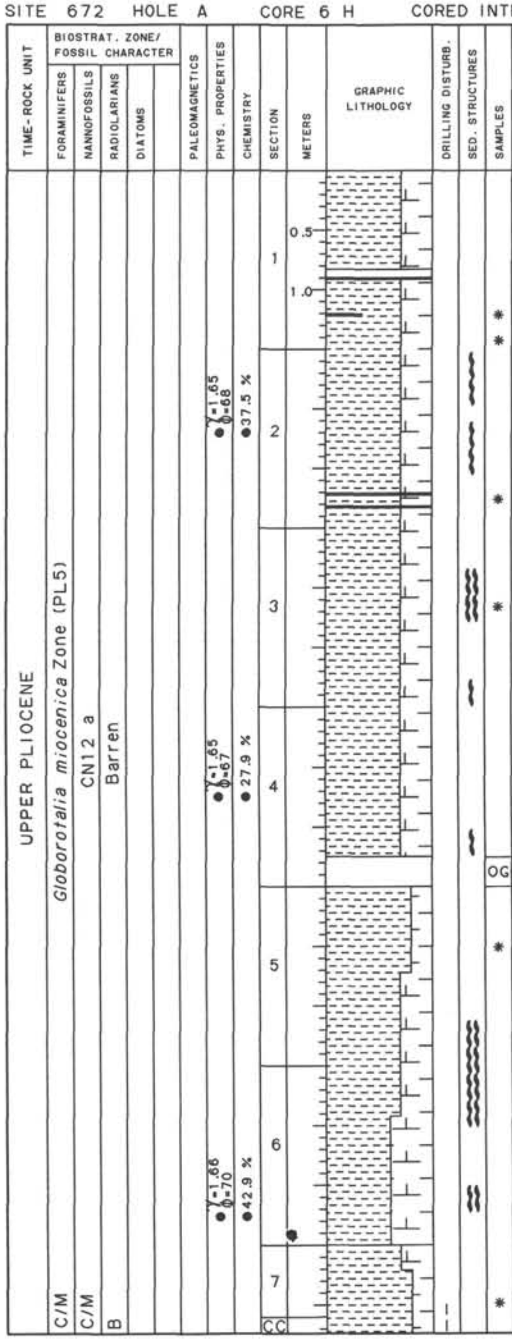

LITHOLOGIC DESCRIPTION

CALCAREOUS CLAY and MUD plus MARL

CALCAREOUS CLAY and MUD plus MARL; gray to light olive-gray (5Y5/1, 5Y6/3, 10Y5/1); nannofossil-rich.

Minor lithology: dispersed ash material and discrete ash beds, dark gray (2.5Y5/2), both lithic and vitric ash; horizontal bedding.

SMEAR SLIDE SUMMARY (%):

	1, 126 M	1, 150 D	2, 126 M	3, 69 M	5, 56 M	7, 60 D
TEXTURE:						
Sand	30	—	100	80	—	—
Silt	70	8	—	20	15	12
Clay	—	92	—	—	85	88
COMPOSITION:						
Feldspar	15	—	1	25	—	Tr
Rock fragments	37	—	55	38	—	—
Clay	—	75	—	—	70	70
Volcanic glass	30	—	40	30	1	—
Calcite/dolomite	—	4	—	—	—	—
Accessory minerals						
Fibrous zeolites	—	—	—	—	Tr	—
Orthopyroxene	2	—	2	2	—	—
Clinopyroxene	1	—	—	Tr	—	—
Opaques	1	1	2	5	8	—
Hornblende	3	—	—	—	Tr	—
Foraminifers	—	5	—	—	8	3
Nannofossils	—	15	—	—	10	20
Sponge spicules	—	Tr	—	—	—	—
Chitinozoa	—	—	—	—	—	Tr
Bioclasts	—	—	—	—	2	3

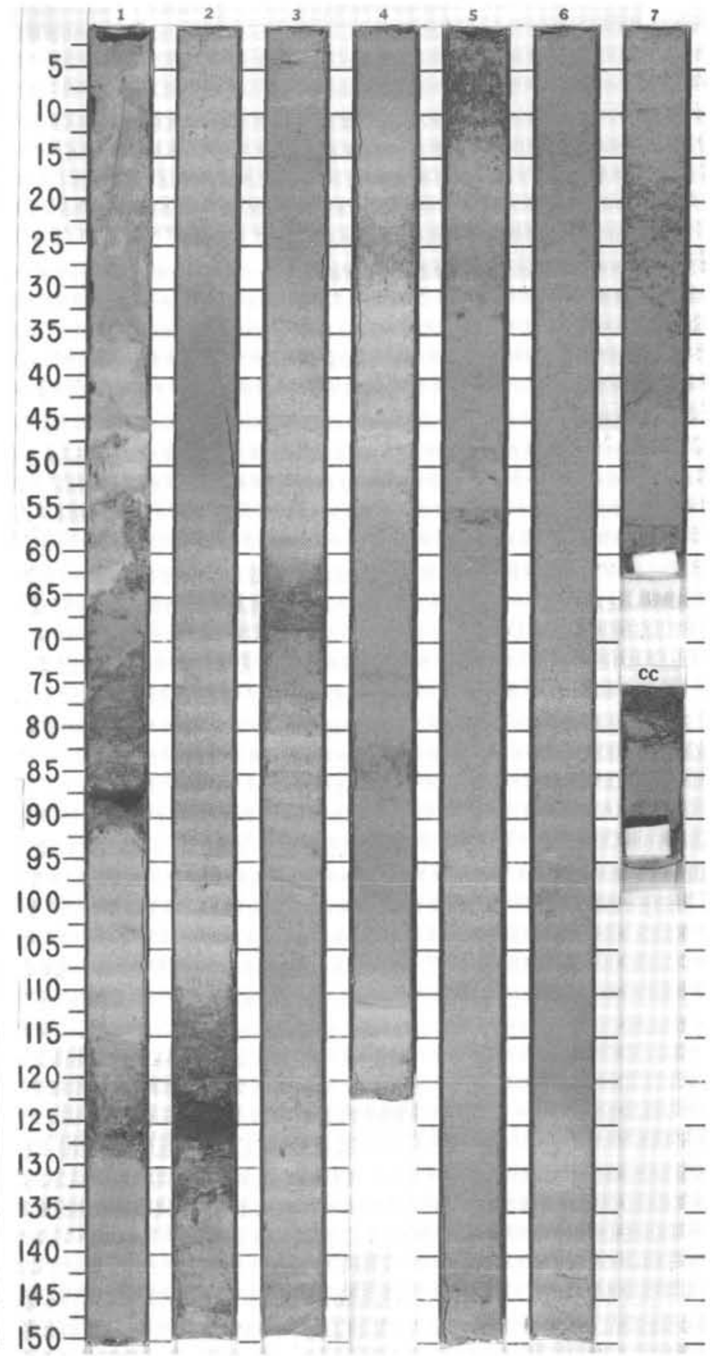

SITE 672 HOLE A CORE 7 H CORED INTERVAL 5023.8-5033.3 mbsl; 50.8-60.3 mbsf

TIME-ROCK UNIT	FORAMINIFERS	NANNOFOSSILS	RADIOLARIANS	DIATOMS	PALEOMAGNETICS	PHYS. PROPERTIES	CHEMISTRY	SECTION
UPPER PLIOCENE	*Globorotalia miocenica* Zone (PL5)	CN12 a	Barren			γ=1.69 φ=65; γ=1.68 φ=64; γ=1.68 φ=64	17.5 %; 27.6 %; 31.8 %	1, 2, 3, 4, 5, 6, 7, CC
	A/G	A/G	B					

Samples: *, PP, IW

LITHOLOGIC DESCRIPTION

CALCAREOUS CLAY plus MARL

CALCAREOUS CLAY plus MARL; light brownish and olive-gray (2.5Y6/2, 5Y6/2); nannofossil-rich.

Minor lithology: vitric and minor lithic ash dispersed through sediment and in discrete beds.

SMEAR SLIDE SUMMARY (%):

	1, 56 M	3, 77 D	4, 60 D	4, 123 M	5, 84 M
TEXTURE:					
Sand	10	—	—	—	8
Silt	20	15	2	5	25
Clay	70	85	98	95	67
COMPOSITION:					
Quartz	—	—	—	—	5
Feldspar	2	Tr	Tr	1	15
Clay	59	50	78	70	35
Volcanic glass	10	2	—	1	40
Accessory minerals					
Clinopyroxene	Tr	1	—	—	—
Opaques	—	1	—	—	2
Hornblende	—	Tr	—	—	1
Mn oxides	—	1	—	—	—
Foraminifers	—	5	—	5	—
Nannofossils	25	30	20	20	—
Radiolarians	—	1	—	1	—
Sponge spicules	1	—	Tr	—	—
Silicoflagellates	2	—	—	—	—
Bioclasts	—	10	—	2	1
Altered grains	—	—	—	—	2

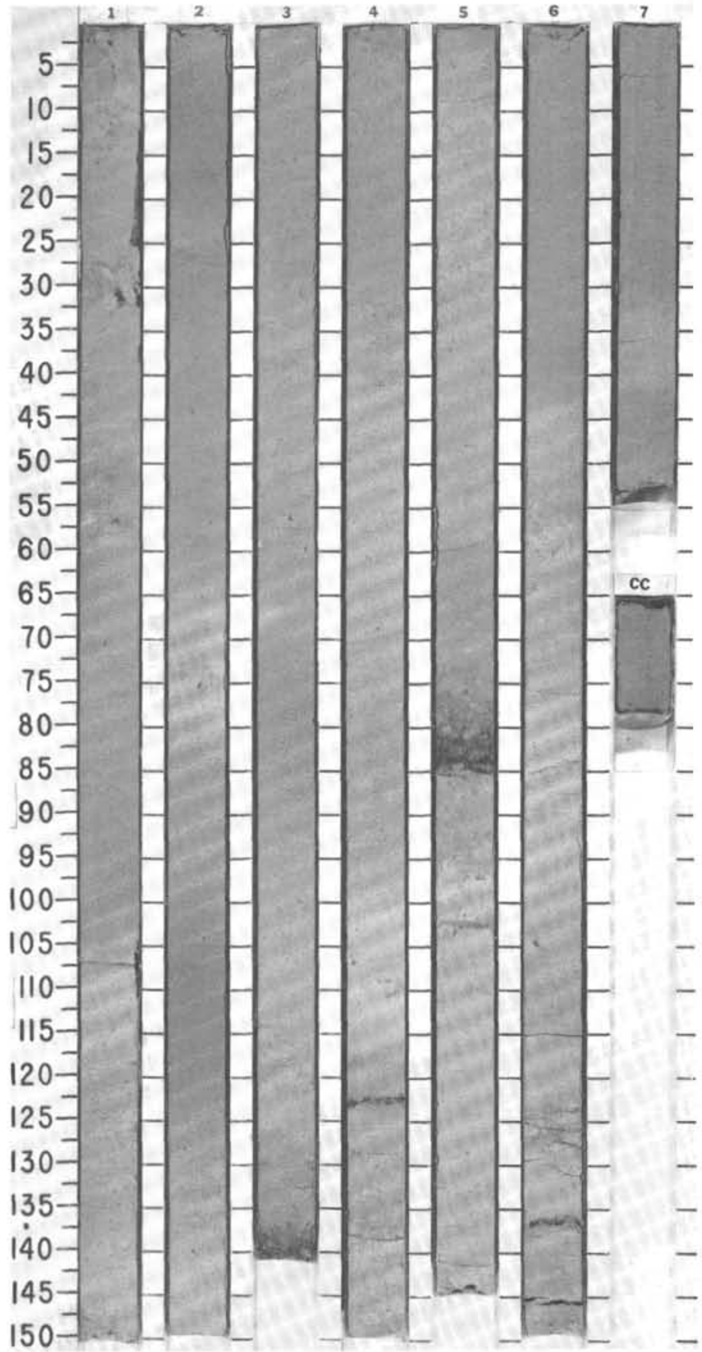

SITE 672 HOLE A CORE 8 H CORED INTERVAL 5033.3-5042.8 mbsl; 60.3-69.8 mbsf

TIME-ROCK UNIT	FORAMINIFERS	NANNOFOSSILS	RADIOLARIANS	DIATOMS	PALEOMAGNETICS	PHYS. PROPERTIES	CHEMISTRY	SECTION	METERS	GRAPHIC LITHOLOGY	DRILLING DISTURB.	SED. STRUCTURES	SAMPLES
UPPER PLIOCENE	*Globorotalia miocenica* Zone (PL3/PL4) C/P	CN12a A/G	Barren B			γ=1.68 φ=67; γ=1.64 φ=67; γ=1.70 φ=65; γ=1.63 φ=66	32.1 %; 38.8 %; 32.6 %; 41.5 %	1, 2, 3, 4, 5, 6, 7, CC	0.5, 1.0				* * * *

LITHOLOGIC DESCRIPTION

CALCAREOUS CLAY and MUD plus MARL

CALCAREOUS CLAY and MUD plus MARL; light gray, light brownish gray, and gray (2.5Y6/2, 10YR6/3, 5Y6/1); nannofossil-rich.

Minor lithology: disseminated and discrete vitric and lithic ash, dark gray (7.5YR3/1). Normal faults dipping 44°–68° show slickensided surfaces associated with bedding dipping 7° in Sections 1 through 4.

SMEAR SLIDE SUMMARY (%):

	1, 80 D	2, 60 M	4, 94 D	6, 116 D
TEXTURE:				
Silt	7	20	18	22
Clay	93	80	82	78
COMPOSITION:				
Feldspar	—	5	2	1
Clay	76	68	81	67
Volcanic glass	Tr	3	2	1
Accessory minerals				
Opaques	1	5	—	—
Hornblende	—	—	—	1
Mn oxides	Tr	—	—	—
Foraminifers	5	5	5	15
Nannofossils	15	10	5	10
Sponge spicules	Tr	—	—	—
Bioclasts	2	4	5	5

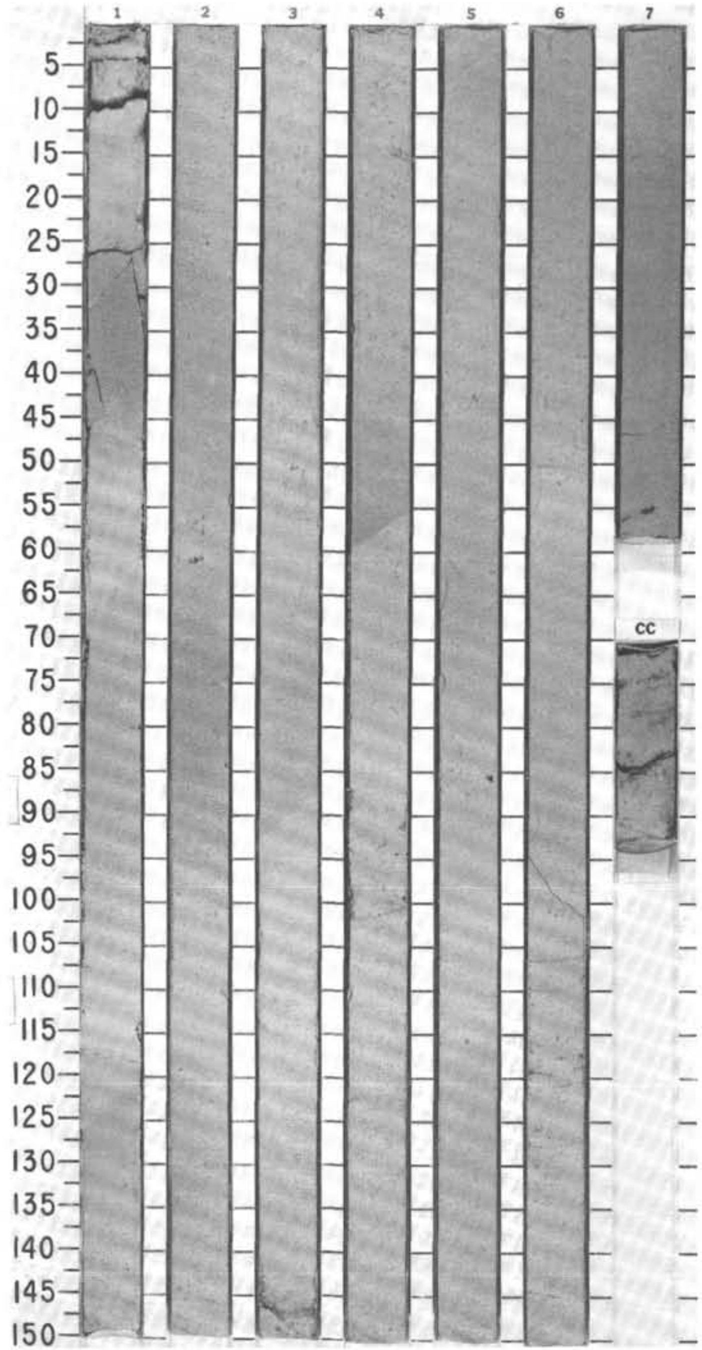

SITE 672 HOLE A CORE 9 H CORED INTERVAL 5042.8-5052.3 mbsl; 69.8-79.3 mbsf

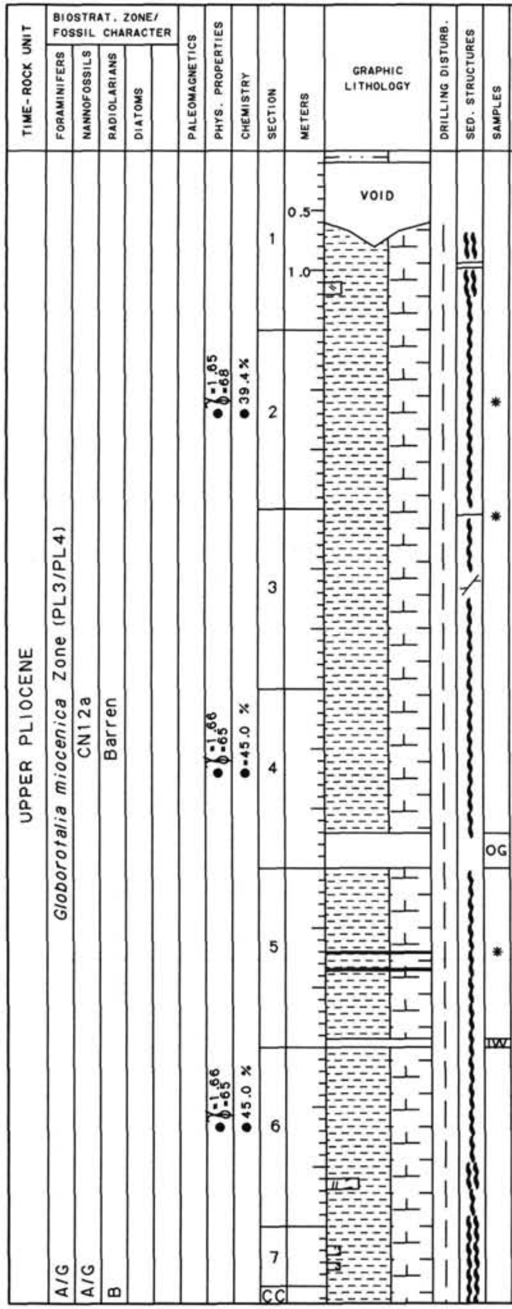

LITHOLOGIC DESCRIPTION

CALCAREOUS CLAY and MUD plus MARL

CALCAREOUS CLAY and MUD plus MARL; light brownish gray, light gray, and light olive-gray (2.5Y6/2, 5Y7/2, 5Y6/2, 5Y5/2); nannofossil-rich with some foraminifers.

Minor lithology: ash occurs dispersed through sediment and in discrete beds, dark gray (5Y4/1). Two normal faults dip 50° in Section 3, 60–75 cm.

SMEAR SLIDE SUMMARY (%):

	2, 57 D	3, 4 D	5, 70 M
TEXTURE:			
Sand	—	—	3
Silt	8	10	40
Clay	92	90	57
COMPOSITION:			
Feldspar	—	—	5
Clay	74	87	55
Volcanic glass	Tr	Tr	40
Accessory minerals			
Bright red(?)	—	—	Tr
Foraminifers	1	—	—
Nannofossils	25	13	—
Radiolarians	Tr	—	—

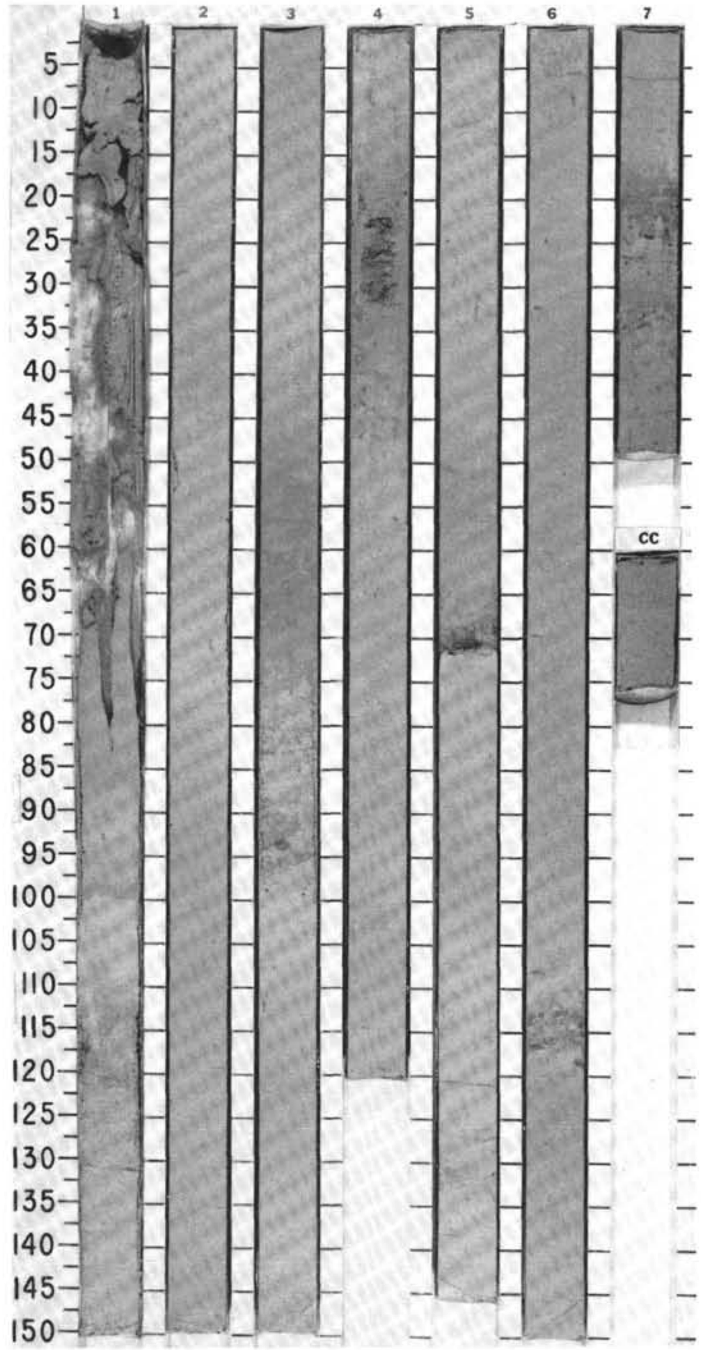

SITE 672 HOLE A CORE 10 H CORED INTERVAL 5052.3-5061.8 mbsl; 79.3-88.8 mbsf

TIME-ROCK UNIT	FORAMINIFERS	NANNOFOSSILS	RADIOLARIANS	DIATOMS	PALEOMAGNETICS	PHYS. PROPERTIES	CHEMISTRY	SECTION	METERS	GRAPHIC LITHOLOGY	DRILLING DISTURB.	SED. STRUCTURES	SAMPLES
LOWER PLIOCENE	*Globorotalia margaritae* Zone (PL2) A/G	CN11 A/G	Barren B			●γ=1.60 ●φ=69; ●γ=1.64 ●φ=67; ●γ=1.72 ●φ=62	●45.9 %; ●39.7 %; ●39.5 %	1, 2, 3, 4, 5, 6, 7, CC	0.5, 1.0	VOID			* * *

LITHOLOGIC DESCRIPTION

MARL

MARL; light gray to light olive-gray (5Y6/1, 5Y6/2); nannofossil-rich and foraminifer-rich.

Minor lithology: ash occurs dispersed throughout sediment and in discrete beds, dark gray (5Y3/1). Two 60°-dipping faults in Section 6, 40–65 cm; one displays reverse offset of 3 cm.

SMEAR SLIDE SUMMARY (%):

	1, 50 D	3, 60 D	5, 68 M
TEXTURE:			
Silt	10	5	75
Clay	90	95	25
COMPOSITION:			
Feldspar	—	—	5
Clay	75	88	25
Volcanic glass	Tr	2	70
Foraminifers	3	—	—
Nannofossils	22	10	—

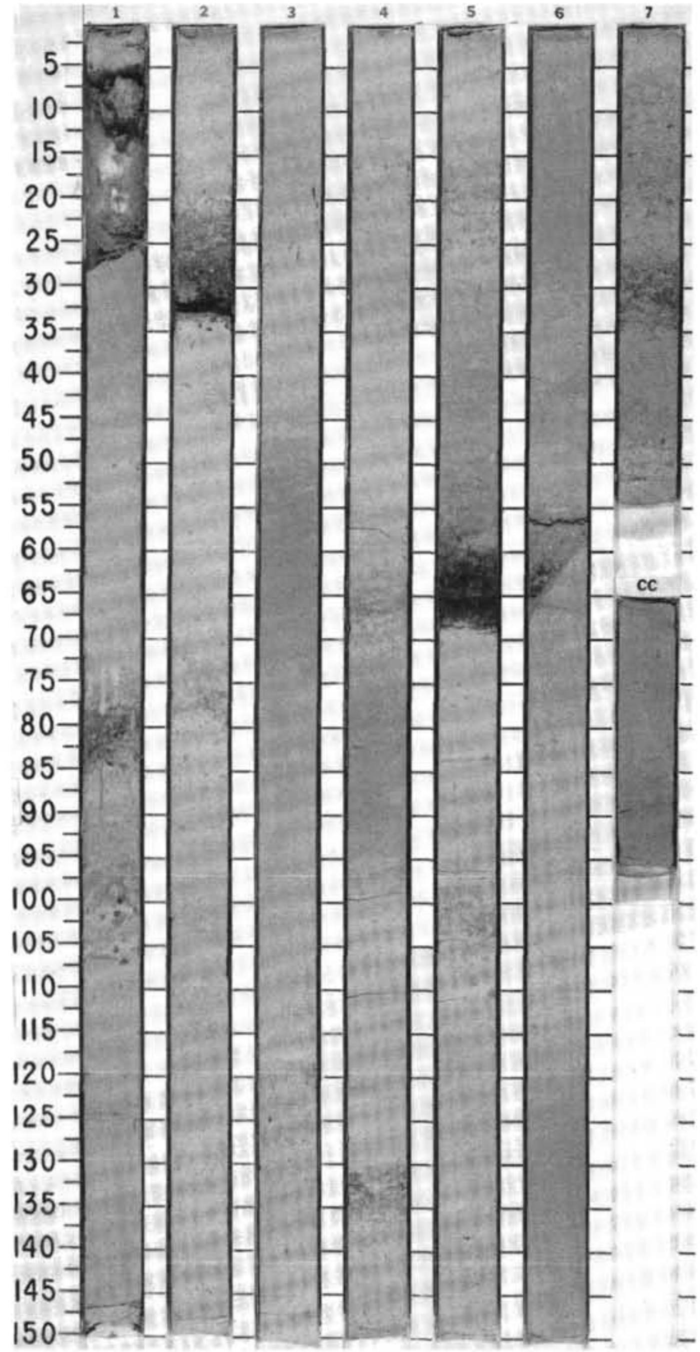

SITE 672 HOLE A CORE 11 H CORED INTERVAL 5061.8-5071.3 mbsl; 88.8-98.3 mbsf

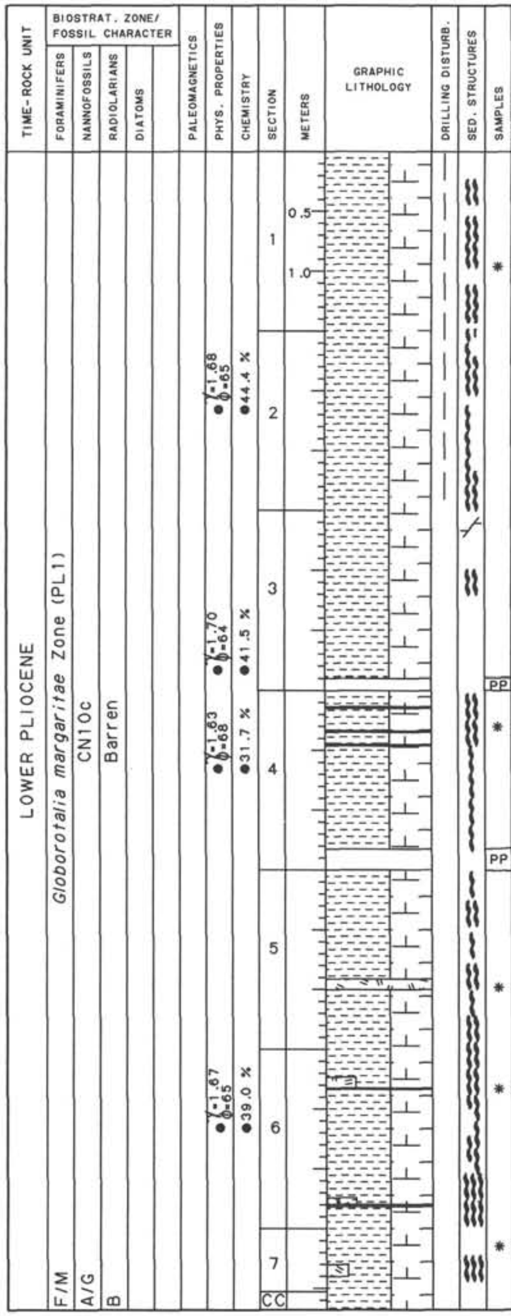

LITHOLOGIC DESCRIPTION

CALCAREOUS MUD and MARL

CALCAREOUS MUD and MARL; gray, light olive-gray, pale olive, light gray, and light brownish gray (5Y6/1, 5Y6/2, 5Y6/3, 5Y7/2, 2.5Y6/2); nannofossil- and foraminifer-rich.

Minor lithology: crystalline and vitric ash occurs dispersed throughout the sediment and as discrete beds, gray to dark gray (2.5Y4/0, 2.5Y3/0). A single fault with possible normal displacement is recorded at Section 3, 20 cm.

SMEAR SLIDE SUMMARY (%):

	1, 100 D	4, 35 M	5, 95 M	6, 32 M	7, 20 D
TEXTURE:					
Sand	5	2	5	—	—
Silt	25	63	65	75	5
Clay	70	35	30	25	95
COMPOSITION:					
Feldspar	—	40	15	40	—
Rock fragments	—	—	10	10	—
Clay	75	35	30	25	55
Volcanic glass	—	15	20	20	—
Accessory minerals					
Glauconite(?)	—	Tr	—	—	—
Pyroxene	—	3	—	—	—
Opaques	—	5	25	5	—
Foraminifers	3	1	—	—	3
Nannofossils	20	—	—	—	40
Bioclasts	2	1	—	—	2

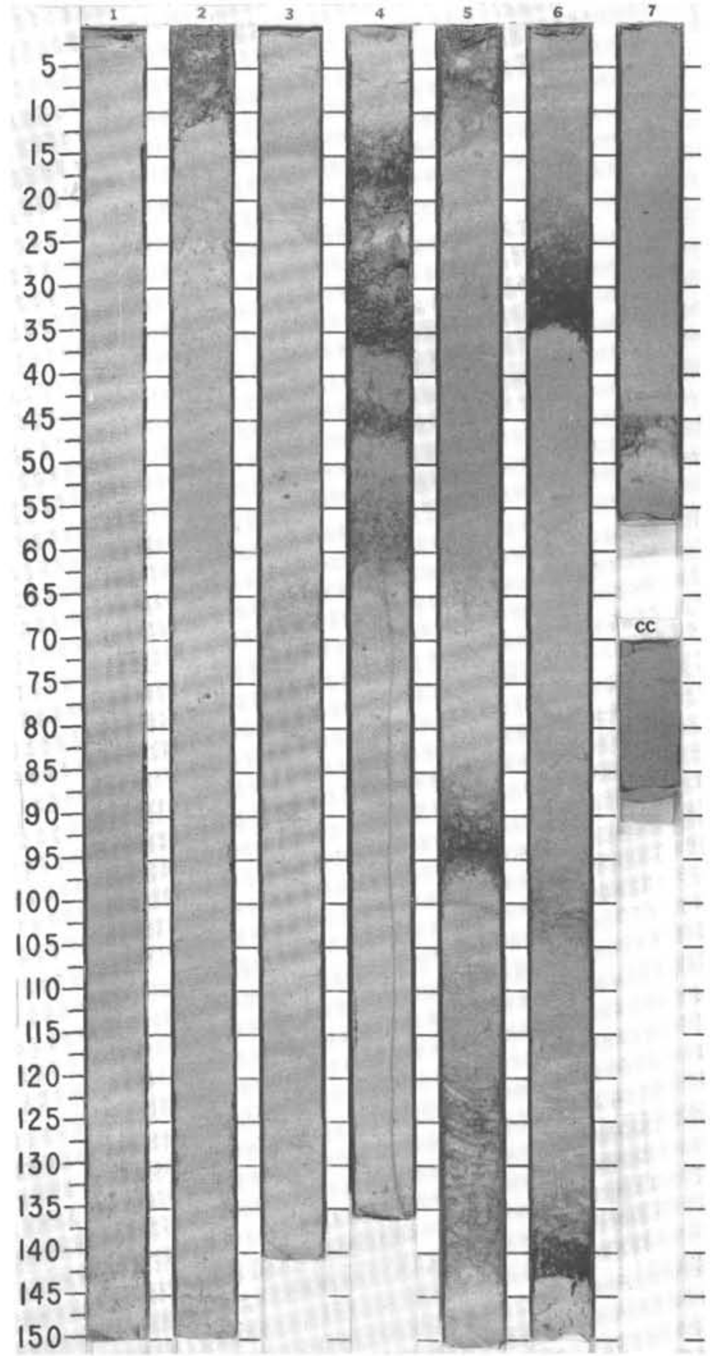

SITE 672 HOLE A CORE 12 H CORED INTERVAL 5071.3-5080.8 mbsl; 98.3-107.8 mbsf

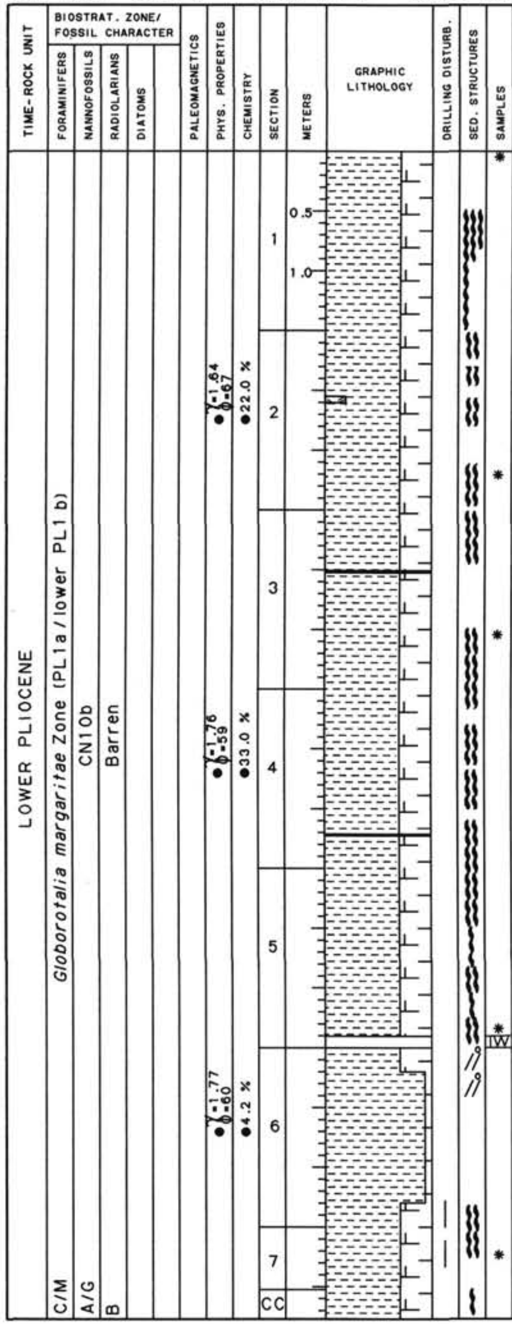

LITHOLOGIC DESCRIPTION

CALCAREOUS CLAY and MUD, MARL, and MUD

CALCAREOUS CLAY and MUD, MARL, and MUD; grayish brown, light gray, and olive-brown (2.5Y5/2, 2.5Y7/2, 2.5Y5/4); nannofossil-rich; *Zoophycos* burrows.

Minor lithology: vitric and crystalline ash occurs disseminated throughout the sediment and in discrete beds, gray and pale green (N5/0, 5G7/2). Several normal faults range in dip from 35°–85° and are intimately associated with "vein structures" that also dip steeply in Section 3, 70–105 cm, Section 5, 20–60 cm, and Section 6, 0–53 cm.

SMEAR SLIDE SUMMARY (%):

	1, 6 M	2, 127 D	3, 110 D	5, 142 D	7, 31 M
TEXTURE:					
Sand	2	Tr	—	—	Tr
Silt	78	20	10	5	20
Clay	20	80	90	95	80
COMPOSITION:					
Quartz	Tr	—	—	—	—
Feldspar	25	1	Tr	Tr	—
Rock fragments	15	—	—	—	—
Clay	20	65	60	70	50
Volcanic glass	25	2	—	Tr	20
Accessory minerals					
Pyroxene	3	Tr	—	—	—
Opaques	5	1	—	—	Tr
Hornblende	—	—	—	Tr	—
Foraminifers	Tr	5	—	—	—
Nannofossils	Tr	25	35	25	30
Sponge spicules	—	—	—	1	Tr
Bioclasts	—	—	5	2	—

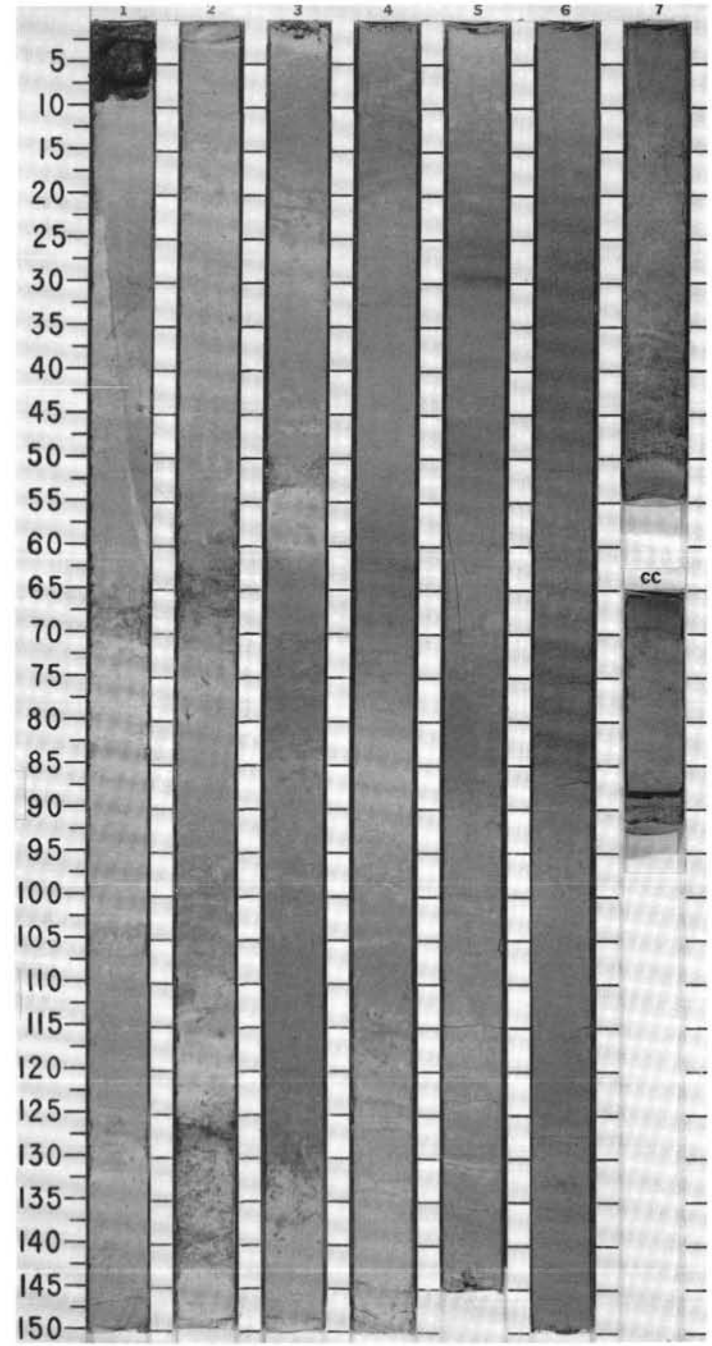

SITE 672 HOLE A CORE 13 H CORED INTERVAL 5080.8-5090.3 mbsl; 107.8-117.3 mbsf

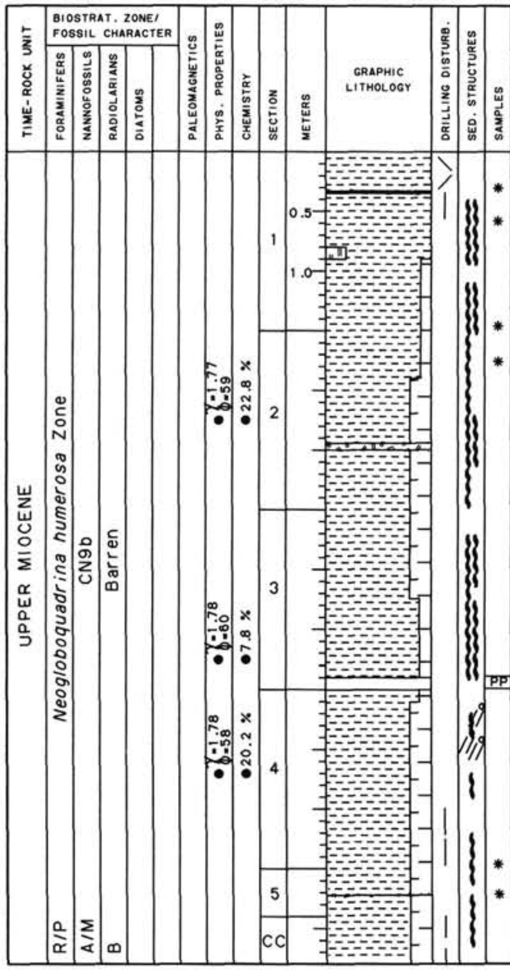

LITHOLOGIC DESCRIPTION

CALCAREOUS CLAY and CLAY plus MARL

CALCAREOUS CLAY and CLAY plus minor MARL; light olive-gray to olive (5Y6/2, 5Y5/4); nannofossil-rich.

Minor lithology: ash occurs disseminated throughout sediment and as discrete beds, dark gray and greenish gray (2.5Y3/0, 5BG7/1). "Vein structure" is observed in Section 4.

SMEAR SLIDE SUMMARY (%):

	1, 36 M	1, 64 D	1, 143 D	2, 27 M	4, 149 D	5, 26 M
TEXTURE:						
Sand	2	—	Tr	Tr	Tr	—
Silt	58	5	5	5	2	60
Clay	40	95	95	95	98	40
COMPOSITION:						
Quartz	Tr	—	—	—	—	—
Feldspar	20	—	Tr	Tr	1	2
Rock fragments	20	—	—	—	—	30
Clay	40	65	90	72	90	40
Volcanic glass	12	5	—	Tr	Tr	28
Accessory minerals						
Zeolites	—	Tr	—	—	—	—
Pyroxene	2	—	—	—	—	—
Opaques	5	Tr	Tr	—	—	Tr
Hornblende	—	—	—	Tr	—	—
Foraminifers	—	—	Tr	—	—	—
Nannofossils	Tr	35	10	25	8	Tr
Bioclasts	—	Tr	Tr	2	Tr	—

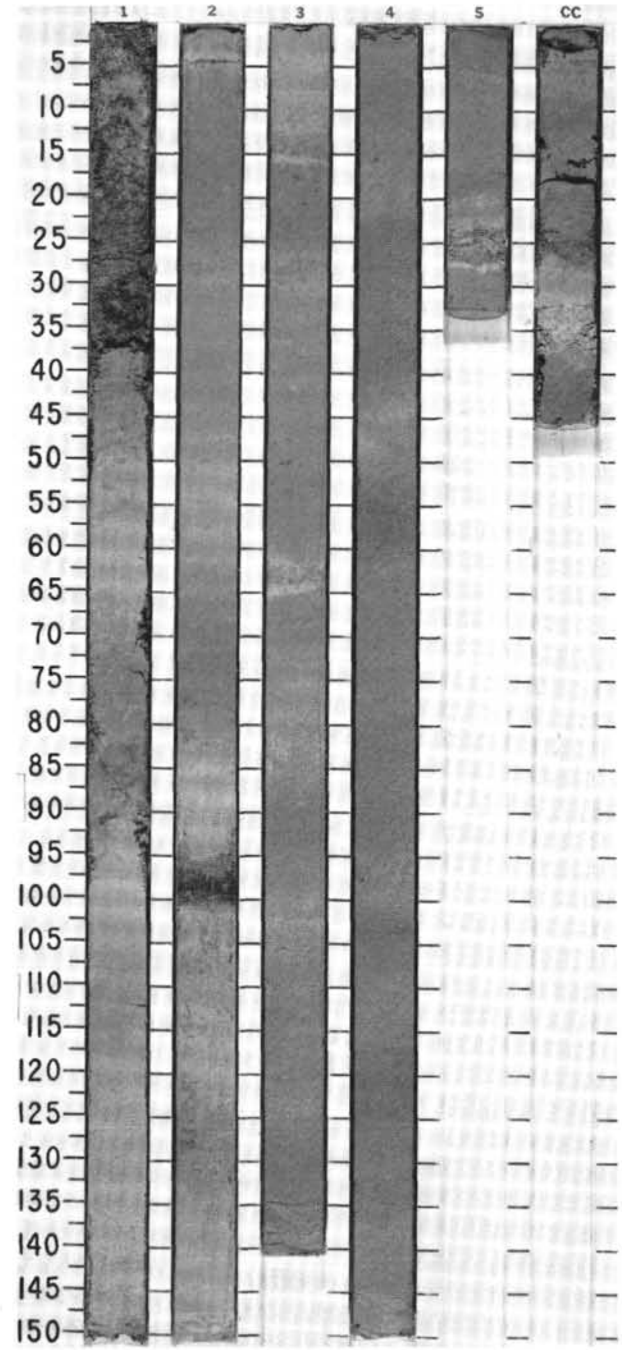

SITE 672 HOLE A CORE 14 H CORED INTERVAL 5090.3-5096.3 mbsl; 117.3-123.3 mbsf

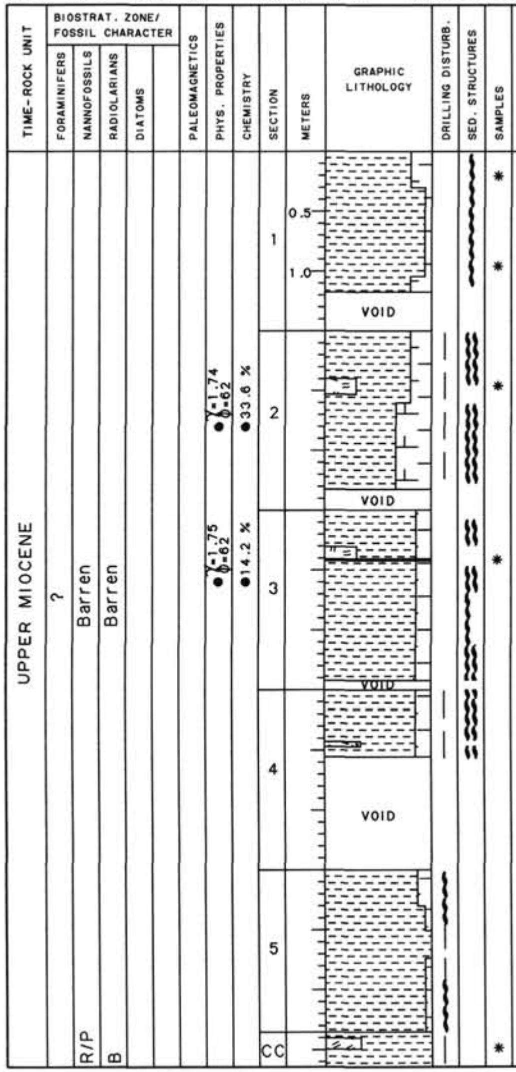

LITHOLOGIC DESCRIPTION

CALCAREOUS CLAY and MARL

CALCAREOUS CLAY and MARL; pale brown, light brownish gray, and grayish brown (10YR6/3, 2.5Y6/2, 2.5Y5/2); nannofossil-rich.

Minor lithology: ashy beds occur in Sections 2, 3, 4, and CC as dispersed crystalline and vitric ash material, light greenish gray (5G6/2, 5G7/2).

SMEAR SLIDE SUMMARY (%):

	1, 20 D	1, 96 D	2, 45 M	3, 47 M	CC M
TEXTURE:					
Sand	—	—	5	10	5
Silt	5	2	20	90	45
Clay	95	98	75	—	50
COMPOSITION:					
Quartz	—	—	1	—	—
Feldspar	—	—	2	10	1
Clay	78	93	77	—	64
Volcanic glass	—	—	15	86	35
Calcite/dolomite	—	1	—	—	—
Accessory minerals					
Orthopyroxene	—	—	—	2	—
Clinopyroxene	—	—	—	2	—
Opaques	—	Tr	—	—	Tr
Fe/Mn hydroxide	—	2	—	—	—
Nannofossils	20	—	5	—	—
Bioclasts	2	—	—	—	—

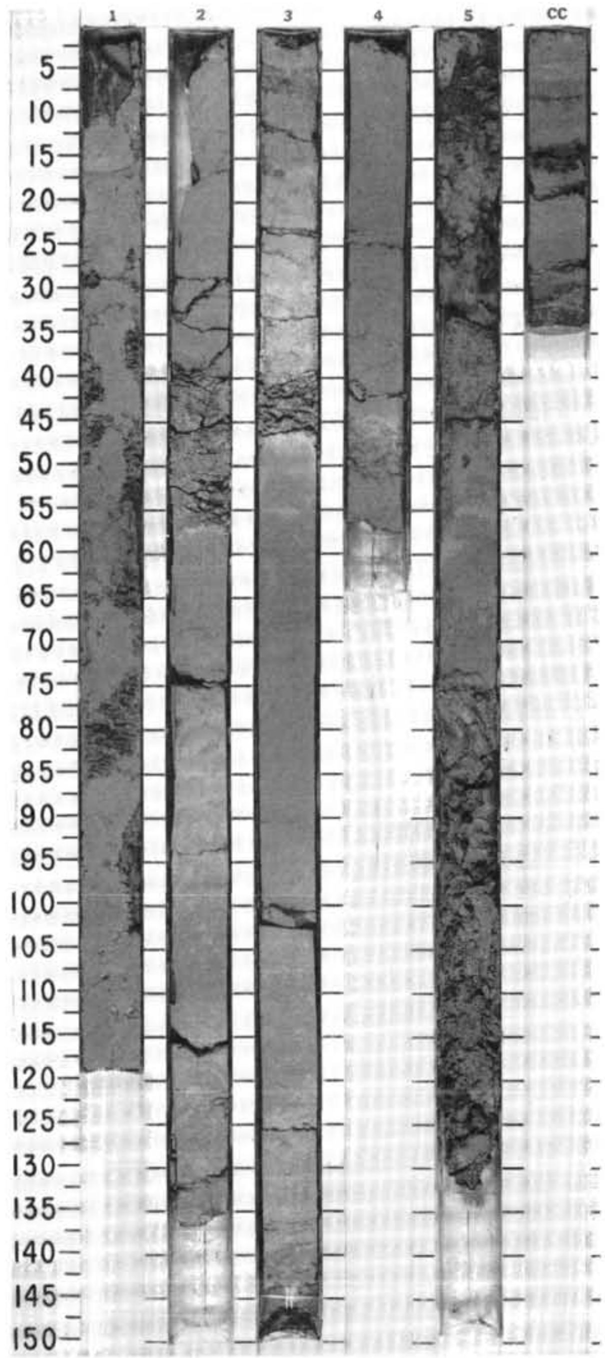

SITE 672 HOLE A CORE 15 X CORED INTERVAL 5096.3-5105.8 mbsl; 123.3-132.8 mbsf

TIME-ROCK UNIT	FORAMINIFERS	NANNOFOSSILS	RADIOLARIANS	DIATOMS	PALEOMAGNETICS	PHYS. PROPERTIES	CHEMISTRY	SECTION	METERS	GRAPHIC LITHOLOGY	DRILLING DISTURB.	SED. STRUCTURES	SAMPLES
UPPER MIOCENE ?	B Barren	B Barren	B Barren			●γ=1.58 ●φ=72	●0.9 %	1, 2, 3	0.5, 1.0				IW
						●γ=1.54 ●φ=74	●0.2 %	4, 5, CC					* * *

BIOSTRAT. ZONE/ FOSSIL CHARACTER

LITHOLOGIC DESCRIPTION

CLAYSTONE and MUDSTONE

CLAYSTONE and MUDSTONE; gray, grayish brown, and light grayish brown (5Y6/1, 5Y5/2, 5Y6/2).

Minor lithology: vitric and crystalline ash dispersed throughout the sediment, creating slightly darker colored horizons. Mostly massive with local *Planolites* and other burrows.

SMEAR SLIDE SUMMARY (%):

	4, 6 D	4, 53 M	5, 48 M
TEXTURE:			
Sand	—	Tr	—
Silt	15	25	2
Clay	85	75	98
COMPOSITION:			
Feldspar	3	Tr	Tr
Clay	85	94	98
Volcanic glass	10	—	—
Calcite/dolomite	—	2	—
Accessory minerals			
Opaques	2	Tr	Tr
Fe/Mn hydroxide(?)	—	Tr	Tr
Nannofossils	—	3	—
Sponge spicules	—	—	Tr
Bioclasts	—	—	2

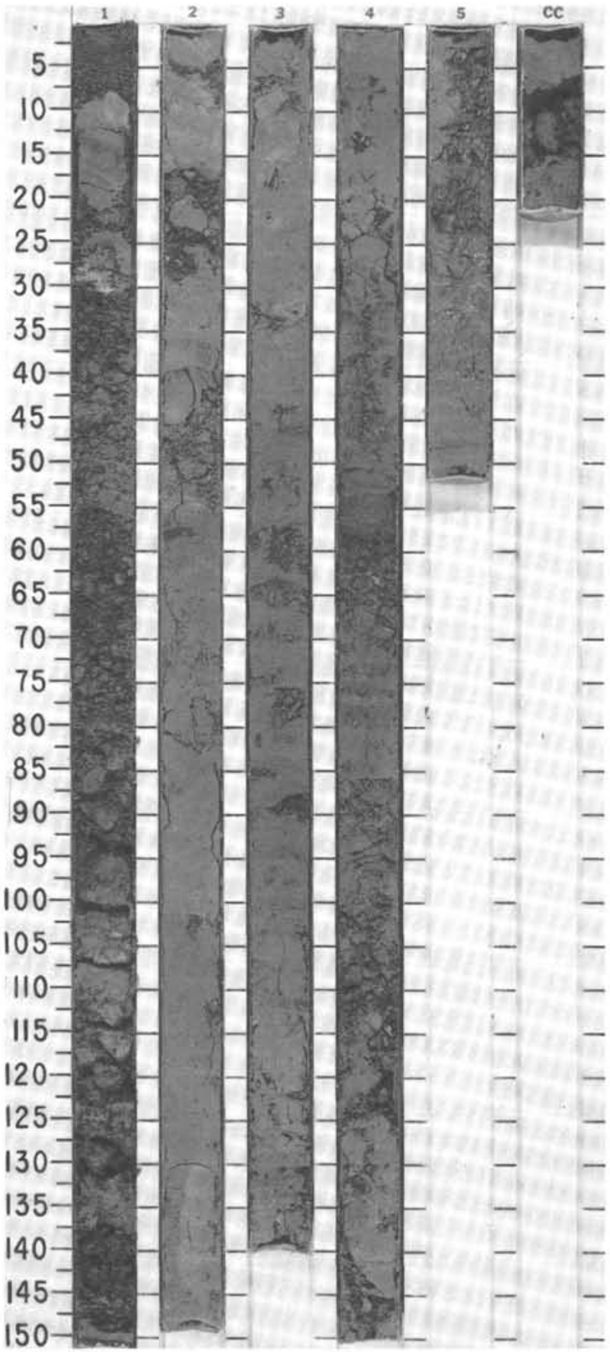

SITE 672 HOLE A CORE 16 X CORED INTERVAL 5105.8-5115.3 mbsl; 132.8-142.3 mbsf

TIME-ROCK UNIT	BIOSTRAT. ZONE/ FOSSIL CHARACTER: FORAMINIFERS	NANNOFOSSILS	RADIOLARIANS	DIATOMS	PALEOMAGNETICS	PHYS. PROPERTIES	CHEMISTRY	SECTION	METERS	GRAPHIC LITHOLOGY	DRILLING DISTURB.	SED. STRUCTURES	SAMPLES
UPPER MIOCENE	Barren B	Barren B	Barren B					1	0.5, 1.0	VOID			*
								2					*
								CC					

LITHOLOGIC DESCRIPTION

CLAYSTONE and MUDSTONE

CLAYSTONE and MUDSTONE; greenish gray and dark greenish gray (5GY6/1, 5BG4/1); strongly bioturbated; *Planolites* identified.

SMEAR SLIDE SUMMARY (%):

	1, 77 D	CC, 3 M
TEXTURE:		
Silt	—	45
Clay	100	55
COMPOSITION:		
Feldspar	Tr	1
Mica	Tr	—
Clay	100	55
Volcanic glass	Tr	—
Accessory minerals		
Opaques	Tr	44
Dark red grain	Tr	—
Sponge spicules	Tr	—

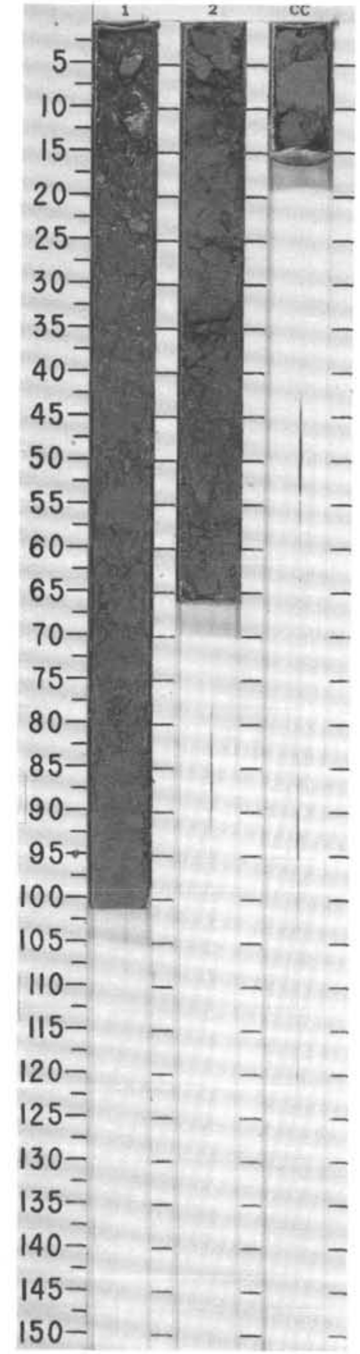

SITE 672 HOLE A CORE 17 X CORED INTERVAL 5115.3-5124.8 mbsl; 142.3-151.8 mbsf

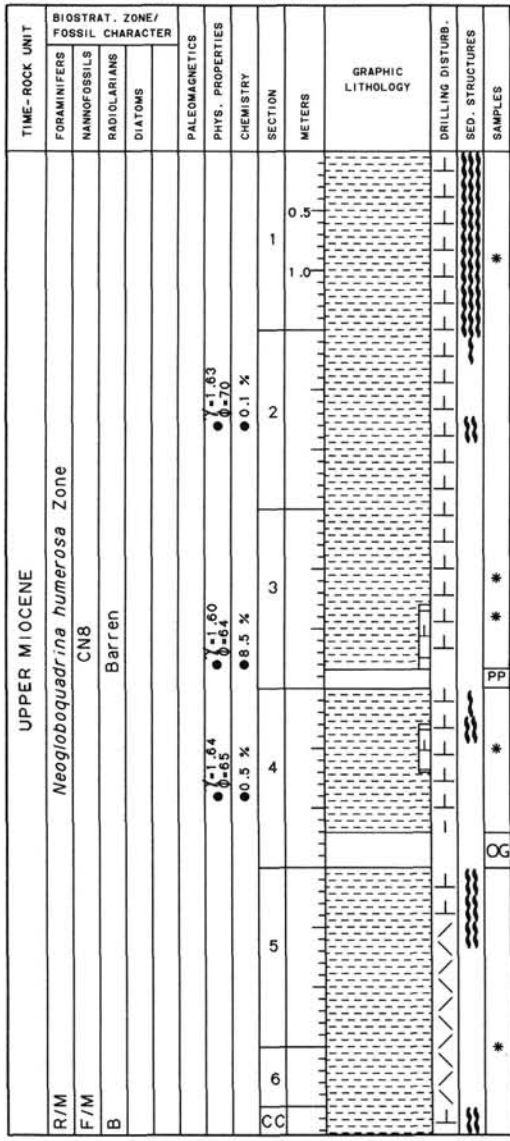

LITHOLOGIC DESCRIPTION

CLAYSTONE and CALCAREOUS MUDSTONE

CLAYSTONE and CALCAREOUS MUDSTONE; greenish gray, dark greenish gray, olive-gray, and grayish brown (5GY5/1, 5G4/1, 5Y5/2, 2.5Y5/2); silt fraction in mudstone consists of foraminifers.

Minor lithology: minor ash dispersed through sediment in Section 1; bioturbation moderate to slight; a near-vertical fault with normal displacement in Section 3.

SMEAR SLIDE SUMMARY (%):

	1, 91 M	3, 57 D	3, 97 D	4, 50 D	5, 148 D
TEXTURE:					
Silt	5	1	20	2	3
Clay	95	99	80	98	97
COMPOSITION:					
Quartz	—	Tr	—	—	—
Feldspar	4	Tr	1	Tr	2
Rock fragments	4	—	—	—	—
Clay	88	98	80	95	97
Calcite/dolomite	—	—	—	Tr	—
Accessory minerals					
Pyrite	2	1	1	—	1
Dark reddish mineral	1	—	—	—	—
Mn oxide	1	Tr	—	Tr	Tr
Nannofossils	—	Tr	15	5	—
Sponge spicules	—	Tr	—	—	—
Bioclasts	Tr	1	3	—	—

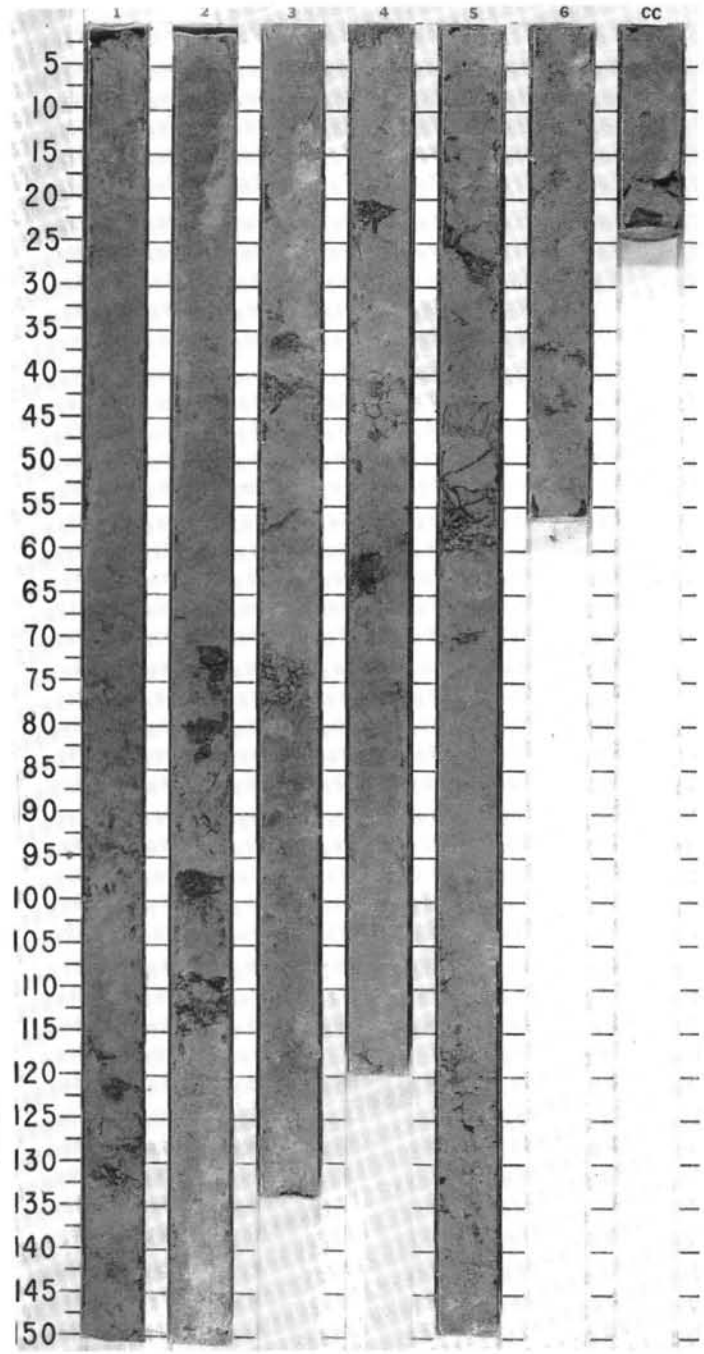

SITE 672 HOLE A CORE 18 X CORED INTERVAL 5124.8-5134.3 mbsl; 151.8-161.3 mbsf

TIME-ROCK UNIT	FORAMINIFERS	NANNOFOSSILS	RADIOLARIANS	DIATOMS	PALEOMAGNETICS	PHYS. PROPERTIES	CHEMISTRY	SECTION	METERS	GRAPHIC LITHOLOGY	DRILLING DISTURB.	SED. STRUCTURES	SAMPLES
UPPER MIOCENE	Barren	CN7	Barren					1	0.5, 1.0	VOID			
								2					*
								3					IW
						• γ=1.65 • φ=63	• 14.0 %	4					*
	B	F/M	B					CC					

LITHOLOGIC DESCRIPTION

CLAYSTONE, MUDSTONE, and CALCAREOUS CLAYSTONE

CLAYSTONE, MUDSTONE, and CALCAREOUS CLAYSTONE; olive-gray, greenish gray, and brownish gray (5Y4/2, 5GY6/2, 10Y5/2); slightly to moderately burrowed with *Zoophycos* recognized in Section 4, 54–63 cm.

SMEAR SLIDE SUMMARY (%):

	2, 137 D	4, 50 D
TEXTURE:		
Silt	11	5
Clay	89	95
COMPOSITION:		
Quartz	—	Tr
Feldspar	1	1
Clay	88	84
Volcanic glass	—	Tr
Accessory minerals		
Opaques	10	—
Foraminifers	—	Tr
Nannofossils	—	15
Bioclasts	—	2

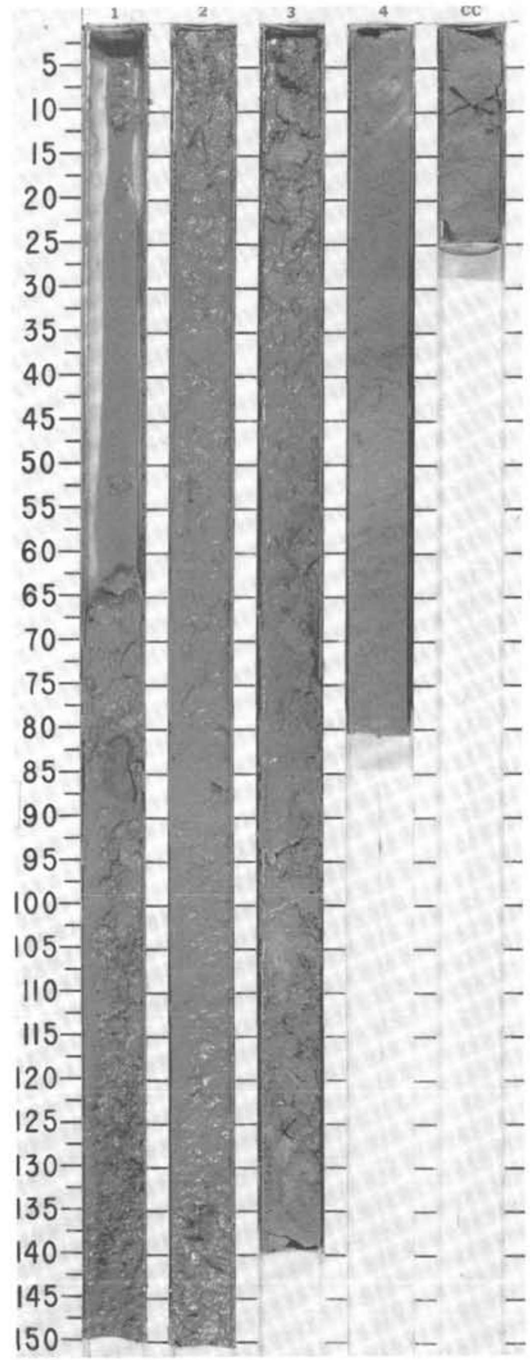

SITE 672 HOLE A CORE 19 X CORED INTERVAL 5134.3-5143.8 mbsl; 161.3-170.8 mbsf

TIME-ROCK UNIT	FORAMINIFERS	NANNOFOSSILS	RADIOLARIANS	DIATOMS	PALEOMAGNETICS	PHYS. PROPERTIES	CHEMISTRY	SECTION	METERS	GRAPHIC LITHOLOGY	DRILLING DISTURB.	SED. STRUCTURES	SAMPLES
?	Barren B	Barren B	Barren B			●γ=1.52 ●φ=74 ●γ=1.56 ●φ=72	●0.0 % ●0.0 %	1 2 3 4 5 6 CC	0.5 1.0				* * * PP *

LITHOLOGIC DESCRIPTION

CLAYSTONE

CLAYSTONE; greenish gray to olive-gray and olive-brown (5GY5/1, 5Y5/2, 2.5Y5/3); slightly to intensely burrowed with at least three burrow generations; includes *Planolites* and *Chondrites*.

Minor lithology: dispersed ash found in Section 3.

SMEAR SLIDE SUMMARY (%):

	2, 16 M	2, 73 D	3, 23 D	CC, 31 D
TEXTURE:				
Silt	7	2	3	—
Clay	93	98	97	100
COMPOSITION:				
Quartz	—	Tr	—	—
Plagioclase	3	1	1	Tr
Rock fragments	—	Tr	—	—
Mica	Tr	—	Tr	—
Clay	89	97	93	100
Volcanic glass	5	1	1	Tr
Accessory minerals	3	1	3	—
Hornblende	Tr	—	—	—
Deep red mineral	—	Tr	Tr	—
Nannofossils	—	—	1	Tr
Sponge spicules	Tr	Tr	1	Tr
Bioclasts	—	—	Tr	Tr

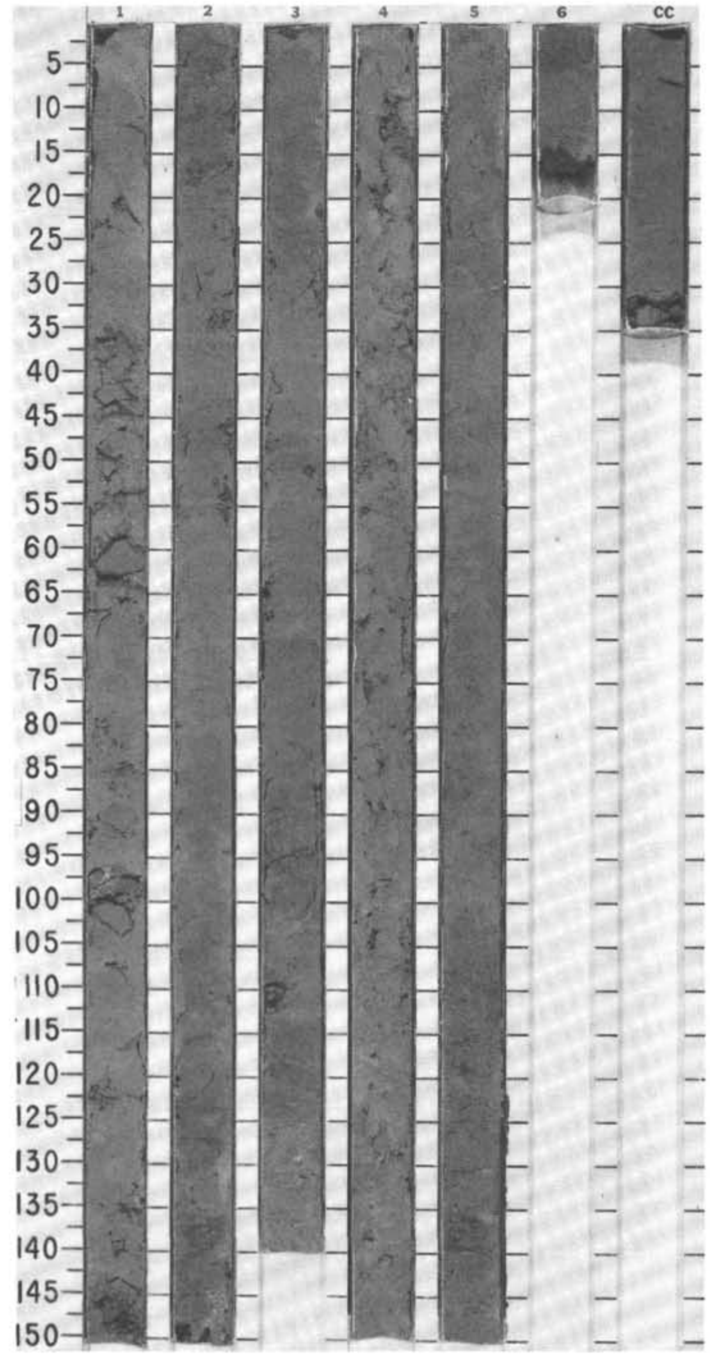

SITE 672 HOLE A CORE 20 X CORED INTERVAL 5143.8-5153.3 mbsl; 170.8-180.3 mbsf

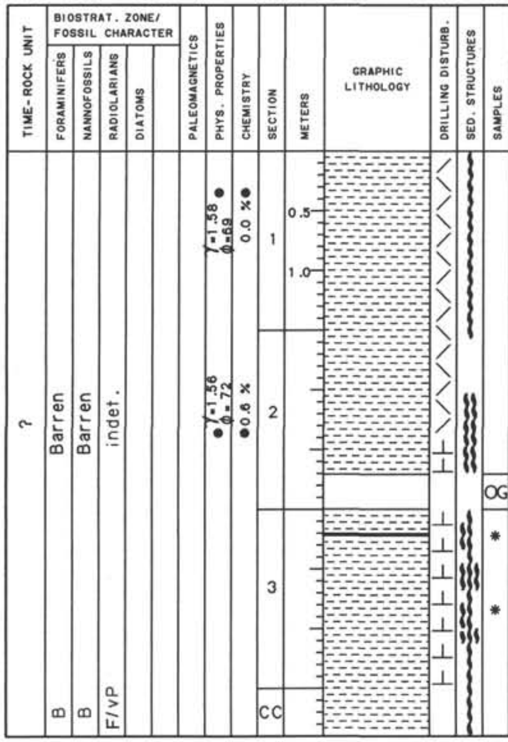

LITHOLOGIC DESCRIPTION

CLAYSTONE

CLAYSTONE; greenish gray (5GY5/1, 5GY6/1); with slight to intense burrowing causing mottling of sediment.

Minor lithology: discrete vitric ash beds found in Sections 2, 3, and CC, dark gray (N2, N4); ash also concentrated in burrows. "Vein structure" developed in low-angle normal shear zones throughout core.

SMEAR SLIDE SUMMARY (%):

	3, 19 M	3, 85 D
TEXTURE:		
Sand	1	Tr
Silt	15	5
Clay	84	95
COMPOSITION:		
Feldspar	Tr	—
Clay	40	95
Volcanic glass	60	5

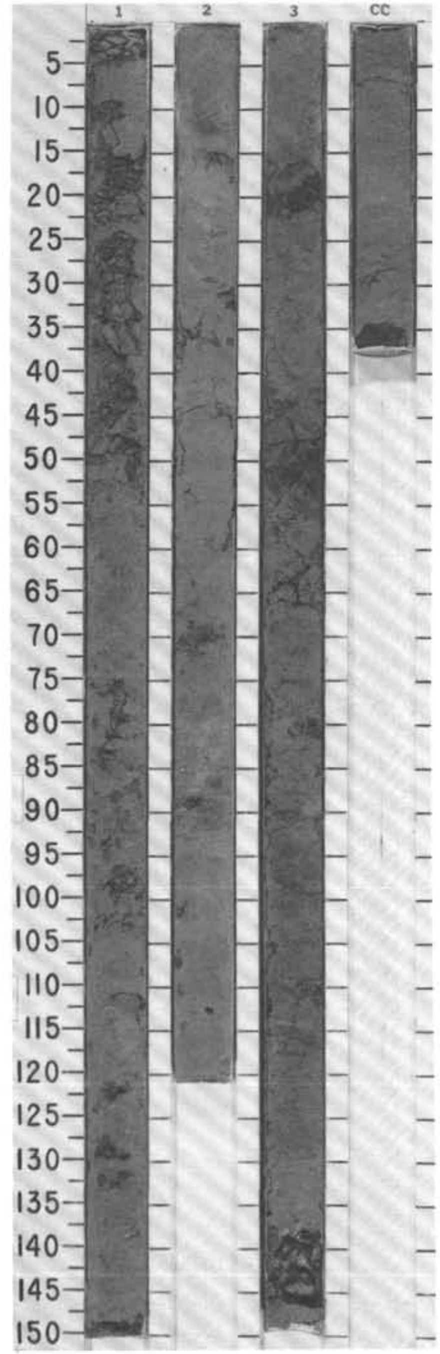

SITE 672 HOLE A CORE 21 X CORED INTERVAL 5153.3-5162.8 mbsl; 180.3-189.8 mbsf

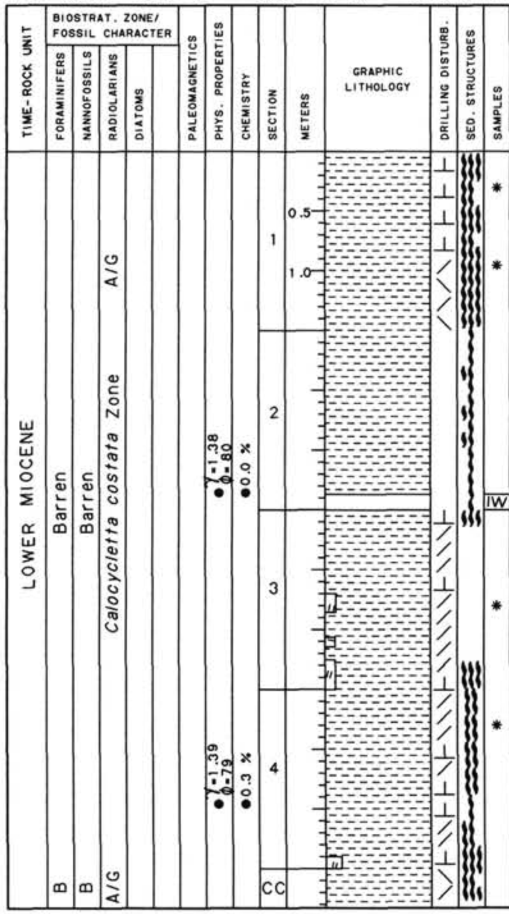

LITHOLOGIC DESCRIPTION

CLAYSTONE

CLAYSTONE, light brownish gray, pale olive, olive, and yellowish brown (2.5Y6/3, 5Y6/3, 5Y5/3, 10YR5/4); slightly to strongly bioturbated, with *Zoophycos*, *Chondrites* and *Planolites* identified.

Minor lithology: disseminated ash occurs in dark layers in Section 3. Two generations of "vein structure," the first is sigmoidal and steeply dipping and records downward flow of material; the second is at low angles and mostly shows normal shear offset. Bedding dip around 20–30°, locally as much as 65–75°.

SMEAR SLIDE SUMMARY (%):

	1, 31 D	1, 93 D	3, 83 D	4, 32 M
TEXTURE:				
Sand	—	Tr	—	—
Silt	5	6	8	5
Clay	95	94	92	95
COMPOSITION:				
Quartz	5	—	—	Tr
Feldspar	—	Tr	—	Tr
Clay	95	93	92	95
Volcanic glass	—	3	5	3
Accessory minerals				
Mn oxides	—	—	Tr	—
Diatoms	—	Tr	Tr	—
Radiolarians	—	3	3	2
Sponge spicules	—	Tr	Tr	Tr

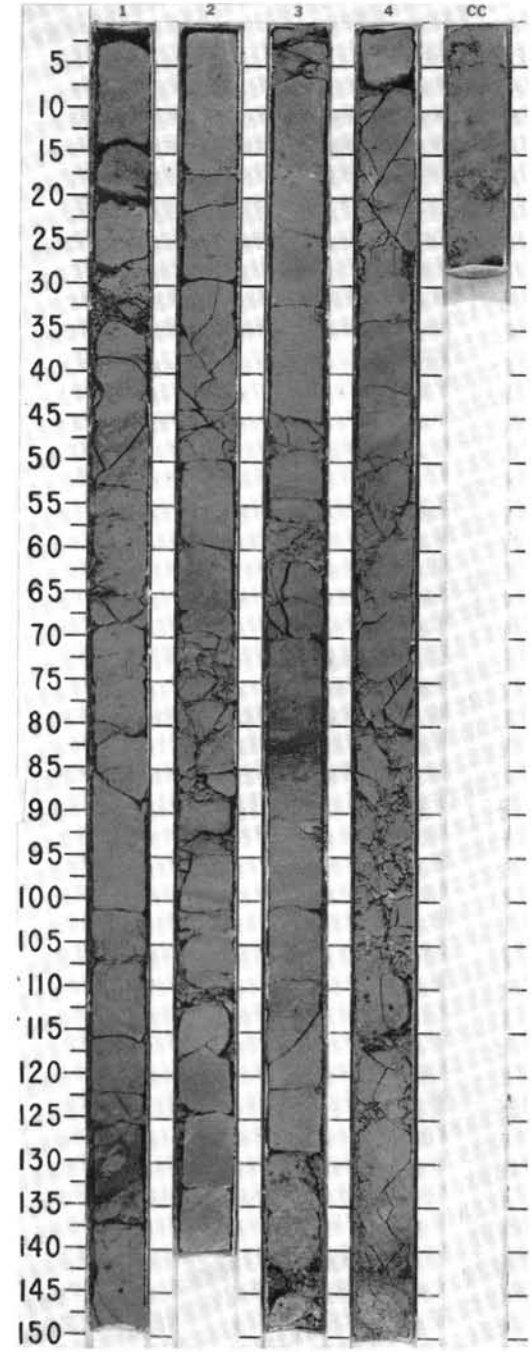

SITE 672 HOLE A CORE 22 X CORED INTERVAL 5162.8-5172.3 mbsl; 189.8-199.3 mbsf

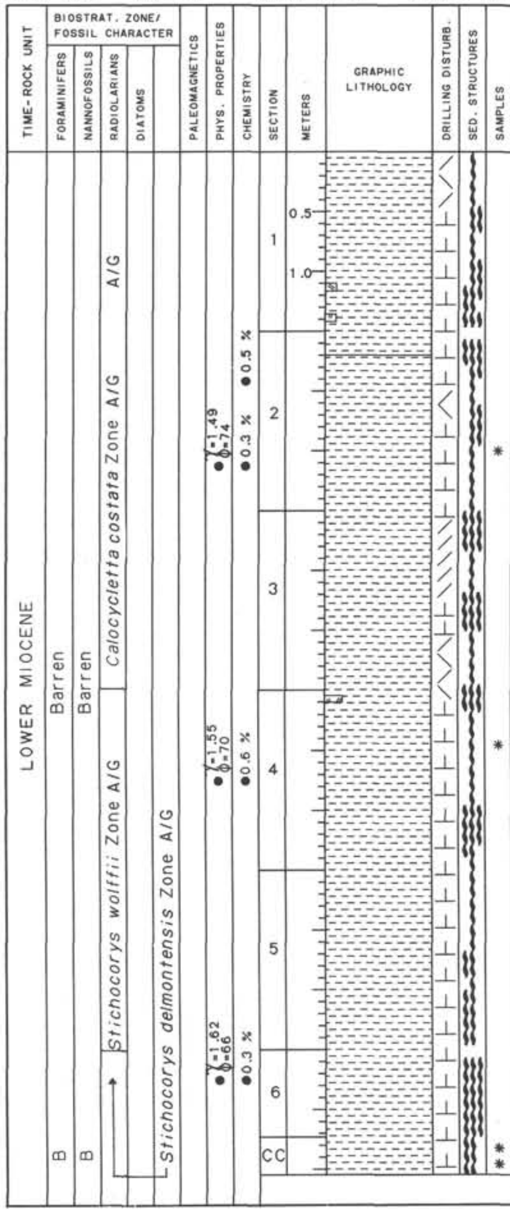

LITHOLOGIC DESCRIPTION

CLAYSTONE

CLAYSTONE; pale olive, light olive-gray, light brownish gray, and brown (5Y6/3, 5Y6/2, 2.5Y6/3, 7.5YR5/4); slight to intense bioturbation.

Minor lithology: minor ash-rich mudstone, vitric and crystal ash, in Sections 1–5. "Vein structure" developed in Sections 1–3.

SMEAR SLIDE SUMMARY (%):

	2, 105	4, 45	CC, 13	CC, 24
TEXTURE:				
Sand	1	3	3	2
Silt	5	15	7	10
Clay	94	82	90	88
COMPOSITION:				
Quartz	—	—	—	2
Feldspar	2	3	—	2
Clay	91	82	87	80
Volcanic glass	5	10	10	6
Accessory minerals				
Opaque/Mn oxide	—	—	—	10
Radiolarians	2	5	3	Tr

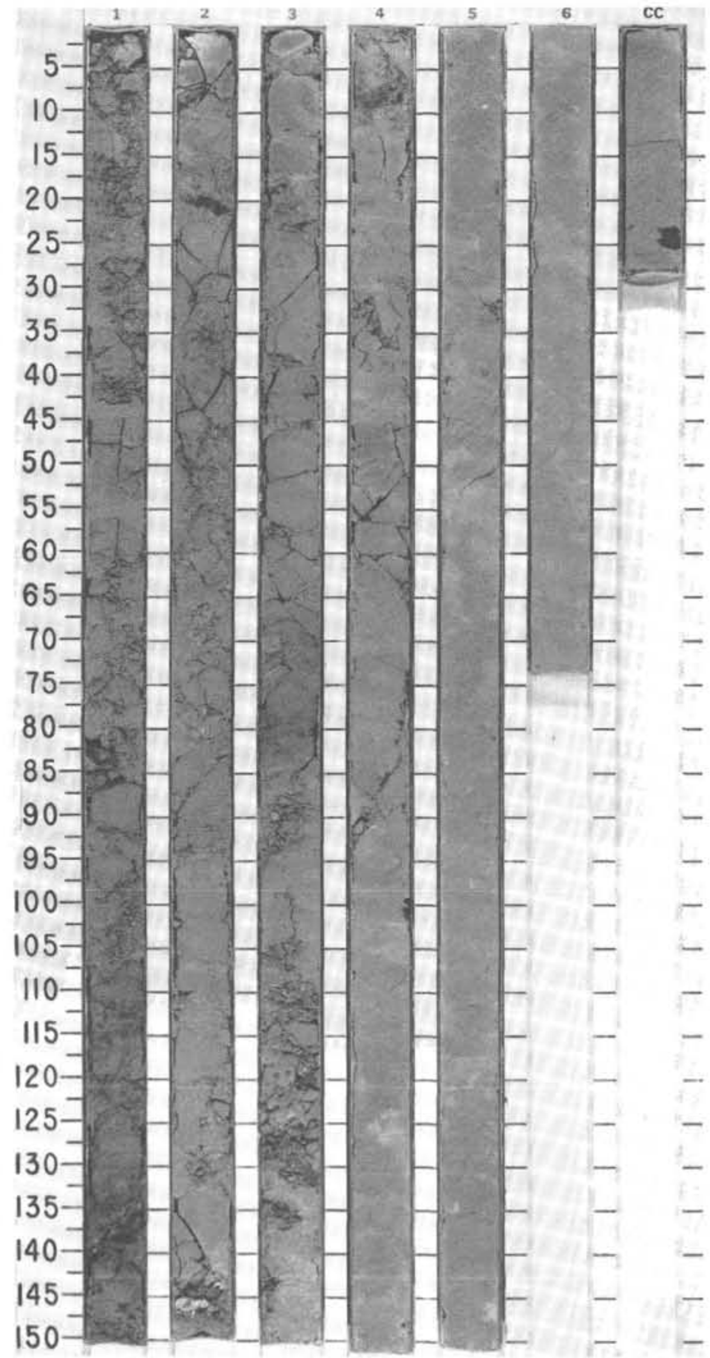

SITE 672 HOLE A CORE 23 X CORED INTERVAL 5172.3-5181.8 mbsl; 199.3-208.8 mbsf

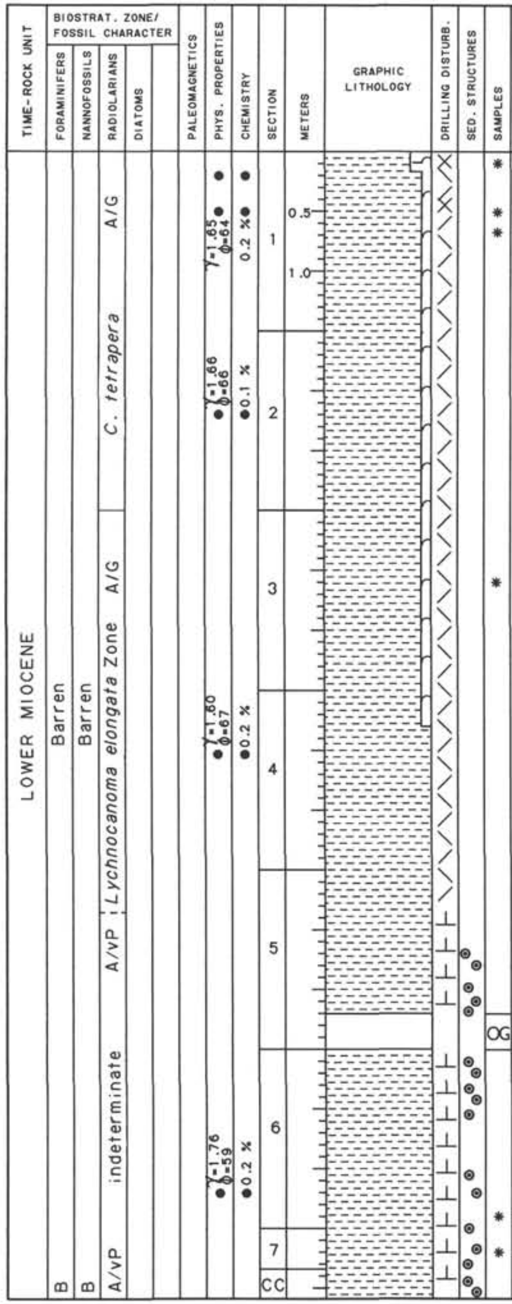

LITHOLOGIC DESCRIPTION

MUDSTONE, CLAYSTONE, and SILICEOUS MUDSTONE

MUDSTONE, CLAYSTONE, and SILICEOUS MUDSTONE; light yellowish brown, pale olive, and olive (10YR6/4, 5Y6/3, 10Y6/2, 5Y5/3), unbioturbated with zeolite concretions (0.5–1.0 mm diameter); SILICEOUS MUDSTONE consists of radiolaria in silt fraction.

SMEAR SLIDE SUMMARY (%):

	1, 7 M	1, 54 D	1, 64 D	3, 60 D	6, 147 D	7, 20 M
TEXTURE:						
Sand	—	—	—	—	—	5
Silt	20	25	5	20	1	80
Clay	80	75	95	80	99	15
COMPOSITION:						
Feldspar	Tr	—	—	—	—	—
Clay	80	83	95	80	99	15
Volcanic glass	—	—	—	10	—	5
Calcite/dolomite	—	—	—	—	Tr	—
Accessory minerals	—	—	—	—	Tr	—
Dissem. pyrite	—	15	—	—	—	—
Authigenic zeolite	—	—	—	—	—	80
Radiolarians	20	1	5	10	Tr	—
Sponge spicules	—	1	—	Tr	—	—
Silicoflagellates	Tr	—	—	—	—	—

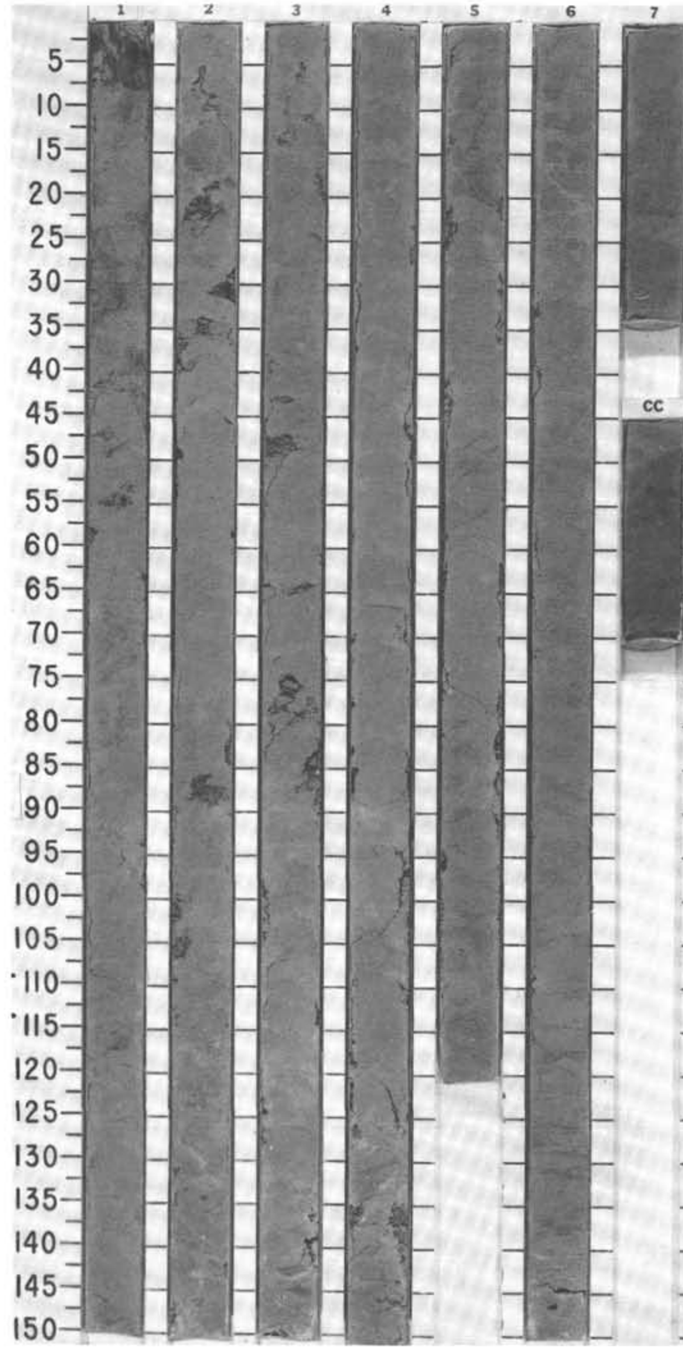

SITE 672 HOLE A CORE 24 X CORED INTERVAL 5181.8-5191.3 mbsl; 208.8-218.3 mbsf

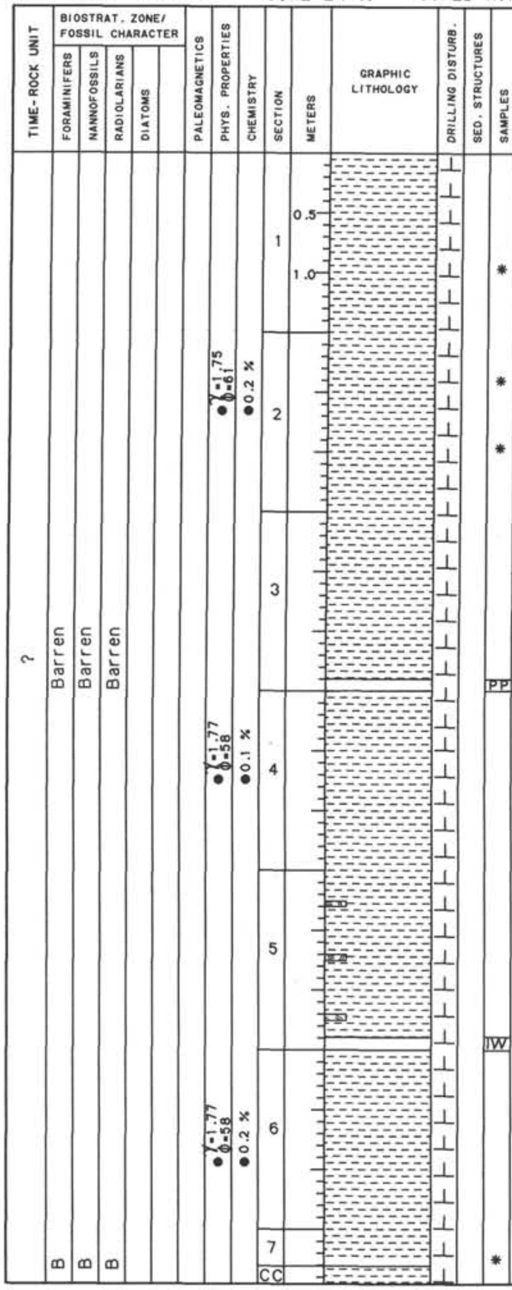

LITHOLOGIC DESCRIPTION

CLAYSTONE

CLAYSTONE; light olive-gray, greenish gray, olive, olive-gray, and bluish gray (5Y6/2, 5G6/1, 5G5/2, 5Y5/3, 5Y5/2, 5G6/2).

Minor lithology: very minor siltstone in Section 6; unbioturbated. Dispersed altered ash may be responsible for bluish/greenish gray beds.

SMEAR SLIDE SUMMARY (%):

	1, 96 D	2, 48 M	2, 93 D	7, 27 D
TEXTURE:				
Silt	5	85	5	8
Clay	95	15	95	92
COMPOSITION:				
Quartz	—	60	—	—
Clay	95	15	95	97
Volcanic glass	5	20	5	—
Calcite/dolomite	—	—	—	2
Accessory minerals	—	50	—	1
Pyroxene	—	Tr	—	—

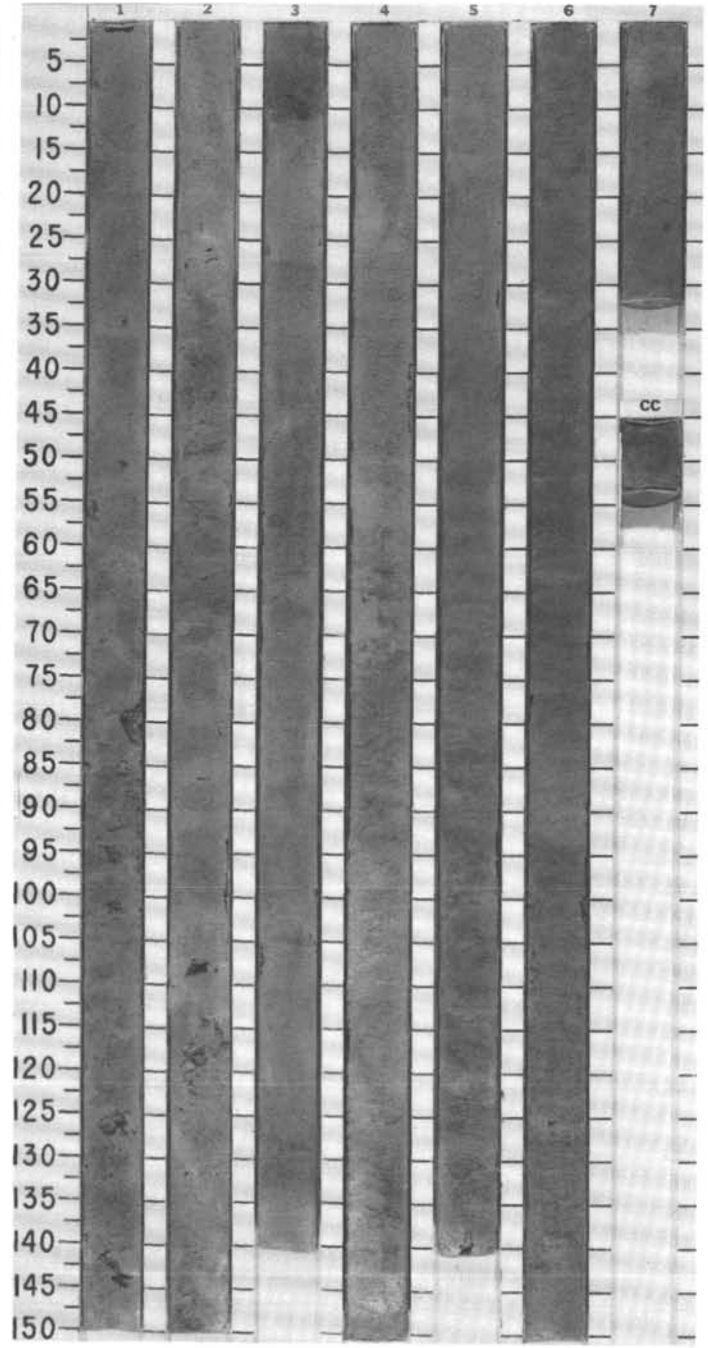

SITE 672 HOLE A CORE 25 X CORED INTERVAL 5191.3-5200.8 mbsl; 218.3-227.8 mbsf

TIME-ROCK UNIT	BIOSTRAT. ZONE/ FOSSIL CHARACTER: FORAMINIFERS	NANNOFOSSILS	RADIOLARIANS	DIATOMS	PALEOMAGNETICS	PHYS. PROPERTIES	CHEMISTRY	SECTION	METERS
?	Barren B	Barren B	Barren B			●γ=1.84 ●φ=58	●0.2 %	2	
						●γ=1.84 ●φ=58	●0.2 %	3	
						●γ=1.92 ●φ=55	●0.2 %	4	
								1	0.5, 1.0
								CC	

GRAPHIC LITHOLOGY / DRILLING DISTURB. / SED. STRUCTURES / SAMPLES

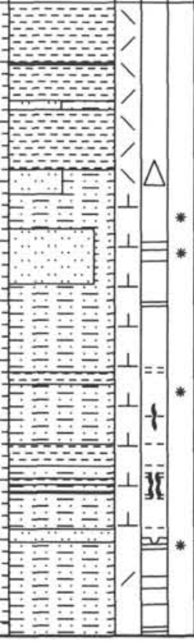

LITHOLOGIC DESCRIPTION

MUDSTONE, CLAYSTONE, and SILTSTONE

MUDSTONE, CLAYSTONE, and minor SILTSTONE; grayish green, greenish gray, and dark greenish gray (10Y5/2, 5G5/2, 5G5/1, 5G6/1, 5Y4/4, 5B6/1, 5GY5/1); unbioturbated; silty intervals are quartz-rich and planar-laminated.

SMEAR SLIDE SUMMARY (%):

	2, 57 M	2, 32 D	3, 26 D	4, 7 M
TEXTURE:				
Silt	80	60	2	100
Clay	20	40	98	—
COMPOSITION:				
Quartz	70	40	1	95
Feldspar	3	1	—	—
Mica (biotite)	—	—	—	Tr
Clay	20	40	98	—
Volcanic glass	2	10	—	—
Dolomite	Tr	—	—	—
Accessory minerals				
Zeolites	—	8	—	—
Chlorite	—	—	—	1
Opaques	5	1	1	3
Hornblende	—	—	—	1
Zircon(?)	—	—	—	Tr
Glaucophane	—	—	—	Tr

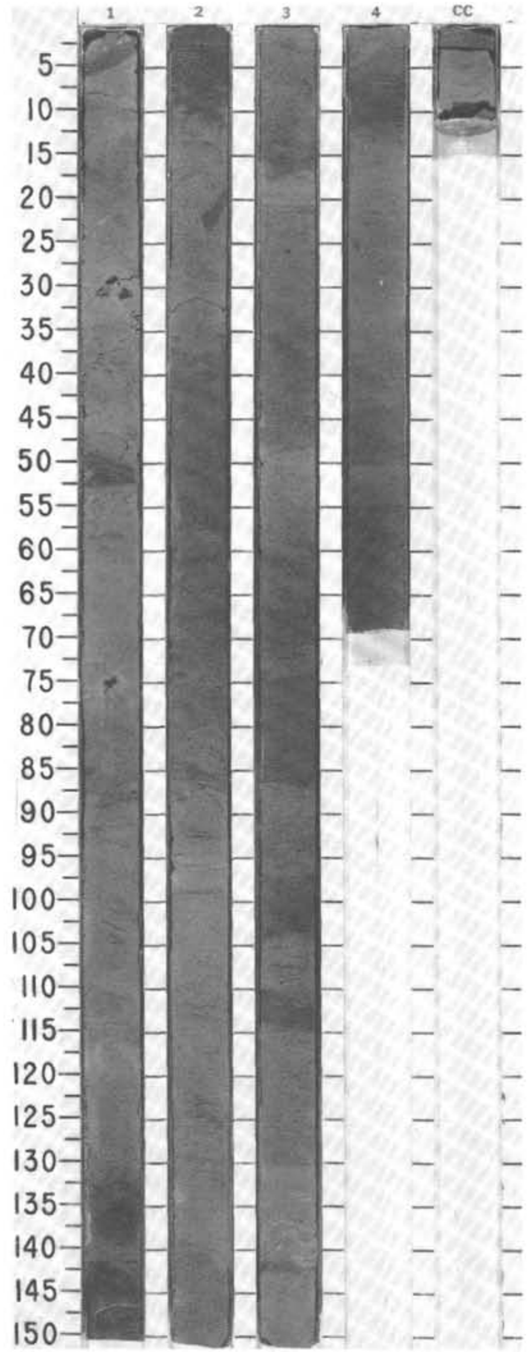

SITE 672 HOLE A CORE 26 X CORED INTERVAL 5200.8-5210.3 mbsl; 227.8-237.3 mbsf

TIME-ROCK UNIT	BIOSTRAT. ZONE/FOSSIL CHARACTER: FORAMINIFERS	NANNOFOSSILS	RADIOLARIANS	DIATOMS	PALEOMAGNETICS	PHYS. PROPERTIES	CHEMISTRY	SECTION	METERS
UPPER OLIGOCENE	*Globigerina ciperoensis* Zone; R/P	CP19; A/M	Barren; B			γ=1.84 ϕ=58; γ=1.86 ϕ=54	0.5 %; 0.2 %	1, 2, 3, 4, CC	0.5, 1.0

GRAPHIC LITHOLOGY · DRILLING DISTURB. · SED. STRUCTURES · SAMPLES (OG)

LITHOLOGIC DESCRIPTION

MUDSTONE, CLAYSTONE, and CALCAREOUS MUDSTONE

MUDSTONE and CLAYSTONE, gray, dark greenish gray, and dark gray to black (5B4/1, 5G5/2, 5B4/1, 5Y5/3); and CALCAREOUS MUDSTONE, light greenish gray and light brownish gray (5G7/2, 5Y5/3). CALCAREOUS MUDSTONE is mildly to moderately bioturbated. Beds dip at 10° near base of core.

SMEAR SLIDE SUMMARY (%):

	1, 117 D	2, 50 D	2, 96 D	2, 100 M	4, 93 D
TEXTURE:					
Silt	3	—	70	2	21
Clay	97	100	30	98	79
COMPOSITION:					
Quartz	—	—	68	—	18
Feldspar	—	—	Tr	—	—
Rock fragments	—	—	Tr	—	—
Clay	30	100	30	72	79
Calcite/dolomite	3	—	—	—	1
Accessory minerals					
Zeolites	—	—	—	Tr	—
Opaques	2	—	2	—	2
Fe/Mn hydroxides	5	—	—	—	Tr
Nannofossils	60	—	—	28	—
Sponge spicules	Tr	—	—	—	—
Amphibole/glaucophane	—	—	—	—	Tr

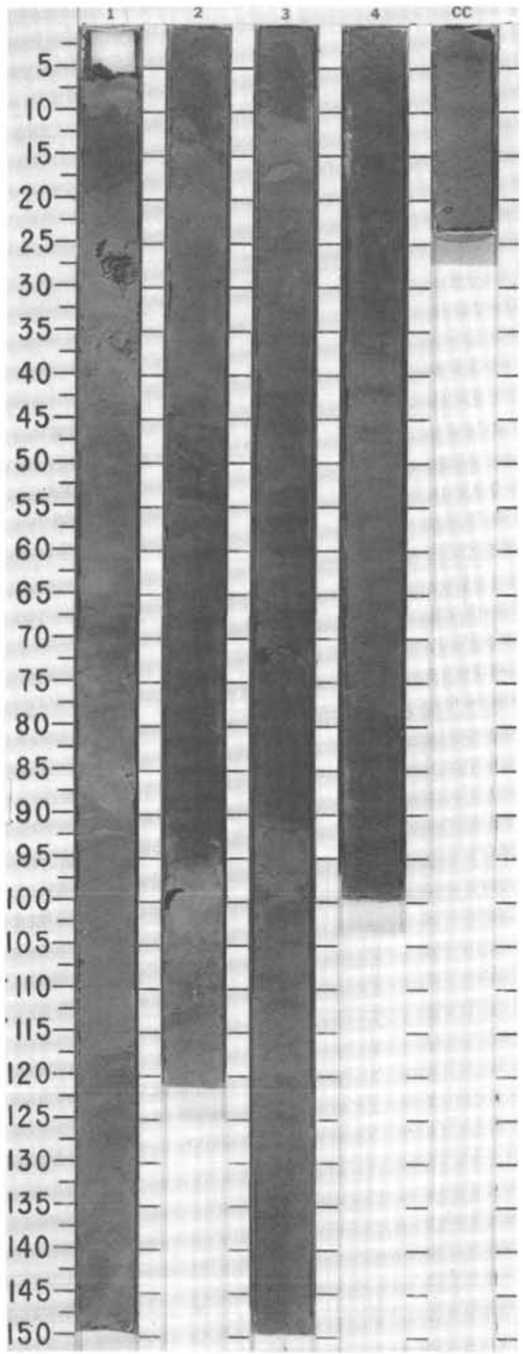

SITE 672 HOLE A CORE 27 X CORED INTERVAL 5210.3-5219.8 mbsl; 237.3-246.8 mbsf

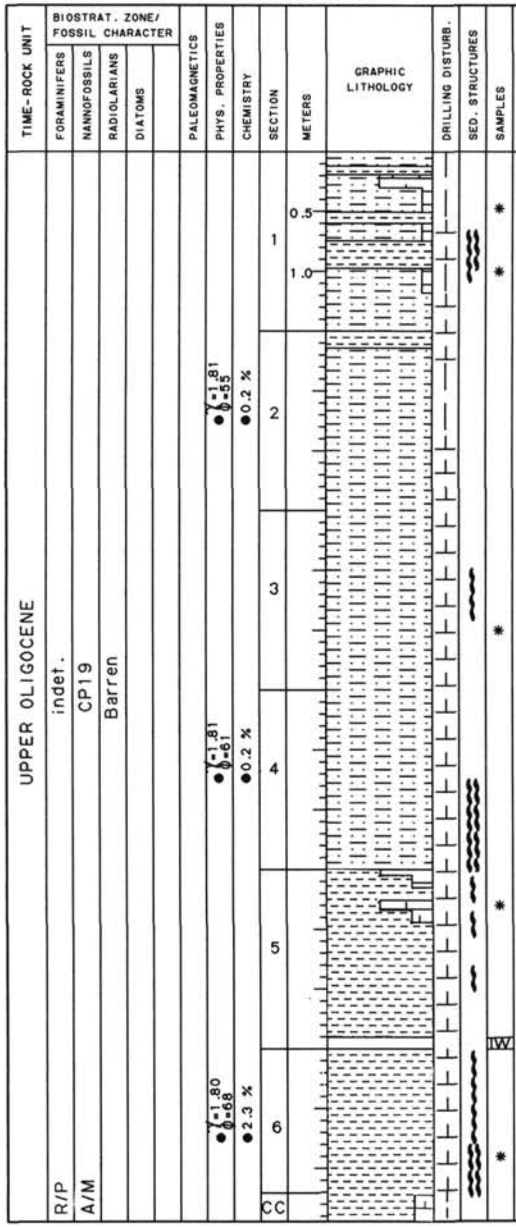

LITHOLOGIC DESCRIPTION

MUDSTONE, CLAYSTONE, CALCAREOUS CLAYSTONE, and MARLSTONE

MUDSTONE, CLAYSTONE, CALCAREOUS CLAYSTONE, and MARLSTONE; dark gray, greenish gray, gray, pale green, and pale blue-green (5Y4/1, 5G4/2, 5Y5/1, 5G4/2, 5G5/2); thinly bedded (1-cm to 5-cm thick beds); slightly bioturbated; *Planolites* identified. Glauconite(?) appears as authigenic mineral. Bedding horizontal.

SMEAR SLIDE SUMMARY (%):

	1, 42 D	1, 106 D	3, 102 D	5, 29 M	6, 86 M
TEXTURE:					
Silt	10	40	5	10	100
Clay	90	60	95	90	—
COMPOSITION:					
Quartz	Tr	25	5	—	—
Feldspar	—	10	—	—	—
Pumice fragments	—	Tr	—	—	—
Clay	49	50	95	40	—
Volcanic glass	Tr	—	—	—	—
Calcite/(dolomite?)	—	—	—	5	—
Accessory minerals					
Glauconite(?)	—	Tr	—	—	100
Opaques	Tr	3	Tr	1	—
Reddish semi-opaque	—	1	—	—	—
Foraminifers	Tr	—	—	Tr	—
Nannofossils	50	5	—	54	—
Sponge spicules	—	Tr	—	—	—
Bioclasts	1	—	—	—	—

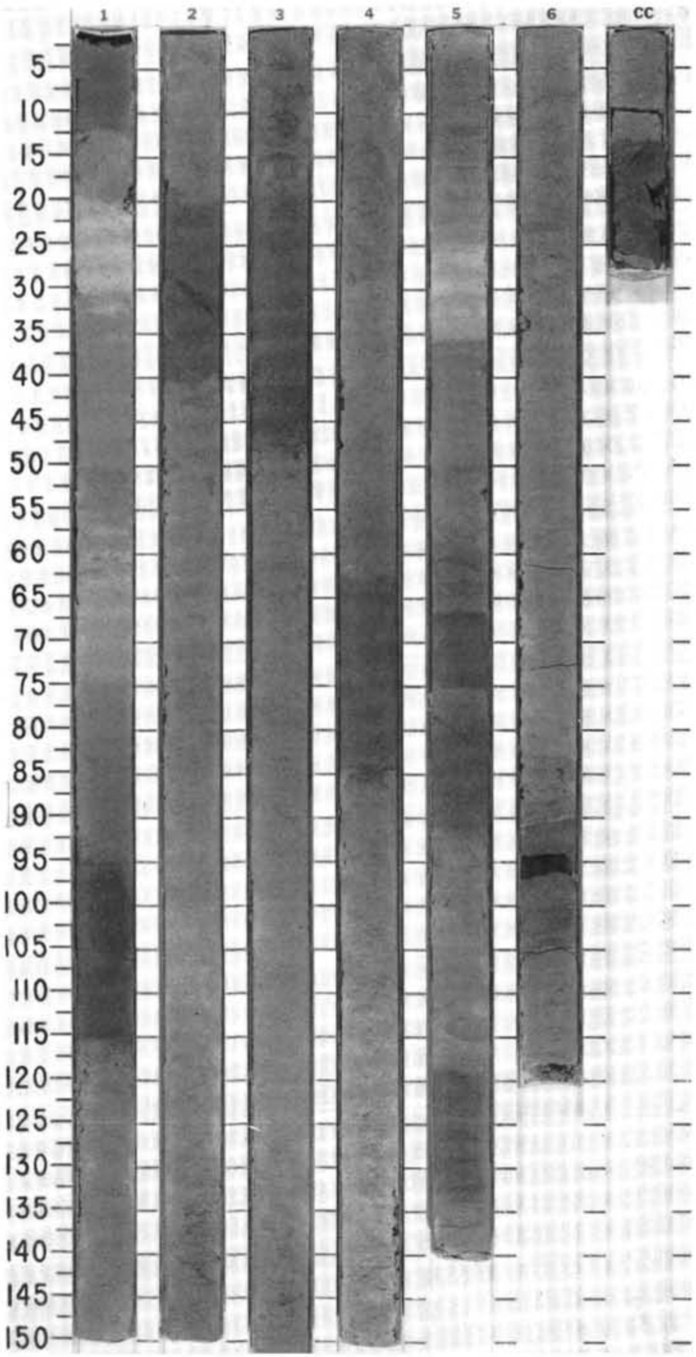

SITE 672 HOLE A CORE 28 X CORED INTERVAL 5219.8-5229.3 mbsl; 246.8-256.3 mbsf

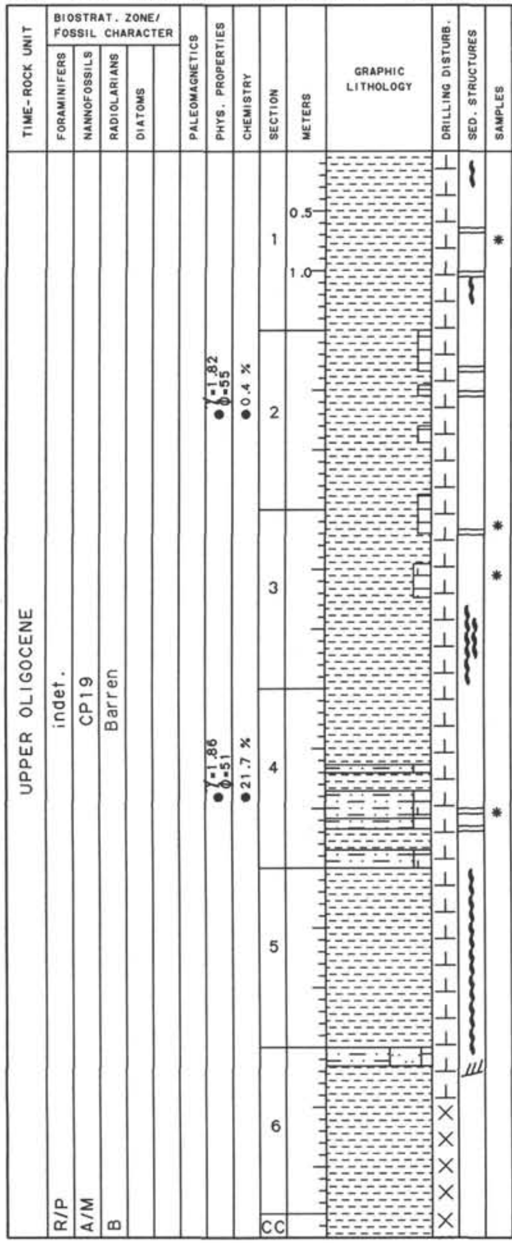

LITHOLOGIC DESCRIPTION

CLAYSTONE, CALCAREOUS CLAYSTONE, and SILTSTONE

CLAYSTONE and CALCAREOUS CLAYSTONE; dark greenish gray, gray, grayish green, very dark gray, and pale green (5G4/1, 5Y4/1, 5G5/2, 5Y3/1, 5G6/2); slightly bioturbated; *Planolites* identified. Minor SILTSTONE forms planar laminations. A 60° dipping fault in Section 3.

SMEAR SLIDE SUMMARY (%):

	1, 80 D	3, 18 M	3, 56 D	4, 109 M
TEXTURE:				
Silt	2	80	5	90
Clay	98	20	95	10
COMPOSITION:				
Quartz	1	70	—	75
Feldspar	—	—	—	2
Mica	—	1	—	—
Clay	98	8	83	3
Calcite/dolomite	—	1	—	—
Accessory minerals	1	5	2	10
Glauconite	—	1	—	Tr
Glaucophane	—	Tr	—	—
Chlorite	—	Tr	—	—
Foraminifers	—	1	Tr	2
Nannofossils	Tr	10	15	12
Radiolarians	—	1	—	—
Sponge spicules	—	2	—	—
Fish remains	—	Tr	—	—
Bioclasts	—	—	—	1

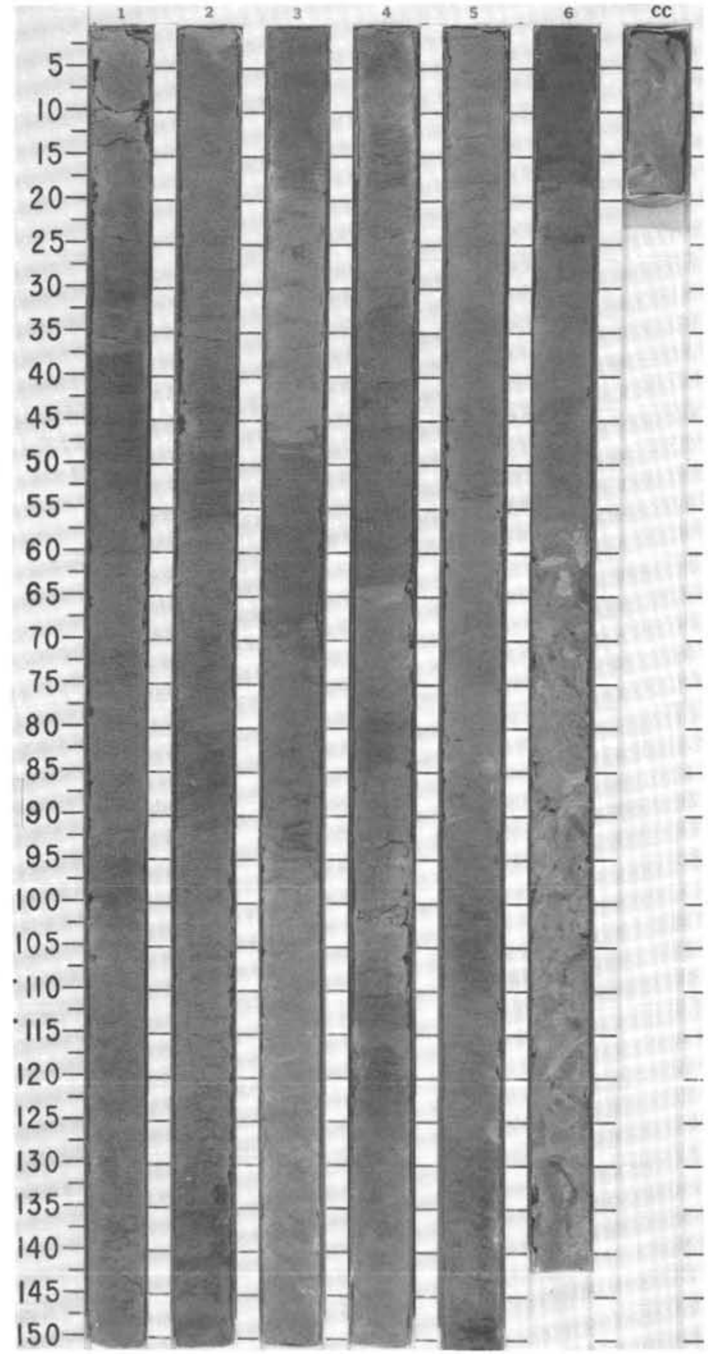

SITE 672 HOLE A CORE 29 X CORED INTERVAL 5229.3-5238.8 mbsl; 256.3-265.8 mbsf

TIME-ROCK UNIT	FORAMINIFERS	NANNOFOSSILS	RADIOLARIANS	DIATOMS	PALEOMAGNETICS	PHYS. PROPERTIES	CHEMISTRY	SECTION	METERS	GRAPHIC LITHOLOGY	DRILLING DISTURB.	SED. STRUCTURES	SAMPLES
LOWER OLIGOCENE	R/P indet.	A/M CP18	B Barren			● γ=1.78 ● φ=56; ● γ=1.78 ● φ=59	● 0.4 %; ● 0.3 %	1, 2, 3, 4, 5, 6, 7, CC	0.5, 1.0	Drill Breccia; Drill Breccia			* * *; OG

LITHOLOGIC DESCRIPTION

CLAYSTONE, CALCAREOUS CLAYSTONE, MARLSTONE, and CHALK

CLAYSTONE, CALCAREOUS CLAYSTONE, MARLSTONE, and CHALK; dark greenish gray, greenish gray, pale green, dark blue gray, and gray (5G4/1, 5G6/1, 5GY6/1, 5BG4/1, 5Y5/1, 5G6/2); mostly massive, but locally slightly to moderately burrowed; *Planolites* identified. Planar laminations in Sections 2, 3, and 4.

SMEAR SLIDE SUMMARY (%):

	1, 54 D	1, 76 D	1, 99 D
TEXTURE:			
Silt	3	25	15
Clay	97	75	85
COMPOSITION:			
Quartz	Tr	—	Tr
Feldspar	Tr	—	—
Clay	94	25	25
Calcite/dolomite	—	Tr	—
Accessory minerals	1	1	Tr
Foraminifers	—	3	2
Nannofossils	Tr	70	70
Bioclasts	—	1	2

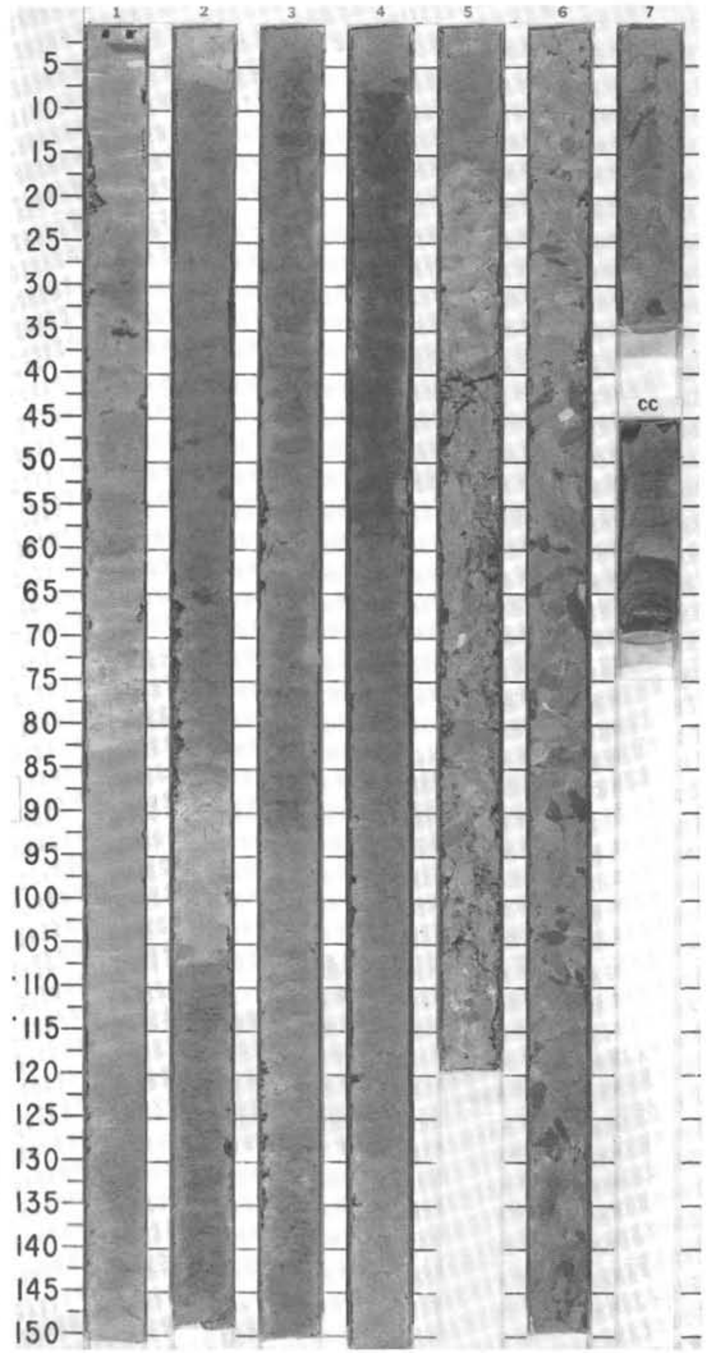

SITE 672 HOLE A CORE 30 X CORED INTERVAL 5238.8-5248.3 mbsl; 265.8-275.3 mbsf

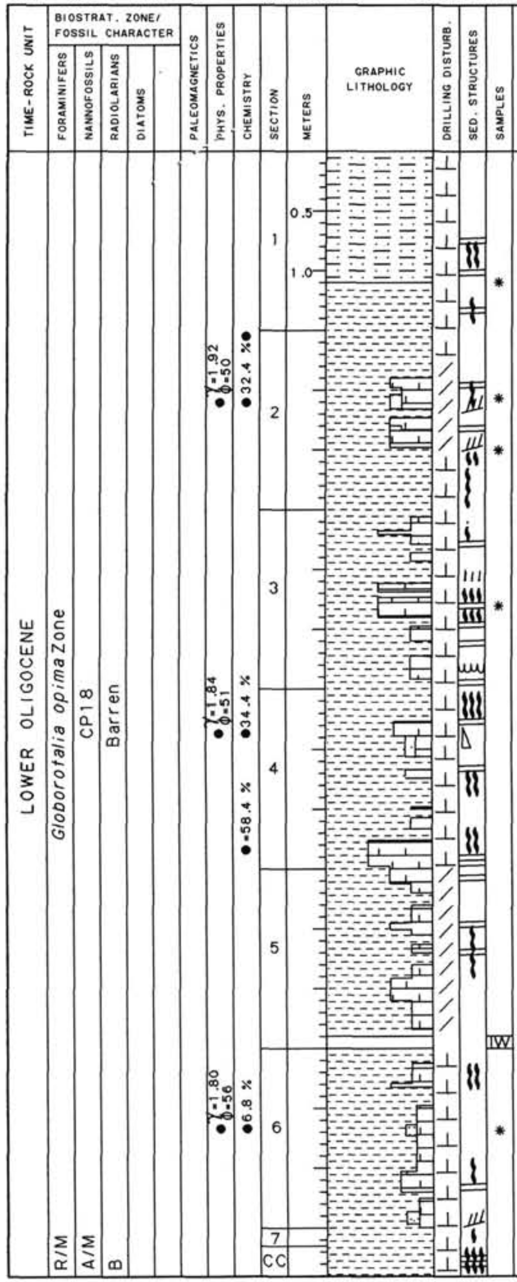

LITHOLOGIC DESCRIPTION

MUDSTONE, CALCAREOUS MUDSTONE, and MARLSTONE

MUDSTONE, CALCAREOUS MUDSTONE, and MARLSTONE; varicolored grayish green, gray, greenish gray, and light greenish gray (5G5/2, 5Y5/1, 5Y4/1, 5G5/1, 5G6/1, 5GY7/1); thinly interbedded (beds mostly 10–20 cm thick); moderately bioturbated to unbioturbated; parallel-laminated and ripple cross-laminated in siltier intervals. Fining-upward sequence in Section 4; convolute lamination in Section 3. Bedding dips 5°–7° at top of core and is nearly horizontal at bottom.

SMEAR SLIDE SUMMARY (%):

	1, 110 D	2, 63 D	2, 104 D	3, 80 D	6, 72 M
TEXTURE:					
Silt	25	12	15	5	13
Clay	75	88	85	95	87
COMPOSITION:					
Quartz	15	3	1	1	3
Feldspar	10	1	Tr	Tr	1
Mica	Tr	—	Tr	—	—
Clay	75	71	97	47	69
Volcanic glass	—	—	2	Tr	3
Accessory minerals	Tr	2	Tr	—	—
Hornblende	Tr	—	—	—	—
Foraminifers	—	5	—	1	5
Nannofossils	—	15	Tr	50	15
Bioclasts	—	—	—	1	—

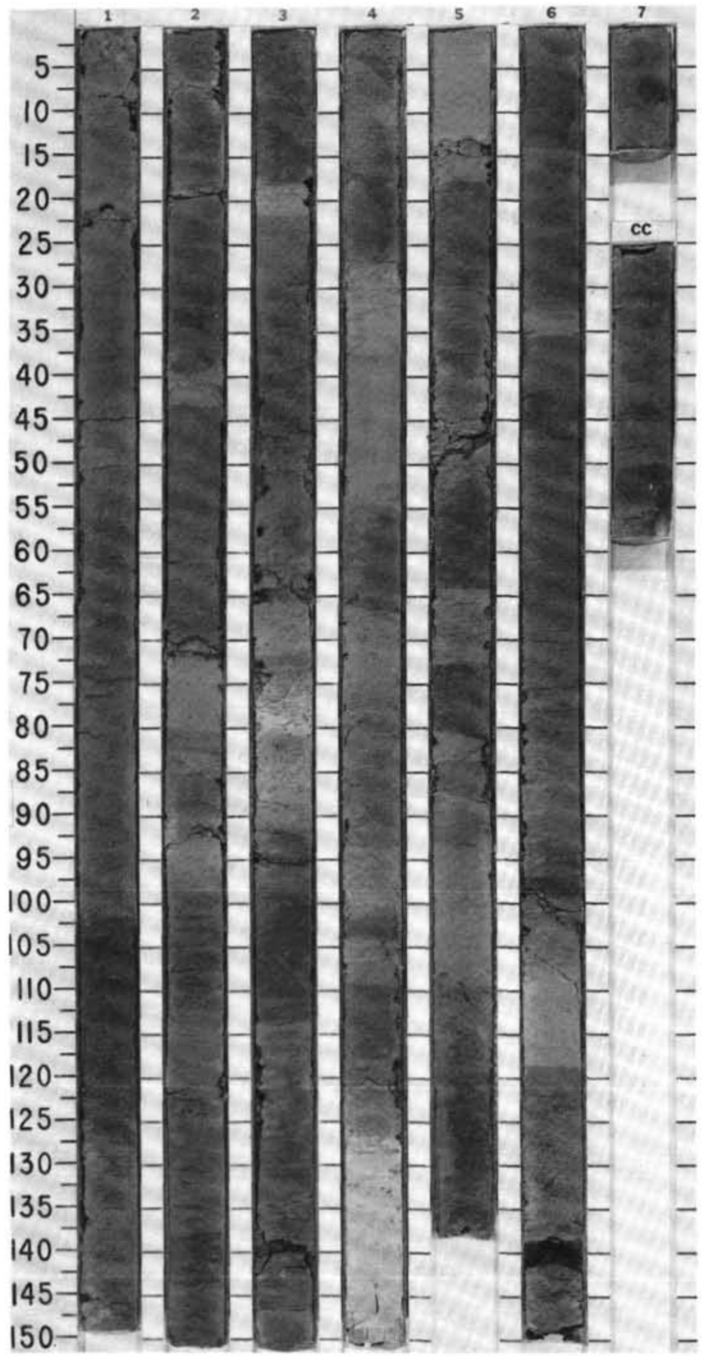

SITE 672 HOLE A CORE 31 X CORED INTERVAL 5248.3-5257.8 mbsl; 275.3-284.8 mbsf

TIME-ROCK UNIT	BIOSTRAT. ZONE/ FOSSIL CHARACTER: FORAMINIFERS	NANNOFOSSILS	RADIOLARIANS	DIATOMS	PALEOMAGNETICS	PHYS. PROPERTIES	CHEMISTRY	SECTION	METERS	GRAPHIC LITHOLOGY	DRILLING DISTURB.	SED. STRUCTURES	SAMPLES
LOWER OLIGOCENE ?	Barren	Barren	Barren			● γ=1.79 ϕ=60	● 32.4 %	1	0.5, 1.0				*
							● 0.2 %	2					*
								3					
						● γ=1.87 ϕ=53	● 33.3 %	4					
	B	B	B					CC					

LITHOLOGIC DESCRIPTION

MUDSTONE, CALCAREOUS MUDSTONE, and MARLSTONE

MUDSTONE, CALCAREOUS MUDSTONE, and MARLSTONE; varicolored gray, dark blue-green, pale blue-green, and olive (N4, 5G4/1, 5G5/1, 5G7/1, 5BG4/1, 10Y4/2, 5GY6/1); thinly interbedded (5–30-cm thick beds). MARLSTONE is typically parallel-laminated and siltier at base and has burrowed tops; beds are normally graded. Ripple cross-lamination identified in Section 4 and CC. Bedding is horizontal.

SMEAR SLIDE SUMMARY (%):

	1, 75 D	2, 99 D
TEXTURE:		
Silt	10	11
Clay	90	89
COMPOSITION:		
Quartz	4	9
Feldspar	1	1
Clay	65	89
Volcanic glass	—	1
Foraminifers	5	—
Nannofossils	25	—
Radiolarians	Tr	—

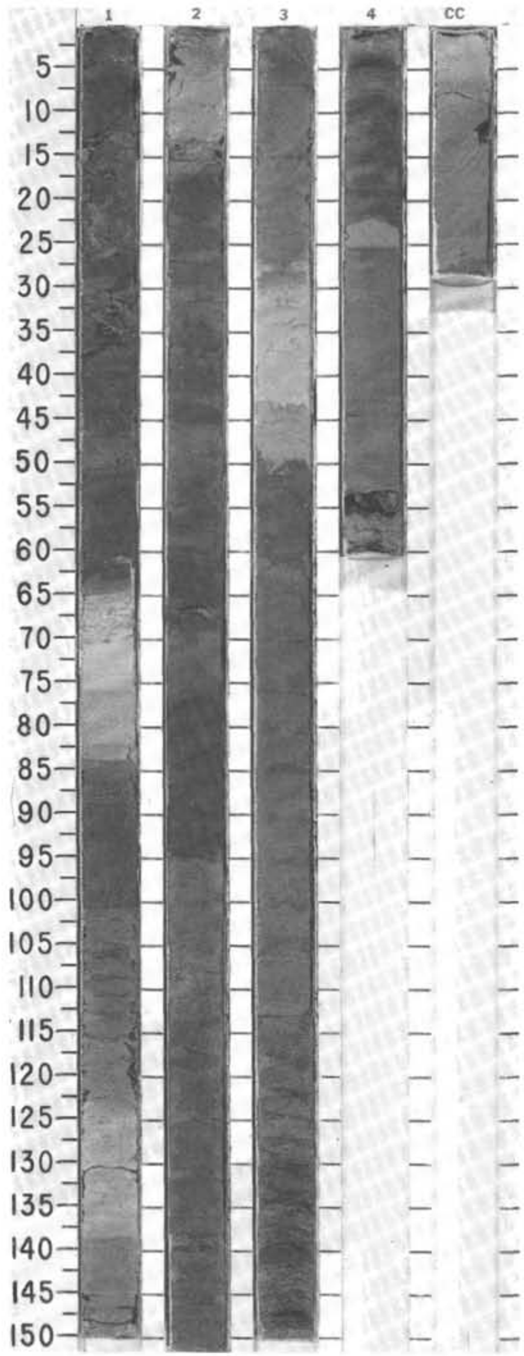

SITE 672 HOLE A CORE 32 X CORED INTERVAL 5257.8-5267.3 mbsl; 284.8-294.3 mbsf

TIME-ROCK UNIT: LOWER OLIGOCENE (rew. EOCENE)

BIOSTRAT. ZONE/FOSSIL CHARACTER:
- FORAMINIFERS: *Globorotalia opima* Zone — F/G
- NANNOFOSSILS: indet. (Lower Oligocene) — A/M
- RADIOLARIANS: indet. — R/vP
- DIATOMS

PALEOMAGNETICS

PHYS. PROPERTIES: γ=1.88, φ=50; γ=1.86, φ=53

CHEMISTRY: 25.8 %; 39.0 %; 32.6 %

SECTION: 1, 2, 3, 4, 5, CC

METERS: 0.5, 1.0

GRAPHIC LITHOLOGY / DRILLING DISTURB. / SED. STRUCTURES / SAMPLES

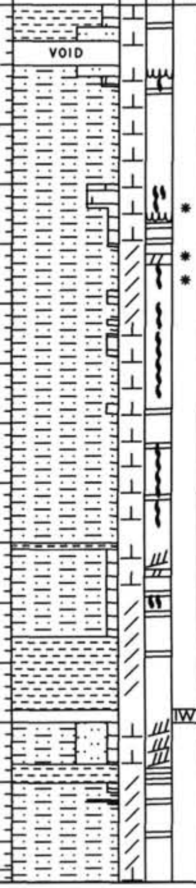

LITHOLOGIC DESCRIPTION

MUDSTONE, CALCAREOUS MUDSTONE, and MARLSTONE

MUDSTONE, CALCAREOUS MUDSTONE, and MARLSTONE; varicolored olive-gray, greenish gray, light greenish gray, grayish green, and very dark gray (5Y4/2, 5GY5/1, 5G5/1, 5G7/1, 5G4/2, 5G5/2, 5Y3/1); 30–100 cm thick, slightly to moderately bioturbated at the top of beds; parallel-lamination and minor convolute-lamination at base of beds; ripple cross-lamination identified in Sections 2 and 5.

SMEAR SLIDE SUMMARY (%):

	2, 16 M	2, 57 M	2, 78 D
TEXTURE:			
Sand	—	2	—
Silt	2	18	12
Clay	98	80	88
COMPOSITION:			
Quartz	2	10	12
Clay	58	80	86
Volcanic glass	—	—	Tr
Foraminifers	Tr	5	2
Nannofossils	30	5	—

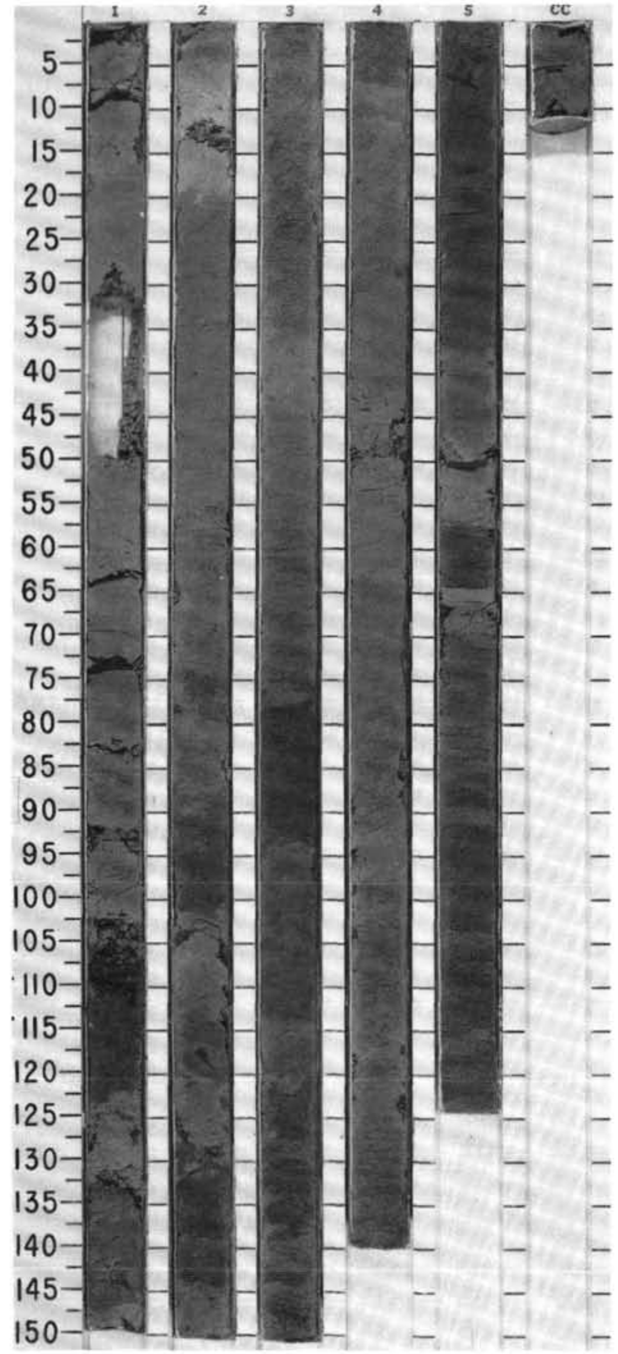

SITE 672 HOLE A CORE 33 X CORED INTERVAL 5267.3-5276.8 mbsl; 294.3-303.8 mbsf

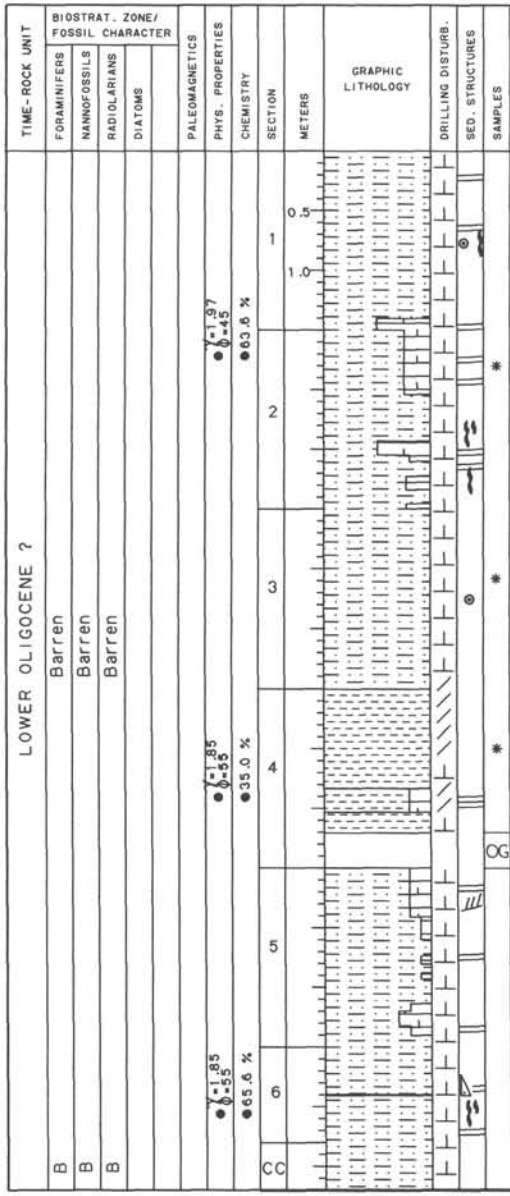

LITHOLOGIC DESCRIPTION

CLAYSTONE, MUDSTONE, and CALCAREOUS MUDSTONE

CLAYSTONE, MUDSTONE, and CALCAREOUS MUDSTONE; varicolored light greenish gray, olive, dark greenish gray, greenish gray, and gray (5GY7/1, 10Y6/2, 5G4/1, 5GY4/1, 5G5/1, 5G6/1, 5Y4/1, 5Y5/1); foraminifers make up silt fraction in CALCAREOUS MUDSTONE; thinly interbedded (10–50 cm thick beds); slight bioturbation at top of beds. Parallel-laminated throughout but most common at base of beds; fining-upward sequence identified in Section 5; sub-horizontal bedding.

SMEAR SLIDE SUMMARY (%):

	2, 33 D	3, 46 D	4, 62 D
TEXTURE:			
Silt	20	20	2
Clay	80	80	98
COMPOSITION:			
Quartz	3	16	2
Feldspar	—	4	—
Clay	70	80	98
Volcanic glass	1	—	—
Calcite/dolomite	1	—	—
Foraminifers	5	—	—
Nannofossils	20	—	—
Radiolarians	1	—	—

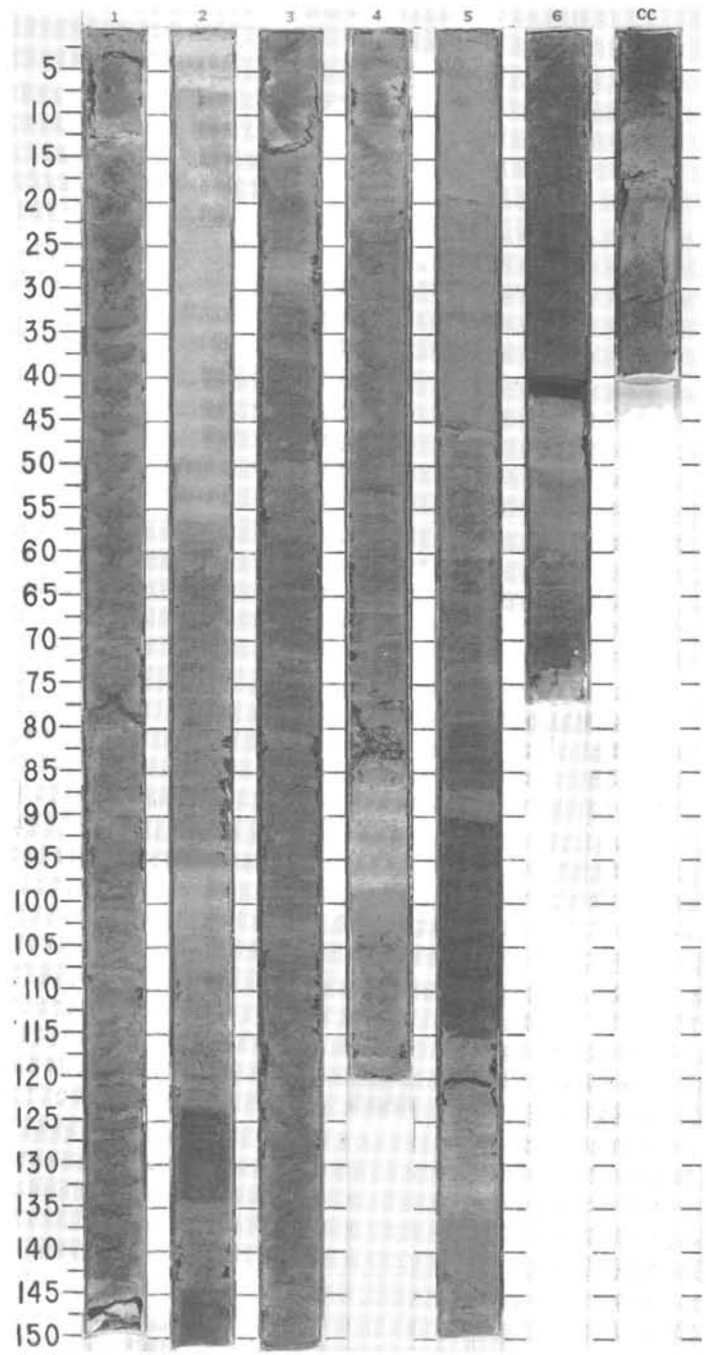

SITE 672 HOLE A CORE 34 X CORED INTERVAL 5276.8-5286.3 mbsl; 303.8-313.3 mbsf

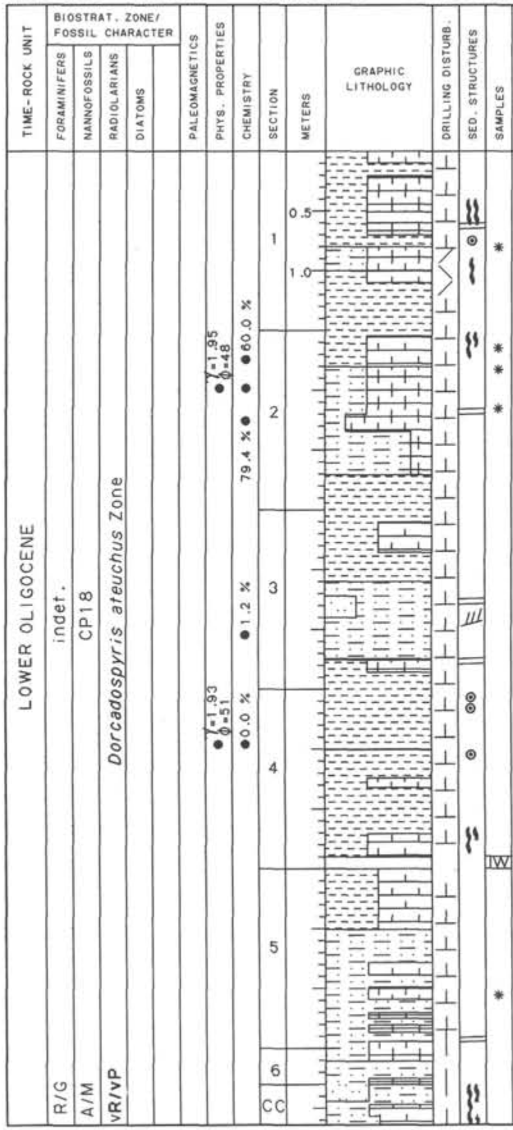

LITHOLOGIC DESCRIPTION

CLAYSTONE, CALCAREOUS MUDSTONE, and CHALK

CLAYSTONE, CALCAREOUS MUDSTONE, and CHALK; varicolored dark greenish gray, grayish green, light greenish gray, and greenish gray (5GY4/1, 5Y5/3, 5GY4/1, 5G4/2, 5G5/2, 5G7/2, 5GY7/1, 5GY5/1, 5GY6/1); thinly interbedded (10–50-cm thick beds); beds slightly to moderately bioturbated at top, parallel laminated at base (where silt-sized particles are present); foraminifers make up silty fraction.

Minor lithology: pyrite concretions (<1 mm diameter) occur locally in Sections 1 and 4. Horizontal bedding.

SMEAR SLIDE SUMMARY (%):

	1, 80 D	2, 23 D	2, 48 D	2, 72 D	5, 106 D
TEXTURE:					
Sand	—	—	—	—	Tr
Silt	2	10	10	50	65
Clay	98	90	90	50	35
COMPOSITION:					
Quartz	—	Tr	—	2	25
Clay	98	23	35	33	30
Calcite/dolomite	—	5	5	—	—
Accessory minerals	2	—	—	—	—
Foraminifers	—	Tr	—	35	15
Nannofossils	—	70	60	15	10
Sponge spicules	—	—	—	10	15
Bioclasts	—	2	—	5	5

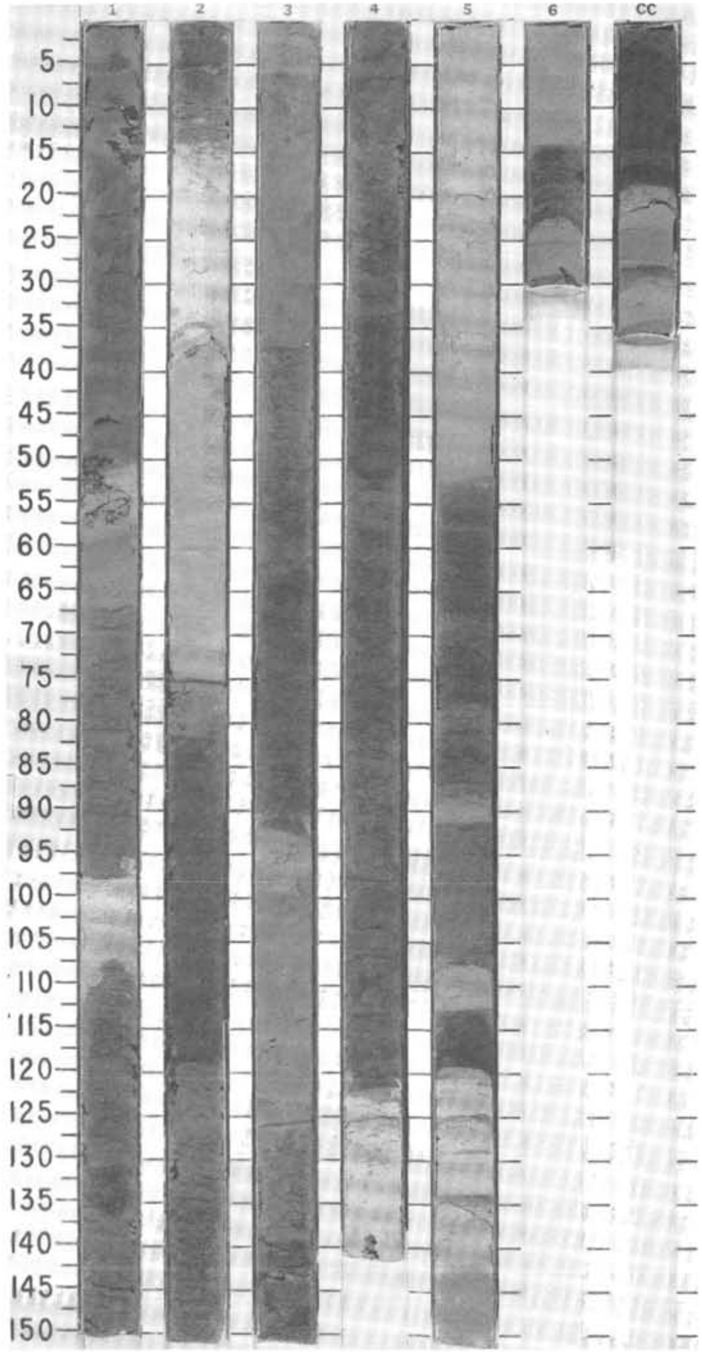

SITE 672 HOLE A CORE 35 X CORED INTERVAL 5286.3-5295.8 mbsl; 313.3-322.8 mbsf

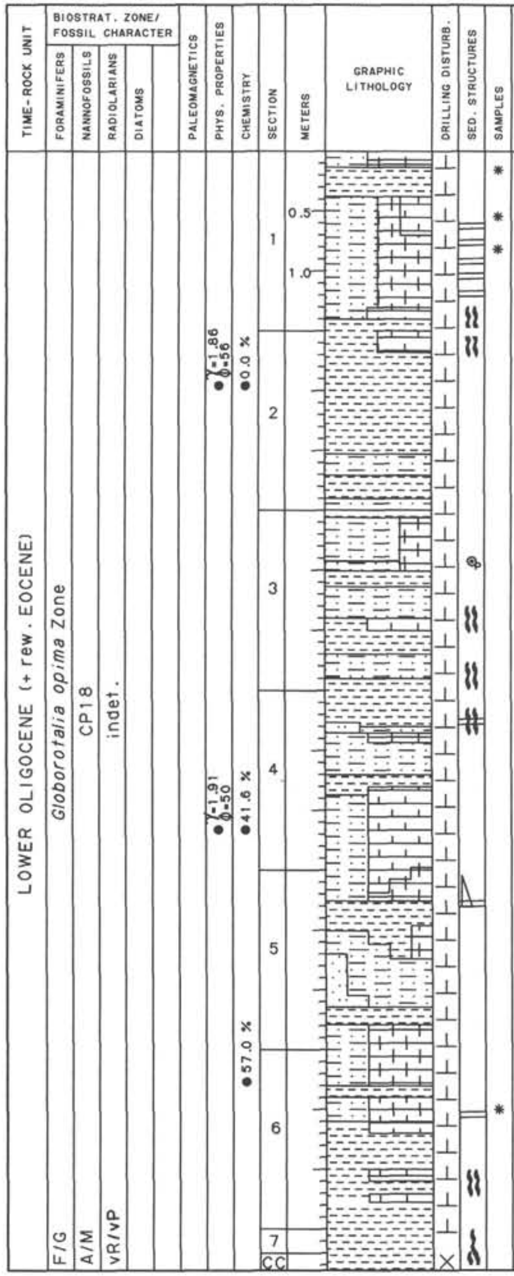

LITHOLOGIC DESCRIPTION

CLAYSTONE and SILTY CALCAREOUS MUDSTONE; and MARLSTONE and CLAYSTONE

CLAYSTONE and SILTY CALCAREOUS MUDSTONE; dark gray, grayish green, gray, pale green, and greenish gray (5Y4/1, 5G5/2, 5Y3/1, 5G7/2, 5G4/2, 5G5/1); interbedded (20–90-cm thick beds); locally moderately bioturbated MARLSTONE and CLAYSTONE; parallel lamination in SILTY CALCAREOUS MUDSTONE.

Minor lithology: minor pyrite concretions.

SMEAR SLIDE SUMMARY (%):

	1, 16 D	1, 54 M	1, 81 D	6, 54 M
TEXTURE:				
Sand	—	10	10	Tr
Silt	Tr	60	40	95
Clay	100	30	50	5
COMPOSITION:				
Quartz	Tr	40	30	55
Feldspar	—	Tr	Tr	Tr
Mica	—	—	Tr	—
Clay	100	30	45	5
Calcite/dolomite	—	—	Tr	—
Accessory minerals	Tr	5	5	15
Foraminifers	—	3	2	3
Nannofossils	—	10	15	2
Radiolarians	—	2	—	Tr
Sponge spicules	—	5	Tr	20
Fish remains	—	—	—	Tr
Bioclasts	—	5	—	—

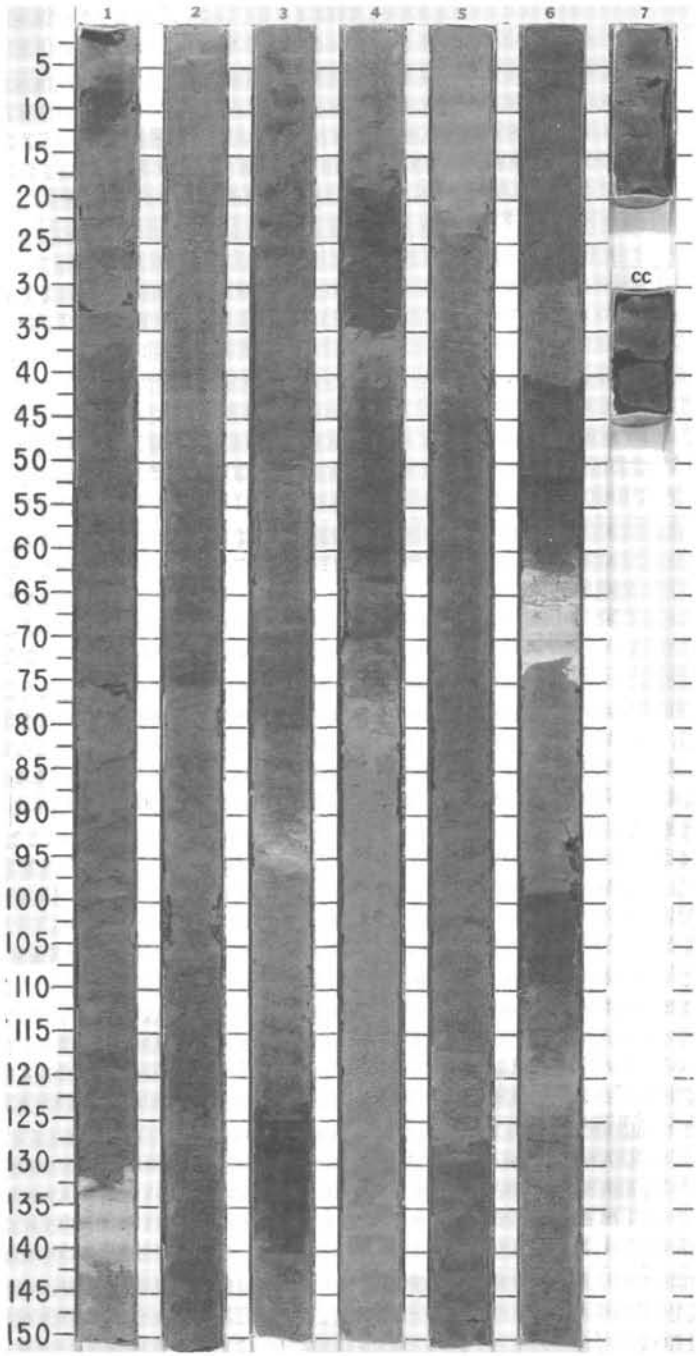

SITE 672 HOLE A CORE 36 X CORED INTERVAL 5295.8-5305.3 mbsl; 322.8-332.3 mbsf

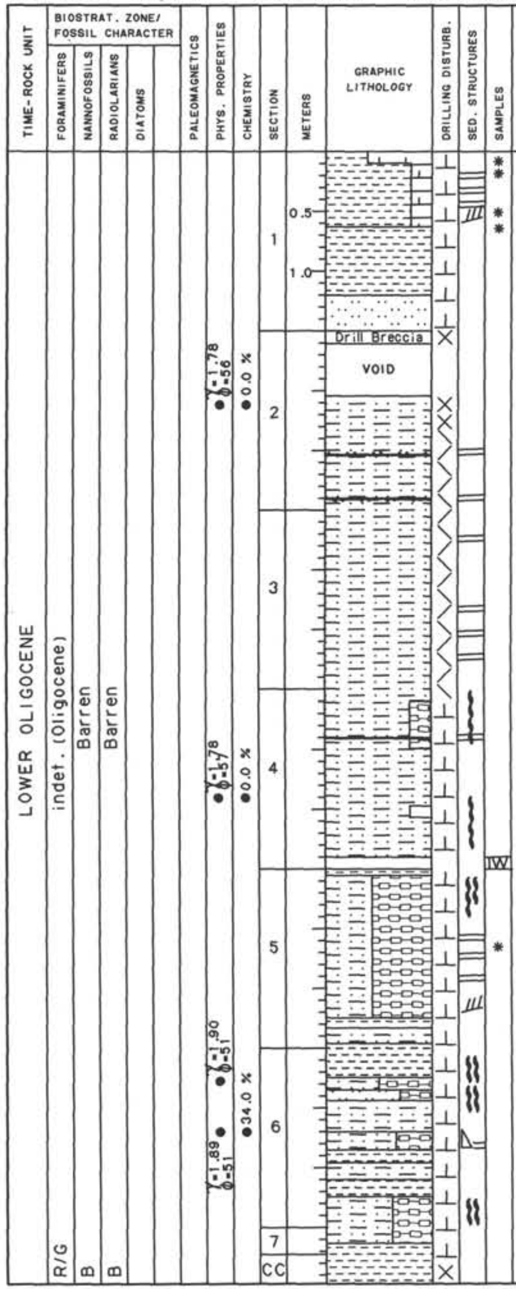

LITHOLOGIC DESCRIPTION

MARLSTONE, CALCAREOUS MUDSTONE, and MUDSTONE

Gray and light gray MARLSTONE (5G7/2, 5Y5/3); light olive-gray and olive-gray CALCAREOUS MUDSTONE (5Y6/2, 5Y5/2) laminated in places; and dark olive-gray and greenish gray MUDSTONE (5G5/2, 5GY5/2, 5Y4/1, GY4/1).

Minor lithology: dark gray siltstone, (5Y3/1), laminated and graded in Section 6.

SMEAR SLIDE SUMMARY (%):

	1, 10 D	1, 18 D	1, 52 D	1, 64 D	5, 72 D
TEXTURE:					
Sand	—	—	Tr	—	2
Silt	10	15	25	5	20
Clay	90	85	75	95	78
COMPOSITION:					
Quartz	Tr	Tr	10	Tr	5
Feldspar	—	—	—	Tr	—
Clay	40	75	70	94	10
Volcanic glass	—	—	—	3	—
Calcite/dolomite	—	—	—	—	2
Accessory minerals	Tr	2	—	Tr	Tr
Pyroxene	—	Tr	—	—	—
Hornblende	—	—	—	—	Tr
Glaucophane	—	—	—	—	Tr
Foraminifers	Tr	1	5	—	8
Nannofossils	60	20	10	Tr	70
Radiolarians	—	—	—	—	1
Sponge spicules	—	—	2	—	2
Bioclasts	—	1	3	—	—

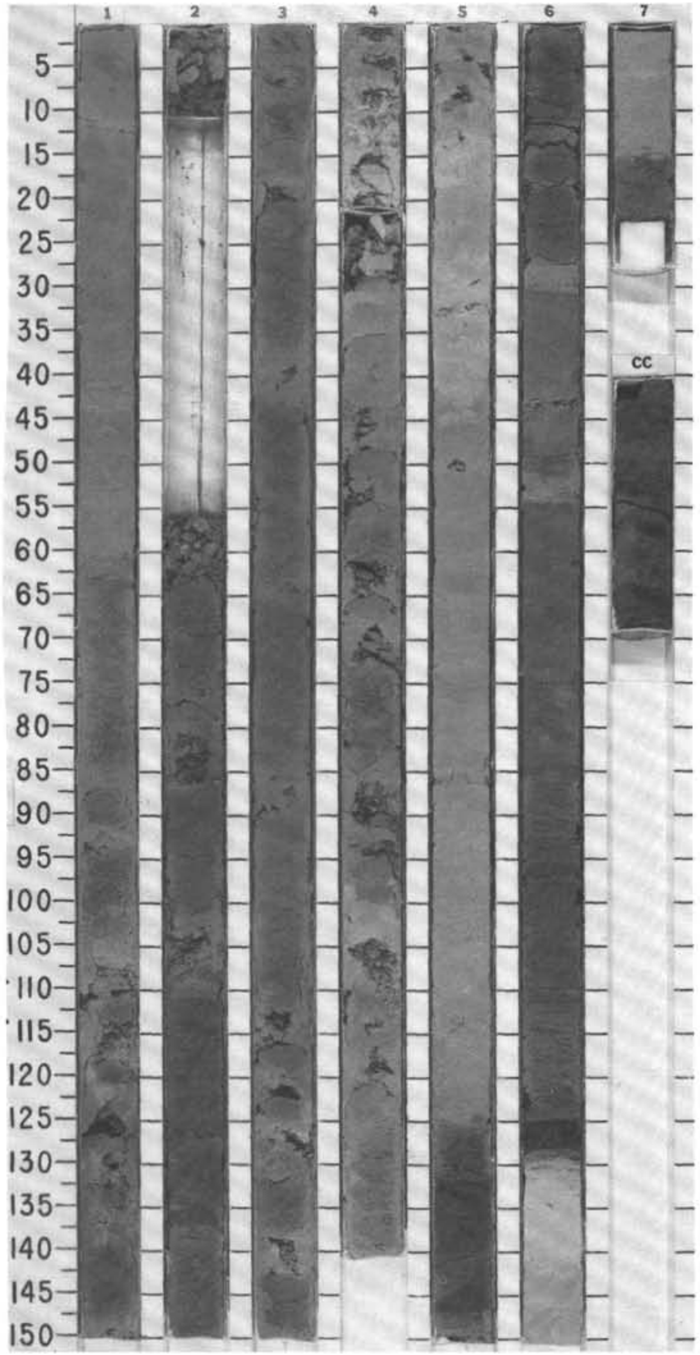

SITE 672 HOLE A CORE 37 X CORED INTERVAL 5305.3-5314.8 mbsl; 332.3-341.8 mbsf

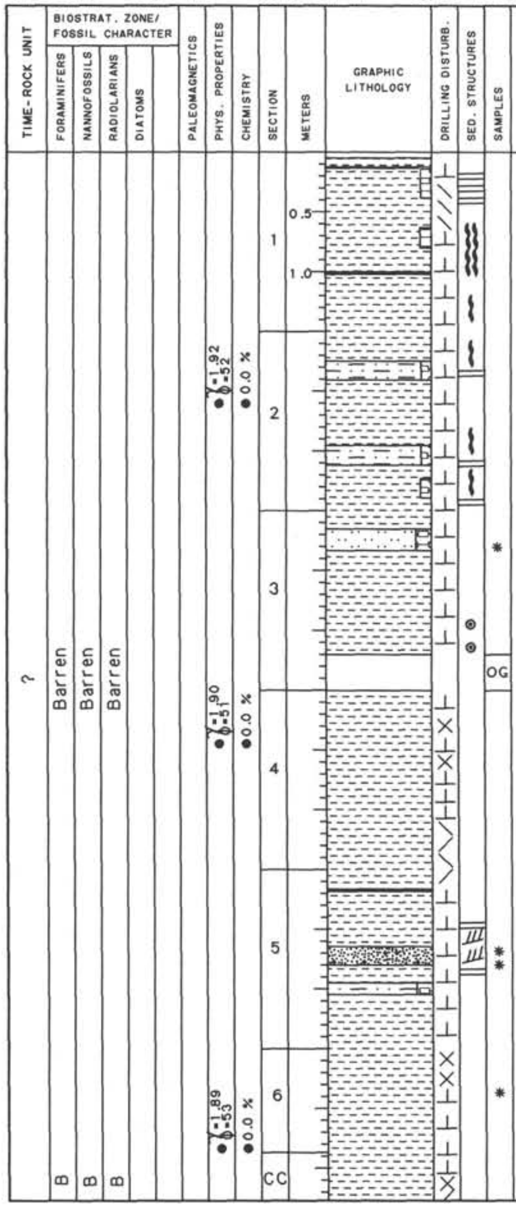

LITHOLOGIC DESCRIPTION

MUDSTONE, CLAYSTONE, CALCAREOUS CLAYSTONE, CHALK, and MARLSTONE

Finely laminated MUDSTONE, dark gray (N/4) and dark greenish gray and greenish gray (5G4/1, 5G4/2, 5G5/1); MUDSTONE and CLAYSTONE, locally pyritiferous, greenish gray and light greenish gray (5GY7/1, 5GY6/1); CALCAREOUS CLAYSTONE, commonly finely laminated at base and burrowed at top of bed, delicate *Planolites* burrows also present locally; CHALK and MARLSTONE, pale greenish gray (5GY7/1).

Minor lithology: dark gray laminated and ripple cross-bedded siltstone and sandstone (5GY4/1). Bedding dips 0° to 4°. A normal fault dipping at 60° in Section 5.

SMEAR SLIDE SUMMARY (%):

	3, 27 D	5, 72 M	5, 74 M	6, 40 M
TEXTURE:				
Sand	—	50	—	—
Silt	20	45	46	5
Clay	80	5	54	95
COMPOSITION:				
Quartz	15	70	40	Tr
Feldspar	2	1	4	—
Rock fragments	—	—	1	—
Clay	70	5	55	95
Accessory minerals	—	2	5	Tr
Glauconite	Tr	20	—	4
Pyroxene	2	—	—	—
Foraminifers	3	—	—	—
Nannofossils	10	—	—	—
Plant debris	Tr	—	—	—
Bioclasts	—	Tr	Tr	—

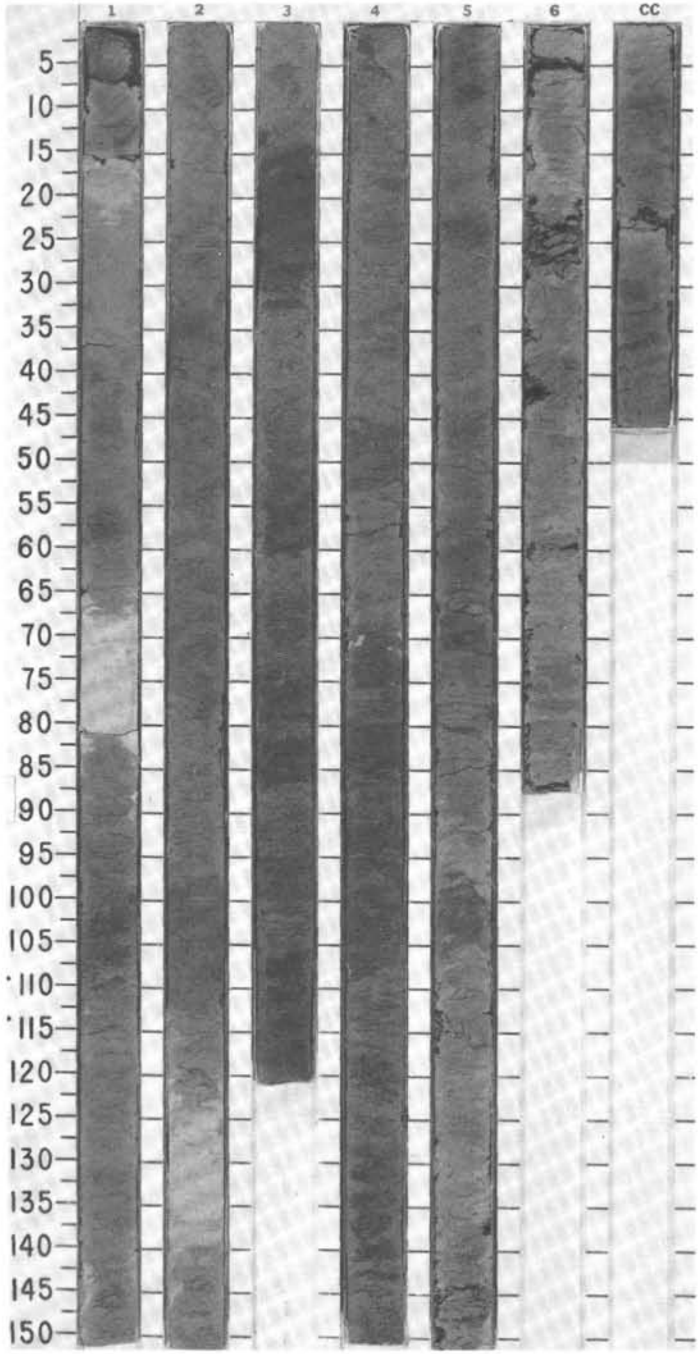

SITE 672 HOLE A CORE 38 X CORED INTERVAL 5314.8-5324.3 mbsl; 341.8-351.3 mbsf

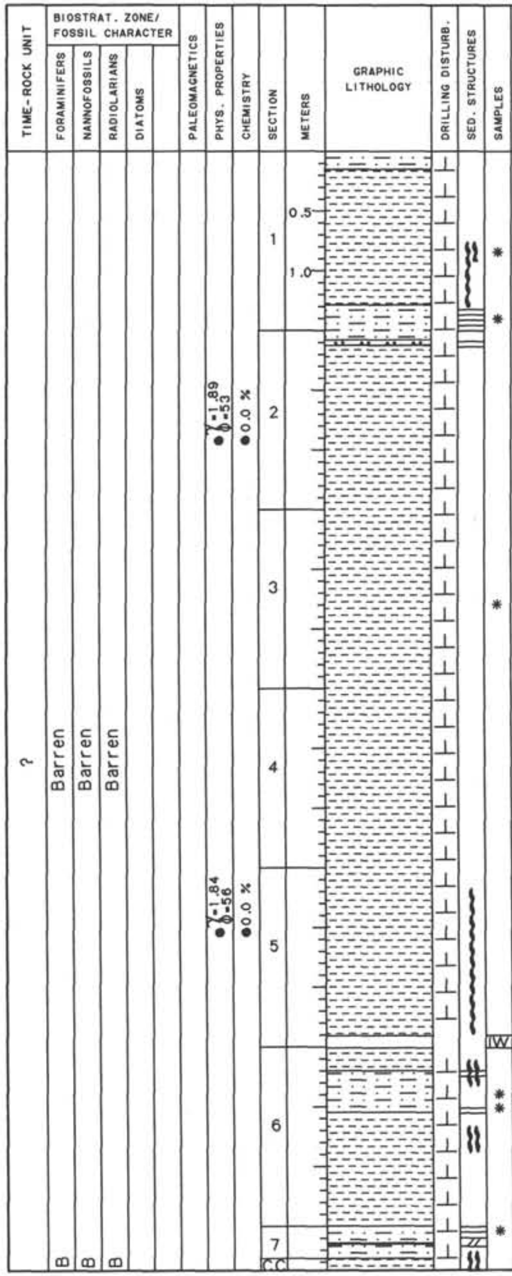

LITHOLOGIC DESCRIPTION

CLAYSTONE, MUDSTONE, and SILTY MUDSTONE

Grayish green and greenish gray (5G5/2, 5GY5/1) CLAYSTONE; dark greenish gray and greenish gray (5GY4/1, 5GY5/1) MUDSTONE; and dark gray (5Y4/1) laminated and locally cross-bedded SILTY MUDSTONE. Bedding dips 3°–7°.

Minor lithology: green glauconitic mudstone (5Y4/2) in Section 6, 21–42 cm.

SMEAR SLIDE SUMMARY (%):

	1, 83 D	1, 140 M	3, 76 D	6, 39 M	6, 43 M	7, 6 M
TEXTURE:						
Sand	—	Tr	—	—	—	1
Silt	1	70	Tr	35	51	84
Clay	99	30	100	65	49	15
COMPOSITION:						
Quartz	1	60	Tr	10	92	Tr
Feldspar	Tr	1	—	—	Tr	—
Rock fragments	—	2	—	—	5	—
Clay	99	30	100	75	—	15
Accessory minerals	—	5	—	15	1	—
Glauconite	—	—	—	—	1	85
Glaucophane	—	—	—	—	Tr	—
Pyroxene	—	—	—	—	Tr	—
Microcline	—	Tr	—	—	—	—
Zircon	—	Tr	—	—	Tr	—

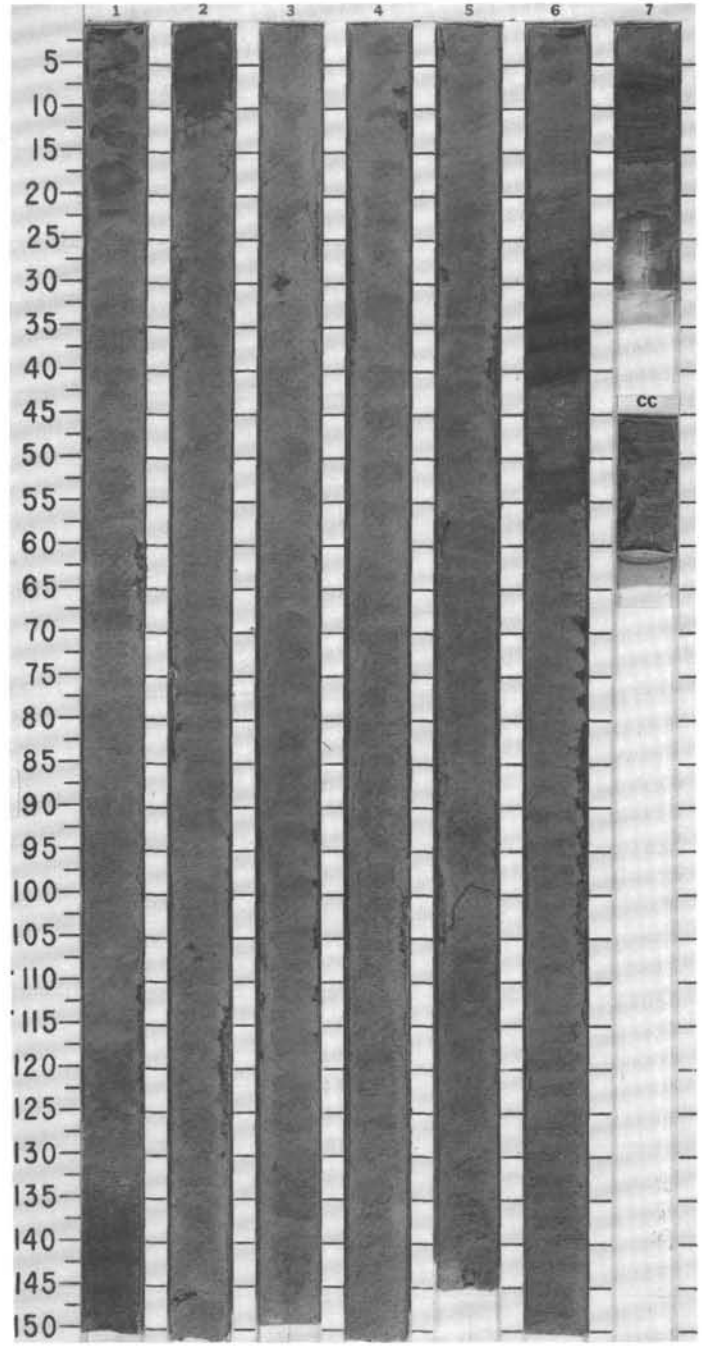

SITE 672 HOLE A CORE 39 X CORED INTERVAL 5324.3-5333.8 mbsl; 351.3-360.8 mbsf

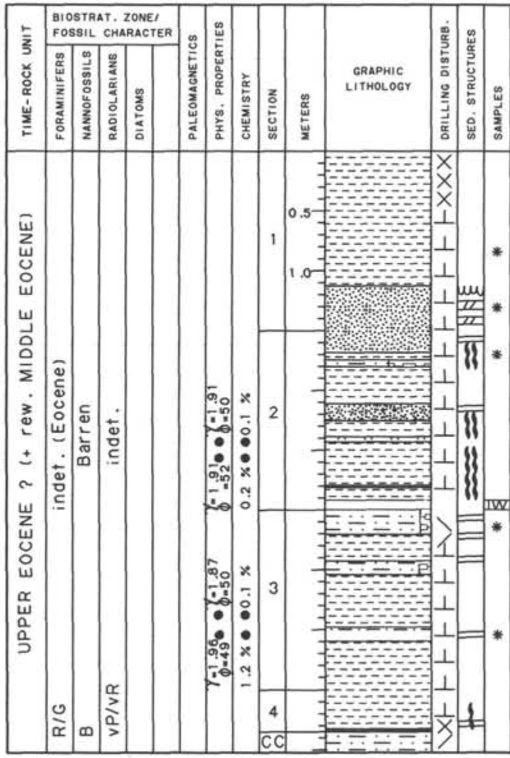

LITHOLOGIC DESCRIPTION

CLAYSTONE; MUDSTONE; and SILTSTONE, SANDSTONE and SILTY/SANDY MUDSTONE

Greenish gray (5G5/2) CLAYSTONE; dark to medium gray (5G4/2) MUDSTONE; very dark gray (5Y4/1, 5Y3/1) laminated and locally cross-bedded SILTSTONE, SANDSTONE and SILTY/SANDY MUDSTONE.

Minor lithology: chalk and marlstone, light greenish gray (5GY6/1) with bioturbated tops.

SMEAR SLIDE SUMMARY (%):

	1, 89 D	1, 136 D	2, 28 D	3, 20 D	3, 112 D
TEXTURE:					
Sand	—	50	5	45	—
Silt	5	30	40	30	10
Clay	95	20	55	25	90
COMPOSITION:					
Quartz	Tr	65	10	70	1
Feldspar	—	1	1	—	—
Clay	95	18	81	25	89
Accessory minerals	—	5	1	2	—
Glauconite	—	Tr	1	1	—
Pyrite	5	—	—	—	—
Foraminifers	—	5	3	Tr	—
Nannofossils	—	5	3	1	10
Radiolarians	—	Tr	—	Tr	—
Sponge spicules	—	Tr	—	—	—
Fish remains	—	Tr	—	—	—
Plant debris	—	Tr	—	—	—
Bioclasts	—	—	Tr	1	Tr

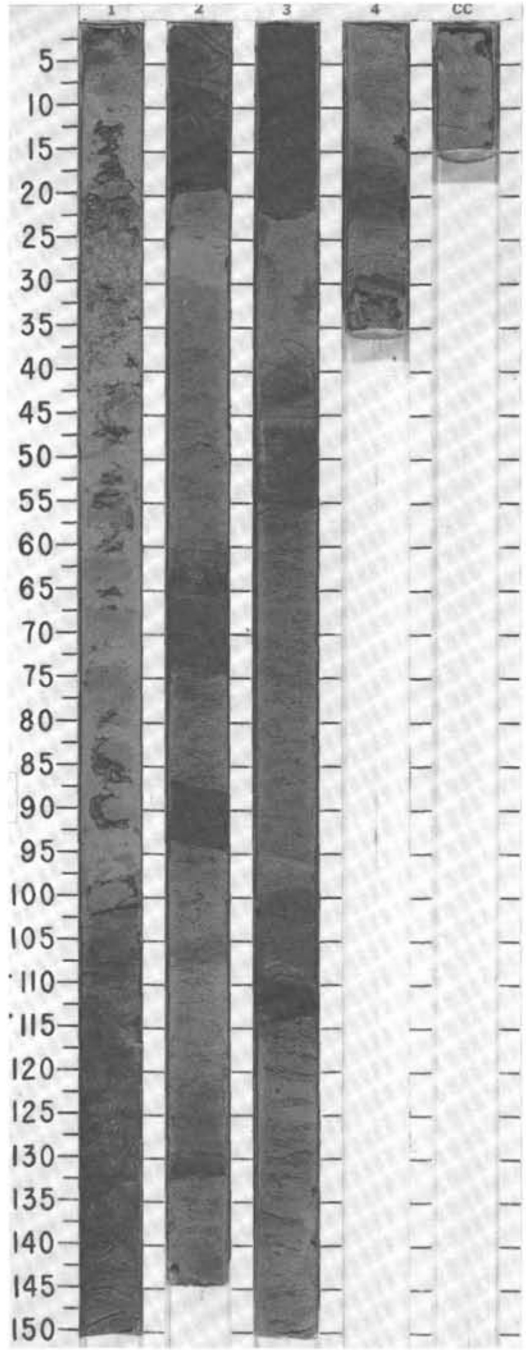

SITE 672 HOLE A CORE 40 X CORED INTERVAL 5333.8-5343.3 mbsl; 360.8-370.3 mbsf

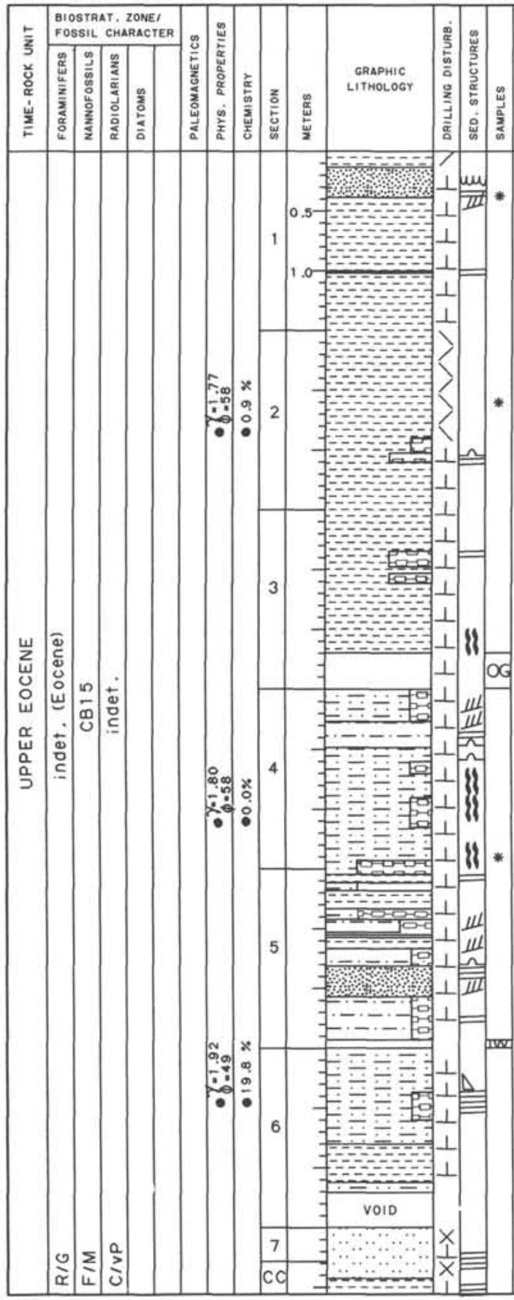

LITHOLOGIC DESCRIPTION

CLAYSTONE, MARLSTONE, and CALCAREOUS CLAYSTONE; SANDSTONE; and MUDSTONE and SANDY MUDSTONE

Greenish gray (5G5/2, 5G5/1) CLAYSTONE and whitish green (5GY7/1) MARLSTONE and CALCAREOUS CLAYSTONE, with commonly laminated bases and burrowed tops, and slump folding in Section 2; dark gray (5Y4/1), laminated and cross-laminated, medium-grained SANDSTONE; and grayish green (5G5/2) MUDSTONE and SANDY MUDSTONE. Bedding dips of 10°. A normal fault dipping 80° with a displacement of 7 cm in Section 6.

Minor lithology: dark gray (N4) laminated siltstone.

SMEAR SLIDE SUMMARY (%):

	1, 36 D	2, 70 D	4, 148 M
TEXTURE:			
Sand	60	—	—
Silt	20	Tr	20
Clay	20	100	80
COMPOSITION:			
Quartz	40	—	—
Feldspar	5	—	—
Rock fragments	15	—	—
Clay	23	95	25
Calcite/dolomite	—	—	55
Accessory minerals	2	—	—
Authigenic sulphate	2	—	—
Glauconite	2	—	—
Zeolites	3	—	—
Pyroxene	—	—	5
Foraminifers	5	—	—
Nannofossils	3	5	15

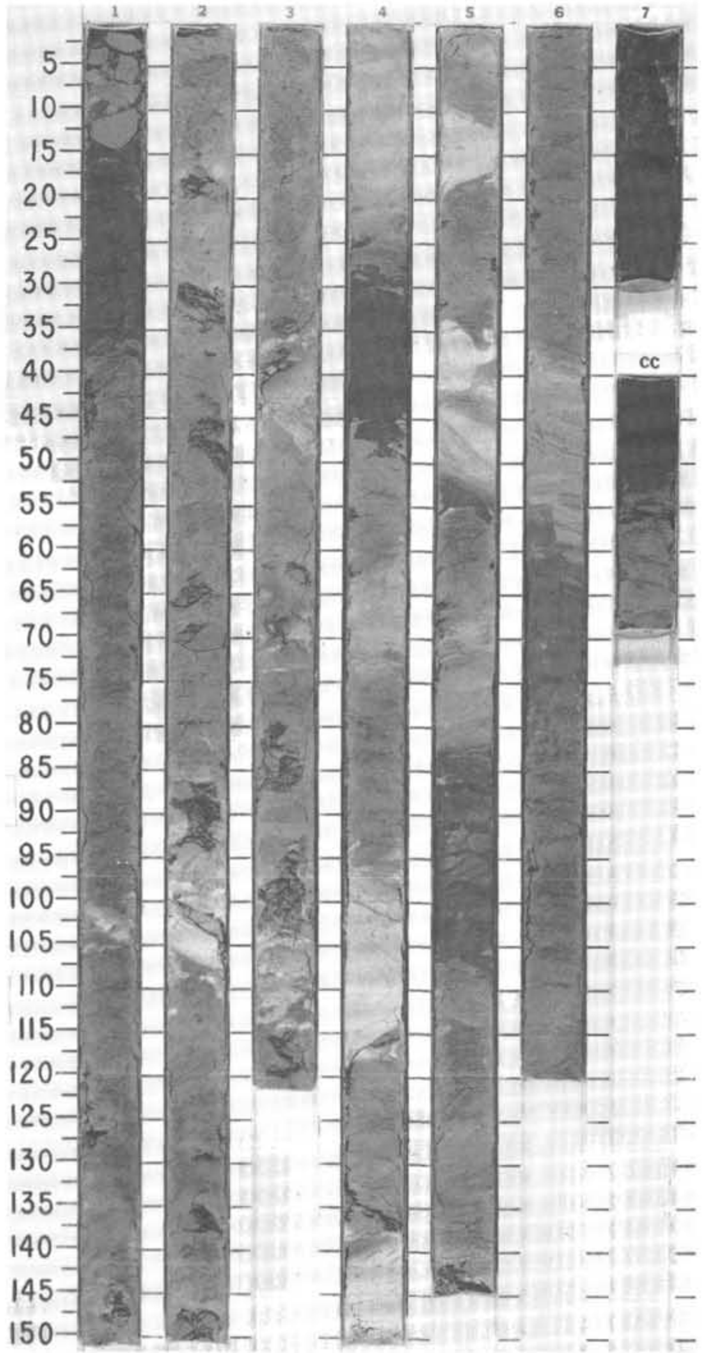

SITE 672 HOLE A CORE 41 X CORED INTERVAL 5343.3-5352.8 mbsl; 370.3-379.8 mbsf

TIME-ROCK UNIT	FORAMINIFERS	NANNOFOSSILS	RADIOLARIANS	DIATOMS	PALEOMAGNETICS	PHYS. PROPERTIES	CHEMISTRY	SECTION	METERS	GRAPHIC LITHOLOGY	DRILLING DISTURB.	SED. STRUCTURES	SAMPLES
MIDDLE EOCENE	*Truncorotaloides rohri* Zone A/M	CP14 F/M	indet. C/vP			●γ=2.03 ●φ=41 ●γ=1.86 ●φ=52	●32.3 % ●10.0 % ●0.1 % ●	1 2 CC	0.5 1.0	Drill Breccia			* * * *

LITHOLOGIC DESCRIPTION

MARLSTONE and CALCAREOUS MUDSTONE; CLAYSTONE; SANDY MUDSTONE; and MUDDY SANDSTONE

Pale green bioturbated and laminated (5GY7/1) MARLSTONE and CALCAREOUS MUDSTONE with burrowing more concentrated at the top of individual horizons; green (5G5/1) CLAYSTONE, dark olive-brown and green (5G5/1, 5G4/1) laminated; SANDY MUDSTONE, dark olive-brown (5Y4/1) laminated; and MUDDY SANDSTONE, cross-laminated and convolute-laminated.

SMEAR SLIDE SUMMARY (%):

	1, 82 D	1, 128 D	2, 130 D	2, 148 M
TEXTURE:				
Sand	40	1	1	1
Silt	20	40	5	50
Clay	40	59	94	49
COMPOSITION:				
Quartz	40	3	6	10
Feldspar	Tr	—	Tr	—
Clay	48	16	94	49
Accessory minerals				
Glauconite	Tr	—	Tr	2
Opaques (pyrite?)	5	—	Tr	—
Limonite(?)	1	—	—	—
Foraminifers	3	1	—	7
Nannofossils	3	—	—	2
Bioclasts	—	80	Tr	30

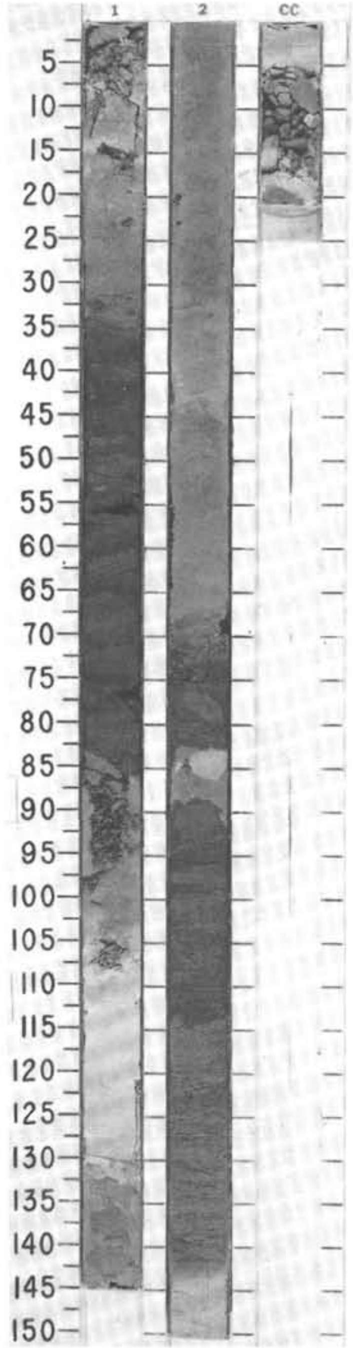

SITE 672 HOLE A CORE 42 X CORED INTERVAL 5352.8-5362.3 mbsl; 379.8-389.3 mbsf

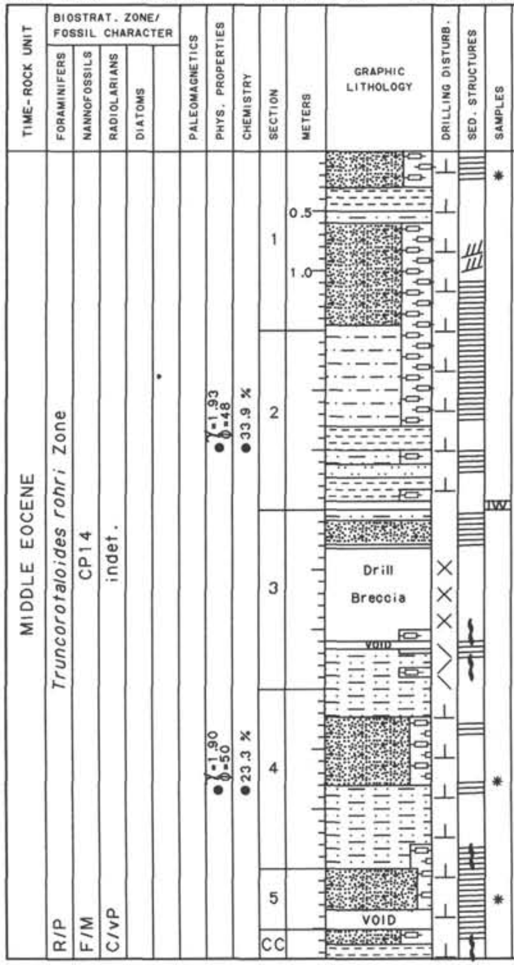

LITHOLOGIC DESCRIPTION

MARL; MUDSTONE and CLAYSTONE; SILTSTONE; and CALCAREOUS SANDSTONE

Pale green (5GY7/1) MARL with laminated bases and burrowed tops; greenish gray (5G5/1) MUDSTONE and CLAYSTONE; gray-brown (5Y4/1) laminated SILTSTONE; and laminated and cross-laminated bioclast-rich CALCAREOUS SANDSTONE, light greenish gray and greenish gray (5GY6/1, 5GY7/1). Beds dip at 35°–63° above faults that dip 60°–80° in Section 4. Well-developed scaly clay horizon 1 cm wide occurs along the fault zone. Bedding is horizontal at the base of the core.

SMEAR SLIDE SUMMARY (%):

	1, 21 D	4, 72 D	5, 30 D
TEXTURE:			
Sand	10	2	10
Silt	25	30	20
Clay	65	68	70
COMPOSITION:			
Quartz	28	32	30
Rock fragments	5	—	—
Clay	62	58	60
Accessory minerals			
Opaques	2	Tr	Tr
Foraminifers	3	—	—
Nannofossils	—	10	10

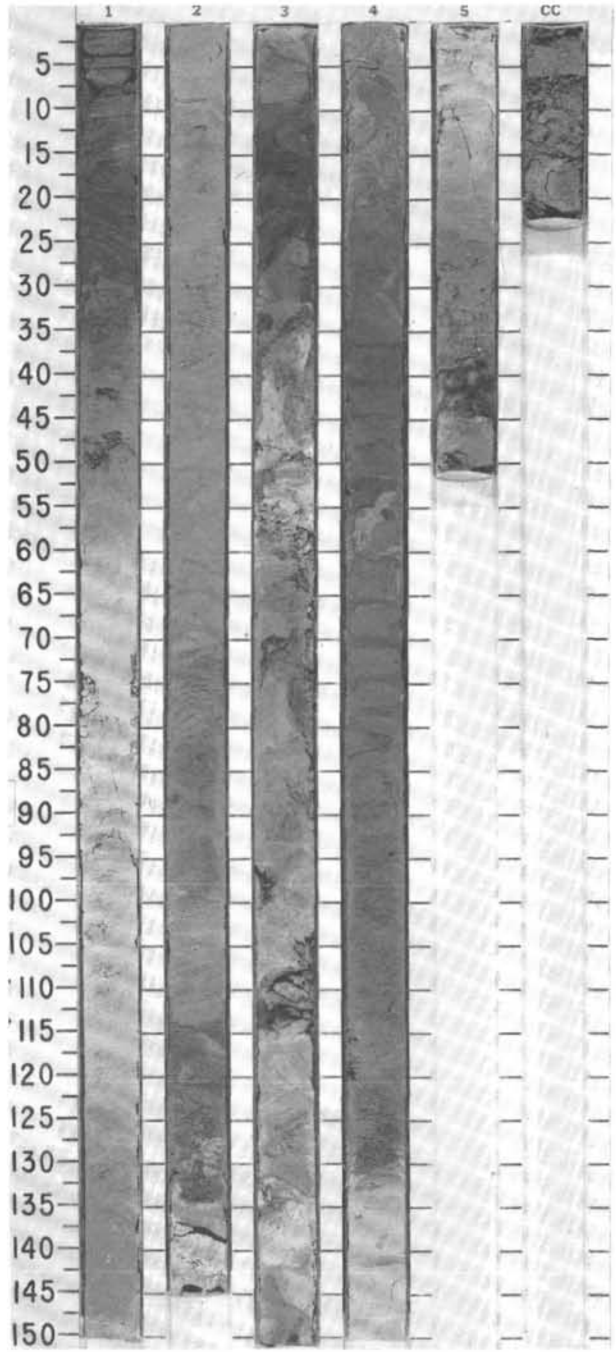

SITE 672 HOLE A CORE 43 X CORED INTERVAL 5362.3-5371.8 mbsf; 389.3-398.8 mbsf

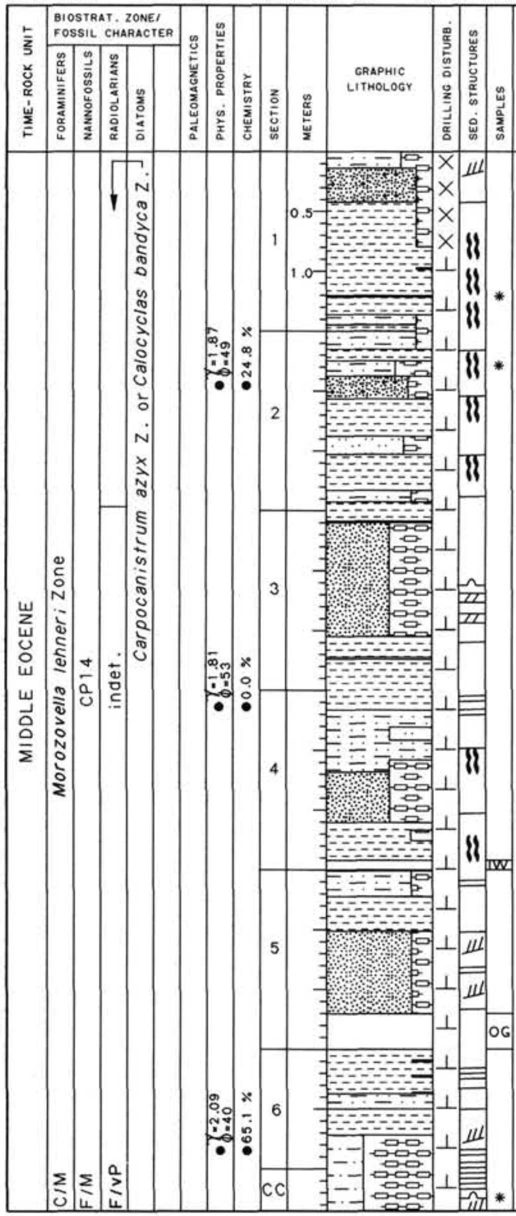

LITHOLOGIC DESCRIPTION

CLAYSTONE; CALCAREOUS MUDSTONE and SILTSTONE; and CALCAREOUS SANDSTONE

Greenish gray (5G5/2) CLAYSTONE; dark green (10Y4/1) CALCAREOUS MUDSTONE and SILTSTONE; pale green (10Y6/2) laminated and cross-laminated CALCAREOUS SANDSTONE.

Minor lithology: pale green (5G6/2) calcareous mudstone.

SMEAR SLIDE SUMMARY (%):

	1, 120 D	2, 30 D	CC, 20 D
TEXTURE:			
Sand	13	Tr	50
Silt	85	80	40
Clay	2	20	10
COMPOSITION:			
Quartz	76	12	10
Feldspar	—	1	—
Clay	—	15	15
Calcite/dolomite	2	36	55
Accessory minerals			
Glauconite	1	1	Tr
Pyrite	2	—	—
Fe/Mn hydroxide(?)	1	—	—
Biotite(?)	Tr	—	—
Foraminifers	10	30	20
Nannofossils	2	5	—
Diatoms	Tr	—	—
Sponge spicules	2	—	—
Fish remains	—	Tr	—
Bioclasts	3	—	—

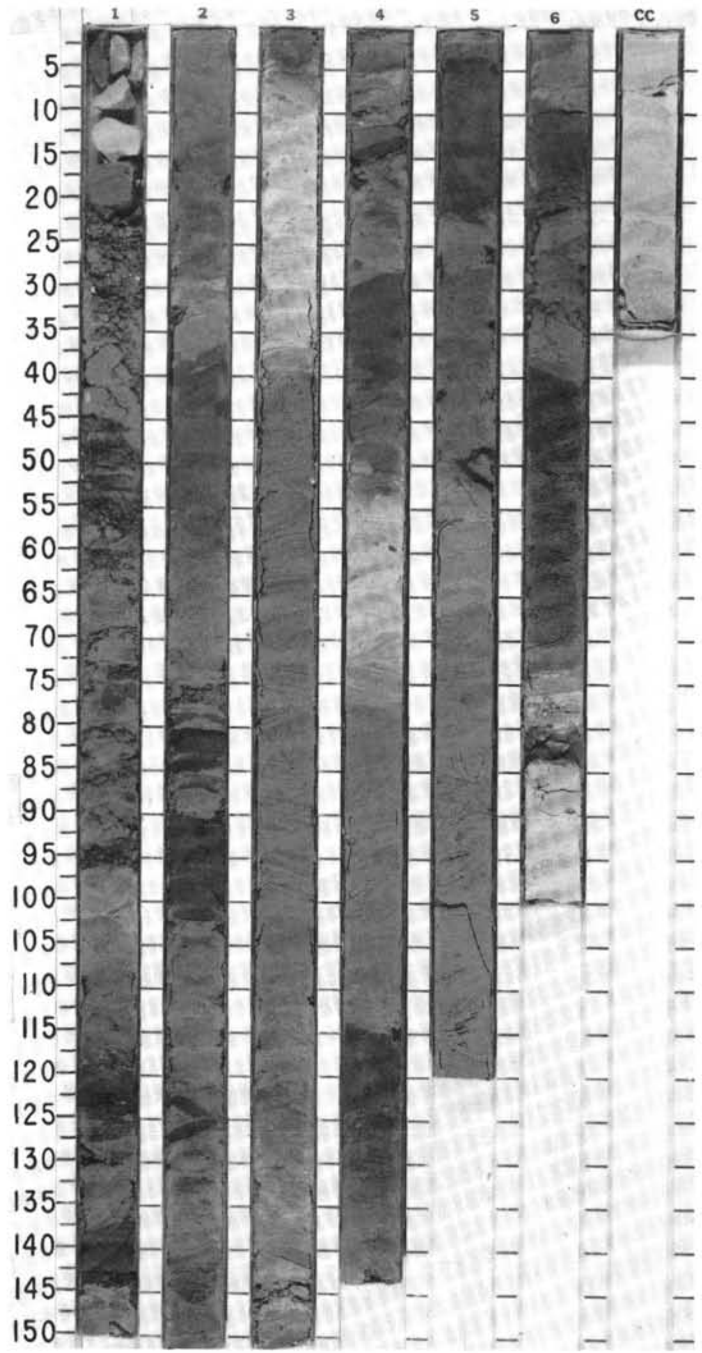

SITE 672 HOLE A CORE 44 X CORED INTERVAL 5371.8-5381.3 mbsl; 398.8-408.3 mbsf

TIME-ROCK UNIT	FORAMINIFERS	NANNOFOSSILS	RADIOLARIANS	DIATOMS	PALEOMAGNETICS	PHYS. PROPERTIES	CHEMISTRY	SECTION	METERS
MIDDLE EOCENE	*Morozovella lehneri* Zone	CP14	indet.			γ=1.90 ϕ=47; γ=1.84 ϕ=51	11.8 %; 39.8 %	1, 2, 3, 4, CC	0.5, 1.0
	F/G	F/M	F/vP						

GRAPHIC LITHOLOGY / DRILLING DISTURB. / SED. STRUCTURES / SAMPLES

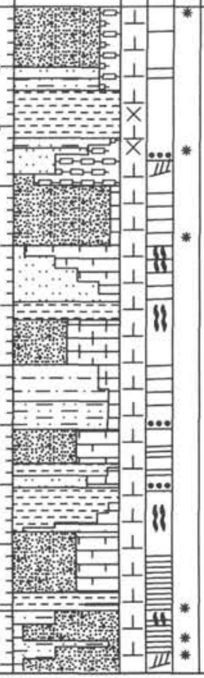

LITHOLOGIC DESCRIPTION

CLAYSTONE; CHALK, MARLY CHALK, and SILTY INDURATED CHALK; *CALCAREOUS SANDSTONE or MUDSTONE; and CALCAREOUS* CLAYSTONE

Dark green (5G5/2) CLAYSTONE, pale blue to white (5GY7/1) CHALK, MARLY CHALK, and SILTY INDURATED CHALK; plus dark gray (N4) CALCAREOUS SANDSTONE or MUDSTONE. CHALK has laminations and slumps; SANDSTONE and MUDSTONE are cross-stratified; CHALK and MARLY CHALK are bioturbated. Calcareous beds exhibit sequences with sharp base, laminated lower part, and an upper part grading into CALCAREOUS CLAYSTONE. Bedding is horizontal.

SMEAR SLIDE SUMMARY (%):

	1, 2 D	1, 127 D	2, 43 D	4, 53 M	CC, 21 D	CC, 33 D
TEXTURE:						
Sand	85	60	2	—	—	20
Silt	15	40	88	15	90	60
Clay	—	—	10	85	10	20
COMPOSITION:						
Quartz	62	15	50	—	—	3
Feldspar	—	Tr	Tr	—	—	—
Rock fragments	—	—	Tr	—	—	—
Clay	—	—	10	70	10	20
Calcite/dolomite	2	—	25	—	—	15
Accessory minerals						
Glauconite	1	—	1	—	—	Tr
Pyrite	5	—	—	—	—	—
Pyroxene(?)	—	Tr	—	—	—	—
Zircon	—	—	Tr	—	—	—
Foraminifers	20	20	5	—	10	20
Nannofossils	—	—	1	30	80	40
Fish remains	Tr	Tr	Tr	—	Tr	—
Bioclasts	10	65	5	—	—	2

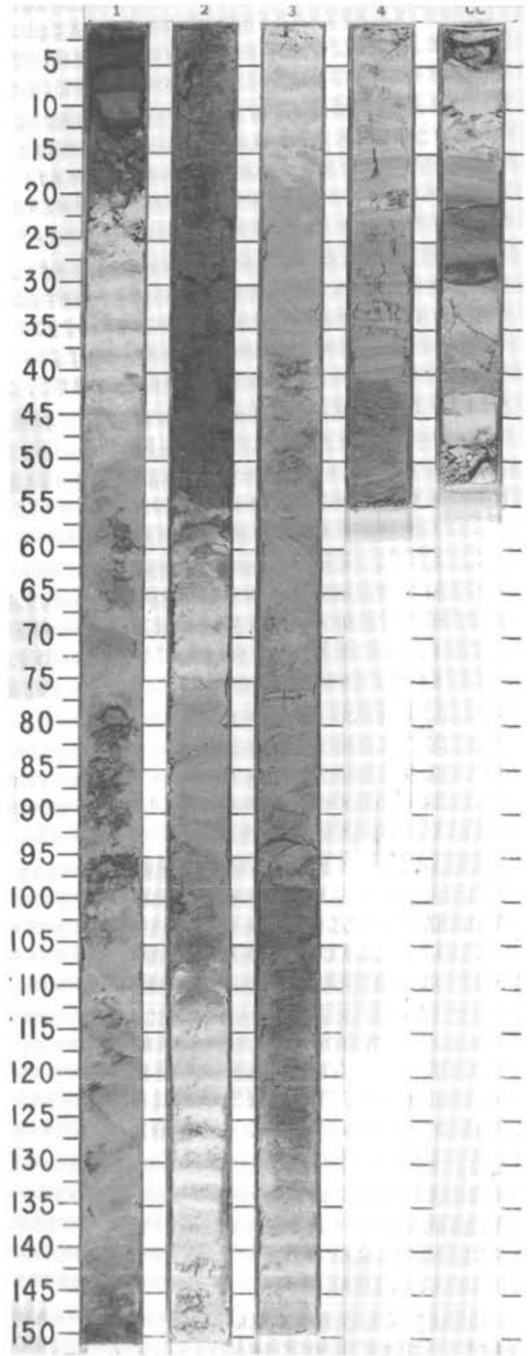

SITE 672 HOLE A CORE 45 X CORED INTERVAL 5381.3-5390.8 mbsl; 408.3-417.8 mbsf

TIME-ROCK UNIT	FORAMINIFERS	NANNOFOSSILS	RADIOLARIANS	DIATOMS	PALEOMAGNETICS	PHYS. PROPERTIES	CHEMISTRY	SECTION	METERS	GRAPHIC LITHOLOGY	DRILLING DISTURB.	SED. STRUCTURES	SAMPLES
MIDDLE EOCENE	B Barren	CP14 F/M	*Podocyrtis mitra* Zone - *Podocyrtis goetheana* Zone A/P					1	0.5				* *
								CC					

LITHOLOGIC DESCRIPTION

CALCAREOUS MUDSTONE, CALCAREOUS SANDSTONE, and INDURATED CHALK

Light brown (5GY6/1) CALCAREOUS MUDSTONE, green (5G6/1) CALCAREOUS SANDSTONE, and light greenish gray (5G6/1) INDURATED CHALK; commonly laminated at base and bioturbated at bottom.

SMEAR SLIDE SUMMARY (%):

	1, 49 D	1, 66 D
TEXTURE:		
Sand	25	95
Silt	70	5
Clay	5	Tr
COMPOSITION:		
Quartz	30	70
Mica	—	Tr
Clay	5	Tr
Calcite/dolomite	45	3
Accessory minerals		
Glauconite	1	2
Opaques	Tr	—
Epidote	—	Tr
Authigenic albite(?)	—	Tr
Foraminifers	10	20
Nannofossils	2	Tr
Bioclasts	5	2

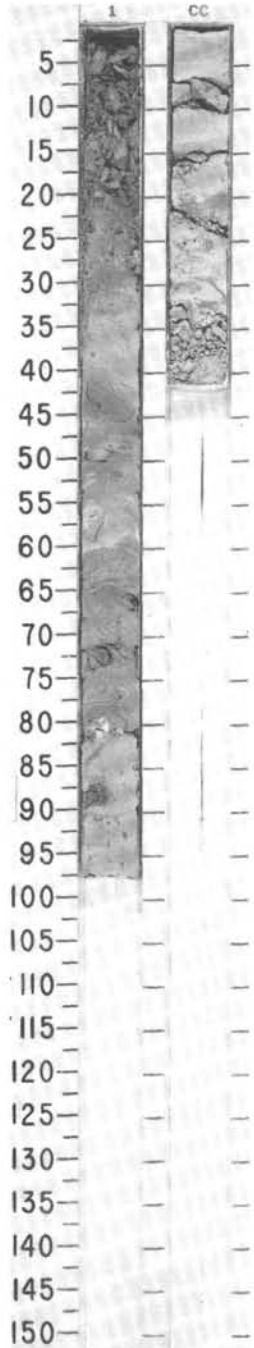

SITE 672 HOLE A CORE 46 X CORED INTERVAL 5390.8-5400.3 mbsl; 417.8-427.3 mbsf

TIME-ROCK UNIT	FORAMINIFERS	NANNOFOSSILS	RADIOLARIANS	DIATOMS	PALEOMAGNETICS	PHYS. PROPERTIES	CHEMISTRY	SECTION	METERS	GRAPHIC LITHOLOGY	DRILLING DISTURB.	SED. STRUCTURES	SAMPLES
MIDDLE EOCENE	Barren	CP14	R/VP *Podocyrtis mitra* Zone - *P. goetheana* Zone			γ=2.00 φ=42; γ=1.92 φ=47	51.2 %; 24.3 %	1, 2, CC	0.5, 1.0				* IW
	F/M												

LITHOLOGIC DESCRIPTION

CALCAREOUS MUDSTONE and MUDSTONE; CLAYSTONE; CALCAREOUS SANDSTONE; and INDURATED CHALK

Dark brownish green (5Y4/2) CALCAREOUS MUDSTONE and MUDSTONE; dark olive-gray (5G4/2) CLAYSTONE; laminated CALCAREOUS SANDSTONE (5G5/2); and pale bluish green (5GY7/1) INDURATED CHALK.

SMEAR SLIDE SUMMARY (%):

	1, 115 D
TEXTURE:	
Sand	20
Silt	73
Clay	7
COMPOSITION:	
Quartz	5
Feldspar	Tr
Clay	5
Calcite	50
Accessory minerals	
Glauconite	Tr
Glaucophane	Tr
Auth. albite, zeolite(?)	1
Dolomite	3
Foraminifers	25
Nannofossils	5
Radiolarians	Tr
Sponge spicules	Tr
Bioclasts	6

SITE 672 HOLE A CORE 47 X CORED INTERVAL 5400.3-5409.8 mbsl; 427.3-436.8 mbsf

TIME-ROCK UNIT	FORAMINIFERS	NANNOFOSSILS	RADIOLARIANS	DIATOMS	PALEOMAGNETICS	PHYS. PROPERTIES	CHEMISTRY	SECTION	METERS	GRAPHIC LITHOLOGY	DRILLING DISTURB.	SED. STRUCTURES	SAMPLES
MIDDLE EOCENE	F/M	CP14	F/P *Podocyrtis mitra* Zone					CC					* * *

LITHOLOGIC DESCRIPTION

CHALK and INDURATED CHALK; CLAYSTONE and CALCAREOUS SANDY SILTSTONE

Laminated pale greenish gray (5BG5/1) CHALK and INDURATED CHALK; dark greenish gray (5G5/1) CLAYSTONE and CALCAREOUS SANDY SILTSTONE with cross-bedding and laminations. CHALK is bioturbated. Bedding dips up to 12°.

SMEAR SLIDE SUMMARY (%):

	CC, 19 M	CC, 39 D	CC, 51 D
TEXTURE:			
Silt	4	90	85
Clay	96	10	15
COMPOSITION:			
Feldspar	—	Tr	—
Clay	75	5	—
Calcite/dolomite	5	90	69
Accessory minerals	—	Tr	—
Glauconite	Tr	—	—
Hornblende	Tr	—	—
Biotite	Tr	—	—
Authigenic sulphate	10	—	—
Foraminifers	2	Tr	1
Nannofossils	5	5	30
Radiolarians	Tr	—	—
Sponge spicules	Tr	—	—

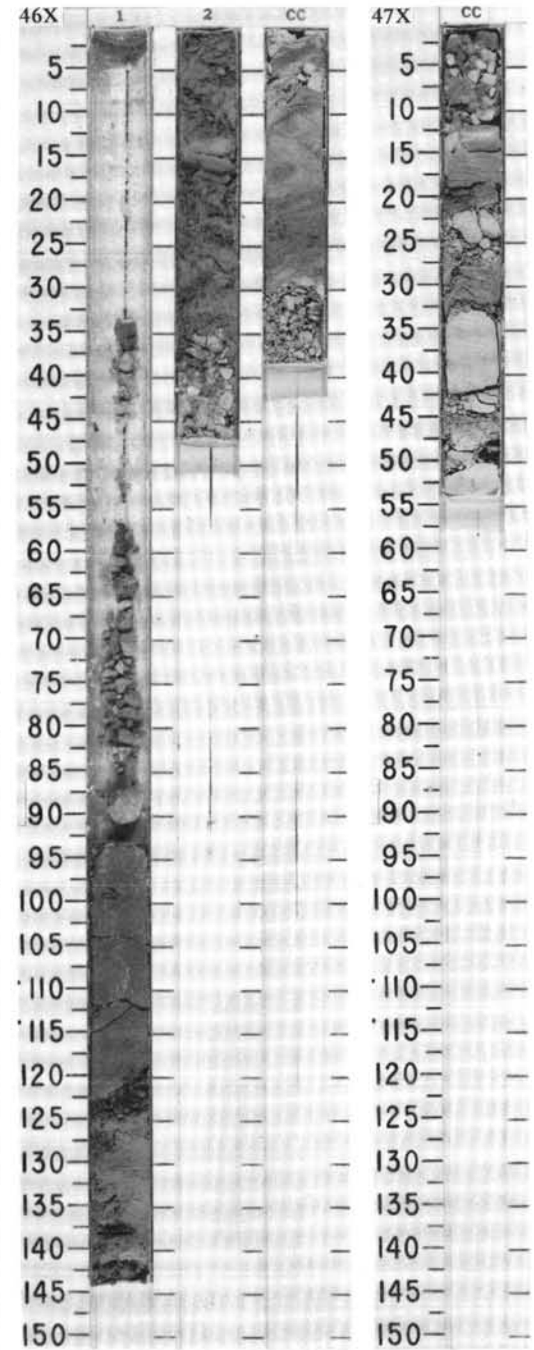

SITE 672 HOLE A CORE 48 X CORED INTERVAL 5409.8-5419.3 mbsl; 436.8-446.3 mbsf

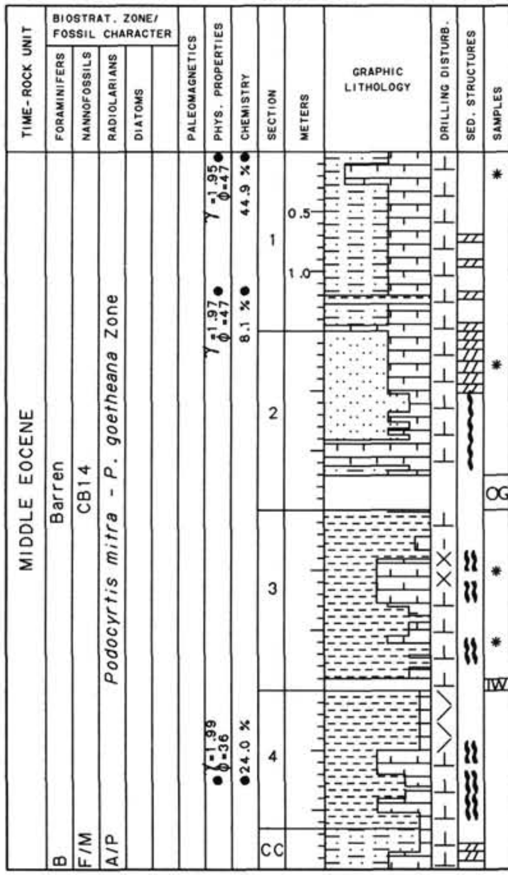

LITHOLOGIC DESCRIPTION

CALCAREOUS SANDY SILTSTONE; CALCAREOUS SILTSTONE grading into CALCAREOUS MUDSTONE and CHALK; and CLAYSTONE

Gray (10Y6/1) CALCAREOUS SANDY SILTSTONE with cross-bedding; laminated CALCAREOUS SILTSTONE (5GY6/1) grading into bioturbated CALCAREOUS MUDSTONE and CHALK; and dark olive-gray (5G4/2), slightly calcareous CLAYSTONE. Normal fault in CC dips 45°.

SMEAR SLIDE SUMMARY (%):

	1, 19 D	2, 27 D	3, 64 D	3, 112 M
TEXTURE:				
Sand	90	60	—	—
Silt	8	30	10	15
Clay	2	10	90	85
COMPOSITION:				
Quartz	8	30	1	Tr
Clay	—	5	—	59
Calcite/dolomite	2	20	50	—
Accessory minerals	1	3	Tr	Tr
Glauconite	1	2	—	—
Foraminifers	85	35	—	—
Nannofossils	2	5	49	40
Diatoms	—	—	—	Tr
Sponge spicules	1	—	—	—
Fish remains	Tr	—	—	—
Bioclasts	—	2	—	—

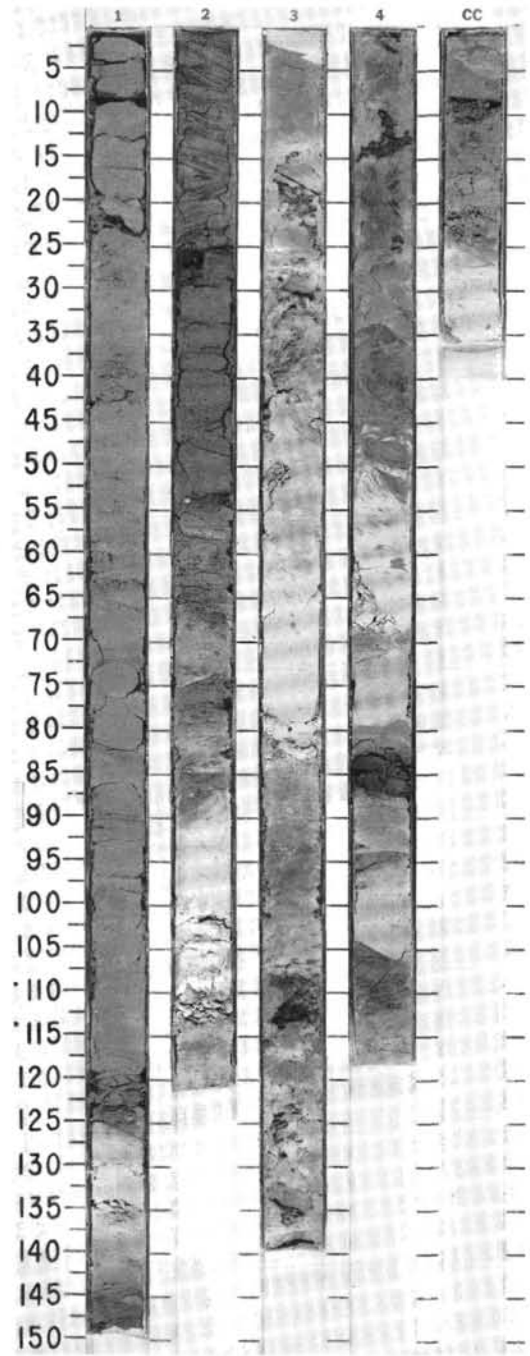

SITE 672 HOLE A CORE 49 X CORED INTERVAL 5419.3-5428.8 mbsl; 446.3-455.8 mbsf

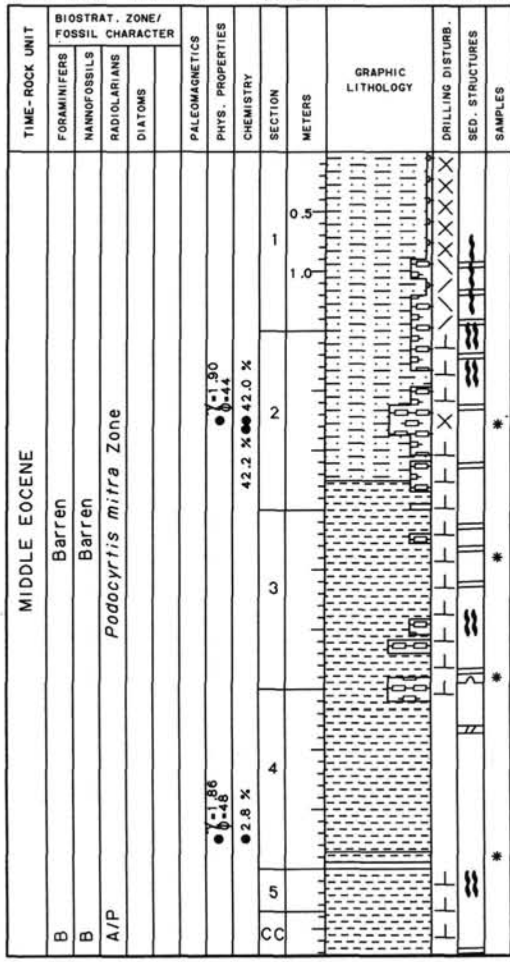

LITHOLOGIC DESCRIPTION

MUDSTONE, CALCAREOUS MUDSTONE, and SILTY INDURATED CHALK

Interbedded greenish gray (5G5/1) MUDSTONE, laminated bluish gray (5GY7/1) CALCAREOUS MUDSTONE and SILTY INDURATED CHALK. Slump in base of calcareous sequences and bioturbations at top of calcareous sequences.

SMEAR SLIDE SUMMARY (%):

	2, 76 D	3, 40 D	3, 140 D	4, 136 M
TEXTURE:				
Sand	1	5	—	1
Silt	49	15	3	2
Clay	50	80	97	97
COMPOSITION:				
Quartz	10	3	1	1
Feldspar	—	Tr	—	—
Clay	50	91	97	97
Accessory minerals	1	1	—	—
Glauconite	Tr	—	—	—
Foraminifers	3	3	1	2
Nannofossils	1	1	Tr	—
Bioclasts	35	1	1	Tr

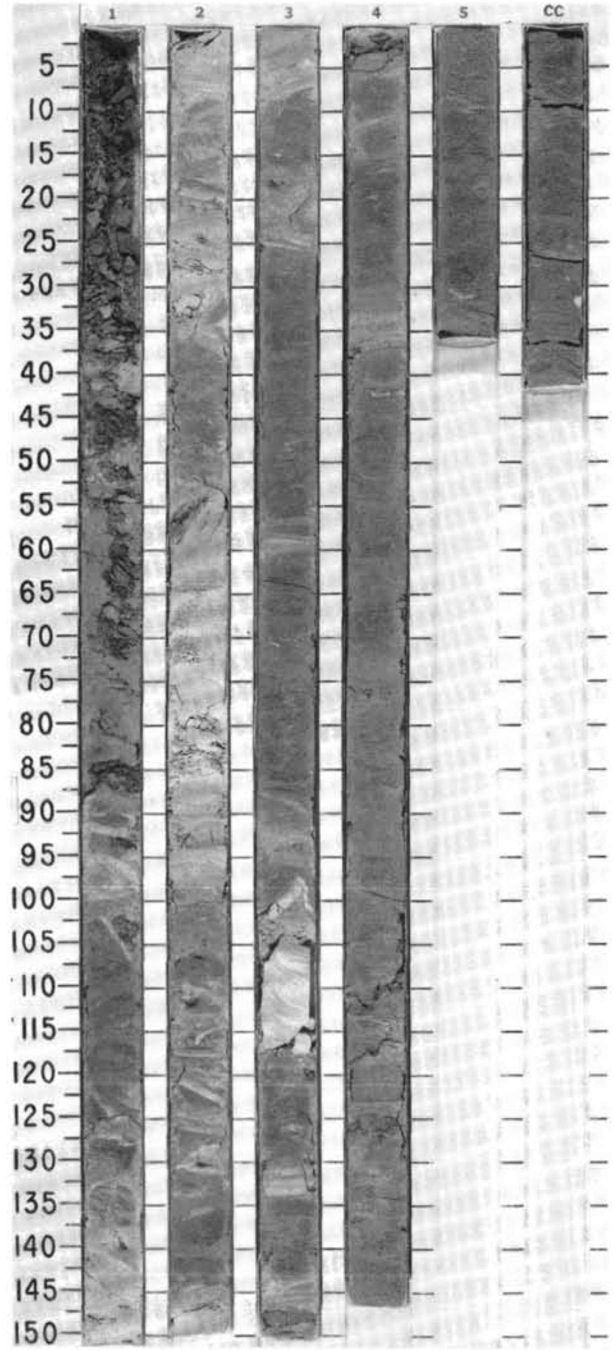

SITE 672 HOLE A CORE 50 X CORED INTERVAL 5428.8-5438.3 mbsl; 455.8-465.3 mbsf

TIME-ROCK UNIT	FORAMINIFERS	NANNOFOSSILS	RADIOLARIANS	DIATOMS	PALEOMAGNETICS	PHYS. PROPERTIES	CHEMISTRY	SECTION	METERS	GRAPHIC LITHOLOGY	DRILLING DISTURB.	SED. STRUCTURES	SAMPLES
MIDDLE EOCENE	Barren	Barren B	*Podocyrtis ampla* Zone - *P. mitra* Zone C/P			●γ=1.82 φ=49; ●γ=1.88 φ=46	●0.0 %; ●0.2 %	1, 2, 3, 4, CC	0.5, 1.0				*

BIOSTRAT. ZONE/ FOSSIL CHARACTER

LITHOLOGIC DESCRIPTION

MUDSTONE and CLAYSTONE

Bluish green (5G5/1) MUDSTONE and varicolored (5G5/1 to 5GY5/1) CLAYSTONE; massive to locally bioturbated.

SMEAR SLIDE SUMMARY (%):

	2, 34 M	2, 63 D	3, 37 M	3, 76 D	3, 86 D
TEXTURE:					
Sand	—	—	—	—	5
Silt	40	2	30	2	1
Clay	60	98	70	98	94
COMPOSITION:					
Quartz	20	2	10	Tr	1
Feldspar	—	—	20	—	1
Clay	60	98	68	98	93
Accessory minerals	Tr	—	3	—	—
Authigenic sulphate	10	—	—	—	—
Radiolarians	10	—	—	—	5

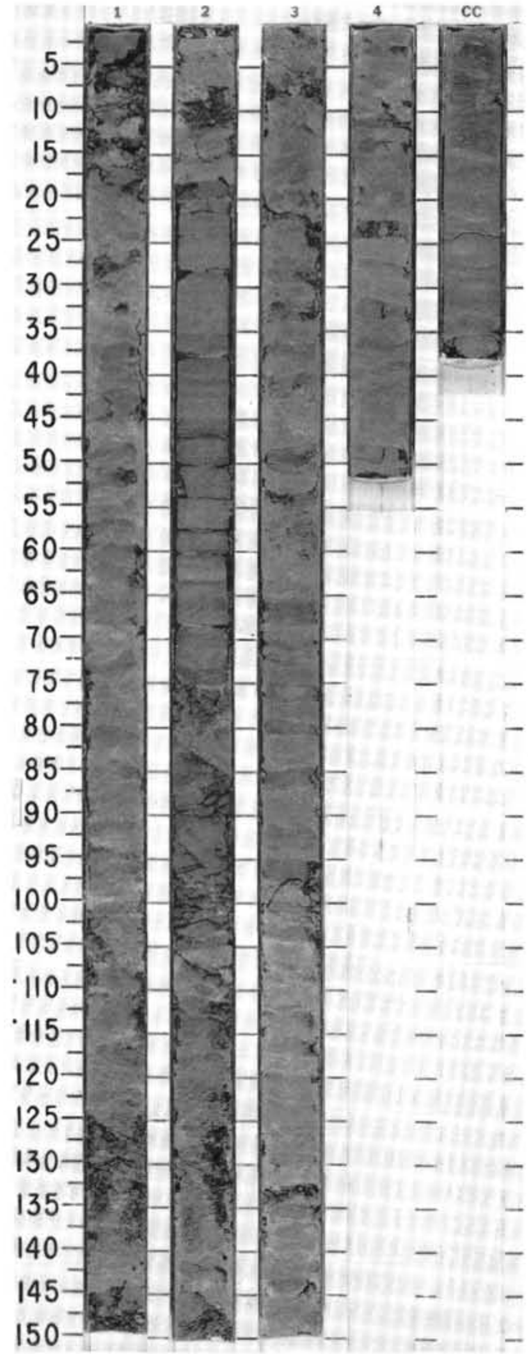

SITE 672 HOLE A CORE 51 X CORED INTERVAL 5438.3-5447.8 mbsl; 465.3-474.8 mbsf

TIME-ROCK UNIT	FORAMINIFERS	NANNOFOSSILS	RADIOLARIANS	DIATOMS	PALEOMAGNETICS	PHYS. PROPERTIES	CHEMISTRY	SECTION	METERS	GRAPHIC LITHOLOGY	DRILLING DISTURB.	SED. STRUCTURES	SAMPLES
MIDDLE EOCENE	B Barren	B Barren	C/P *Dictyoprora mongolfieri* Zone - *Podocyrt mitra* Zone			γ=1.87 ϕ=51; γ=1.81 ϕ=54	0.4 %; 0.2 %	1, 2, 3, CC	0.5, 1.0				*, IW, *, *

SILICEOUS MUDSTONE

Green to reddish brown (5G5/1 to 10YR5/2) radiolarian-rich SILICEOUS MUDSTONE, locally bioturbated.

SMEAR SLIDE SUMMARY (%):

	1, 20 M	3, 15 D	CC, 20 D
TEXTURE:			
Silt	30	1	3
Clay	70	99	97
COMPOSITION:			
Quartz	—	1	5
Clay	69	99	95
Radiolarians	30	Tr	—
Sponge spicules	1	—	—

SITE 672 HOLE A CORE 52 X CORED INTERVAL 5447.8-5457.3 mbsl; 474.8-484.3 mbsf

TIME-ROCK UNIT	FORAMINIFERS	NANNOFOSSILS	RADIOLARIANS	DIATOMS	PALEOMAGNETICS	PHYS. PROPERTIES	CHEMISTRY	SECTION	METERS	GRAPHIC LITHOLOGY	DRILLING DISTURB.	SED. STRUCTURES	SAMPLES
LOWER EOCENE	B Barren	B Barren	C/P *Dictyoprora mongolfieri* Zone			γ=1.86 ϕ=49	0.1 %	1, CC					*, *

CLAYSTONE and SILICEOUS CLAYSTONE

Reddish brown (7.5YR4/3) CLAYSTONE and SILICEOUS CLAYSTONE; massive.

SMEAR SLIDE SUMMARY (%):

	1, 24 D	CC, 26 D
TEXTURE:		
Silt	1	1
Clay	99	99
COMPOSITION:		
Quartz	1	1
Clay	99	99

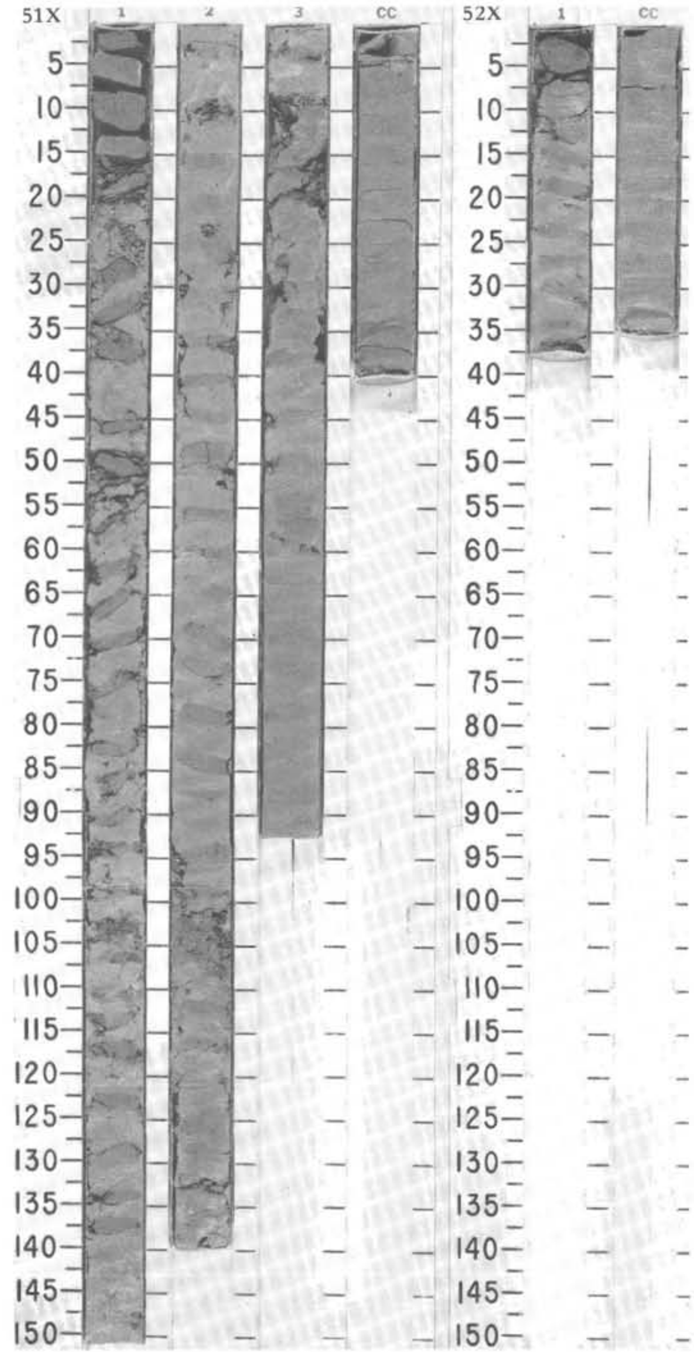

SITE 672 HOLE A CORE 53 X CORED INTERVAL 5457.3-5466.8 mbsl; 484.3-493.8 mbsf

TIME-ROCK UNIT	FORAMINIFERS	NANNOFOSSILS	RADIOLARIANS	DIATOMS	PALEOMAGNETICS	PHYS. PROPERTIES	CHEMISTRY	SECTION	METERS
LOWER EOCENE	Barren B	Barren B	*Buryella clinata* Zone - *Theocotyle cyrptocephala* Zone C/P			γ=1.79 ϕ=62 ; γ=1.80 ϕ=59	0.0 % ; 0.0 %	1, 2, 3, 4, 5, 6, CC	0.5, 1.0

GRAPHIC LITHOLOGY / DRILLING DISTURB. / SED. STRUCTURES / SAMPLES

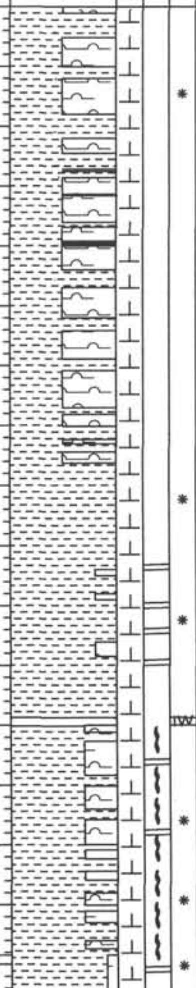

LITHOLOGIC DESCRIPTION

SILICEOUS CLAYSTONE and CLAYSTONE

Alternating beds of brown (7.5YR5/2) SILICEOUS CLAYSTONE and greenish gray (5GY6/1) CLAYSTONE, massive to locally fissile.

SMEAR SLIDE SUMMARY (%):

	1, 76 D	3, 123 D	4, 68 M	5, 75 D	5, 144 M	CC, 10 M
TEXTURE:						
Sand	—	—	—	Tr	—	—
Silt	50	5	—	5	30	15
Clay	50	95	100	95	70	85
COMPOSITION:						
Clay	50	95	99	98	70	83
Volcanic glass	—	—	—	Tr	—	—
Accessory minerals	—	—	Tr	—	—	5
Chlorite	—	—	1	—	—	—
Authigenic albite(?)	—	—	—	Tr	—	—
Hornblende(?)	—	—	—	Tr	Tr	—
Authigenic sulphate	—	—	—	—	Tr	2
Radiolarians	50	5	—	1	30	10